MOLECULAR INTERACTIONS IN PHARMACEUTICAL PREFORMULATION AND SUPRAMOLECULAR COMPLEXES

S.R. KAMBLE

PhD

UNIVERSITY OF BRADFORD

2018

MOLECULAR INTERACTIONS IN PHARMACEUTICAL PREFORMULATION AND SUPRAMOLECULAR COMPLEXES

“STRUCTURAL PROPERTIES GOVERNING DRUG-PLASMA PROTEIN BINDING AND INVESTIGATION OF AMINO ACIDS CO-CRYSTALS”

Sharad Ramchandra KAMBLE

Submitted for the degree of

Doctor of Philosophy

School of Biomedical Sciences and Pharmacy

Faculty of Life Sciences

UNIVERSITY OF BRADFORD

2018

Abstract

Sharad Ramchandra Kamble

Title: “Molecular Interactions in Pharmaceutical Preformulation and Supramolecular Complexes”.

Subtitle: ‘Structural Properties Governing Drug-Plasma Protein Binding and Investigation of Amino Acids Co-crystals’.

Keywords: Drug-Plasma Protein Binding, HPLC, Linear Free Energy Relationship, Abraham’s descriptors, Amino acids, Co-crystallisation, Non-Hygroscopic Effervescent Tablets.

The study of pharmaceutical preformulation includes the evaluation of pharmacokinetic, pharmacodynamic and physicochemical properties of the drug molecules that aid the formulation. However, it has a limited role in determining drug dosage optimisation in the formulation. The study of drug-Plasma Protein Binding (PPB), and the lipophilicity, solubility, and ionic behaviours of the desired drug molecules addresses the gap and enhances our undertraining related to the behaviour of the drug molecules in the body.

The High-Performance Liquid Chromatography (HPLC) technique was used in the current study to assess drug-PPB interaction. Using Michael Abraham’s ‘Linear Free Energy Relationship’ (LFER) method, two major plasma proteins namely, Human Serum Albumin as HSA and α-1-Acid Glycoprotein as AGP, were used and the structural properties governing drug-plasma protein binding was determined. This is the first time that the effect of ionised species on PPB has been quantitatively evaluated.

In addition, the molecular interactions also play a key role in the supramolecular complexes of co-crystals. The project also evaluated the co-crystallisation

process and its effect on physicochemical properties of the drug. In the current study, amino acids (AAs) have been observed to be a prominent source of coformers. The AAs showed co-crystals formation with carboxylic acids, non-steroidal anti-inflammatory drug (NSAID) and citric acid which overcome the hygroscopicity problems and improved the physical stability issues during storage. This study has also identified a new formulation which is helpful for improvement in the stability of effervescent tablets at various relative humidity (RH) conditions which will reduce the manufacturing cost associated with the production of effervescent tablets.

Declaration

This thesis is a presentation of my original research work. Wherever contributions of others are involved, every effort is made to indicate this clearly, with due reference to the literature, and acknowledgement of collaborative research and discussions.

The work was done under the guidance of Professor Anant Paradkar and Dr Xiangli Liu, at the University of Bradford, West Yorkshire, England, UK.

Mr. Sharad Ramchandra Kamble

In my capacity as supervisor of the candidate's thesis, I certify that the above statements are true to the best of my knowledge.

Professor Anant R. Paradkar
Director, Centre for Pharmaceutical Engineering Sciences
Date:

Dr. Xiangli Liu
Lecturer in Pharmacy and Medical Sciences
Date:

Professor Marcus Rattray
Head of School of Pharmacy and Medical Sciences,
University of Bradford, Bradford, West Yorkshire, England, UK.

Preface

This research work has been carried out at the Centre of Pharmaceutical Engineering Science, University of Bradford, Bradford, West Yorkshire, England, the United Kingdom between April 2014 to September 2017 under the supervision of Dr Xiangli Liu and Professor Anant Paradkar. The contents of this work are original, and references to the published work have been cited in this thesis.

Publication of this current work

1. Kamble, S., Loadman, P., Abraham, M. H. and Liu, X. (2018) Structural properties governing drug-plasma protein binding determined by high-performance liquid chromatography method. *Journal of Pharmaceutical and Biomedical Analysis* 149, 16-21.

Manuscripts (*in preparation*)

1. Kamble, S.R., Pagire, S., Liu, X. and Paradkar, A., "Processability improvement study in the effervescent tablet formulation".
2. Kamble, S.R., Pagire, S., Liu, X. and Paradkar, A., "Amino acid co-crystals and single crystal of citric acid - L-cysteine monohydrate".

Presentation of research work in conferences

A part of the results of this dissertation was presented at the following conferences.

1. Presented poster entitled as, "amino acids co-crystals" in 'APS 7th International PharmSci conference 2016', 5th - 7th September 2016, at Technology and Innovation Centre, University of Strathclyde, Glasgow, UK.

2. Presented poster entitled as, “amino acids co-crystals” in ‘Research and Development Day 2017’ at University of Bradford, School of Pharmacy and Medical Sciences (incorporating Centre for Pharmaceutical Engineering and Institute of Cancer Therapeutics) under Faculty of Life Sciences on 6th June 2017.
3. Oral presentation on, “amino acids co-crystals” was given in, ‘3rd Post Graduate Research Symposium 2017’, at the University of Bradford, School of Pharmacy and Medical Sciences (incorporating Centre for Pharmaceutical Engineering and Institute of Cancer Therapeutics) under Faculty of Life Sciences on 7th June 2017.

Inspirational Thoughts

"Science knows no country because knowledge belongs to humanity and is a torch which illuminates the world."

---- Louis Pasteur.

[I think 'Science knows no country (also *religion, class, castes, races and gender)'* need to be added to this brilliant quote by Louis Pasteur]

"*Atta Deep Bhava*" means "*You are the creator of your future.*"

---- Buddha.

"*Educate, Organise and Agitate for Better Humanity.*"

---- Dr B.R. Ambedkar.

(MA., Ph.D., M.Sc., D. Sc, Barrister-at-Law, L.L.D., D. Litt)

("Symbol of Knowledge". We are because He was)

Dedicated to

"My Beloved Family Members, Parents, Relatives, Friends and Teachers."

Acknowledgement

I sincerely acknowledge the funding source as, “Chhatrapati Rajarshee Shahu Maharaj Scholarship for Higher Studies in Foreign Countries” programme of ‘Department of Social Justice and Welfare, Government of Maharashtra, India’ for providing the financial support to pursue my PhD study.

I would like to thank my supervisors, Dr Xiangli Liu and Prof Anant Paradkar. I would like to express my sincere gratitude to Dr Xiangli Liu for her continuous support and guidance in this study. I am thankful to her, for giving me constant motivation and suggestions throughout the work. I also appreciate her continuous feedback and advice at various stages of the PhD. Her cordial co-operation, enthusiasm and keen interest had indeed helped me throughout this research work.

It is an indeed privilege to express a broad sense of gratitude towards Professor Anant Paradkar for his support and guidance from the starting of this journey to every stage of PhD. His patience, serenity and cheerful nature, strong support and wise advice and constant encouragement had indeed helped me to build up inner strength, uplift confidence required to accomplish the work. Besides this, he stood supportive guardian as well.

I would like to thank and express my gratitude to the Centre for Pharmaceutical Engineering Sciences, School of Pharmacy, and Centre for Skin Sciences. Also, the Analytical Centre and Institute of Cancer Therapeutics of Faculty of Life Sciences of the University of Bradford, for providing the necessary infrastructure and all the facilities required for carrying out this research work.I am also thankful to the entire technician and technical staff especially Dr Richard Telford, Dr Alexander Surtees, Stuart Fox and Andrew Healey who helps whenever needed.

I would like to appreciate the help from Paul Loadman from Institute of Cancer Therapeutics, University of Bradford to avail the HPLC facilities and his valuable suggestions during the initial studies. I am also very thankful and appreciates the help of Dr Michael Abraham, UCL, London in data analysis in the drug-PPB study without which this work would not be completed.

I would like to express my gratitude to Dr Sudhir, Dr Niten and Dr Venu Vangala for their help and significant valuable suggestions during the mid-end part of research work.

I am very thankful to Mrs Sue Baker, International student advisor for her help and immense support in non-academic issues. I would like to thank Anne Costigan, subject librarian for her help in various aspects of endnote programme.

I would like to thank Mrs Shamim for her help in administrative issues. I am also very thankful to Mr Toheed Raza for his constant help and support in Information Technology (IT) related queries and problems throughout studies. I would like to thank all Library staff for their help in reference books availability, providing printing facilities and laptop loan facilities during initial days and throughout the PhD.

I am sincerely thankful to Hub team, PGR administrative team and University finance team for helping me to solve financial issues and support during the critical economic conditions.

The special thanks go to all CPES colleagues, who helped throughout the research work. I got constant help, feedback and moral support from all of them every time and every situation. I would like to specially acknowledge help of Dr Sudhir, Dr Sachin, Dr Ujjwala, Dr.Ratnadeep, Dr Amit, Dr Clive, Dr Chaitrali, Dr Hrushikesh, Dr Prafulla, Dr Kartik, Dr Rohan, Dr Abdul, Dr Yousuf, Dr Suyog, Dr

Bhanvi, Dr Parineeta, Dr Mukesh,Dr Niten, Bashir, Aniket, Azad, Muthana, Fatima, Hanan and Asim.

I would like to express my sincere thanks to all my Teachers, colleagues, friends from my schools and colleges as well as staff members at workplaces. It includes Lupin ltd., Zytex Biotech pvt., ltd., and Dr.R.N.Cooper hospital workplaces. My respected teachers from primary school Vidya Mandir Apati, secondary school Panhala Vidya Mandir Panhala, Rajarshee Chhatrapati Shahu Maharaj Jr. college, Rajaram college, Kolhapur and Post graduation department of Microbiology of Yashwantrao Chavan College of Science, Karad for their support, help and continuous encouragement at every stage of life.

This work would not have been possible without immense support from my family members and relatives. Especially Pappa (father) Mr Ramchandra M.Kamble and Aai (mother) Mrs Savita R. Kamble, Uncle Bhaskar M. Kamble (Bapu), my beloved Aai (mother) Late Mrs Rekhatai, my grandparents late Mr M.S.Kamble (Aba) and Late Mrs S.M.Kamble (Aajji). Late Mr S.S.Kamble (Tatya), uncle Late Mr M.S.Kamble (Dada) and cousin brother late Mr M.M.Kamble (Appa). My beloved brothers and sisters, father-in-law, mother-in-law, brother-in-law and sister-in-law, dear villagers of Apati, friends from Global café Bradford, who encouraged me in every stage of life.I am also thankful for their blessings, constant encouragement and unconditional love and support.

I must acknowledge my lovely wife Mrs Snehal S. Kamble and my gorgeous daughter Miss Swarali S. Kamble, for their unconditional love and constant moral support without which I would not have finished this work.

Table of Contents

List of Figures

List of Tables

List of Abbreviations

Chapter 1 Introduction

The journey of a drug molecule passes through various stages from discovery to development and finally reaches the formulation. The preformulation studies are required for the development of formulations. These studies involve the thoughtful assessment of physicochemical, pharmacokinetic and pharmacodynamic properties of the selected drug molecule. It is helpful to meet the expected requirements for the drug design, development and delivery.

In the preformulation studies, the drug-plasma protein binding (drug-PPB) study also becomes the vital part. It is a necessity nowadays along with the studies of solubility, lipophilicity and ionic behaviour of the desired drug molecule before its formulation (Vuignier *et al.* 2010a). Additionally, the selection of the crystalline material of considerable stability and solubility is one of the crucial parts of the solid-state preformulation studies of an active pharmaceutical ingredient (API) (Jones *et al.* 2006).

Drug-PPB has an impact on the pharmacokinetic and pharmacodynamic activity of the drug molecule. This impact includes the disposition of drugs, their transportation and availability at the liver metabolism and excretion as well as the final drug concentration at the site of action. Because, once drug entered and distributed around the circulatory system, it binds to plasma proteins in varying degrees. In general, such binding is reversible and an equilibrium exists between bound and free molecular forms of the drug. In most cases, only the free drug molecules can cross membrane barriers, be distributed to tissues and then exert therapeutic effects (Lindup and Orme 1981; Vuignier et al. 2010a). Thus, it is necessary to study the drug-PPB before formulation. Ghafourian *et al.* have explained that this molecular binding is happening due to the hydrophobic and electrostatic interactions such as van der Waals and hydrogen

bonding (Ghafourian and Amin 2013). It was observed by Vuignier *et al.* that, the drug-PPB was studied in many ways, like Equilibrium Dialysis (ED), Ultra-Filtration (UF) and Ultra-Centrifugation (UC) methods (Vuignier *et al.* 2010a). However, those previous methods were time-consuming, non-robust and showed inconsistency in results when repeated. Recently, Ghafourian *et al.*in 2013, have shown a 'quantitative structure-activity relationship' based approach for drug-PPB in their studies (Ghafourian and Amin 2013). They observed PPB could be modelled using simple regression trees or multiple linear regressions with reasonable model accuracies. Thus, it could be helpful to identify the governing molecular factors for a high PPB. Valko *et al.* reported that there is involvement of ionic behaviour of molecules in drug-PPB. They used the fast gradient HPLC technique in their drug-PPB study (Valko *et al.* 2003). The current study also focuses on investigating such molecular interactions, and it is based on an approach of 'structural properties governing drug-PPB' using HPLC method and quantification of the ionic effects by using multiple linear regression (MLR) by Minitab 16 software and LFER method application.

Similarly, there is another area where such molecular interactions are involved and explored widely, is the area of supramolecular complexes. The best example is co-crystals. "Co-crystals are the crystalline materials made up of two or more different molecules. Specifically, drug molecules and the co-crystal former molecule known as coformer are held together in one single lattice, either by hydrogen bonds, halogen bonds or π-π interactions". Since last few decades, the term "co-crystals" was under debate. Recently, in August 2016 United States Food and Drug Administration (US-FDA) department accepted the co-crystal term as described above (FDA 2016).

The co-crystallisation technique has recently demonstrated increased interest and plays an important role in the field of solid-state drug dosage formulations. The co-crystallisation improves the physicochemical properties of the active pharmaceutical ingredient (API) (Jones *et al.* 2006). These properties include stability, solubility, hygroscopicity and compressibility which could improve through the co-crystallisation process. It suggests that the co-crystallisation process can be used to reduce the hygroscopicity of the reacting molecules. Therefore, the reacting molecules improve in-process stability and storage stability to tolerate the change of different relative humidity (RH) conditions.

The physical stability of the drug or its formulation depend on their hygroscopicity. If they are hygroscopic, they could interact with surrounded moisture and may dissociate. The structural integrity collapses and molecules stability is damaged. Therefore to avoid such contacts with moisture, these hygroscopic drug formulations are carried out in controlled environmental conditions. The final products are also packaged in an airtight, leakproof, moisture-proof packaging materials and are stored in a moisture controlled area. It increases the cost of manufacturing as well as storage.

However, through the process of cocrystallisation, such hygroscopic compounds may improve their physical stability and make them less or non-hygroscopic. It will be helpful for reducing the cost of manufacturing, packaging and storage.

1.1 Aims and Objectives

The main aim of this research was to identify the molecular interactions involved in the pharmaceuticals preformulation and the supramolecular complexes limited to the co-crystals area of studies. To investigate such interactions role in drug-plasma protein binding studies as well as in the co-crystal formation. To do

an investigation of the role of structural properties in the molecular interactions between the drug and plasma protein. To understand how to use these interactions data for dosage optimisation in the formulation and to avoid the toxic effect. To understand the competitors in binding and choose alternative generally recognised as safe (GRAS) molecule to avoid moisture uptake in solid-state formulation through co-crystal technique. To improve the storage stability of the hygroscopic molecules by making them less/ non-hygroscopic through co-crystal method.

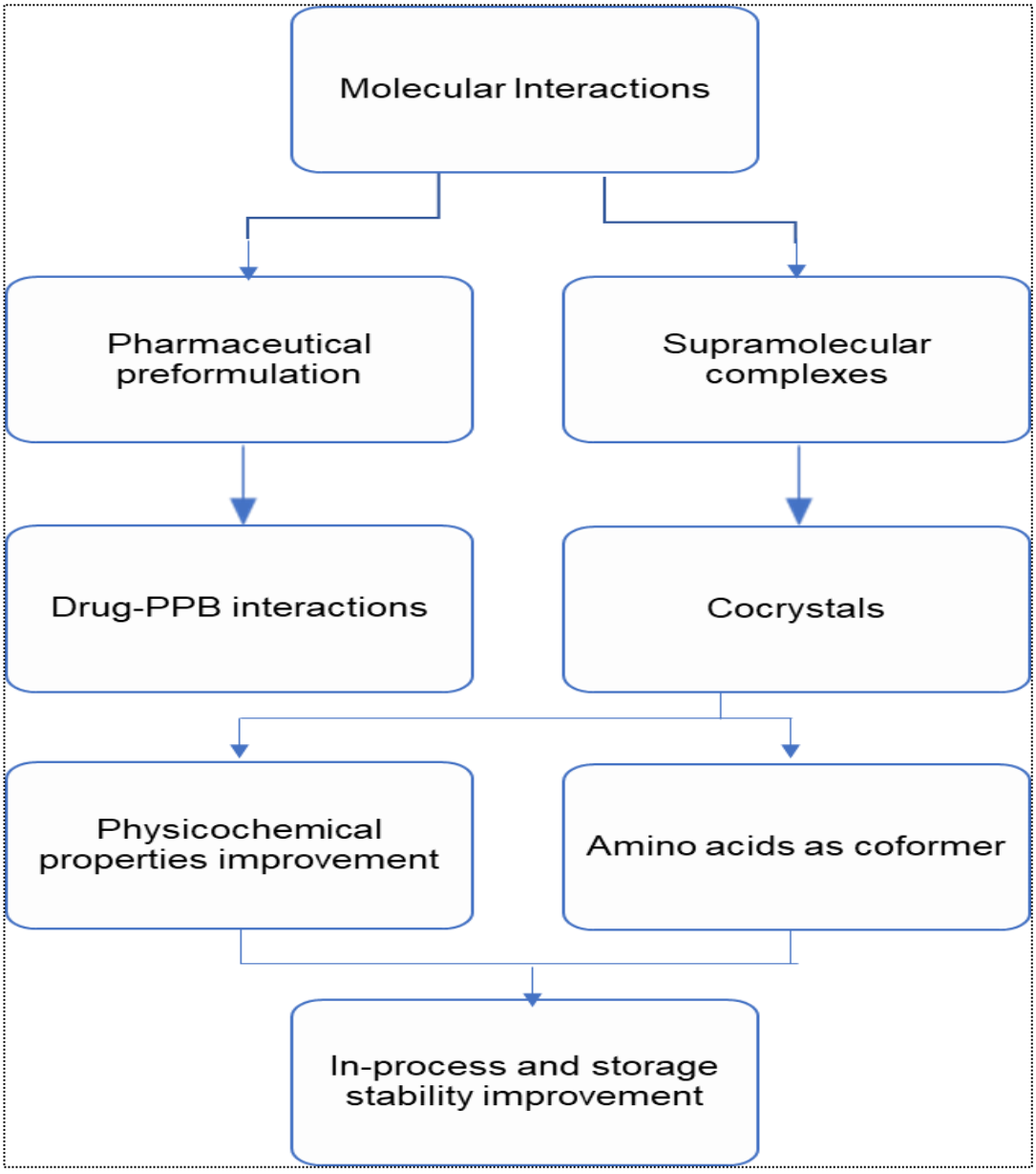

Figure 1.1 Research structure of the current work

Specific aims and objectives of this research work were:

1) To investigate drug-plasma protein interaction by using the high-performance liquid chromatography technique.
2) To identify structural properties which are important for drug-plasma protein binding using a broad range of structurally diverse compounds including drugs.
3) To develop computational models for predicting drug-plasma protein binding interaction based on these properties.
4) To develop the HPLC method for Drug- Human serum albumin/HSA and Drug-α-1-acid glycoprotein/AGP (plasma proteins) interaction studies and use of linear free energy relationship method for data analysis.
5) To check amino acids as a coformers and synthesis of co-crystals.
6) To improve the in-process and storage stability of hygroscopic compounds using the co-crystallisation method and its application.
7) To understand the molecular interaction of drug-plasma protein binding and supramolecular complexes such as co-crystals.

1.2 Thesis outline

The thesis outline is represented in Figure 1.2 and after that described in detail. Figure 1.2 indicates the outline of the thesis.

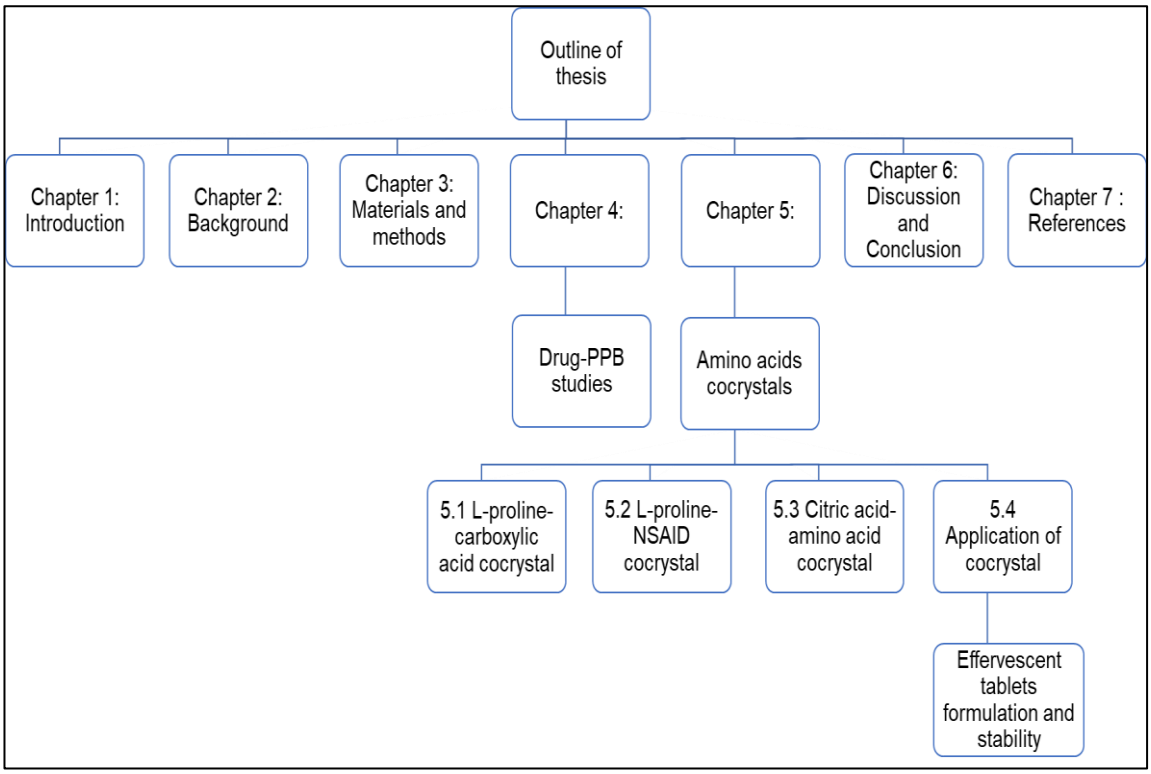

Figure 1.2 Outline of Thesis

Chapter 1 provides an introduction, aims and objectives and thesis outline.

Chapter 2 provides background and is divided into two major sections; firstly, the concept of a drug-plasma protein binding is presented, including its importance in the preformulation studies, molecular interactions bases and methods of drug-PPB studies. The second section describes the molecular interactions involved in the supramolecular complex limited to the co-crystal formation. The physicochemical properties improvement through the co-crystal process was carried out with the use of amino acids as coformers.

Chapter 3 describes details of the materials and methods adopted in the present research work and have been divided into two major sections; drug-PPB study and amino acids co-crystals.

Chapter 4 contains the results and discussion of the drug-plasma protein binding study. An important outcome of this study is first time quantification of the ionic behaviour of the drug and chemical compounds responsible for the

drug-PPB. Therefore, it will be helpful for the drug dosage optimisation in the formulations.

Chapter 5 includes information of cocrystallisation, amino acids as coformer. It covers four sub-chapters as L-proline-carboxylic acids cocrystals, L-proline-NSAID cocrystals, citric acid-amino acids cocrystals and application of cocrystals.

Chapter 5.1 explains how the L-proline amino acid and carboxylic acid co-crystals formed and how they are helping to reduce the hygroscopicity of the L-proline. One new co-crystal form obtained through this research work along with the two already known co-crystals of L-proline and carboxylic acids.

Chapter 5.2 showed the L-proline and non-steroidal anti-inflammatory drugs co-crystals formation. As per the report of Tilborg *et al.*, this was only the confirmation to find out their ability to form co-crystals with L-proline.

Chapter 5.3 describes the co-crystal formation of amino acids with the pharmaceutically important compound - citric acid. Through this research work, five-cocrystals were obtained. One single crystal was obtained successfully amongst the five cocrystals of amino acids with citric acid. The obtained single crystal was 1:1 L-cysteine-citric acid cocrystal hydrate. It adopts one H_2O molecule in their crystal lattice.

Chapter 5.4 gives information about the application of the obtained co-crystal in effervescent tablet formulation. It had successfully shown the improvements in physical stability in various relative humidity conditions over 28 days of studies.

Chapter 6 provides overall summary (global discussion) and conclusions of the work presented in this thesis followed by the scope of future work.

Chapter 7 contains references to published work cited within the thesis.

Chapter 2 Background

This chapter includes the literature survey for the drug-plasma protein binding studies and the co-crystals. It also gives in-detail information about the techniques and methodology used in these studies and current study focus.

2.1 Drug-plasma protein binding study

The drug-PPB is an important process that determines the activity and pharmacokinetics of many drugs in the body. After distributing with the circulatory system, the drug is bind to plasma proteins in varying degrees. In general, such binding is reversible, and equilibrium exists between bound and free molecular forms. In most cases, only the free drug molecules can cross membrane barriers, distribute to tissues and then exert therapeutic effects (Lindup and Orme 1981; Vuignier *et al.* 2010a). Figure 2.1 gives us a general idea regarding the drug distribution and the process of protein binding (Vuignier *et al.* 2010a).

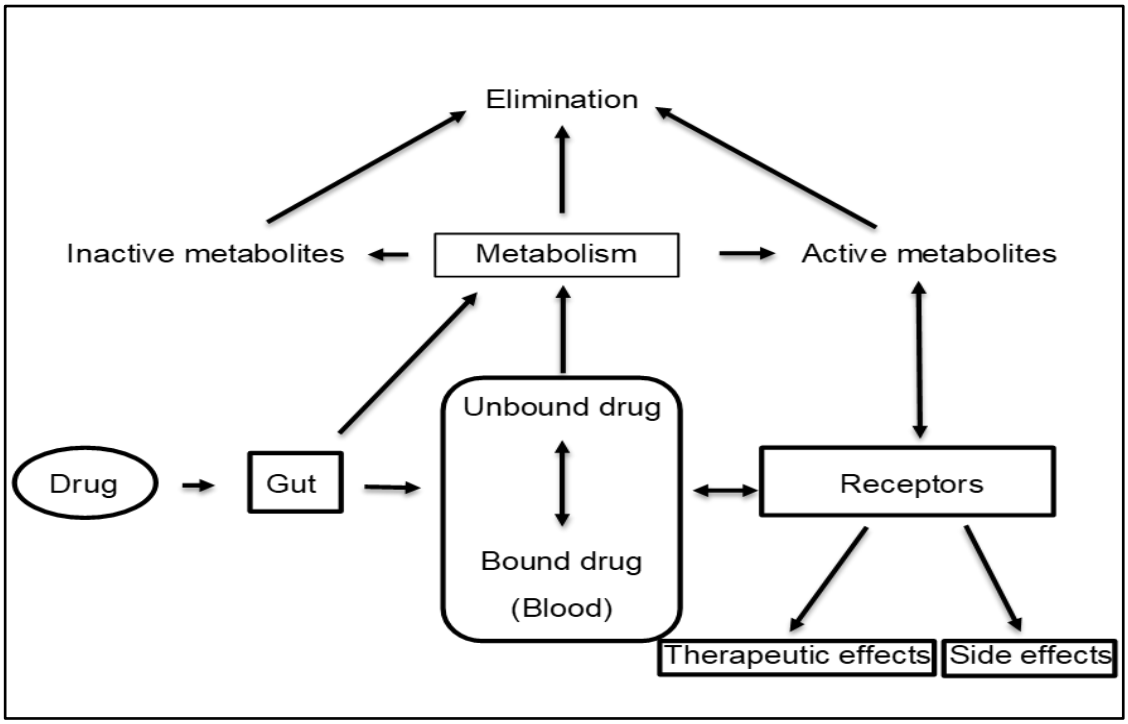

Figure 2.1 Drug distribution and binding with protein (Vuignier *et al.* 2010a).

Drug-plasma protein binding acts as a reservoir for free drug concentration and prolongs the duration of drug action. Therefore drug-plasma protein binding is considered as an important property and needs to be characterised in the early stage of drug discovery (Wan and Holmen 2009).

In plasma, two major proteins, Human Serum Albumin known as HSA and α1-Acid Glycoprotein described as AGP are present in relatively high quantities. They can bind a variety of drugs with much affinity (Trainor 2007).

2.1.1 Human serum albumin

The 66–kDa, globular protein HSA is made up of 585 amino acids. It measures merely about 4.5% of the weight of human blood and exists as a major component of plasma protein. It is present at a relatively constant concentration of ~600μM in the plasma of healthy individuals. HSA tends to bind with endogenous ligands (e.g. metal ions and fatty acids) as well as drugs. Though there are multiple drugs–binding sites on HSA, Trainor observed that two are predominant amongst them and these have a slight inclination for binding to neutral and acidic drugs (Trainor 2007). Figure 2.2 shows three–dimensional structure of HSA (left side image) and locations of sites I and II (right side image), which were discovered by Sudlow, hence called Sudlow site I and II also (Sudlow *et al.* 1975; Wa *et al.* 2006).

2.1.1.1 The binding sites of HSA

The structural information about the low affinity as well as high-affinity binding sites is useful in the designing of new drug molecules. The understanding of structural information helps the researchers to decide whether to avoid the binding of the drug to HSA or modify the drug to achieve desired activity considering the extent of binding (Hein *et al.* 2010). Therefore, Yang *et al.* said

that the studies of drug binding sites on HSA are still essential since past (Yang et al. 2014). Sudlow *et al.* have done revolutionary studies in this field during 1975–76, in which they used a fluorescent probe displacement method to discover binding sites (Sudlow *et al.* 1975; Sudlow *et al.* 1976).

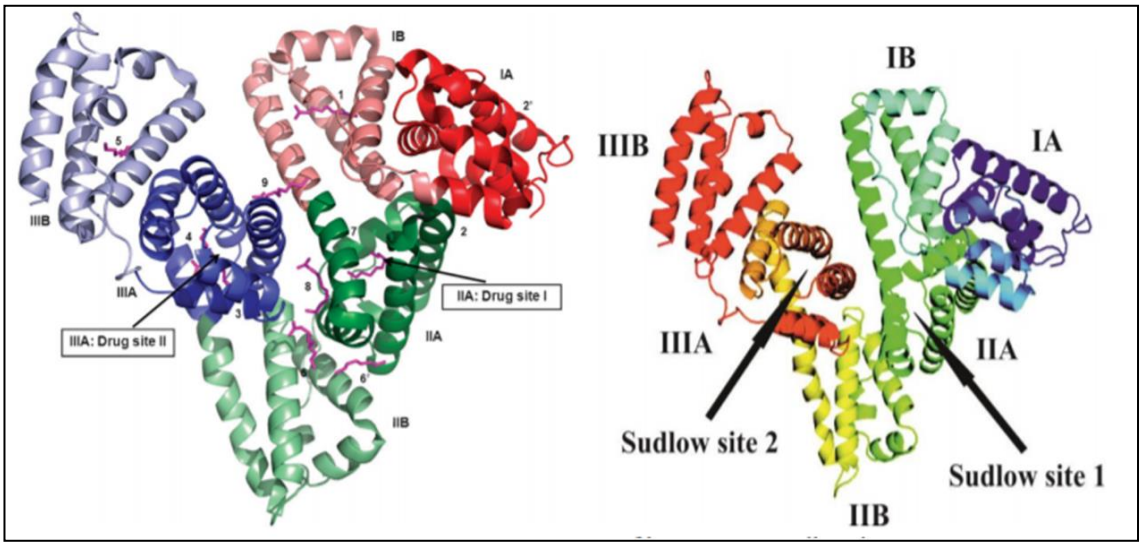

Figure 2.2 Three–dimensional structure of HSA (left) and the known locations of Sudlow site I and II (Sudlow *et al*. 1975; Reilly *et al*.).

After careful observation, two unique binding sites on the HSA were discovered by Sudlow *et al.* in 1975. These are called as the site I (sometimes also described as warfarin binding site or henceforth as Sudlow site I) and site II (sometimes referred to the benzodiazepine binding site or Sudlow site II) as mentioned in Figure 2.2.

2.1.2 Alpha (α) –1 – acid glycoprotein (AGP)

The AGP is heavily glycosylated; an acidic, 38–kDa to 48–kDa protein. It includes a single amino acid chain of 204 residues. Its concentration in plasma varies from 0.55 to 1.4mg/ml, corresponding to ~2–31µM. AGP is a protein which synthesises in the liver in an acute phase, and thus, it can elevate in certain disease states as high as up to 3mg/ml in concentration, i.e. about 60µM (Kremer *et al.* 1988). AGP shows a preference for binding to basic drugs. There

are multiple drugs–binding sites described in AGP, but one site is to be most important which particularly binds to basic drugs (Kaliszan *et al*. 1995). Figure 2.3 shows crystal structure of AGP.

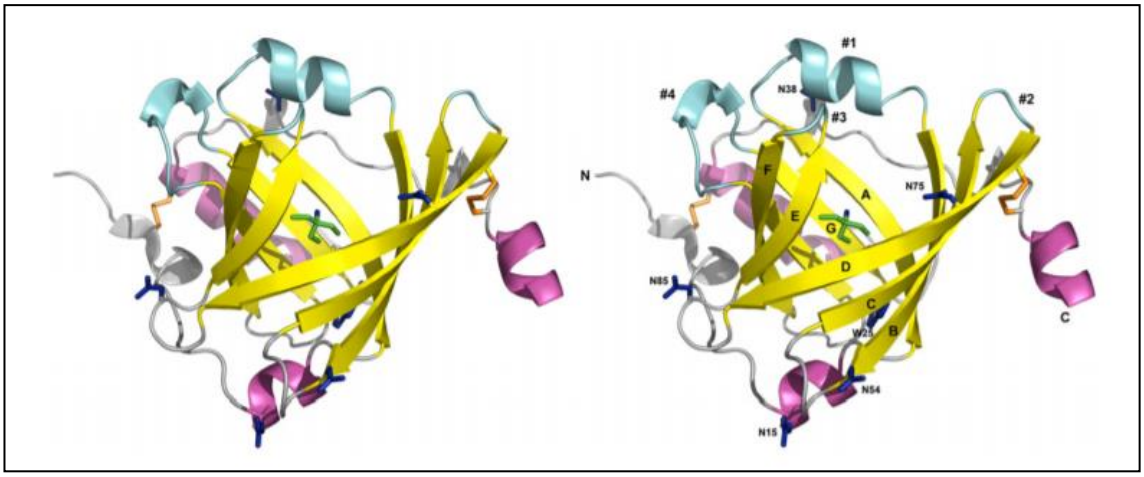

Figure 2.3 The refined crystal structure of human AGP at 1.8 Å resolutions shown as a ribbon cartoon in stereo view (Schonfeld *et al.* 2008).

It was observed that immunoglobulins and lipoproteins also might be involved in binding, but they have a lesser effect (Singh and Mehta 2006; Trainor 2007; Howard *et al.* 2010; Vuignier *et al.* 2010b).

2.1.3 Techniques in plasma proteins binding (PPB) studies

Numbers of techniques have been established for the quantitative determination of drug–PPB interactions *in vitro*. In these, Equilibrium Dialysis, Ultra–Filtration, and Ultra–Centrifugation have been used most commonly and conventionally (Vuignier *et al.* 2010a), along with Capillary electrophoresis (CE), Surface–Plasmon Resonance (SPR)-based assays (Sprunger *et al.*), and Liquid Chromatography/LC.

2.1.3.1 Equilibrium dialysis

Equilibrium dialysis (ED) is based on the difference between the size and weight of the drug molecules. A standard ED experiment involves two partitions which are divided by a semi-permeable membrane. This membrane performs

as a molecular strainer, to permit only those molecules less than a specific molecular size and weight to permeate through it. Preferably the selected membrane is flawlessly permeable to the drugs, due to its low molecular size and weight and resistant to the drug-protein complex, as well as the protein due to their higher molecular size or weight.

In ED, the protein is retained one side of the semi-permeable membrane and on the other side is present the drug molecule which is to be tested. Afterwards, within a precisely defined time span, equilibrium exists, and the unbound drug percentage is available, for the measurement from the second section. This method was in use for many years for the drug–PPB interaction studies. Additionally, this has executed in solutions of drug molecule and protein, which helps to establish a right equilibrium, throughout the full experiment. As a result, ED is recognised as the reference method (Vuignier *et al.* 2010a).

The drawbacks of ED include:

a) It takes a long time to establish equilibrium (around 12–48 hours).
b) It necessitates a preliminary set of studies, such as the measurement of the necessary time required to establish the equilibrium.
c) The volume shift linked with the form of osmotic pressure exerted by proteins.
d) Another possible problematic situation associated with ED is unstable volume which happens because of the semipermeable membrane and the presence of proteins. This changed volume can range from +10 to +30%.
e) The Donnan effect, which is the general attachment of proteins or drugs to the walls of the cell and the dialysis membrane, is another problem in ED.

f) The reduced aqueous solubility of the drug molecules is also the major problem and restraining factor for the use of equilibrium dialysis technique (Vuignier *et al.* 2010a).

2.1.3.2 Ultrafiltration

The ultrafiltration (UF) technique was recognised as a speedy substitute to ED. Its analysis speed had increased by pressure to increase the potency of the mixture of drug-protein solution to pass through the membrane. UF helps to reduce the process and analysis time by obtaining results more quickly. This will allow to pass the unbounded protein through membrane in less time than the ED. However, as in ED, the Donnan effect including protein escape (due to applied pressure, small size protein could be pass through the membrane) creates problems for the use of UF also (Vuignier *et al.* 2010a).

2.1.3.3 Ultracentrifugation

Ultracentrifugation (UC) is another technique related to ED and UF but more advanced. In this procedure, a mixture of drug and protein solutions is placed into a centrifugation chamber. Then centrifugation is carried out until the entire protein as well as the drug-protein complex is deposited at the bottom of the tube. As compared with the protein, the drug sedimentation coefficient is smaller; hence, the free drug molecule left over in the supernatant which can easily be calculated from it. UC becomes advanced in nullifying the complications related to the effects of the membrane, i.e. membrane absorption and as well as the Donnan effect.

However, the equipment costs are higher than that of ED and UF. Additionally, with different types of drugs, comparative studies exposed that, there is measurable difference arose amongst the results obtained by ED and UC. Because the unbound drug quantity assessment can be exaggerated with

physical phenomena, such as sedimentation, back dispersion, and viscidness (Sebille *et al.* 1990; Vuignier *et al.* 2010a).

Furthermore, these methods are shows some limitations such as very low throughput and poor reproducibility (Oravcova *et al.* 1996). Therefore, in comparison to these conventional methods, the HPLC method that employs stationary phases immobilised with plasma proteins observed an interesting approach because of the speed, simplicity and specificity of analysis and automation capability (Valko *et al.* 2003; Vuignier *et al.* 2013).

In the liquid chromatography techniques, it is characteristically promising to carry out carefully controlled measurements and to help in achieving reproducibility in data generation. The development in the discovery of new methods and evaluating or modernise the established methodologies by inspired endeavours is the result of the increased number of compounds expected to be checked for PPB data (Trainor 2007).

2.1.3.4 Chromatographic techniques

2.1.3.4.1 Liquid chromatography or LC

Liquid chromatographic techniques have been used to evaluate drug–PPB interactions. LC is a technique which used for a mixture to separate into its parts. A chromatography technique was firstly discovered by a Russian botanist Mikhail Tswett in the late 1890s for his work on chlorophyll by using a column of calcium carbonate (Scott 1995). However, it has been modified in various ways by different researchers over a period as per their requirement. LC is further divided into size–exclusion chromatography in short SEC and affinity chromatography (AC).

2.1.3.4.2 Size–exclusion chromatography or SEC

In the SEC technique, the molecules are separated based on their size or their hydrodynamic volume capacity. A combination of the drug and the protein pass out through the column which is made up of porous material. This material has a pore size such that, it will only permit the unbound free drugs molecules to enter it. However, the drug-protein complex will not be able to enter and hence elute first. Thus, it is also called gel permeation chromatography or gel filtration chromatography. Proteins and drugs are both used free in a solution in SEC. However, it was observed that, for drug-protein analysis, this SEC method not suitable due to poor column efficiency and low protein yield. Therefore, nowadays it is rarely used. Recent columns are more robust but, have a short lifetime.

Along with the techniques mentioned above, there are other procedures which have also been applied to study drug-protein interaction. These techniques include X-ray crystallography, fluorescence spectroscopy, absorption spectroscopy, surface–plasmon resonance and Nuclear Magnetic Resonance (NMR) spectroscopy. However, the technique which has gained enormous popularity in this field is high–performance affinity chromatography (Sebille *et al.* 1990; Singh and Mehta 2006; Kim and Wainer 2008; Hage *et al.* 2009; Vuignier *et al.* 2010a).

2.1.3.4.3 High–performance affinity chromatography (HPAC)

High–performance affinity chromatography (HPAC) based on the technique in which the protein has immobilised on support like silica inside the column. The injection of the interacting solute (in this case the drug) in a large–plug (i.e. frontal analysis-FA) or small–plug (i.e. zonal elution-ZE) is used to check the pattern of drug-protein interaction. High attraction drugs will interact with the

immobilised protein and delayed elution, as compared to the drug that has less or no affinity towards the protein (Vuignier *et al.* 2010a). This HPAC can use only a small amount of protein for many studies is the main advantage, which made this method valuable. Additionally, same preparation of protein can be used for multiple experiments which can reduce the variations from run-to-run. Furthermore, other notable impacts of HPAC are its simplicity of automation and capacity to study the behaviour of chiral drug's enantiomers (Vuignier *et al.* 2010a). The newly developed chiral HSA columns have a stationary phase which has based on immobilised HSA protein.

It has been widely described as an instrument to evaluate drug–PPB connections when used in an isocratic chromatographic method (Singh and Mehta 2006). In this method, drugs with high affinities interact strongly with the immobilised protein and are eluted later than drugs with no or fewer affinities. The affinity is expressed by the retention factor k, which is calculated through Eq. 1

$$k = \frac{(t_R - t_0)}{t_0} \quad \text{..... Eq.1}$$

In this Eq.1, t_R and t_0 are the retention times of the solute and an unretained compound respectively.

In this current study, the data obtained from the HPLC experiments have been analysed with the help of Abraham's LFER method of partitioning solutes determination. The interaction between these drugs and immobilised plasma proteins (HSA and AGP) was measured using the HPLC method. In order to establish quantitative structure-drug-plasma protein binding relationships and to unravel the structural parameters governing the interaction mechanisms, which are very important in drug design, a LFER model was used (Abraham and Acree 2010a; Abraham and Acree 2010c; Abraham 2011).

2.1.4 Linear free energy relationship (LFER)

The partitioning of solutes ruled by structural determinants in chromatography systems and could be explained by the analytical method developed by Abraham *et al.* This method is known as, "Linear Free Energy Relationship (LFER)" (Abraham and Martins 2004; Zhang et al. 2011). It was used in this study to analyse the data obtained from HPLC experiments. This LFER will be helpful for comparison between diverse separating systems including *in vivo* and *in-vitro* ones. Also, it can serve to distinguish the partitioning of solutes governed by structural determinants in these systems (Abraham *et al.* 2004; Abraham and Zhao 2005; Sprunger *et al.* 2007). They developed an equation for it. See Eq.2 below:

$$SP = c + eE + sS + aA + bB + vV \quad \text{.....Eq.2}$$

Where *E*, *S*, *A*, *B*, and *V* represents solute descriptors. *E* means the excess molar refraction in ($cm^3\ mol^{-1}$)/10, *S* stands for solute dipolarity / polarisability, *A* and *B* represent overall solute–hydrogen bond acidity and hydrogen bond basicity respectively, and *V* is representing the McGowan characteristic volume of the solute in ($cm^3\ mol^{-1}$)/100. SP stands for a set of solute properties in each system, for example, SP may be the skin permeability log K_p, or maybe the retention factor log *k* as in our HSA–HPLC and AGP- HPLC study, for some solutes.

The detailed information about the descriptors is as below.

2.1.4.1 Solute property (SP)

Solute Property is the property related to some free energy, such as distribution constant, retention factor, specific retention volume, relative adjusted retention time or retention index value (Poole 2003).

In this study, SP stands for the retention factor, i.e. log *k*. This log *k* value of a solute is linearly related to its partition coefficient between the two phases. For example, water - octanol phase.

2.1.4.2 Excess molar refraction (E)

Excess molar refraction is also closely related to the solute size used in the same correlation equation. E calculated from the refractive index of the solute at 20°C.Excess molar refraction is straight forward for liquids as well as for solids. Refractive index values are easily estimated using available software for molecular property estimations. Also, *E* like the molar refraction is almost an additive quantity and values for solids. It can estimate through the addition of fragments with known *E* values (Poole 2003).

Calculation of Excess molar refraction can be done from the refractive index of the solute, at 20°C for the sodium D- line, η, as per following equation Eq 3.

$$E = 10V\left[\frac{\eta^2-1}{\eta^2+2}\right] - 2.832\,V + 0.526 \ldots\ldots\ldots\ldots\ldots\ldots\ldots\ldots\ldots\text{Eq.3.}$$

In this Eq.3, '*V'* means McGowan's characteristic volume.

The units used for *V* are $cm^3.mol^{-1}/100$ as per Eq.3, and therefore, *E* is writing in $cm^3.mol^{-1}/10$.

For example, calculation of excess molar refraction '*E'*, for toluene, has carried out by using equation mentioned above as Eq.3. The refractive index (η) for toluene at 20°C (sodium D – line) = 1.496 and '*V* 'for toluene is 0.857 in $cm^3.mol^{-1}/100$.

E = 10 x 0.857 $[(1.496)^2$- 1) / $(1.496)^2$+2)] – 2.832 x 0.857 + 0.526 = 0.601 in $cm^3.mol^{-1}/10$.

2.1.4.3 Dipolarity/polarisability (S)

'S' is the descriptor for the dipolarity/polarisability of solute. It would be useful to have descriptors, related to the propensity of a solute to engage in dipole-dipole

and induced dipole-dipole interactions (Poole). In the event it was impossible to separate out descriptors for the two types of interactions but, Abraham *et al.* constructed a solute descriptor for dipolarity/polarisability *S*, combining the two interactions. The dipolarity/polarisability descriptor was initially determined through gas chromatographic measurements on polar stationary phases but it is now more commonly determined in combination with the hydrogen-bonding solute descriptors from liquid-liquid distribution constants and chromatographic measurements by using Abraham's descriptor and LFER method (Poole 2003).

2.1.4.4 Hydrogen bond acidity (A) and hydrogen bond basicity (B)

During the development of solvation parameter model, Abraham *et al.* commenced the process by defining descriptors for solute hydrogen bond acidity (α_2^{H}) or A as well as solute hydrogen bond basicity (β_2^{H}) or B (Poole 2003).

The solute structure has influences on the distribution process due to a consequence of hydrogen bonding of the solute to any surrounding solvent molecules, not just to one. Therefore the scales of "summation" or "overall" hydrogen bonding is needed, that refers to the tendency of interaction with a large excess of solvent molecules by a solute molecule (Poole). These hydrogen bond descriptors denoted as $\sum\alpha_2^{\mathrm{H}}$ alternatively, $\sum A$ and $\sum\beta_2^{\mathrm{H}}$ alternatively, $\sum B$ to distinguish them from the 1:1 descriptors. New values of the effective hydrogen bonding solute descriptors now determined in conjunction with other solute descriptors using liquid-liquid distribution and chromatographic measurements. There is a small complexity that few solutes (sulfoxides, anilines, pyridines) show variable hydrogen bond basicity in distribution systems where the organic phase absorbs an appreciable amount of water. A new solute descriptor $\sum\beta_2^0$ alternatively, B^0 was defined for these solutes and should be

used in octanol-water distribution systems, for example, reversed-phase and micellar electrokinetic chromatography. For the same solutes $\sum\beta_2^H$ alternatively, $\sum B$ should be used for all other applications and always for gas chromatography. Except for the solutes types indicated above, the two hydrogen bond basicity scales are identical. It should also note that the scales of hydrogen bond acidity and basicity are non-related to the expression of pKa based proton transfer acidity and basicity (Poole 2003).

2.1.4.5 McGowan's characteristic volume (V)

The McGowan's characteristic volume, 'V' is in units of $cm^3.mol^{-1}/100$, It can calculate for any molecule whose structure is known by simple summation rules. Each atom has a defined characteristic volume, and the molecular volume is the sum of all atomic volumes less than 6.56 $cm^3.mol^{-1}$ for each bond, no matter whether single, double or triple (Poole 2003).

This can be calculated as follows: -

Calculation of McGowan's characteristic volume (*V*), for toluene

Atomic volumes: (atomic volumes = atomic weight/density of that element)

C=16.35, H=8.71, N=14.39, O=12.43, F=10.48, Si=26.83, P=24.87, S=22.91, Cl=20.95, B=18.23, Br=26.21, I=34.53 (Poole).

Subtract 6.56 for each bond of any type.

$$V = [Sum\ of\ all\ atomic\ volumes - 6.56(Number\ of\ bonds)] \quad \text{.....Eq.4.}$$

Toluene = 7 carbon atoms + 8 hydrogen atoms – 15 bonds = 114.45+69.68-98.40=85.73 in $cm^3.mol^{-1}$. After scaling V = 0.857 in $cm^3.mol^{-1}/100$.

Eq.2 had tried efficiently in wide-ranging systems, which includes a various number of partitions from water to organic solvent (Abraham 2003; Abraham and Acree 2005; Abraham and Zhao 2005). Also various artificial membrane system models (Gil-Agusti *et al.* 2006; Sprunger *et al.* 2007; Wang *et al.* 2009)

and biological processes (Zhao *et al.* 2001; Zhao *et al.* 2003; Abraham and Martins 2004).In Eq.2, (c, e, s, a, b and v) or coefficients are obtained by multiple linear regression (MLR) analysis and used to characterise the given system.

However, Eq.2 was set up only for neutral solutes (Zhao *et al.* 2001; Abraham 2003; Zhao *et al.* 2003; Abraham and Martins 2004; Abraham and Acree 2005; Abraham and Zhao 2005; Gil-Agusti *et al.* 2006; Sprunger *et al.* 2007). Therefore, in the sense of use in ionic species extended by Abraham and Acree (Abraham and Acree 2010b; Abraham and Acree 2010a; Abraham and Acree 2010c; Abraham and Acree 2010d) and developed Eq.5. This equation 5 includes the same five descriptors of equation 2, but also an addition to a new descriptor for cations, J^+ as well as for anions, J^-.

$$SP = c + eE + sS + aA + bB + vV + j^+J^+ + j^-J^-$$ .....Eq.5.

In this, J^+ = 0 for anions and J^-=0 for cations, whereas both J^+ and J^- = 0 for neutral compounds. In another word, Eq.5 reverts Eq.2, when Eq.5 is only assembled for neutral species (Zhang et al. 2011). Sometimes, in certain particular systems, in the case of some solutes revised hydrogen bond basicity, B^0, has to be used in its place of *B* (Abraham 1993). The examples of these solutes are aniline, toluidine, pyridine, alkyl pyridines and sulfoxides, excluding sulfones, and the systems which are of ever two-phase systems where water is in contact with an organic phase which itself contains a considerable amount of water. Examples of such systems include water–wet octanol and water–wet ether (Abraham *et al.* 2013).

The obtained results of this study of drug-PPB have been explained in chapter 4

2.2 Molecular interactions in supramolecular complexes of co-crystals

The molecular interactions have been explored widely in the field of supramolecular complexes. The best example is that of co-crystals.

The co-crystals were synthesised and explored for their ability to improve the physicochemical properties of the drug molecules (Jones *et al.* 2006). During improvement of physicochemical properties, various molecular interactions happened in between the drug or APIs molecules and the coformer molecules.

2.2.1 General background of co-crystals

The solid-state properties of drugs including crystal polymorphism, solvate or hydrate formation, salt formation, particle size and manufacturing ability may have an impact on two important properties. These properties are solubility and stability. These two properties play an essential role in the successful drug development.These improved properties make the drug suitable for oral administration (Buxton 2017).

The orally administered drugs have covered three-quarters of the total drug market (Bergström 2005). In general, oral ingestion is the most convenient and accessible route of drug delivery. The oral route is conventional because of its ease of administration, high patient obedience, affordable, minimum sterility restraints and elasticity in the strategy of the dosage form (Savjani *et al.* 2012). Still, the unpredictability about the absorption, disposition, metabolism, excretion and toxicity (ADMET) (Van De Waterbeemd and Gifford 2003) properties remains the main issues for the cessation of clinical testing of the many desired drug candidate molecules (Kennedy 1997; Borchardt *et al.* 2005).

The drug is required to be in solution to be absorbed as well as permeated with ease through the intestinal membrane. The aqueous solubility (Savjani *et al.*

2012) and intestinal permeability (Artursson and Karlsson 1991) are the two most important factors influencing drug absorption (Bergström 2005). Studies on drug absorption from the gastrointestinal tract are therefore of reflective importance in the discovery and development of new drugs (Stenberg *et al.* 2001; Van De Waterbeemd and Gifford 2003).

Based on the solubility and permeability properties of the drugs, they are classified into four categories and known as Biopharmaceutics Classification System (BCS) See Table 2.1

Table 2.1 Biopharmaceutics Classification System (BCS) (Amidon *et al*. 1995).

BCS Class	Solubility	Permeability
I	High (85-90% in 15-30 minutes)	High (85-90% in 15-30 minutes)
II	Low (at least 85% up to extended time)	High (85% in 15 minutes)
III	High (85% in 15-30 minutes)	Low (extended period of time)
IV	Low (variable)	Low (variable)

This Biopharmaceutics Classification System (BCS) developed by Amidon and co-workers in 1995 to reduce the need for *in vivo* bioequivalency studies and also adopted by the United States Food and Drugs Administration (USFDA)(FDA) department. The BCS is a scientific framework for classifying a drug substance based on its aqueous solubility and intestinal permeability (Amidon *et al.* 1995). "*A highly soluble drug is defined as a drug where the highest marketed dose (highest dose strength) is soluble in 250 ml of aqueous media in over the entire gastrointestinal pH range (1.2–7.4), a conservative definition (Shah and Amidon 2014)*". The Scientists are still focusing on improving the solubility properties of BCS class II drugs in order to bring them

into the main development process. In this field, co-crystals have shown some promising results. One must consider the impact of the solid-state properties of drugs on solubility, hygroscopicity, stability and manufacturability (Shevchenko *et al.* 2012).

It was observed that most marketed pharmaceuticals contain molecular crystals due to their physical stability. The molecular arrangement in a crystal governs its physical properties and, in some instances, its chemical properties. Therefore, they dramatically influence the processing as well as solid-state drugs formulations. They also act as essential drug properties such as stability and rate of dissolution. In-depth knowledge about the relationship between physical structures and the physicochemical properties of pharmaceutical solids is essential for selecting the most suitable form of API for the development of a drug product (Datta and Grant 2004).

During drug development, it was observed that the modifications in the active pharmaceutical ingredients are limited up to the polymorphs, salts and hydrates or solvates. According to literature almost half of the drugs have been delivered in the form of salts (Wermuth *et al.* 2002).

Salt formation involves one acid or basic molecule and requires an API with at least one ionisable centre (Yadav *et al.* 2015). Thus, neutral APIs are not suitable for salt formation. Moreover, most of the salt forms of the API are hygroscopic and have shown a tendency to absorb atmospheric moisture and exhibit stability problems. In contrast, co-crystals can be formed with ionisable or neutral APIs and have shown better stability than salts forms (Aitipamula *et al.* 2012a).

2.2.2 Co-crystals

Over the last few decades a new term, “Co-crystals” has emerged as a new type of modification technique to tailor the physicochemical properties of the crystalline API (Jones *et al.* 2006; Thakuria *et al.* 2013). It was defined and accepted by the FDA in August 2016. The definition is mentioned already in Chapter 1 under section ‘1.0 Introduction, in paragraph 4’. Figure 2.4 represents the general scheme of the co-crystals formation.

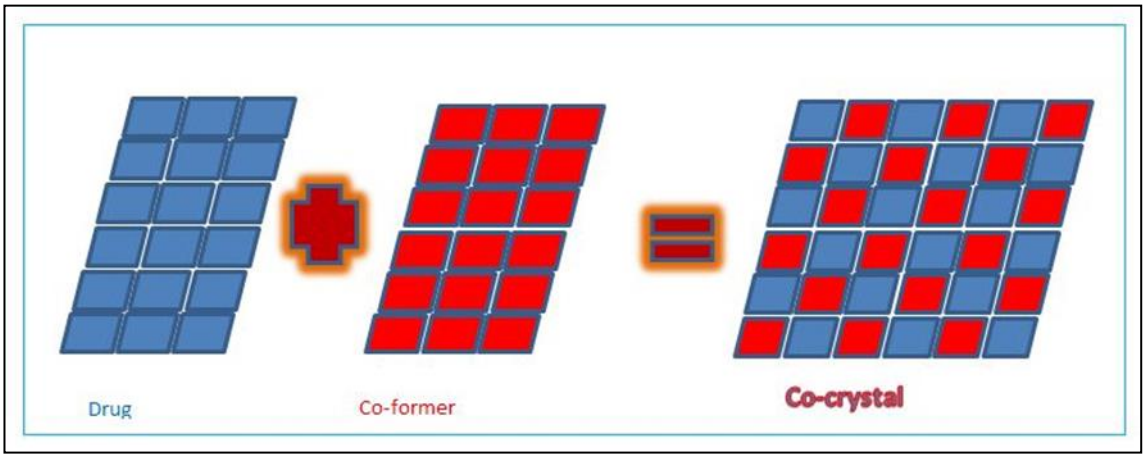

Figure 2.4 Representation of co-crystallisation

Pharmaceutical co-crystals have opened vast opportunities for the engineering of solid state dosage forms beyond the conventional solid-state forms of an API, such as salts and polymorphs. As US-FDA says, co-crystals can be tailored to enhance the drug product bioavailability and stability to enhance processability of APIs during drug product manufacture. Co-crystals capabilities lead to another advantage of co-crystal as they generate a diverse array of solid state forms for APIs that lack ionisable functional group, which is a prerequisite for salt formation (FDA 2016).The co-crystal technology opened the fascinating formulation strategy of creating crystal forms with acceptable stability and improved physicochemical properties. Co-crystals offer new opportunities for intellectual properties (Trask and Day 2007) or may be extending the life of

current patented or patentable formulations resulting in an increasing number of research groups attracted towards co-crystal synthesis and their applications into the pharmaceutical formulations. It is well known that co-crystals have stability and advantages in synthesis over the hydrate, solvate (Vishweshwar et al. 2006) and salt (Schultheiss and Newman 2009).

2.2.3 Coformer

In the process of co-crystallisation, coformer might be a stabilising excipient or a second active drug molecule (Jones *et al.* 2006). These are the inert molecules which will adhere to the drug molecule by hydrogen bonding, halogen bond or π-π interactions and not by a covalent bond. These molecules are recognised as safe (Bolla and Nangia) and not interact with drug molecule. For example, few carboxylic acids like adipic acid, glutaric acid (McNamara *et al.* 2006; Losev *et al.* 2011; Zakharov *et al.* 2012; Zakharov *et al.* 2013). Also, fumaric acid, succinic acid (Jones *et al.*), malic acid (Shete *et al.*), malonic acid (Aitipamula *et al.* 2010), and citric acid. Some of the compounds like saccharin (Shan and Zaworotko) and caffeine (Ghosh et al. 1991; Trask et al. 2005a; Trask et al. 2005b; Guo et al. 2009; Aher et al. 2010; Aitipamula et al. 2012b; Pagire et al. 2013a; Apshingekar et al. 2016b) are used as co-crystals coformer. The nicotinamide (Bhogala *et al.* 2005; Sheikh *et al.* 2009; Kelly *et al.* 2012; Soares and Carneiro 2013; Patil *et al.* 2014; Soares and Carneiro 2014) is also used as co-crystals coformer. However, there are some limitations to the use of these chemicals repeatedly in high concentration. It can adversely affect human beings as high amount become toxic to health. Every drug and excipient has certain recommended daily dosage allowance (RDA) decided by the food and drug administration department of USA (US-FDA) (FDA 2000) and world health organisation (WHO) to avoid their lethal effects.

2.2.4 Amino acids as coformers

In the current study, amino acids were considered as a CCF. In fact, amino acids are more favourable coformers as they are neutral molecules, safe and natural to human beings. They are safer as compared to the other chemical compounds already in use as a CCF. Some of the amino acids possess the ability to be in zwitterionic state at physiological condition around pH 7.0-7.4 (Tilborg *et al.* 2014). This zwitterionic forms bearing capacity of amino acids is more promising for the bonding as well as tailoring the physicochemical properties of the drug molecule. These amino acids are an excellent source of hydrogen bond donor and hydrogen bond acceptor which can be helpful in bonding and synthons formation. It has binary pKa values as well. Therefore, there are more possibilities of hydrogen bonding and cocrystal formation. Please see the Table 2.2.Thus, the co-crystals of amino acids were prepared by using the liquid assisted grinding method.

Table 2.2 Amino acids - names, structures, physicochemical properties and reported co-crystals

Sr. No.	Name of Amino Acid / non-polar, aliphatic residues	3 letter codes	Single letter code	Structure	Co-former/ Reported cocrystals	pKa		Isoelectric point (pI)	Potential H-bonds	Hygroscopicity / Hydropathy index / Hydropathy	Acidic/ Basic	Solubility (g/100g water)	Molecular weight (Da)	Melting point °C
						pK_1 (α-COOH)	pK_2 (α-$^+NH^3$)							
1	Glycine	Gly	G	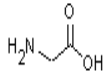	Glutaric Acid Tartaric Acid Phthalic Acid Urea	2.33	9.6	6.06	0	-0.4/ Hydrophobic	Neutral	25.23	75.06	233
2	Alanine	Ala	A	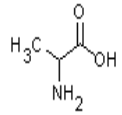	L-ala-val-ala.H_2O L-ala- S-mandelic acid L-ala-L-ala nitrate L-ala-R-mandelic acid hemihydrate	2.35	9.59	6.01	0	1.8/ Hydrophobic	Neutral	16.63	89.09	314-316
3	Valine	Val	V	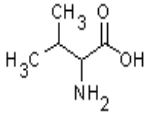	L-val/D-2-aminobutanoic acid L val/ fumaric acid D-val/L-leu L-val/D-norvaline L val/ D met DL val/ succinic Acid D-val/L-Isoleucine L-val/D-norleucine	2.35	9.62	6	0	4.2 / Hydrophobic	Neutral	5.87	117.14	315
4	Leucine	Leu	L	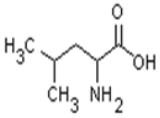	No	2.33	9.74	6.01	0	3.8 / Hydrophobic	Neutral	2.19	131.17	293

The ‘sc’ in ‘pKa’ values stands for the ‘side-chain’ group (Tilborg *et al.* 2014).

Table No. 2.2 Amino acids - names, structures, physicochemical properties and reported co-crystals (Continue...)

Sr. No.	Name of Amino Acid	3 letter codes	Single letter code	Structure	Co-former/ Reported cocrystals	pKa		Isoelec-tric point (pI)	Potential H-bonds	Hygroscopi-city	Acidic/ Basic	Solubility (g/100g water)	Molecular weight (Da)	Melting point °C
	non-polar, aliphatic residues					pK_1 (α-COOH)	pK_2 (α-$^+NH^3$)			Hydropathy index / Hydropathy				
5	Isoleucine	Ile	I	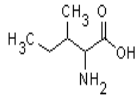	No	2.66	9.7	6.05	0	4.5/ Hydrophobic	Neutral	3.17	131.17	286-288
6	L-proline	Pro	P	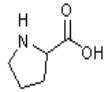	L-pro/$MnCl_2.H_20$ L-pro/LiCl L-pro methanolate/thiourea L-pro monohydrate/ 4 aminobenzoic acid DL-pro/Hemisuccinic acid L-pro/L-pro perchlorate L-pro/L-pro nitrate	1.8	10.63	6.3	0	1.6/ Hydrophobic	Neutral	130.07	115.13	228
	aromatic residues													
7	Phenylalanine	Phe	F	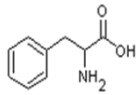	No	2.2	9.31	5.49	0	2.8/ Hydrophobic	Neutral	2.8	165.19	270-275
8	Tyrosine	Tyr	Y	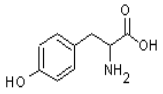	No	2.24	9.21, 10.46 SC	5.64	3	-1.39/ Hydrophobic	Neutral	0.054	181.18	290

The ‘sc’ in ‘pKa’ values stands for the ‘side-chain’ group (Tilborg *et al.* 2014).

Table No. 2.2 Amino acids - names, structures, physicochemical properties and reported co-crystals (Continue...)

Sr. No.	Name of Amino Acid	3 letter codes	Single letter code	Structure	Co-former/ Reported cocrystals	pKa		Isoele-ctric point (pI)	Potential H-bonds	Hygroscop-icity	Acidic/ Basic	Solubility (g/100g water)	Molecular weight (Da)	Melting point °C
						pK_1 (α-COOH)	pK_2 (α-$^+NH^3$)			Hydropathy index / Hydropathy				
	aromatic residues													
9	Tryptophan	Trp	W	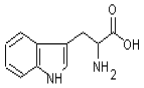	No	2.46	9.41	5.89	1	-0.9/ Hydrophobic	Neutral	1.32	204.22	280-285
	polar, non-charged residues													
10	Serine	Ser	S	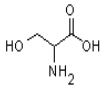	L- ser/ pyridine-2,4 dicarboxylic acid	2.31	9.73	5.68	3	-0.8/ Hydrophillic	Neutral	36.57	105.09	222
11	Threonine	Thr	T	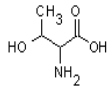	L-thr/ L-ala-thr	2.32	9.03	5.6	3	-0.7/ Hydrophillic	Neutral	9.79	119.11	256
12	Cysteine	Cys	C	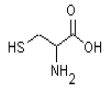	L-cys/S-mandelic acid L-cys/R-mandelic acid	1.92	8.18SC, 10.70	5.05	0	2.5/ Moderate	Neutral	2.56	121.15	220

The ‘sc’ in ‘pKa’ values stands for the ‘side-chain’ group (Tilborg *et al.* 2014).

Table No. 2.2 Amino acids - names, structures, physicochemical properties and reported co-crystals (Continue...)

Sr. No.	Name of Amino Acid	3 letter codes	Single letter code	Structure	Co-former/ Reported cocrystals	pKa		Isoel-ectric point (pI)	Potential H-bonds	Hygrosco-picity	Acidic/ Basic	Solubility (g/100g water)	Molecular weight (Da)	Melting point °C
						pK_1 (α-COOH)	pK_2 (α-$^+NH^3$)			Hydropathy index / Hydropathy				
	polar, non-charged residues													
13	Methionine	Met	M	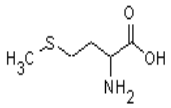	No	2.13	9.28	5.74	0	1.9/ Moderate	Neutral	5.59	149.21	284
14	Asparagine	Asn	N	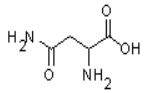	L-asn/L tartaric acid	2.16	8.84	5.41	5	-3.5/ Hydrophillic	Neutral	2.51	132.11	235
15	Glutamine	Gln	Q	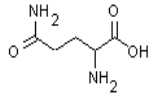	No	2.18, 4.18SC	9.64	5.65	5	-3.5/ Hydrophillic	Neutral	4.25	146.14	185
	positively charged residues													
16	Lysine	Lys	K	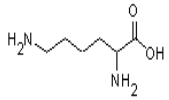	No	2.15	9.16, 10.67 SC	9.6	3	-3.9/ Hydrophillic	Basic	24.66	146.18	215

The ‘sc’ in ‘pKa’ values stands for the ‘side-chain’ group (Tilborg *et al.* 2014).

Table No. 2.2 Amino acids - names, structures, physicochemical properties and reported co-crystals (Continue...)

Sr. No.	Name of Amino Acid	3 letter code	Single letter code	Structure	Co-former/ Reported cocrystals	pKa		Isoelectric point (pI)	Potential H-bonds	Hygroscopicity	Acidic/Basic	Solubility (g/100g water)	Molecular weight (Da)	Melting point °C
						pKa_1 (α-COOH)	pKa_2 (α-$^+NH^3$)			Hydropathy index / Hydropathy				
	positively charged residues													
17	Arginine	Arg	R	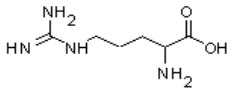	No	2.04	9.04, 12.48 SC	10.76	7	- 4.5/ Hydrophillic	Basic	19.59	174.2	223
18	Histidine	His	H	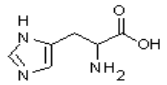	No	2.02	6.22SC, 9.42	7.6	3	- 4.5/ Moderate	Basic	4.36	155.15	285
	negatively charged residues													
19	Aspartate	Asp	D	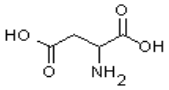	No	1.94, 3.71 SC	9.63	2.85	4	- 3.5/ Hydrophillic	Acidic	0.51	133.1	270
20	Glutamate	Glu	F	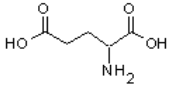	No	2.17	9.01	3.15	4	- 3.5/ Hydrophillic	Acidic	0.88	147.12	205

The ‘sc’ in ‘pKa’ values stands for the ‘side-chain’ group (Tilborg *et al.* 2014).

The synthesised co-crystal of amino acid was checked for the manufacture of effervescent tablets. The improved physical stability property was reported in the current study. It helps to prove the importance of understanding the physicochemical properties like hygroscopicity and stability of the molecule involved in solid-state formulations; and their impact on the development of solid-state dosage forms. The involvement of molecular interactions during this process was understood. The study has found that new crystalline solid material obtained through co-crystallisation techniques can be used for tailor-made physicochemical improvement in APIs for solid-state dosage formulations.

2.2.5 Preparation of co-crystals

Many laboratory levels and scalable type of technologies have been reported and in use for the preparation of co-crystals.These technologies include solution crystallisation technique (Vishweshwar *et al.* 2006) neat grinding and liquid-assisted grinding (Trask *et al.* 2004); sonochemical (Friščić *et al.* 2006; Aher *et al.* 2010) and twin screw hot melt extrusion (Paradkar *et al.* 2003; Dhumal *et al.* 2010). External energy input has been involved in all the methods mentioned above to stimulate the intermolecular interactions between API and the co-crystals coformer. Energy input may be in the form of the shear as in the case of grinding or combination of shear and temperature in extrusion or sonic energy as observed in the ultrasound-assisted method (Pagire *et al.* 2013a).

Recently, a new technique based on the green process approach was utilised for the co-crystal synthesis. Researchers from the University of Bradford have investigated Twin Screw Hot Melt extrusion for the solvent-free continuous production of co-crystals by Paradkar *et al.*2010 (Dhumal *et al.* 2010). An invention by Soares and Corneiro provides in-line Raman spectroscopy as a

process analytical technology (PAT) in the slurry-based co-crystallisation process. It will support the understanding of the co-crystallisation reaction and monitor it. This very helpful PAT avoids the unnecessary treatment of the reaction medium, reduces failure chances and generation of impurities with continuous process monitoring. It will result in an opportunity to adjust process parameters accordingly as well as supporting the green synthesis of co-crystals (Soares and Carneiro 2013).

Recently Mehta *et al.* from the University of Bradford invented spray drying. Apshingekar *et al.* developed ultrasound assisted technologies for co-crystallisation (Apshingekar et al. 2016a). Spherical crystallisation studies for the preparation of pharmaceutical co-crystals had been developed by Pagire *et al.* (Pagire *et al.* 2013b).

2.2.6 Current study and green process

Here, in this current study, the basic simple mechanochemical and green process technique has been used for co-crystallisation study with *amino acids*. This technique is known as liquid-assisted grinding or sometimes known as a solvent assisted grinding (LAG or SAG). It has been used as dry or neat grinding or with a suitable solvent (organic or inorganic), but here in this work water was used to develop a green process technology. However, it failed in some of the trials.

Though there are so many techniques available and have been studied by many researchers and many to come in developing; LAG/SAG stands as a low cost and easy for developing at the laboratory level. The LAG procedure gives a more significant yield for the screening at the research laboratory level.

2.3 Summary

The molecular interactions study is important to understand the drug-PPB interaction as well as the co-crystal formation. The knowledge of the bonding (hydrogen / π-π / electrostatic forces) will help and guide for understanding the activity of drug-PPB. Through the obtained results one can measure the free drug availability for the therapeutic effect as well as the toxicity. It will lead to optimisation of drug dosage in the formulation. Similarly, the study of molecular level interaction, electrostatic forces and hydrogen bonding mechanism will reveal the APIs and coformer molecule interaction for the cocrystal formation. It will guide for new coformer selections and provides alternative competitors information for the bonding with the APIs. The current study will lead to the development of physically stable solid state effervescent formulation.

Chapter 3 Materials and methods

This chapter includes the information about the materials used for the drug-PPB study and amino acids co-crystals study. It also describes the methods used for the experiments and characterisation study.

3.1 Materials

All test compounds obtained from the Sigma–Aldrich Chemie Gmbh Munich, Germany. All solvents including methanol, ethanol, acetonitrile, and propanol were obtained from Fisher Scientific, UK and Sigma–Aldrich, U.K. All the solvents and chemicals were used without further purification.

Deionised as well as filtered water achieved through an ELGA Maxima LS ultrapure water purification system. The chemicals, drugs used in this study are listed in Table 3.1 with their lot numbers.

Table 3.1 List of chemicals, drugs with lot numbers

Sr No.	Name of Chemical/Drug	Source	Lot No.
1	Amino acids kit DLAA	Sigma Aldrich, USA	34H9015
2	Amino acids LAA 10KT	Sigma Aldrich, USA	SLBK8201V
3	L-Arginine	Sigma Aldrich, USA	CDBB2685V
4	L-Cystine	Sigma Aldrich Slovakia	BCBS1903V
5	Sodium Bicarbonate	Sigma Aldrich, USA	SLBP7821V
6	L-Cysteine	Alfa Aesar, UK	10192131
7	L-Methionine	Alfa Aesar, UK	10186273
8	L-Cystine	Alfa Aesar, UK	10191196
9	L-Serine	Alfa Aesar, UK	10135680
10	Succinic acid	Sigma Aldrich, Austria	O5OM0082
11	Citric acid	Sigma Aldrich, USA	SLBD0318V
12	Citric acid	Sigma Aldrich, USA	SLBR3765V
13	Fumaric acid	Sigma Aldrich, Austria	BCBK1778V
14	L-proline	Sigma Aldrich, USA	SLBL4766V
15	Adipic acid	Acros Organics, USA	A016837701
16	Polyvinylpyrrolidone (PVP K30) (In this study K-17)	ISP Technologies Inc. NJ, USA	TX81102
17	Mannitol	Sigma Aldrich, UK	BCBM0366V

Specifications of all solvents used in this research work are listed in Table 3.2.

Table 3.2 Specification of solvents

Sr.No.	Name	Supplier	Grade
1	Ethanol	Fisher Chemicals, UK, Sigma-Aldrich/Merck, UK	HPLC grade
2	Methanol	Fisher Chemicals, UK	HPLC grade
3	Acetonitrile	Fisher Chemicals, UK	HPLC grade
4	Ethyl acetate	Fisher Chemicals, UK	HPLC grade
5	Isopropyl alcohol	Fisher Chemicals, UK, Sigma-Aldrich/Merck, UK	HPLC grade

All instruments/equipment utilised in this study are listed in Table 3.3

Table 3.3 Specification of instruments

Sr.No.	Instrument	Manufacturer	Model
1	DSC	TA Instruments, UK.	Q2000
2	TGA	TA Instruments, UK.	Q5000
3	PXRD	Bruker, Billerica, USA.	D8 powder diffractometer
4	Raman	Renishaw, UK.	RX210 RIAS, 785nm.
5	FT-IR	PerkinElmer	Frontier
6	Tablet Pressing Machine	Karnavati, India.	Rimek mini tablet press
7	DVS	Surface Measurement Systems, UK.	DVS Intrinsic
8	SCXRD	Bruker, Billerica, USA.	Bruker APEX II X8
9	HPLC	Waters, Herts, UK	Waters Alliance 2695,996 PDA
10	HPLC	Shimadzu, Milton Keynes, UK	LC-20AD, SPD-M20A PDA
11	Chiral HSA column	VWR, UK.	100 × 4.0 mm, 5um
12	Chiral AGP column	VWR, UK.	100 × 4.0 mm, 5um
13	SEM	INCAx-sight,Oxford instruments,UK	FEI Quanta 400

All software used in this research work are listed in Table 3.4.

Table 3.4 List of software and their purpose of use in this study

Sr.No.	Software	Purpose
1	TA universal analysis	Thermal analysis
2	PowDLL converter	PXRD pattern analysis
3	GRAM	Vibrational spectral analysis
4	Spectragryph ver.1.2.7	Spectroscopy analysis
5	DVS Intrinsic	DVS analysis
6	Bruker APEX software9	SCXRD data analysis
7	SHELXS10	SCXRD data analysis
8	SHELXL10	SCXRD data analysis
9	EmpowerPro	HPLC data analysis for HSA study
10	LabSolutionsLite	HPLC data analysis for AGP study
11	XT microscope V 2.3	SEM control

3.2 Methods

3.2.1 Drug-PPB studies

In HSA and AGP studies the mobile phase A was 20mM, potassium phosphate buffer solution, pH 7.0, and the mobile phase B was isopropyl alcohol (IPA). The flow rate of mobile phase was kept constant as 0.8ml/min (0.9ml/min in AGP) throughout the analysis. The temperature of the column also kept constant throughout the analysis at around 20˚C, (25°C in AGP experiments), i.e. room temperature. The injection volume was 10µl. In our experiments, we used the isocratic method, in which the mobile phase composition was kept constant at 15% B: 85% A throughout one complete set of test compounds.

The compounds were detected using the maximum absorption wavelength, λmax of the ultraviolet–visible spectroscopy (UV–VIS) detector. Each set of test compounds was repeated twice (n=2) (three times n=3 in AGP) to get the relative data of retention time by using the Empower Pro software (by using the LabSolutionsLite software in AGP studies) which connected to the HPLC system.

3.2.1.1 Validation of our HPLC method

Here in these experiments the aim was to find out primarily the retention times of drug samples but not the concentrations. Thus, normal procedures of HPLC to obtain standard calibration curve was not implicated here. However, the columns integrity was checked from time to time to ensure the obtained results, which are of equal standards. To check column integrity or stability of HSA stationary phase was controlled by injecting 4 compounds namely as, 17α-hydroxyprogesterone, salicylic acid, warfarin and penbutolol (n=5; s.d.≤ 0.03) throughout the study, whereas the compounds used for stability control of AGP column were 17α-hydroxyprogesterone, mefenamic acid, warfarin and penbutolol (n=5; s.d.≤ 0.03).

Any analytical method is based on the purpose to deliver some qualitative and/or quantitative results with an acceptable uncertainty level. By theory, “validation” means “measuring uncertainty”. In fact, method validation is performed by evaluating a series of method-performance characteristics, such as precision, trueness, selectivity/specificity, linearity, operating range, recovery, limit of detection (LOD), limit of quantification (LOQ), sensitivity, ruggedness/robustness, and applicability (Taverniers et al. 2004; Şengül 2016). The LOD and LOQ are two important parameters in quantitative analysis. The definition of LOD is defined by the United States Pharmacopeia as “a parameter of limit tests”. It is the lowest concentration of the analyte that can be detected, but necessarily not quantitated, under the stated experimental conditions”. In contrast, LOQ is defined as a parameter of quantitative assays for low levels of compounds in sample matrices. The LOQ is the lowest concentration in a sample that may be measured with an acceptable level of accuracy and precision under the stated experimental conditions (Şengül 2016). A variety of

approaches are used to calculate detection limits, which are the most important parameters of validation. These approaches are the visual evaluation, signal-to-noise, standard deviation of the blank, and calibration curve methods. In this current study we used the visual evaluation in the form of difference in retention time at different concentration. Therefore, as a result we confirm and use the concentration of our compounds as 100mM to 0.1mM and use in 10-20 µl of injection volume. In few cases we used 0.01mM concentration of the compounds.

$LOD = 3 \times SD + B_{ave}$…Eq. for LOD

$LOQ = 10 \times SD + B_{ave}$…Eq. for LOQ.

SD: standard deviation of measurements B_{ave}: average concentration of spike samples.

In our studies we checked the standard deviation of obtained retention time from 3 subsequent injections. The obtained data processed for retention factor (k) as per the equation (1). The Abraham's linear free energy relationship (LFER) method was used in this study as per the equations 2 and 5, as explained in Chapter 2.

3.2.2 Amino acid cocrystals

Amino acid cocrystals were prepared and by liquid assisted grinding (LAG) technique. The mixture in 1:1 stoichiometric ratio of the amino acid with carboxylic acid/ NSAID molecule/ citric acid was taken into a clean mortar and pestle and grind for 20-25 minutes. This grinding process is catalysed with the addition of 4-6 drops of distilled water or ethanol through 5 ml sterile syringe. This process is known as liquid assisted / solvent assisted grinding (LAG/SAG). In the presence of water sometimes LAG gives sticky material, while in the presence of ethanol it gives free flow powder material. As this experiment was

aimed at the hygroscopicity reduction, all sticky materials were discarded. The obtained free flow powder materials through the LAG process were characterised for cocrystals development using powder crystal X-ray diffractometry, DSC, TGA, Raman, FTIR and dynamic vapour sorption measurements techniques.

3.2.2.1 L-proline - carboxylic acid cocrystals

The L-proline was taken as a 1:1 stoichiometric ratio with each of the nine carboxylic acids to screen for the cocrystal development. The used carboxylic acids are namely as oxalic acid,malonic acid, succinic acid, glutaric acid, adipic acid, malic acid, fumaric acid, ascorbic acid and citric acid. The free-flowing powder materials obtained from the LAG process were subjected to the further characterisation studies using DVS, PXRD, DSC, TGA, Raman and FT-IR techniques for the cocrystal formation and to understand the molecular interaction in between these reacting molecules.

3.2.2.2 L-proline - non-steroidal anti-inflammatory drugs (NSAIDs) co-crystals

The cocrystals of L-proline and NSAIDs was carried out in a 1:1 stoichiometric ratio. These NSAIDs were ibuprofen, flurbiprofen, ketoprofen and aspirin. The obtained free flow powder material was characterised by DVS, PXRD, DSC, TGA, Raman and FT-IR techniques for the cocrystal formation and to understand the molecular interaction in between these reacting molecules.

3.2.2.3 Citric acid-amino acid cocrystals

All amino acids (18 amino acids) were screened for the cocrystal formation with citric acid in the 1:1 stoichiometric ratio by using the LAG method. The obtained free flow powder material was characterised by DVS, PXRD, DSC, TGA,

Raman and FT-IR techniques for the cocrystal formation and to understand the molecular interaction in between these reacting molecules.

3.2.2.4 Single crystal preparation

An attempt was made to obtain a well grown single crystal of the cocrystals obtained using solvent evaporation method. All cocrystal formed were taken in the 1:1 stoichiometric ratio and transfer into the clean conical flasks. Then these mixtures warmed at 60°C until the clear saturated solutions observed in the presence of different solvent systems like methanol, ethanol, acetonitrile, ethyl acetate. All flasks were kept covered with perforated aluminium foil for evaporation without disturbing. After few days (2 days to 3 weeks) crystalline entity was separated and dried. A well grown single crystal was then subjected to the single crystal x-ray diffractometer analysis.

3.2.3 Characterisation methods for amino acids cocrystals

3.2.3.1 Powder X-ray diffraction (PXRD)

PXRD patterns of all samples were recorded at room temperature on a Bruker D8 diffractometer (Billerica, USA) equipped with a Cu Kα radiation source tube, 1.540 Å X-ray wavelengths and the emission filament voltage and ampere were 40 kV and 40 mA respectively. A scanning range of 3° to 30° 2θ° angle was used with a step size of 0.01°at the rate of 1 sec. time count. The scatter slit and receiving slit was 0.2° and 1° respectively.

3.2.3.2 Differential scanning calorimetry (DSC)

DSC was performed using a Differential Scanning Calorimeter *Q2000* from TA Instruments, Crawley, UK. This machine equipped with the RSC90 cooling unit to analyse and comprehend heat flow in the starting crystalline components as well as the resulting crystalline products. Indium metal was used for the calibration of instrument. Approximately 1 to 2 mg of the sample was weighed in

a crimped standard aluminium pan. The top of the pan was pierced with sharp needle to create a tiny hole before crimping. This will allow evaporation of the excessive moisture during experiment. DSC runs were carried out at a heating rate of 10°C/min from 0°C to 300°C under nitrogen atmosphere. DSC data were analysed using TA Universal analysis software version 4.5A.

3.2.3.3 Thermogravimetric analysis (TGA)

TGA was performed using Thermo Gravimetric Analyser *Q5000* from TA Instruments, Crawley, UK, equipped with a water bath. Each cleaned platinum pan was tared to store the weight of the pan as an offset before loading the samples. About 2-3 mg of the sample was loaded in the standard platinum pan and heated as a ramp run from 25°C to 350°C some cases up to 400°C at a heating rate of 10°C /min under nitrogen atmosphere. TGA data were analysed using TA Universal analysis software version 4.5A.

3.2.3.4 Raman spectroscopy

Raman spectra were recorded of all amino acids and chemical compounds and their respected co-crystals by using Raman microscope analyser made by Renishaw (UK), equipped with a diode laser which emits light of wavelength 785nm. Maximum output of the diode laser was 50mV at source point and approximately 20mV at the sample. A 50X objective was used to emit a light beam of diameter 2 µm for 10 secs at the sample. Few particles of each sample were spread over the clean metal coated background glass slide and processed under the 785 nm laser beam. Three acquisitions of each sample were taken at 4 cm^{-1} spectral resolution and scan were collected at wavenumber 100-3500 cm^{-1} and sometimes 100-2000 cm^{-1}. A charged coupled device detector was used to collect the data.

3.2.3.5 Fourier transform infra-red (FT-IR) spectroscopy

FT-IR spectra were recorded of each compound and their respected co-crystals using Perkin-Elmer's make the FT-IR machine. A small amount of powder of a sample was kept on the diamond crystal at the centre of the platform in such a way that it should cover the area of diamond crystal with the help of rotating the vertical shaft. Powdered material was pressed against the diamond crystal to a predetermined pressure, which was confirmed by generation of signal sound. Once the sample was placed correctly, measurements were recorded. Each sample was analysed at four times acquisition rate and from 600 to 4000 wavelengths (cm^{-1}) range. The assembly involves an electronically stabilised source and detector for accurate results with high repeatability.

3.2.3.6 Dynamic vapour sorption (DVS) study

Approximately 40-50 mg sample was carefully transferred to the previously tared DVS pan. Sample sizes were used to give the optimum balance between sensitivity and equilibration time. Sample pan was transferred to the humidity chamber of DVS intrinsic machine. Samples were subjected to an increment program of relative humidity. Relative humidity was maintained using a mixture of dry nitrogen gas and water. The experiment was carried out from 0% RH to 90% RH relative humidity by 10% RH increase in each step and at 25°C temperature programme condition. The step change was done using dm/dt principle, i.e. a change in RH step was achieved when the difference between two time points was less than 0.001%.

3.2.3.7 Single crystal X-ray diffraction (SCXRD)

The single crystal structure was determined using intensity data collected on a Bruker APEX II X8 diffractometer using Cu Kα radiation at 170 K. The data was

collected and processed using the Bruker APEX software9 and the structures were solved using SHELXS10 and refined with SHELXL10.

3.2.3.8 Scanning electron microscopy (SEM)

Scanning electron microscope (INCAx-sight,Oxford instrument, UK) was used to characterise surface and visual morphology of cocrystal. Self-adhesive carbon mounts were used to mount samples on aluminium pin stubs (Agar Scientific, Stansted, UK). SEM images were taken using a FEI Quanta 400 microscope under high vacuum and high voltage of 20KV at working distance as 10mm at various magnification levels 40x to 250x. All samples were gold plated prior to the analysis.

Chapter 4 Drug- plasma protein interaction studies

The drug plasma protein studies are discussed and explained in chapter 1 and 2. The part of this study has been published in the journal of pharmaceutical and biomedical analysis, Volume 149, 5 February 2018, Pages 16-21. The link to this publication is https://doi.org/10.1016/j.jpba.2017.10.022 (Kamble *et al*. 2018).

In 2003, Valko *et al.* have used a fast gradient HPLC method to study a variety of compounds on an immobilised HSA column (Valko *et al.* 2003). Valko *et al.* showed that the ionic compounds are responsible for the drug-plasma protein binding, but they could not quantify them exactly. However, this current study focuses specifically on quantifying the percentage of ionic behaviour responsible for drug-plasma protein binding. As well as an understanding of the molecular interactions involved in this drug-PPB. The following part of this chapter is similar to the published article entitled as, “Structural properties governing drug-plasma protein binding determined by high-performance liquid chromatography method” (This publication is attached to this thesis in the Appendix).

4.1 Results and Discussion

In this study, a set of 65 compounds with a broad structural diversity (in terms of E, S, A, B, V, J^+ and J^-) were selected. The solutes consist of neutrals, acidic and basic compounds which are present as neutral or ionic (cationic or anionic) at the experimental condition of pH 7, which is as close as possible to the physiologic pH and compatible with the stability of the stationary phase (pH no higher than 7.0). Their retention factor log k was determined using immobilised HSA and AGP HPLC columns at the isocratic mobile phase condition. 15% (v/v) of IPA was used as the organic modifier to allow the elution of most of the

solutes in a reasonable time. The two columns were stable during the study period. The stability of HSA stationary phase was controlled by injecting 4 compounds (17α-hydroxyprogesterone, salicylic acid, warfarin and penbutolol) throughout the study, whereas the compounds for stability control of AGP column were 17α-hydroxyprogesterone, mefenamic acid, warfarin and penbutolol. Some of the chromatograms obtained from HSA and AGP studies are shown below in Figure 4.1 and 4.2 respectively.

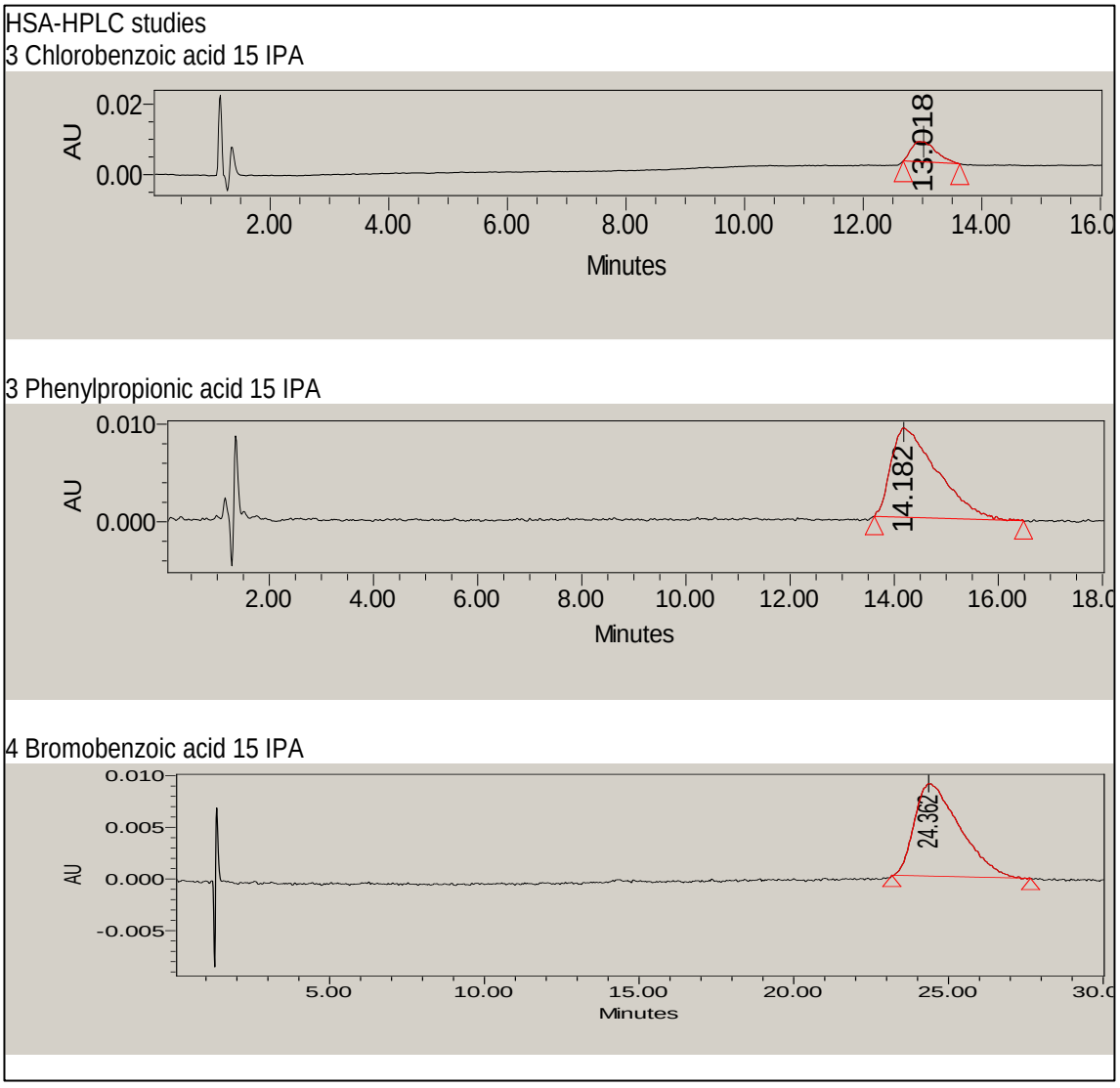

Figure 4.1 HPLC chromatogram from HSA-HPLC studies

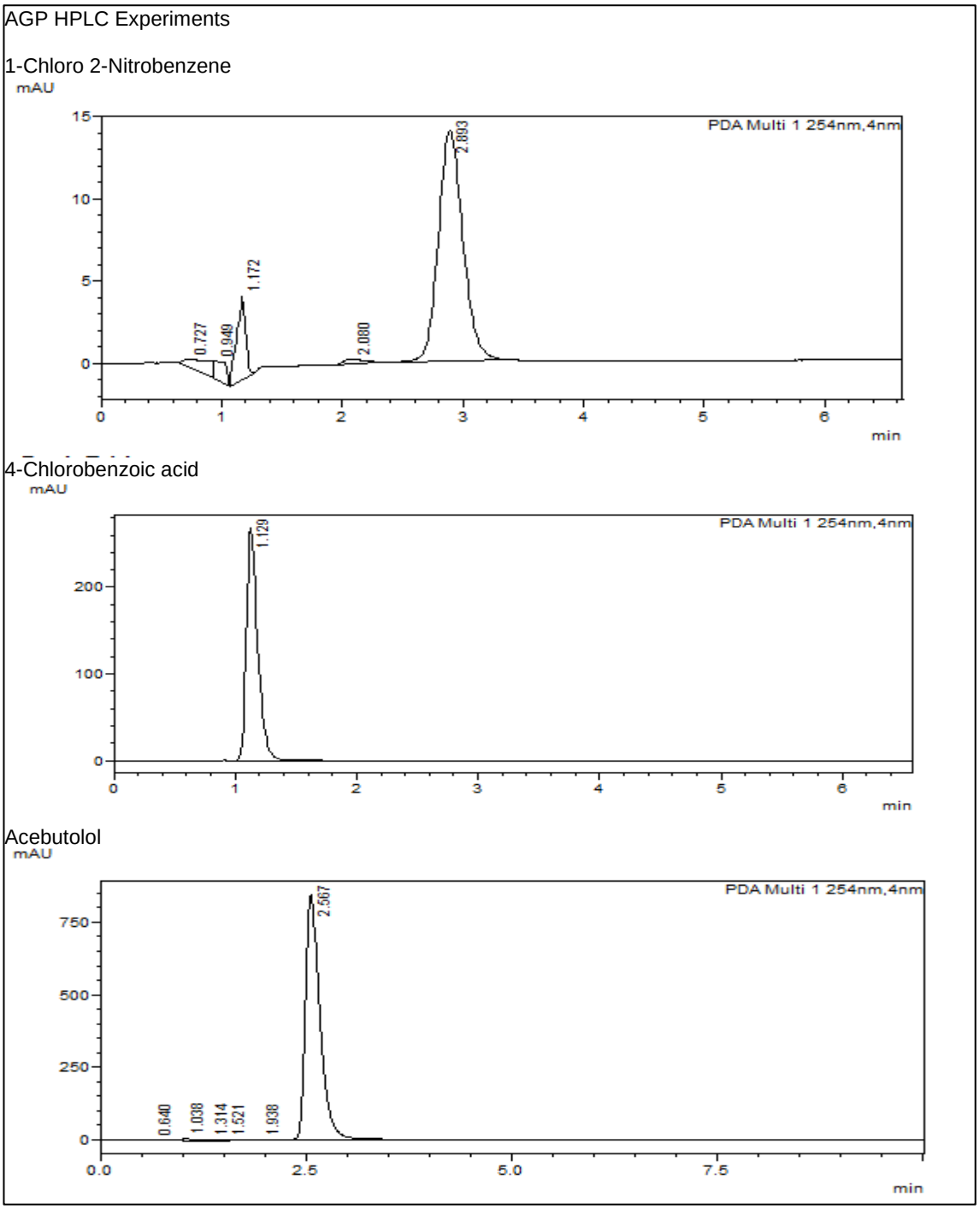

Figure 4.2 HPLC chromatogram from AGP-HPLC studies

The log k values and other physicochemical parameters including dissociation constant pKa, n-octanol/water partition coefficient (log P_{oct}), n-octanol/water distribution coefficient at pH 7 (log $_{D}$7.0), as well as the values of the solute descriptors are shown in Table 4.1.

Table 4.1 Physicochemical parameters of the investigated compounds

	Solutes	**pKa[a]**	**Charge state**	**log k_{HSA}[b]**	**log k_{AGP}[b]**	**log P_{oct}[a]**	**log $D_{7.0}$[c]**	**E**	**S**	**A**	**B**	**V**	**J+**	**J-**
	Neutrals													
1	Acetaminophen	9.50	neutral	-0.35	-0.73	0.51	0.51	1.120	1.63	1.01	0.91	1.1724	0.0000	0.0000
2	Acetophenone	N	neutral	0.05	-0.30	1.58	1.58	0.818	1.01	0.00	0.48	1.0139	0.0000	0.0000
3	Acridine	5.58	neutral	1.22	0.90	3.40	3.38	2.356	1.32	0.00	0.58	1.4133	0.0000	0.0000
4	Aniline	4.60	neutral	-0.21	-0.45	0.90	0.90	0.955	0.96	0.26	0.41	0.8162	0.0000	0.0000
5	2-Chloroaniline	2.64	neutral	0.31	0.05	1.91	1.91	1.033	0.92	0.25	0.31	0.9386	0.0000	0.0000
6	N-Ethylaniline	5.12	neutral	0.15	-0.05	2.16	2.15	0.945	0.85	0.17	0.43	1.0980	0.0000	0.0000
7	Nitrobenzene	N	neutral	0.33	-0.13	1.85	1.85	0.871	1.11	0.00	0.28	0.8906	0.0000	0.0000
8	1-Chloro-2-nitrobenzene	N	neutral	0.75	0.24	2.52	2.52	1.020	1.24	0.00	0.24	1.0130	0.0000	0.0000
9	1-Fluoro-2,4-dinitrobenzene	N	neutral	0.26	-0.29	1.47	1.47	1.006	1.69	0.00	0.45	1.0825	0.0000	0.0000
10	Benzyl alcohol	N	neutral	-0.23	-0.42	1.10	1.10	0.803	0.87	0.39	0.56	0.9160	0.0000	0.0000
11	4-Chlorobenzylalcohol	N	neutral	0.28	-0.09	1.96	1.96	0.911	0.96	0.40	0.50	1.0384	0.0000	0.0000
12	2-Aminobiphenyl	3.84	neutral	0.79	0.72	2.84	2.84	1.600	1.48	0.26	0.41	1.4240	0.0000	0.0000
13	Carbamazepine	N	neutral	0.23	0.71	2.19	2.19	2.154	1.90	0.50	1.15	1.8106	0.0000	0.0000
14	Corticosterone	N	neutral	0.31	0.18	1.94	1.94	1.860	3.43	0.40	1.63	2.7389	0.0000	0.0000
15	*m*-Cresol	10.10	neutral	0.23	-0.11	1.96	1.96	0.822	0.88	0.57	0.34	0.9160	0.0000	0.0000
16	*p*-Cresol	10.26	neutral	0.24	-0.15	1.94	1.94	0.820	0.87	0.57	0.31	0.9160	0.0000	0.0000
17	Estradiol	N	neutral	1.26	0.74	3.03	3.03	1.800	1.77	0.86	1.10	2.1988	0.0000	0.0000
18	Estriol	N	neutral	0.68	-0.03	2.54	2.54	1.970	1.74	1.06	1.63	2.2575	0.0000	0.0000
19	Hydrocortisone	N	neutral	-0.02	-0.15	1.61	1.61	2.030	3.49	0.71	1.90	2.7976	0.0000	0.0000
20	Hydrocortisone- 21-acetate	N	neutral	0.24	0.18	2.19	2.19	1.890	2.88	0.46	2.16	3.0951	0.0000	0.0000
21	2- Naphthol	9.57	neutral	0.94	0.47	2.70	2.70	1.520	1.08	0.61	0.40	1.1441	0.0000	0.0000

22	3-Chlorophenol	9.11	neutral	0.71	0.26	2.50	2.50	0.909	1.06	0.69	0.15	0.8975	0.0000	0.0000
23	4-Bromophenol	9.31	neutral	0.82	0.30	2.59	2.59	1.080	1.17	0.67	0.20	0.9501	0.0000	0.0000
24	4-Chlorophenol	9.40	neutral	0.65	0.17	2.39	2.39	0.915	1.08	0.67	0.20	0.8975	0.0000	0.0000
25	4-Chloro-3,5-dimethyl phenol	9.70	neutral	1.22	0.82	3.27	3.27	0.980	0.94	0.61	0.26	1.1793	0.0000	0.0000
26	4-Chloro-2-methylphenol	9.60	neutral	0.92	0.50	2.78	2.78	0.890	0.91	0.63	0.22	1.0384	0.0000	0.0000
27	3-Nitrophenol	8.40	neutral	0.48	-0.09	2.00	1.98	1.050	1.57	0.79	0.23	0.9493	0.0000	0.0000
28	Phenylacetonitrile	N	neutral	0.10	-0.52	1.56	1.56	0.751	1.03	0.00	0.50	1.0120	0.0000	0.0000
29	Phenytoin	8.33	neutral	0.41	0.25	2.47	2.45	1.713	2.23	0.86	1.00	1.8693	0.0000	0.0000
30	Prednisolone	N	neutral	0.02	-0.12	1.62	1.62	2.210	3.10	0.71	1.92	2.7546	0.0000	0.0000
31	17α-Hydroxyprogesterone	N	neutral	0.78	0.71	3.17	3.17	1.640	3.35	0.25	1.31	2.6802	0.0000	0.0000
32	21-Hydroxyprogesterone	N	neutral	0.81	0.60	3.10	3.10	1.740	3.50	0.14	1.31	2.6802	0.0000	0.0000
33	Salicylamide	8.37	neutral	0.02	-0.26	1.28	1.26	1.160	1.58	0.61	0.51	1.0315	0.0000	0.0000
34	Testosterone	N	neutral	0.78	0.66	3.32	3.32	1.540	2.56	0.32	1.17	2.3827	0.0000	0.0000
	Acidic compounds													
35	Aspirin	3.48	Anion	0.86		1.13	-2.39	1.000	4.15	0.00	3.28	1.2664	0.0000	2.2560
36	4-Bromobenzoic acid	3.97	Anion	1.33		2.86	-0.17	1.150	3.25	0.00	2.60	1.0852	0.0000	2.1480
37	3-Chlorobenzoic acid	3.82	Anion	1.04		2.71	-0.47	0.990	3.13	0.00	2.57	1.0326	0.0000	2.0340
38	4-Chlorobenzoic acid	3.98	Anion	1.07		2.65	-0.37	0.990	3.37	0.00	2.60	1.0326	0.0000	2.1790
39	Flurbiprofen	3.91	Anion		0.14	3.81	0.72	1.590	4.56	0.07	3.36	1.8174	0.0000	2.5383
40	Ibuprofen	4.43	Anion		0.04	3.87	1.30	0.880	3.50	0.08	3.31	1.7556	0.0000	2.4188
41	Mefenamic acid	4.33	Anion		0.63	5.12	2.45	1.800	4.71	0.09	3.14	1.8996	0.0000	2.6427
42	3-Phenylpropanoic acid	4.25	Anion	1.08		1.89	-0.86	0.900	3.43	0.03	3.02	1.1920	0.0000	2.1879
43	4-Phenylbutanoic acid	4.72	Anion	1.50		2.42	0.14	0.910	3.59	0.04	3.01	1.3829	0.0000	2.2184
44	8-Phenyloctanoic acid	5.03	Anion		0.67	4.09	2.12	0.940	3.87	0.07	3.26	1.8965	0.0000	2.4256
45	Salicylic acid	2.97	Anion	0.93		2.26	-1.77	1.050	3.51	0.14	2.18	0.9689	0.0000	1.6351
46	Warfarin	4.98	Anion	1.57	0.35	2.70	0.68	2.130	5.62	0.00	4.40	2.2862	0.0000	2.7628
	Basic compounds													
47	Acebutolol	9.52	Cation	-0.02	0.14	2.02	-0.50	1.450	6.69	3.62	0.00	2.7771	2.2965	0.0000

48	Alprenolol	9.59	Cation	0.31	0.71	3.10	0.51	1.100	4.46	1.78	0.00	2.1802	2.2574	0.0000
49	Atenolol	9.60	Cation	-0.19	0.06	0.16	-2.44	1.300	6.27	2.91	0.00	2.1978	2.4800	0.0000
50	Bupivacaine	8.10	Cation	0.36	0.64	3.41	2.28	1.170	4.67	2.92	0.00	2.5354	1.5920	0.0000
51	Imipramine	9.40	Cation	0.83	1.18	4.80	2.40	1.000	3.66	2.02	0.00	2.4230	1.6110	0.0000
52	Lidocaine	8.01	Cation	0.06	0.26	2.44	1.39	0.960	4.18	2.12	0.00	2.0804	1.7490	0.0000
53	Mepivacaine	7.70	Cation	-0.05	0.23	1.95	1.17	1.170	4.69	2.98	0.00	2.1127	1.5607	0.0000
54	Metoprolol	9.63	Cation	-0.02	0.12	1.95	-0.68	1.020	5.35	2.16	0.00	2.2819	2.3476	0.0000
55	Oxprenolol	9.57	Cation	0.08	0.50	2.51	-0.06	1.160	5.09	2.35	0.00	2.2389	2.2029	0.0000
56	Penbutolol	9.92	Cation	0.81	1.35	4.62	1.70	0.775	4.66	1.98	0.00	2.6195	1.9630	0.0000
57	Pindolol	9.54	Cation	0.21	0.43	1.75	-0.79	1.550	4.60	2.36	0.00	2.0305	2.2661	0.0000
58	Procaine	9.03	Cation	0.01	0.25	2.14	0.11	0.999	4.58	1.86	0.00	1.9982	2.1487	0.0000
59	Promazine	9.36	Cation	1.01	1.34	4.55	2.19	1.900	3.78	1.76	0.00	2.3047	2.5263	0.0000
60	Propafenone	9.62	Cation	0.65	1.09	3.64	1.02	1.680	5.69	3.08	0.00	2.8467	2.3780	0.0000
61	Propranolol	9.47	Cation	0.54	0.98	3.48	1.01	1.690	4.31	2.07	0.00	2.1695	2.4319	0.0000
62	Quinidine	8.56	Cation	0.47	0.77	3.44	1.87	2.320	5.81	1.23	0.00	2.5727	4.1570	0.0000
63	Quinine	9.05	Cation	0.50	0.89	3.44	1.39	2.319	5.81	1.23	0.00	2.5727	4.1565	0.0000
64	Sotalol	9.43	Cation	-0.12	0.11	0.24	-2.19	1.320	6.18	2.38	0.00	2.1225	2.8119	0.0000
65	Verapamil	8.92	Cation	0.57	0.77	3.79	1.86	1.660	7.70	4.33	0.00	3.8076	2.4040	0.0000

[a] Taken from (Zhang et al. 2012) and bioloom Software (Biobyte Corporation, Claremont, U.S.A.).

[b] Calculated from Eq. (NCBI); n=3, s.d.≤ 0.03.

c Calculated according to $logD = logP_{oct} - \log(1 + 10^{pKa-pH})$ for bases and $logD = logP_{oct} - \log(1 + 10^{pH-pKa})$ for acids.

From Table 4.1, one can understand that, there are large log k values of the acidic compounds on the immobilised HSA HPLC column (log k HSA). At the experimental condition of pH 7, the acidic compounds (35-46 in Table 1) are negatively charged. This indicates the strong interaction of anionic species with HSA stationary phase. Four acidic compounds with high lipophilicity (flurbiprofen, ibuprofen, mefenamic acid and 8-phenyloctanoic acid) could not be eluted from the HSA column (within 4 hours), implying the contribution of lipophilicity of the solute to the binding in addition to their negative charges. In this case, we eluted the injected samples by mobile phase with a higher ratio of IPA before next injection. On the contrary, the acidic compounds showed much weaker retention on the AGP HPLC column. All the acidic compounds with log P_{oct} values lower than 3 do not retain in AGP column. The four highly lipophilic acids (flurbiprofen, ibuprofen, mefenamic acid and 8-phenyloctanoic acid) showed a low degree of retention, indicating that the negative charges of the solutes do not favour the interaction with AGP, while lipophilicity plays a role.

Fig 4.3 shows the correlations between the values of log D7.0 and log k on the immobilised HSA (log k HSA) 4.3(1a) and AGP (log k AGP) 4.3(1b) stationary phases from this study. From Fig 4.3 (1a), it can be further verified that anions interact much stronger with HSA stationary phase than 7 cations and neutral compounds. Fig 4.3 (1b) shows that the cations have a higher affinity to AGP stationary phase than anions in general. The neutral compounds bind least to both proteins. Within each set of the solutes, the larger the lipophilicity (expressed by log D7.0), the higher the affinity with the proteins. It is indicating that both electrostatic forces and lipophilicity control the drug binding to immobilised proteins. This is in good agreement with drug binding data from soluble human plasma proteins in previous studies (Urien *et al.* 2001).

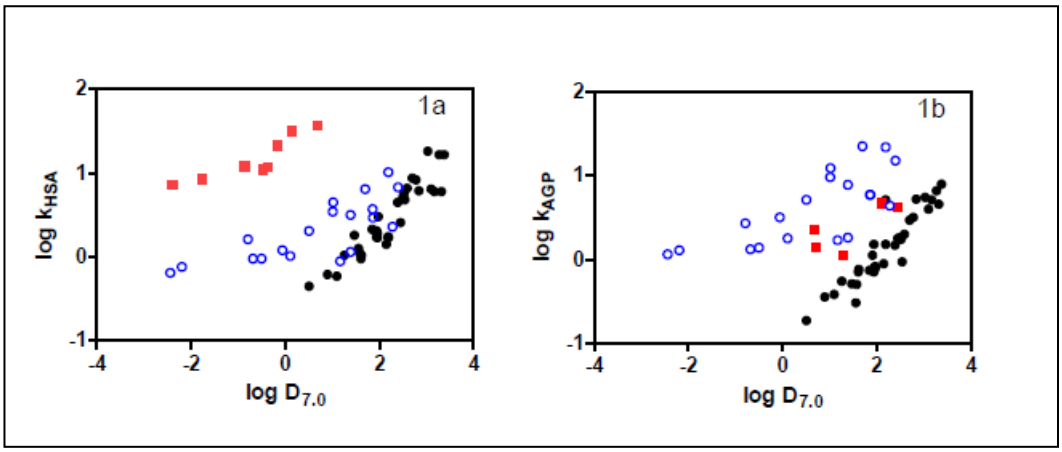

Figure 4.3 Correlations between log D7.0 and log kHSA (1a) as well as log kAGP (1b). Markers: ●, neutral molecules; ■, anions; ○, cations (Kamble *et al*. 2018).

To reveal the structural properties that govern the drug interaction with the immobilised HSA and AGP in HPLC system, the multilinear regression (MLR) of log k against the solute descriptors yielded the LFER model shown in Eq. 6 and Eq. 7.

$$logkHSA = -0.271(\pm 0.298) + 0.470(\pm 0.276)\,E - 0.331(\pm 0.190)\,S - 0.177(\pm 0.197)\,A - 1.233(\pm 0.393)\,B + 1.086(\pm 0.350)\,V - 0.231(\pm 0.229)\,J^{+} + 2.024(\pm 0.460)J^{-}$$

$$N = 61, R2 = 0.812, SD = 0.215, F = 33, Press = 3.204, Q2 = 0.756 \ldots\ldots\ldots Eq.\,6$$

$$\log kAGP = -0.756(\pm 0.315) + 0.428(\pm 0.275)E - 0.354(\pm 0.196)S - 0.156(\pm 0.206)\,A - 1.253(\pm 0.397)\,B + 1.278\,(\pm 0.361)\,V - 0.051(\pm 0.230)\,J^{+} + 1.562(\pm 0.426)\,J^{-}$$

$$N = 58, R2 = 0.796, SD = 0.228, F = 28, Press = 4.143, Q2 = 6.74 \ldots\ldots\ldots Eq.\,7$$

In these equations, 95% confidence limits are given in parentheses; N is the number of compounds; R2 is the squared correlation coefficient; SD is the standard deviation, and F is the Fisher's test. Press and Q2 are the leave-one-out statistics. The values of Q2 are good enough to indicate that Eq. 6 and Eq.

7 are soundly based. The coefficients of Eq. 6 and Eq. 7 showed that for the electrically neutral compounds, McGowan's characteristic molecular volume (V), dipolarity/polarizability (S) and hydrogen bond basicity (B) are the three significant molecular descriptors of solutes determining the interaction with immobilised plasma proteins. Whereas excess molar refraction (E) is less important, and hydrogen bond acidity (A) is not of statistical significance in both systems. For acids and bases in this study, compared logarithm of the retention factors of neutral species and the corresponding anions or cations on the two stationary phases as shown in Table 4.2.

For immobilised HSA stationary phase, we use Eq. 6 to calculate log kHSA for the 8 neutral, acidic compounds and 19 basic compounds using descriptors for the neutral species. These can then be compared to experimental values of log kHSA of the corresponding anions 8 and cations, measured in this study. Over the 8 acidic compounds, the average difference log kHSA (anions) – log kHSA (neutral acids) = 0.80 (±0.03) log units. So that on average the retention factor on immobilised HSA column for the anions is 6.3 times that for the neutral, acidic compounds, further quantitatively verifying the contribution of the electrostatic interactions between the anions and the immobilised HSA. It also means that for the electrically neutral acids, hydrogen bond acidity (A) is not important for binding with the HSA phase.

In the case of 19 basic compounds, the average difference log kHSA (cations) - log kHSA (neutral base) = - 0.14 (±0.01) log units, meaning that retention factor on HSA HPLC column for the protonated base cation is 0.71 times that for the neutral bases. This indicates that positive charge of the solute does not greatly favour the interaction with HSA stationary phase.

Thus, for the first time, this study able to show the effect of negative or positive charge on binding to HSA quantitatively. Valko *et al.* (Valko *et al.* 2003) have used a fast gradient HPLC method to study a variety of compounds on an immobilised HSA column. By comparison of log kHSA with calculated values of log P (octanol) at pH 7.4 (log D), they concluded that acid anions were strongly bound. However, they could not quantify any increased binding due to the negative charge

Table 4.2 The observed log k values of ionic species and predicted log k values of the neutral species of acids and bases in this study by Eq 6 and Eq 7.

Species	**E**	**S**	**A**	**B**	**V**	**J^+**	**J^-**	**$logk_{HSA}$ [a]**	**$logk_{AGP}$ [b]**
Acids									
Aspirin, anion								0.86	
Aspirin	0.781	1.69	0.71	0.67	1.2879	0.0000	0.0000	-0.02	
4-Bromobenzoic acid, anion								1.33	
4-Bromobenzoic acid	1.000	1.01	0.63	0.26	1.1067	0.0000	0.0000	0.63	
3-Chlorobenzoic acid, anion								1.04	
3-Chlorobenzoic acid	0.840	0.95	0.63	0.32	1.0541	0.0000	0.0000	0.45	
4-Chlorobenzoic acid, anion								1.07	
4-Chlorobenzoic acid	0.840	1.02	0.63	0.27	1.0541	0.0000	0.0000	0.49	
Flurbiprofen, anion									0.14
Flurbiprofen	1.440	1.45	0.62	0.76	1.8389	0.0000	0.0000		0.65
Ibuprofen, anion									0.04
Ibuprofen	0.730	0.70	0.57	0.79	1.7771	0.0000	0.0000		0.50
Mefenamic acid, anion									0.63
Mefenamic acid	1.650	1.35	0.65	0.54	1.9211	0.0000	0.0000		1.15
3-Phenylpropanoic acid, anion								1.08	
3-Phenylpropanoic acid	0.750	1.18	0.60	0.60	1.2135	0.0000	0.0000	0.16	
4-Phenylbutanoic acid, anion								1.50	
4-Phenylbutanoic acid	0.760	1.29	0.61	0.57	1.3544	0.0000	0.0000	0.32	
8-Phenyloctanoic acid, anion									0.67
8-Phenyloctanoic acid	0.790	1.28	0.59	0.63	1.9180	0.0000	0.0000		0.70
Salicylic acid, anion								0.93	

Salicylic acid	0.900	0.85	0.73	0.37	0.9904	0.0000	0.0000	0.36	
Warfarin, anion								1.57	0.35
Warfarin	1.980	1.88	0.29	1.57	2.3077	0.0000	0.0000	0.56	0.36
Bases									
Acebutolol, cation								-0.02	0.14
Acebutolol	1.600	2.42	0.90	2.10	2.7556	0.0000	0.0000	-0.08	-0.18
Alprenolol, cation								0.31	0.71
Alprenolol	1.250	1.09	0.15	1.44	2.1587	0.0000	0.0000	0.50	0.32
Atenolol, cation								-0.19	0.06
Atenolol	1.450	1.90	0.62	2.03	2.1763	0.0000	0.0000	-0.47	-0.67
Bupivacaine, cation								0.36	0.64
Bupivacaine	1.320	2.10	0.34	1.33	2.5139	0.0000	0.0000	0.68	0.56
Imipramine, cation								0.89	1.08
Imipramine	1.150	1.45	0.00	1.04	2.4015	0.0000	0.0000	1.12	0.99
Lidocaine, cation								0.06	0.26
Lidocaine	1.110	1.51	0.07	1.24	2.0589	0.0000	0.0000	0.45	0.25
Mepivacaine, cation								-0.05	0.23
Mepivacaine	1.320	2.14	0.34	1.33	2.0912	0.0000	0.0000	0.21	0.00
Metoprolol, cation								-0.02	0.12
Metoprolol	1.170	1.33	0.17	1.76	2.2604	0.0000	0.0000	0.09	-0.07
Oxprenolol, cation								0.08	0.50
Oxprenolol	1.230	1.45	0.15	1.62	2.2174	0.0000	0.0000	0.21	0.04
Penbutolol, cation								0.81	1.35
Penbutolol	0.925	1.15	0.08	1.51	2.5980	0.0000	0.0000	0.73	0.65
Pindolol, cation								0.21	0.43
Pindolol	1.700	1.59	0.30	1.40	2.0090	0.0000	0.0000	0.40	0.18
Procaine, cation								0.01	0.25
Procaine	1.149	1.34	0.26	1.44	1.9767	0.0000	0.0000	0.15	-0.06
Promazine, cation								1.01	1.34
Promazine	2.050	1.49	0.00	1.08	2.2832	0.0000	0.0000	1.35	1.16
Propafenone, cation								0.65	1.09
Propafenone	1.730	2.09	0.29	1.74	2.8252	0.0000	0.0000	0.72	0.63
Propranolol, cation								0.54	0.98
Propranolol	1.840	1.43	0.44	1.31	2.1480	0.0000	0.0000	0.76	0.56
Quinidine, cation								0.47	0.77
Quinidine	2.469	1.23	0.37	1.97	2.5512	0.0000	0.0000	0.76	0.60
Quinine, cation								0.50	0.89
Quinine	2.469	1.23	0.37	1.97	2.5512	0.0000	0.0000	0.76	0.60

Sotalol, cation								-0.12	0.11
Sotalol	1.470	1.55	0.68	2.06	2.1010	0.0000	0.0000	-0.47	-0.68
Verapamil, cation								0.57	0.77
Verapamil	1.807	3.17	0.00	2.37	3.7861	0.0000	0.0000	0.72	0.76

a Observed $logk_{HSA}$ values for ionic species and predicted $logk_{HSA}$ values for neutral species by Eq6

b Observed $logk_{AGP}$ values for ionic species and predicted $logk_{AGP}$ values for neutral species by Eq7

In the same way, here Eq 7 was used to calculate log kAGP for the neutral species of the acids and bases used in this study. After that, compared to experimental values of log kAGP of the corresponding ionic species of neutral, acidic compounds and basic compounds obtained from this work on immobilised AGP stationary phase (shown in Table 2.2). For the 5 acidic compounds, the average difference log kAGP (neutral acids) – log kAGP (anions) = 0.31 (±0.05) log units, so that on average the retention factor on HPLC AGP stationary phase for the neutral, acidic compounds is twice that for the anions. This further quantitatively confirms that anions do not favour interaction with the AGP stationary phase. For the 19 basic compounds, the average difference log kAGP (cation) – log kAGP (neutral base) = 0.32 (±0.02), meaning that the retention factor on HPLC AGP stationary phase for the protonated base cations is about 2.1 times that for neutral bases. This indicates the importance of the positive charge in the drug binding with immobilised AGP phase.

Thus, through these experiments, the aims and objectives from 1 to 4 have been achieved successfully.

Chapter 5 Amino acid cocrystals

5.0 Introduction

Cocrystallisation approach has been used to tailor the physicochemical properties of the drug molecules. Though there is a major focus on improvement in dissolution rate of the drug molecule, cocrystallisation has been successfully used to improve compressional properties (Chattoraj and Sun; Chow *et al.* 2012), photostability (Vangala *et al.* 2011) and controlling hydrate formation (Trask *et al.* 2005b). Recently, Pagire and Paradkar *et al.* used cocrystallisation to control hygroscopicity of carboxylic acids (Paradkar and Pagire 2017).

In all these applications selections of coformer is an important aspect; especially considering the regulatory requirements like the selection of generally recognised as safe (GRAS) molecule. An ideal coformer should have strong synthons to form hydrogen or halogen bond which will maintain stability during processing and storage. Recently, Alsirawan *et al.* demonstrated destabilisation of cocrystals due to the presence of a structurally related molecule in the formulation (Alsirawan *et al.* 2016). Another important aspect in pharmaceutical cocrystals is the safety of using a coformer in the stoichiometric proportion equal to the dose of the drug. Hence, recently there is growing trend towards the use of nutritional supplement molecules as coformers. However, for nutritional supplement molecules also there is a limit due to 'recommended daily dosage allowance' (RDA). Another advantage of nutritional supplement molecules is they are relatively low cost, but this category of molecules suffers from limitations such as instability in the presence of oxygen and moisture.

The amino acid is a major class of nutritional supplement molecules which have high RDAs, low cost and most importantly high chemical diversity in terms of

hydrogen bond donor and acceptor groups and pKa values as shown in Table 2.2. Amino acids have amino and carboxylic groups which are donor and acceptor groups (Tan *et al.* 2006; Liu *et al.* 2016). They have a tendency to form hydrogen bonds with hydroxyl, carboxyl, pyridyl, amide and phenolic groups (Saha *et al.* 2005; Aakeroy *et al.* 2013; Liu *et al.* 2016). Recently, there are few reports of amino acid cocrystals. Cocrystallisation with a fumaric acid has achieved resolution of enantiomers of DL-arginine with fumaric acid (Iwama *et al.* 2014), ezetimibe–L-proline cocrystals have shown five times faster dissolution compared to pure ezetimibe (Shimpi et al. 2014). Liu *et al.* reported 1:2 stoichiometric cocrystal of myricetin with L-proline, which showed 7.7 fold increases in dissolution and three-fold increases in bioavailability of myricetin compared to crystalline myricetin (Liu *et al.* 2016).

Considering, chemical diversity and relatively unexplored molecular cocrystals of amino acids stimulated to investigate applications of cocrystal approach to amino acids. There are many opportunities, but we selected a molecular complex of an amino acid with the carboxylic acid group containing coformer for our research. The major reason for selection of a carboxylic acid group is its tendency of forming a hydrogen bond. It is also found very commonly in most of the drugs and excipients which might be as abundant as amino or amide group. The carboxylic acid group is also associated with performance issues such as hygroscopicity, hydrate formation and acidity of drugs.

The amino acids were screened for their sorption behaviour using DVS and the data are summarised in Table 5.1.

Table 5.1 DVS of amino acids

Sr.No.	Name of compound	dm/dt in % (at 25 °C and 90% RH)
1	L-serine	0.01
2	L-threonine	0.02
3	L-asparagine	0.02
4	L-valine	0.03
5	L-glycine	0.05
6	L-aspartate	0.10
7	L-phenylalanine	0.11
8	L-arginine	0.12
9	L-histidine	0.13
10	L-alanine	0.14
11	L-methionine	0.16
12	L-isoleucine	0.23
13	L-lysine	0.31
14	L-tryptophan	0.33
15	L-glutamate	0.38
16	L-cysteine	0.43
17	L-leucine	0.98
18	**L-proline**	**148.70**

The DVS data shows that most of the amino acids do not absorb significant moisture even at very high levels of %RH at 25 °C. However, L-proline was observed to absorb about 148.70 % moisture and dissolves in the absorbed moisture forming a solution. This state is known as deliquescence. However, L-Serine absorbs 0.1% moisture only at 90% RH. Though there is no clear mechanistic understanding about high hygroscopic nature of L-proline, it is attributed to the presence of polar groups which favour moisture absorption (Lloyd and Phillips 1933).

In the literature, some amino acid co-crystals pairs are reported (Tilborg *et al.* 2014). These include L-glycine – glutaric acid, L-glycine-phthalic acid, L-glycine – tartaric acid, L-glycine–urea, L-serine–ascorbic acid and L-asparagine –

tartaric acid. These all reported pairs use amino acids which are non-hygroscopic amino acids.

Jayasankar *et al.* investigated the role of moisture in cocrystal formation by grinding technique, where deliquescent materials such as fructose, sucrose were added as excipients with the cocrystal pair and demonstrated that the absorbed moisture helps in the synthesis of cocrystals by grinding if temperature and humidity are maintained above deliquescent relative humidity (DRH) (Jayasankar *et al.* 2007). DRH is the function of the chemistry of the material as well as temperature. The substances like sugars and organic and inorganic salts exhibit deliquescence (Parsons *et al.* 2004; Salameh *et al.* 2006; Salameh and Taylor 2006b; Salameh and Taylor 2006a). On the similar basis, we hypothesise that L-proline; a deliquescent amino acid will help the formation of cocrystal in the neat grinding process (Please see Figure 5.1). In this current experiment 'B' is L-proline or citric acid and 'A' is API or another coformer.

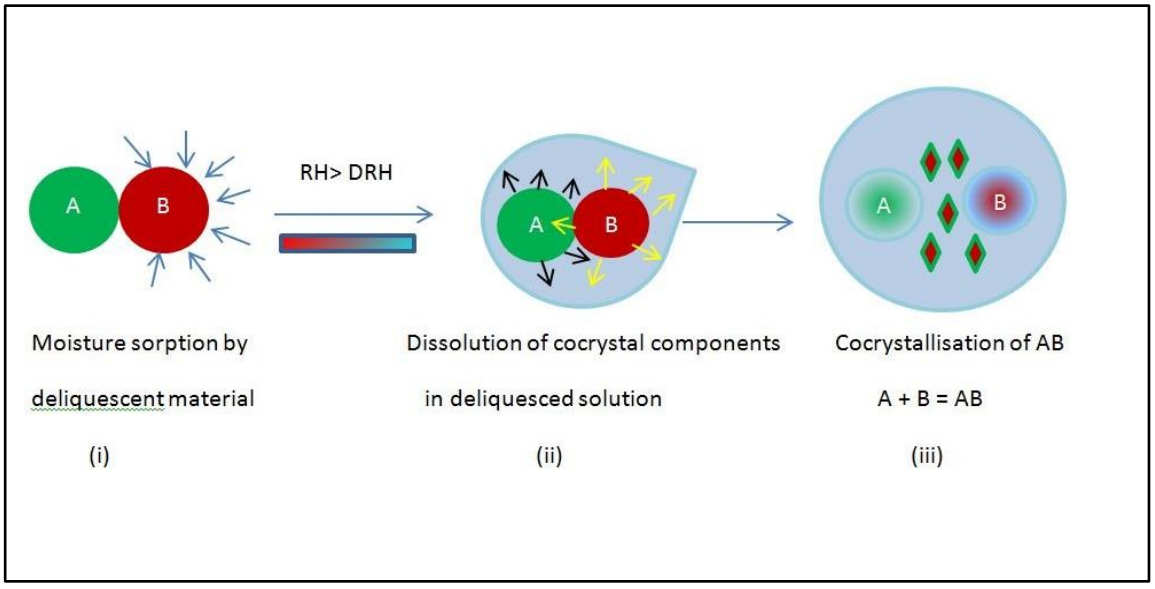

Figure 5.1 Mechanism of cocrystal formation in the presence of deliquescent material updated from Jayasankar *et al.* work.

The DVS isotherm (n=3; s.d. ≤ 0.03)(Figure 5.2) of L-proline shows that L-proline starts absorbing moisture at about 30% RH and continuous to maintain it

at about 15% till 70% RH above which moisture absorption took place at the rapid rate. This DVS profile makes L-proline an ideal deliquescent coformer material to explore cocrystal synthesis by neat grinding. Therefore, we investigated cocrystal synthesis of L-proline cocrystals with nine carboxylic acids.

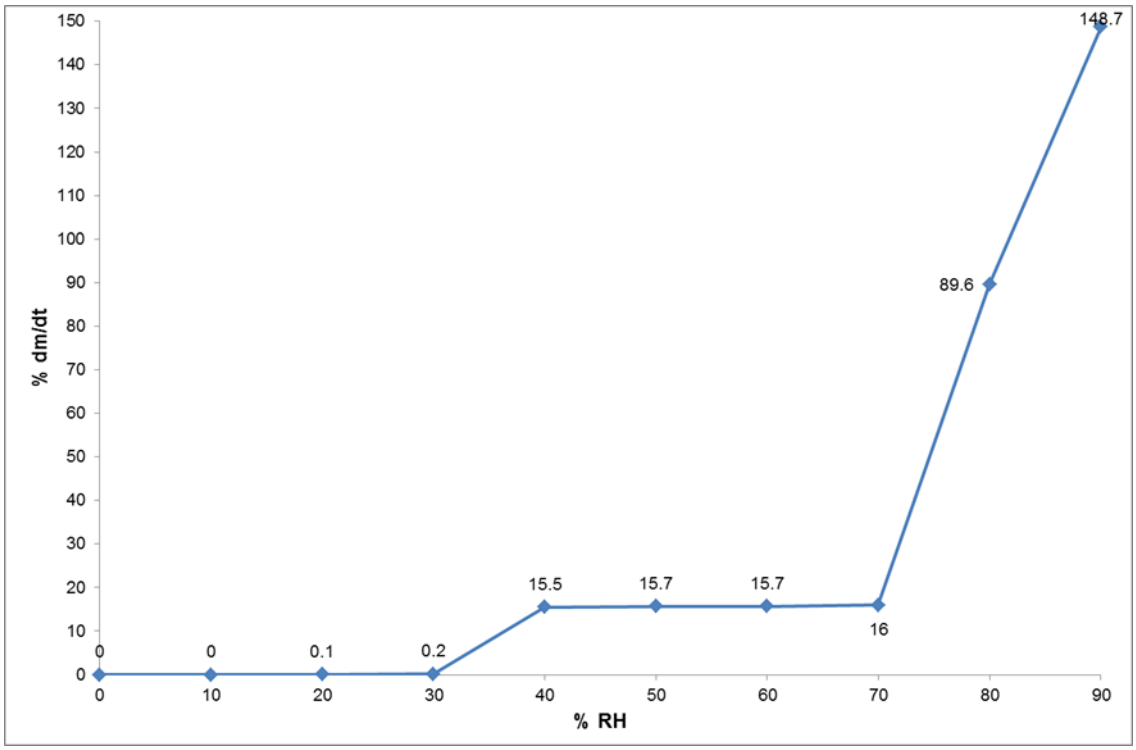

Figure 5.2 DVS of L-proline

5.1 Screening of L-proline-carboxylic acid cocrystallisation

In the current study, total nine carboxylic acids were screened for the co-crystals formation with L-proline. The carboxylic acids include oxalic acid, malonic acid, succinic acid, glutaric acid, adipic acid, malic acid, fumaric acid, ascorbic acid and citric acid. Surprisingly, the neat grinding method for carboxylic acid and L-proline failed to generate cocrystals. This failure can be attributed to the critical amount of moisture required to cause cocrystallisation may not have reached due to the atmospheric humidity condition. In other words, the atmospheric humidity in the day of experiments might be less than

deliquescent relative humidity (DRH). It is relatively challenging to accept reason as at least 15% of moisture is absorbed in 30% RH. To address this issue of DRH few drops of water were added during grinding. These moistures assisted experiments also failed to generate any cocrystal formation instead resulted in a sticky mass (refer Table 5.2).

The separation of cocrystal phase is dependent on the phase solubility behaviour of the cocrystal forming agents and the cocrystal. If the cocrystal has a high solubility or the cocrystal itself is hygroscopic or deliquescent then successful separation of the cocrystal phase will be challenging. Jayasankar *et al.*, when proposed the hypothesis about the role of moisture in cocrystal formation by grinding they have used carbamazepine, theophylline, caffeine and sulfadimidine with nicotinamide, saccharine and carboxylic acids as coformers and sucrose and fructose as deliquescent agents.

It was observed that DRH of sugars decreases significantly in the presence of coformers. The success of these experiments with sugar as deliquescence may be due to relatively less solubility of the cocrystal phase in the slurry state. Similar successes have been shown in slurry experiments of caffeine with carboxylic acids by Pagire *et al.*, Apshingekar *et al.*, in microwave (Pagire *et al.* 2013a) and ultrasound slurry cocrystallisation (Apshingekar et al. 2016b) respectively. Apshingekar *et al.* have shown detained phase diagram during slurry experiments which indicates generation of cocrystal phase in low moisture region. Another reason for the failure of neat grinding process is a depression in DRH of L-proline leading to the formation of dilute slurry dissolving the cocrystal phase. The solubility of coformer does not affect significantly because we have selected some carboxylic acids with high

solubility as well as relatively less soluble NSAIDs molecules like ibuprofen, ketoprofen, flurbiprofen and aspirin.

The next trials were conducted with ethanol as a solvent for liquid assisted grinding. So, including NSAIDs there were total 13 pairs used to carry out LAG of L-proline with carboxylic acid and NSAID. Out of 13 cocrystal experimental pairs, six pairs resulted in sticky mass even with ethanol and only seven pairs provided free-flowing powder (for details refer Table 5.2).

Table 5.2 Screening of non-hygroscopic cocrystal with the LAG method.

Co-crystal pair	**Stoichiometry**	**Reported / New**	**Solvent**	**Results**
L-proline-fumaric acid	1:1	Reported	H_2O EtOH	Sticky Free flow
L-proline-adipic acid	1:1	Reported	H_2O EtOH	Sticky Free flow
L-proline-succinic acid	1:1	New	H_2O EtOH	Sticky Free flow
L-proline-citric acid	1:1	New	H_2O EtOH	Sticky Sticky
L-proline-glutaric acid	1:1	New	H_2O EtOH	Sticky Sticky
L-proline-ascorbic acid	1:1	New	H_2O EtOH	Sticky Sticky
L-proline-malic acid	1:1	New	H_2O EtOH	Sticky Sticky
L-proline-malonic acid	1:1	New	H_2O EtOH	Sticky Sticky
L-proline-oxalic acid	1:1	New	H_2O EtOH	Sticky Sticky
L-proline-aspirin	1:1	New	H_2O EtOH	Sticky Free flow
L-proline-ibuprofen	1:1	New	H_2O EtOH	Sticky Free flow
L-proline-flurbiprofen	1:1	New	H_2O EtOH	Sticky Free flow
L-proline-ketoprofen	1:1	New	H_2O EtOH	Sticky Free flow

The powder mass obtained was further characterised using PXRD for the presence of any new peak (refer Table 5.3). The phases patterns obtained in screening experiments were characterised using PXRD. The new crystalline phase formation confirmed by comparison of the PXRD pattern of generated crystalline phase with that of the starting materials. The newly generated crystalline phase PXRD pattern matched completely with the starting material suggests no new crystalline phase formation occurred. However, the additional new peaks formation with subsequent disappearance of starting material indicates that there is new crystalline phase developed. The results of the screening study are summarised in Table 5.3.

Table 5.3 Summary of screening experiment using PXRD

Co-crystal pair	Stoichio metry	Reported /New	Solvent	PXRD observation	Result
L-proline-fumaric acid	1:1	Reported	H_2O EtOH	No new peaks New peaks	No Yes
L-proline-adipic acid	1:1	New	H_2O EtOH	No new peaks New peaks	No Yes
L-proline-succinic acid	1:1	New	H_2O EtOH	No new peaks New peaks	No Yes
L-proline-citric acid	1:1	New	H_2O EtOH	No new peaks No new peaks	No No
L-proline-glutaric acid	1:1	New	H_2O EtOH	No new peaks No new peaks	No No
L-proline-aspirin	1:1	New	H_2O EtOH	No new peaks New peaks	No Yes
L-proline-ibuprofen	1:1	New	H_2O EtOH	No new peaks New peaks	No Yes
L-proline-flurbiprofen	1:1	New	H_2O EtOH	No new peaks New peaks	No Yes
L-proline-ketoprofen	1:1	New	H_2O EtOH	No new peaks New peaks	No Yes

Thus, only free flow powder formed compounds were subjected to further characterisation study with PXRD, DSC, TGA analysis. Based on the above PXRD results L-proline did not generate any new crystal phases using citric

acid and glutaric acid as cocrystal former. Thus, no further analysis of this pair was performed.

5.1.1 Cocrystal characterisation

5.1.1.1 L-proline- fumaric acid

1 PXRD

All processed and starting materials were analysed using PXRD analyser to investigate the crystal phase (n=3). In the Figure below (Figure 5.3) it is observed that new characteristic crystal peaks at 8.88, 13.12 and 19.92 2θ° are generated in the L-proline-fumaric acid sample. The PXRD pattern of L-proline-fumaric acid is entirely different from individual starting materials as the characteristic peaks of starting materials are absent in the final sample. The PXRD pattern of L-proline-fumaric acid correctly coincides with the previously reported PXRD pattern by Tilborg *et al.* 2013 (Tilborg *et al.* 2013).

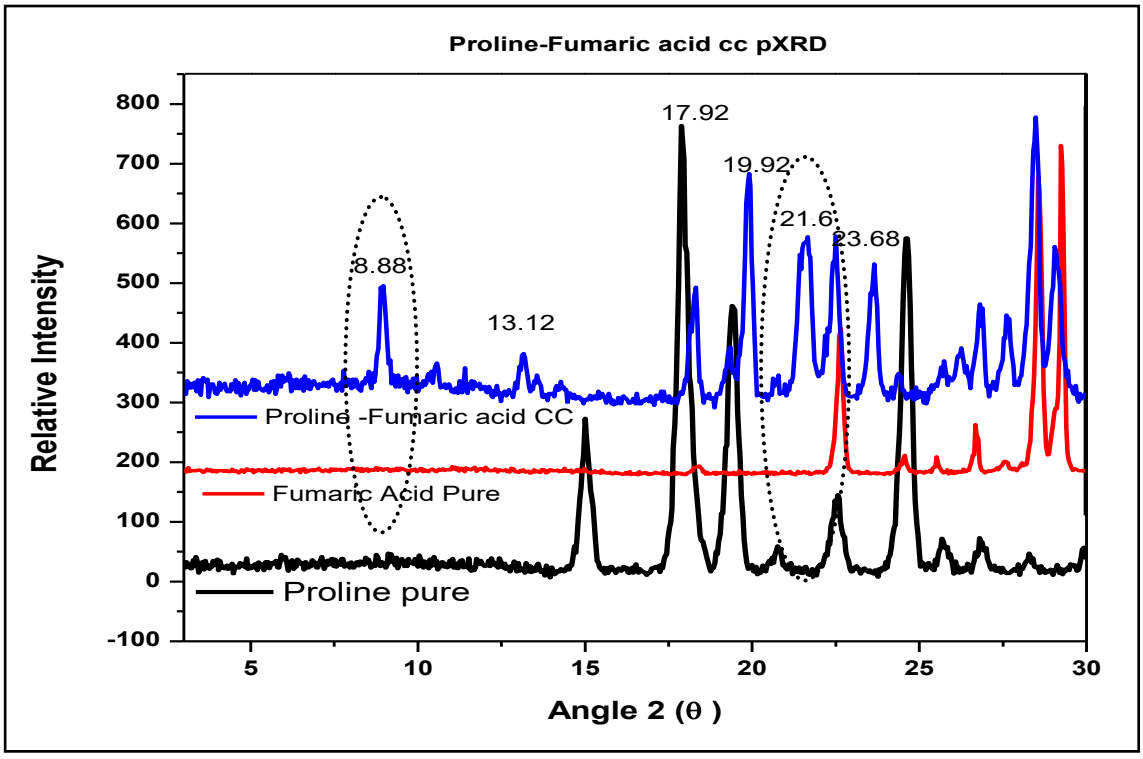

Figure 5.3 PXRD patterns of L-proline-fumaric acid cocrystal and their original material

2 Thermal analysis

2.1 DSC analysis

Below Figure (5.4) describes the DSC thermograms of starting materials, their physical mixtures and processed samples of L-proline and fumaric acid (n=3). Based on the presence of the melting endotherm it is observed that single distinct melting endotherm at 159.2°C followed by degradation was observed for the processed samples of L-proline-fumaric acid cocrystal. This melting endotherm is different from the melting event of L-proline (221°C) (Ash and Ash 2006; Hautala et al. 2016) and fumaric acid (287°C) (Figure 5.5) (Batisai et al. 2014) respectively. Melting endotherm of the L-proline-fumaric acid physical mixture in 1:1 stoichiometric ratio displays endotherm (162.2°C) event which is correlate or gives an idea of cocrystal formation while compared to cocrystal sample. Based on the previous studies by Tilborg *et al.* in 2013, the melting endotherm of L-proline-fumaric acid rightly matches with the cocrystal phase (Tilborg *et al.* 2013). The endothermic event occurred at 217.8°C in L-proline is similar to the event observed by Shimpi *et al*.in their studies (Shimpi *et al*. 2014).

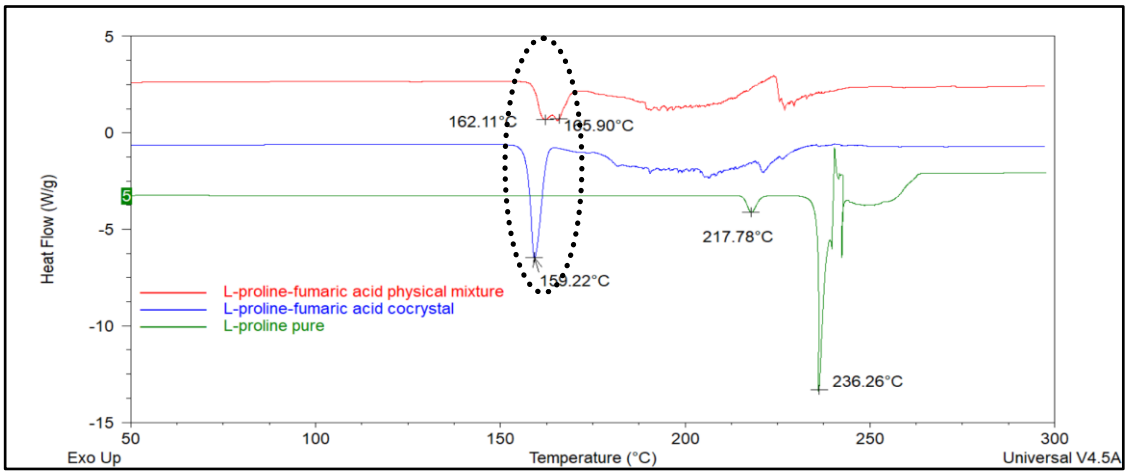

Figure 5.4 DSC thermograms of L-proline pure, L-proline-fumaric acid cocrystal and physical mixture (1:1)

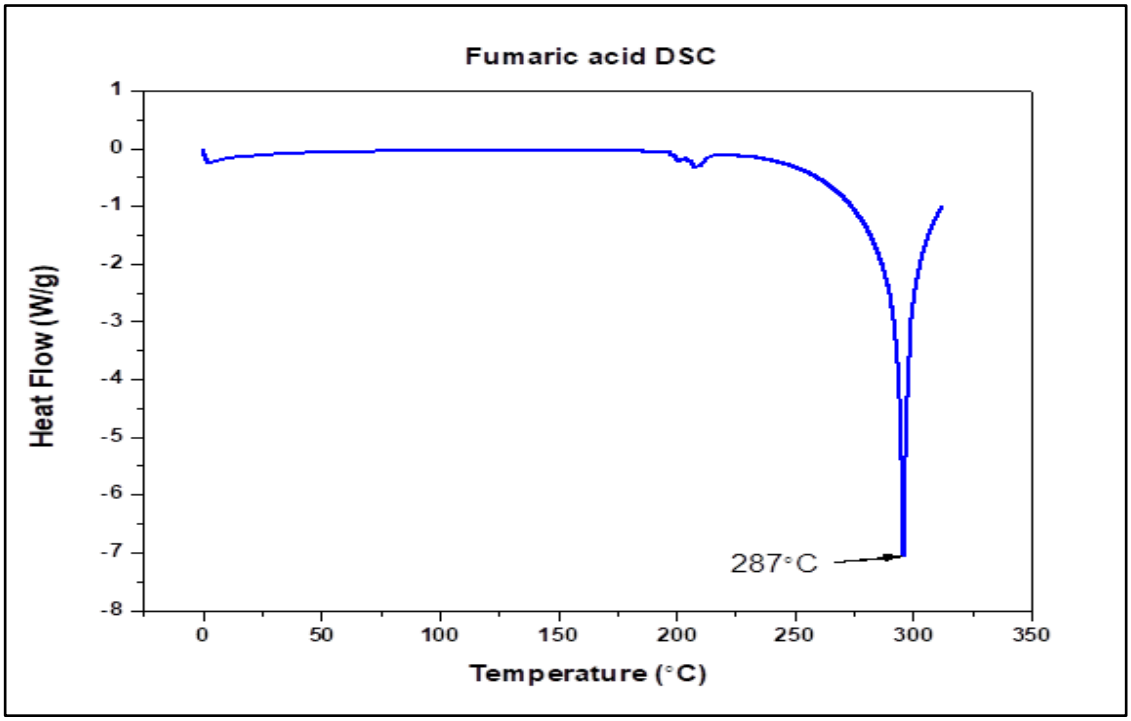

Figure 5.5 DSC thermogram of fumaric acid.

2.2 TGA analysis

TGA analysis was performed to check the onset of melting point and degradation patterns of starting materials, processed materials and their physical mixtures (n=3). Based on the data it is observed that the onset of melting for L-proline–fumaric acid cocrystal at 113.6°C is lower and different from that of onset melting points of both L-proline and fumaric acid or their physical mixture. The presence of single degradation event for cocrystal sample proves that single phase is generated.

The difference in onset melting and single degradation event of the LAG material suggests that there is new crystalline phase has occurred. The results of PXRD and DSC corroborate well with each other. See Figure 5.6.

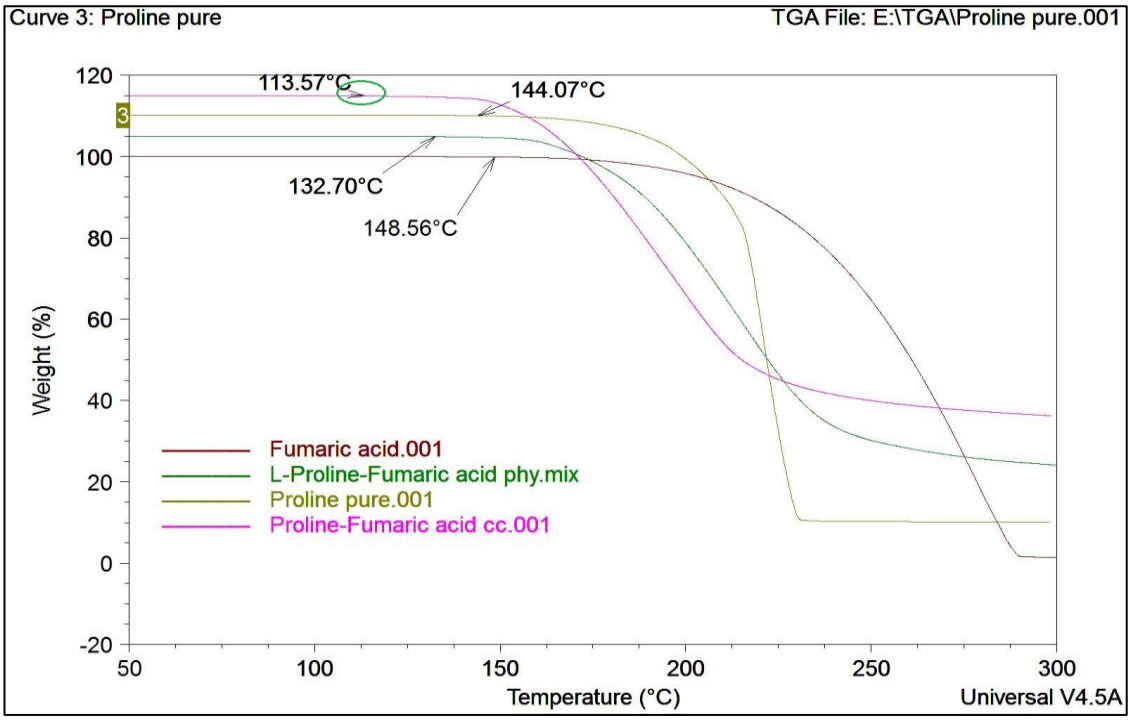

Figure 5.6 TGA of L-proline pure, fumaric acid pure, their physical mixture (1:1) material and L-proline-fumaric acid cocrystal.

3 DVS analysis

DVS analysis was performed to investigate the water uptake profile for L-proline-fumaric acid cocrystal compared to their starting material and physical mixture (n=3; s.d.≤ 0.03). Based upon the DVS profile the moisture absorption capability of L-proline in cocrystal phase with fumaric acid is drastically reduced compared to L-proline raw material and L-proline-fumaric acid physical mixture. Based on the tabular data in Table no 5.4 it is observed that L-proline-fumaric acid cocrystal did not absorb any moisture until 40% RH at 25°C which was further followed by negligible rise by 0.15% moisture uptake until 80%RH after which at 90% RH 81.17% moisture uptake occurred. In comparison with moisture absorption profile of L-proline raw 89.6%, moisture absorption took place at 80% RH followed by forming deliquescent material.

Thus, based on DVS data, upon cocrystallisation of L-proline with fumaric acid the water absorption capacity of L-proline is highly reduced or its stable in the presence of high moisture conditions. Figure 5.7 represents the DVS absorption profile of raw L-proline, a physical mixture of L-proline- fumaric acid and their cocrystal. The change in the water absorption of L-proline in its cocrystal state can be attributed to the hydrogen bond interactions with a carboxylic acid. This indicates that the cocrystallisation helps to reduce the hygroscopicity of L-proline.

Table 5.4 DVS of L-proline, fumaric acid with their physical mix and cocrystal

RH (%)	L-proline-fumaric acid cocrystal (dm/dt)	fumaric acid (dm/dt)	L-proline-fumaric acid physical mix (dm/dt)	L-proline pure (dm/dt)
0.0	0.00	0.00000	0.00	0.0
10.0	0.01	0.00248	0.00	0.0
20.0	0.02	0.00397	0.00	0.1
30.0	0.03	0.00459	0.01	0.2
40.0	0.00	0.00360	0.01	15.5
50.0	0.00	0.00385	0.01	15.7
60.0	0.03	0.00385	7.10	15.7
70.0	**0.07**	0.00497	**27.89**	**16.0**
80.0	0.15	0.00670	35.79	89.6
90.0	**81.17**	0.01217	**66.49**	**148.7**

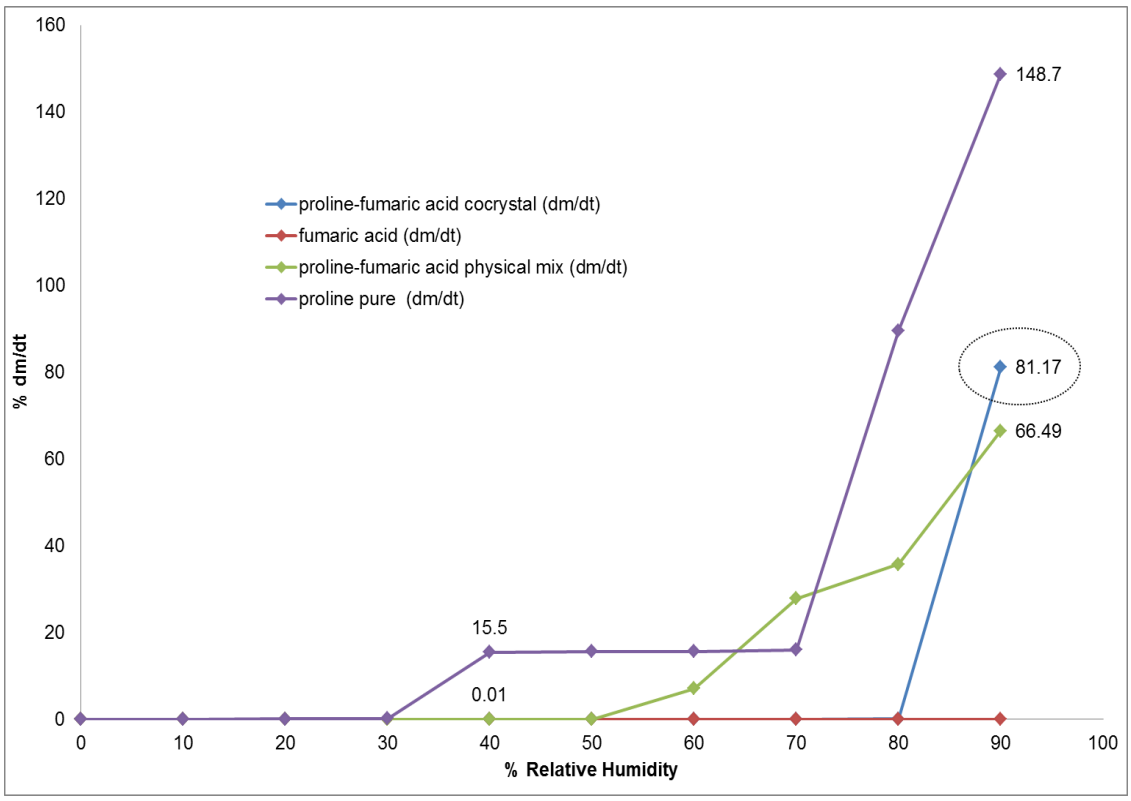

Figure 5.7 DVS of L-proline, fumaric acid and their physical mixture (1:1) and cocrystal.

4 Summary

Based on the PXRD and thermal data generation of L-proline-fumaric acid cocrystal was confirmed. Additionally, the stability of the cocrystal was described by generating comparative moisture absorption profile between L-proline-fumaric acid cocrystal and individual starting materials.

5.1.1.2 L-proline- adipic acid

1 PXRD

Below Figure no 5.8 represents the PXRD pattern of L-proline, adipic acid starting materials and L-proline-adipic acid cocrystal (n=3). The PXRD pattern reveals the absence of characteristic peaks of L-proline (12.5 2θ°) and adipic acid (15 2θ°) in L-proline-adipic acid cocrystal. Instead, a new characteristic peak at 10.88 2θ° angle is observed. This change in the PXRD pattern and generation of new peaks reveals the formation of new crystal phase.

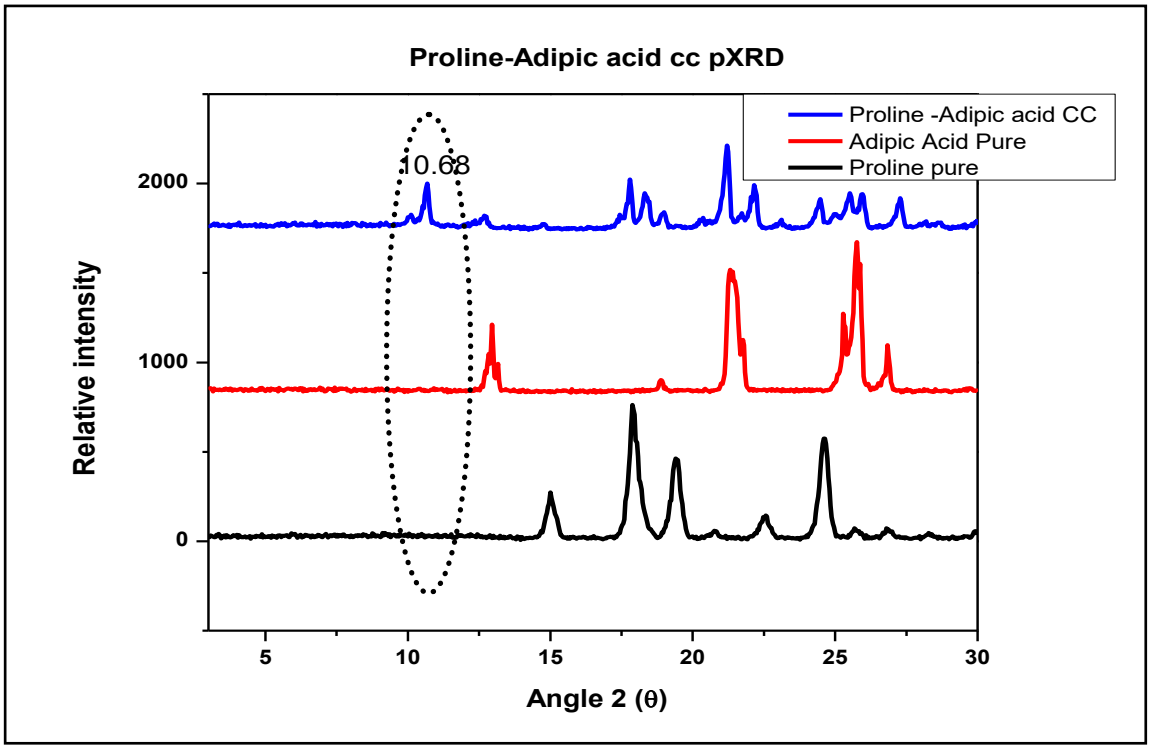

Figure 5.8 PXRD results of L-proline-adipic acid cocrystal

2 Thermal analysis

Thermal analysis was performed to investigate the melting endotherm and phase purity of cocrystal generated for the same.

2.1 DSC data

Below Figure 5.9 represents the DSC thermogram for starting materials of L-proline, adipic acid, physical mixture and processed cocrystal sample of L-proline-adipic acid (n=3). Based on the literature review the melting endotherm event for L-proline and adipic acid is observed at 121°C (Ash and Ash 2006) and 151-154°C (Batisai et al. 2014) respectively. On analysing processed L-proline-adipic acid sample single distinct endotherm was observed at 120.56°C, this endotherm is different when compared to raw material melting endotherms. Thus, it can be concluded that new phase is generated which can be correlated to cocrystal formation. The melting endotherm event observed at 116°C could be a hydrate or solvate formation or may be a solid to solid transition but need

to confirm. The absence of an endothermic event in between 80-110°C reveals that there is no bound or unbound solvent molecule. The physical mix of both showed endotherm at 123.28°C.

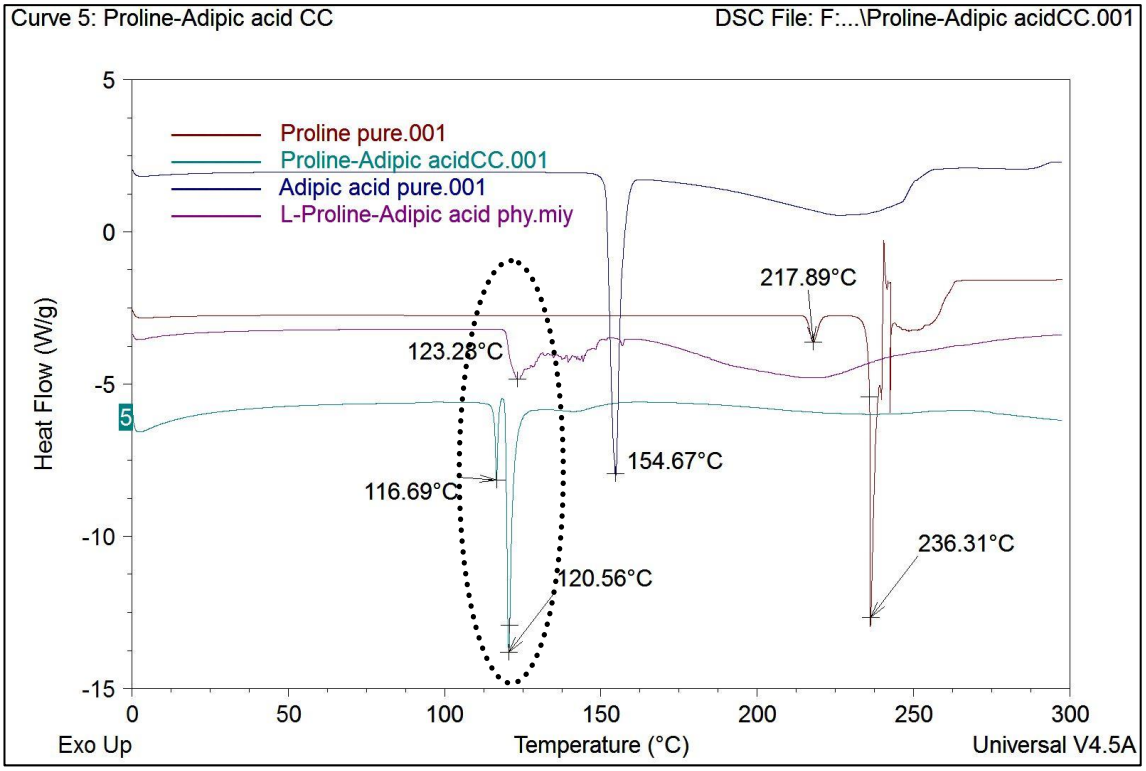

Figure 5.9 DSC of L-proline, adipic acid and their cocrystal and physical mixture (1:1).

2.2 TGA data

TGA analysis was performed for starting materials, their physical mixtures and processed samples (n=3). Based on TGA thermogram the onset of melting event for L-proline-adipic acid cocrystal is different compared to individual components (refer Figure 5.10). L-proline-adipic acid onset melting started at 105.82°C compared to melting event of L-proline at 144.67°C and adipic acid at 120.11°C. The single degradation event suggests that the obtained material is single phase.

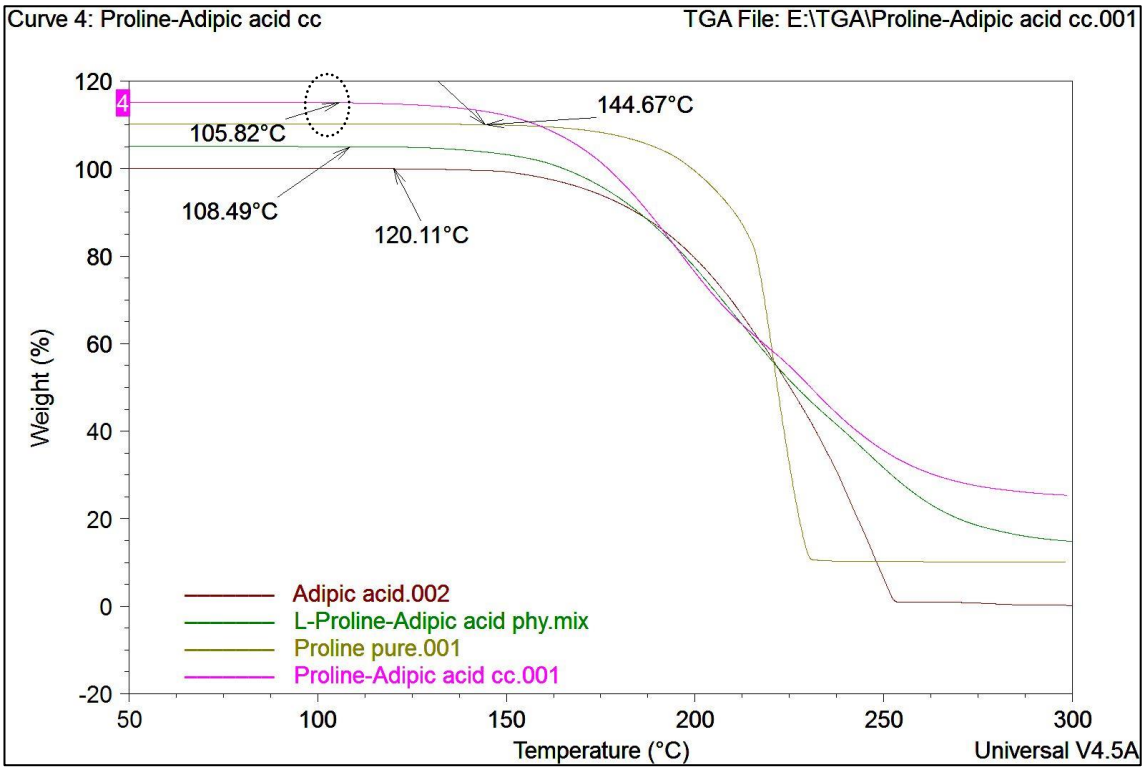

Figure 5.10 L-proline - adipic acid co-crystal TGA with L-proline, adipic acid and their physical mixture (1:1).

3 DVS data

The moisture absorption profile of L-proline, adipic acid, physical mixtures and cocrystal was evaluated using DVS analyser (n=3; s.d.≤ 0.03). Based on the data (refer Table 5.5) it is revealed that cocrystal of L-proline and adipic acid water absorption capacity is negligible until 80%RH compared to L-proline as starting material (89.6%). As adipic acid is non-hygroscopic, it did not absorb any moisture. Below is the Table 5.5 percent moisture uptake of raw, physical mixture and processed samples of L-proline and adipic is reported against percent RH and after that represented pictographically in Figure 5.11.

Table 5.5 DVS of L-proline, adipic acid and their physical mix and cocrystal.

RH (%)	L-proline-Adipic acid cocrystal (dm/dt)	Adipic acid (dm/dt)	L-proline-Adipic acid physical mix (dm/dt)	L-proline pure (dm/dt)
0.0	0.00	-0.00009	0.00	0.0
10.0	0.01	0.00214	0.00	0.0
20.0	0.01	0.00250	0.00	0.1
30.0	0.01	0.00161	0.00	0.2
40.0	0.02	0.00402	0.01	15.5
50.0	0.02	0.00500	0.01	15.7
60.0	0.03	0.00705	5.50	15.7
70.0	**0.04**	0.00937	**20.85**	**16.0**
80.0	0.12	0.01178	19.71	89.6
90.0	**70.66**	0.01795	**48.88**	**148.7**

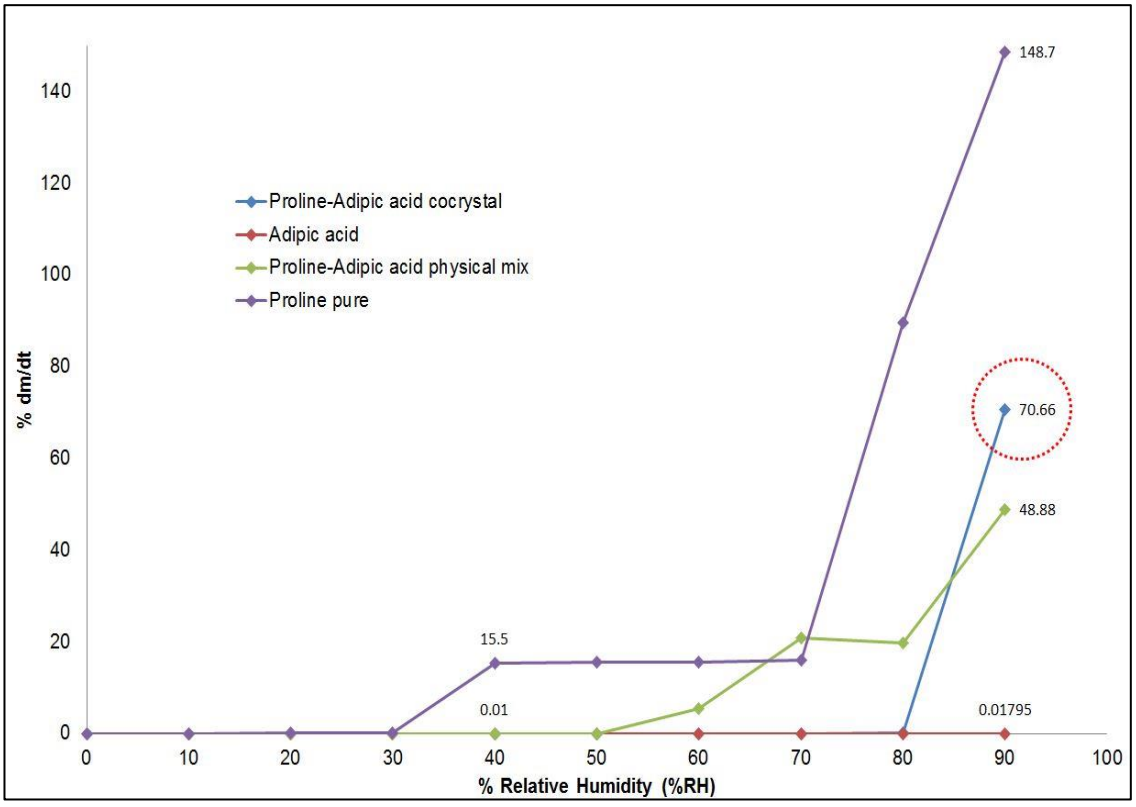

Figure 5.11 DVS of L-proline, adipic acid and their cocrystal and physical mixture (1:1).

4 Summary

These studies suggest that there is the formation of cocrystal between L-proline-adipic acid and it confirms with the PXRD crystalline phase pattern and DSC results. Additionally, it is supported by TGA studies. This study also supports the L-proline-fumaric acid study, that the cocrystallisation can improve the hygroscopicity of the molecules like L-proline. In the current study total, 52.48% reduction in the hygroscopicity of L-proline was observed after cocrystallisation with adipic acid.

5.1.1.3 L-proline-succinic acid

1 PXRD

L-proline- succinic acid in 1:1 stoichiometric ratio was processed using liquid assisted grinding (n=3). The PXRD analysis was performed to check generation of new crystal peaks. Below Figure 5.12 describes the PXRD data for raw and processed samples of L-proline and succinic acid. PXRD patterns displayed that L-proline and succinic acid retains their characteristic peaks at 15, 17.88 2θ° angle and 26.5 2θ° angle respectively. In LAG sample of L-proline-succinic acid new characteristic peaks are observed at 9 and 13.8 2θ° angle which are not present in starting materials of L-proline and succinic acid. This change in the PXRD pattern and generation of new peaks reveals the formation of new crystal phase.

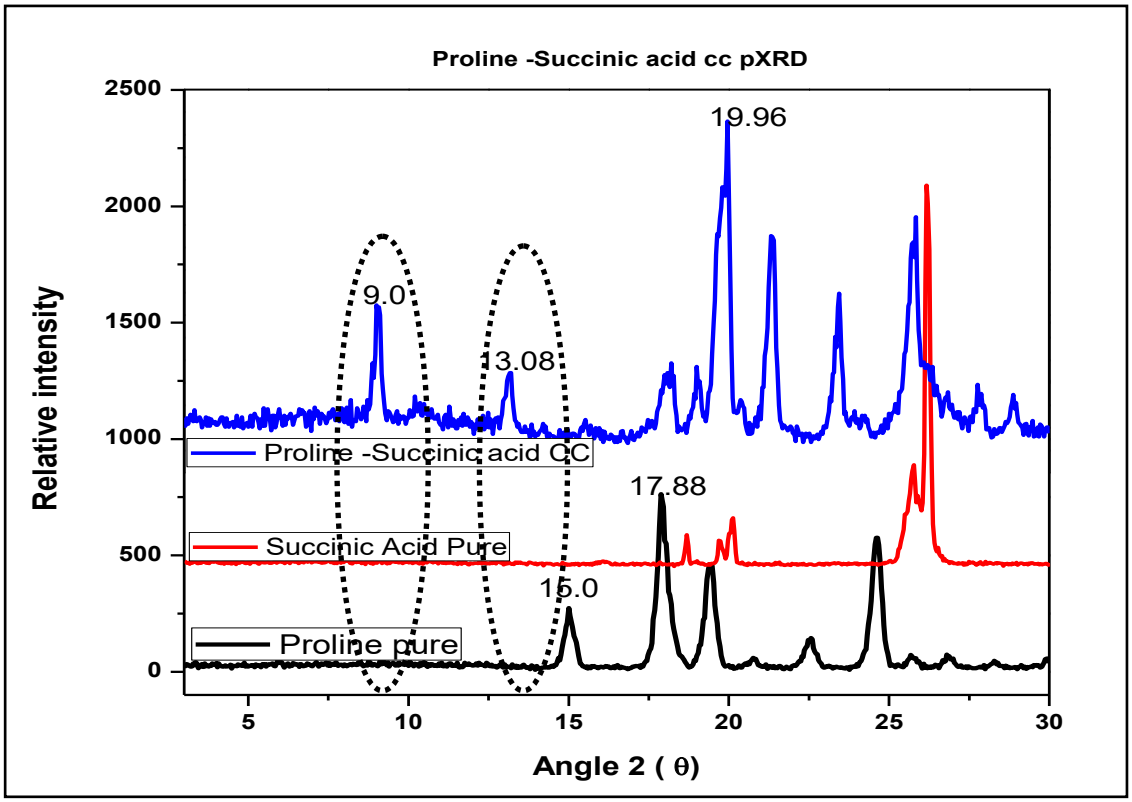

Figure 5.12 PXRD results of L-proline-succinic acid cocrystal

2 Thermal analysis

2.1 DSC data

The DSC analysis of the L-proline, succinic acid raw materials, their physical mix and LAG processed sample was carried out 3 times (Figure 5.13). DSC thermogram of L-proline-succinic acid reveals a distinct characteristic endothermic peak at 115.55°C, which is different from the melting events of individual starting materials. This correlates with the melting peak observed in the physical mix DSC analysis of the L-proline and succinic acid. As per the PubChem records, the melting point of L-proline is 121°C (Ash and Ash 2006), and a melting point of succinic acid is 185-190°C (Soewandhi). Based on the DSC data new crystal phase of L-proline-succinic acid is generated, similar results were also observed in the PXRD analysis

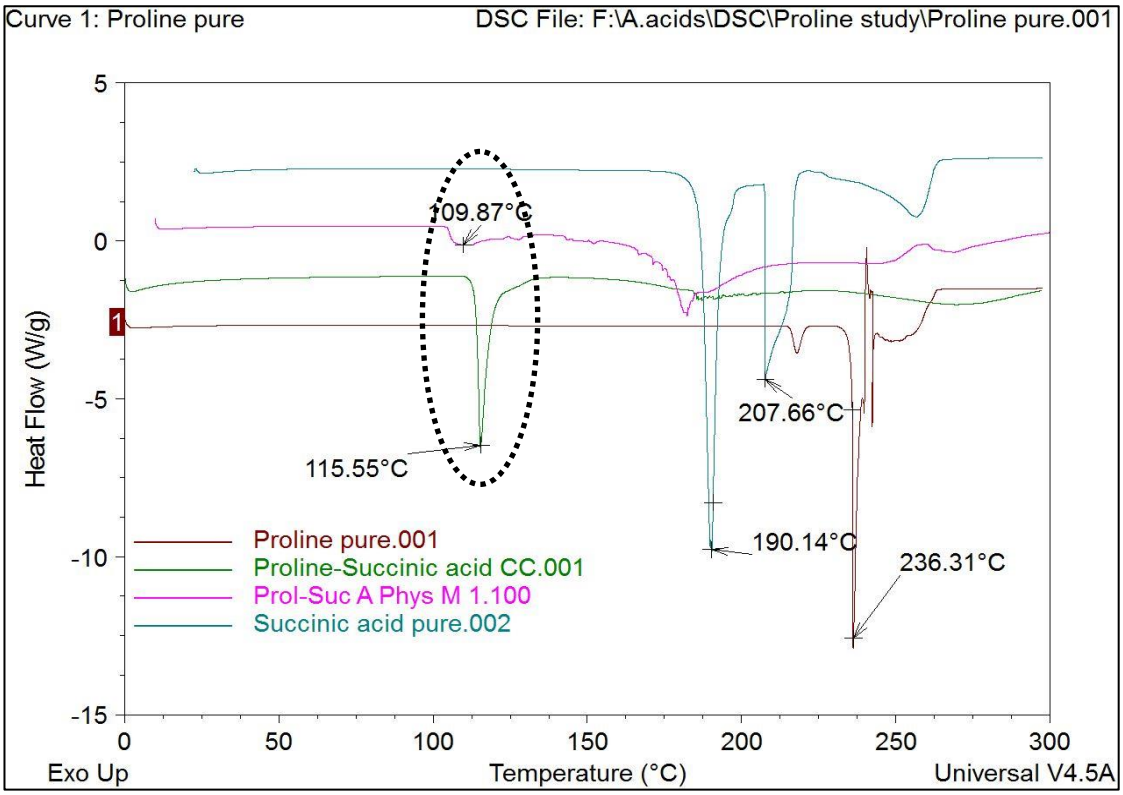

Figure 5.13 DSC of L-proline, succinic acid and their cocrystal and physical mixture (1:1).

2.2 TGA data

In the thermogravimetric analysis (Figure 5.14) of the L-proline-succinic acid cocrystal (n=3), it was observed that the onset melting pattern of the material is different from that of the starting material. The cocrystal material onset melting start point observed at 97.10°C temperature. However, the L-proline showed onset melt at 144.67°C temperature. The succinic acid showed onset melt at 111.39°C. The difference in the onset melting pattern and single phase degradation pattern indicates the new crystalline phase formation and absence of impurities.

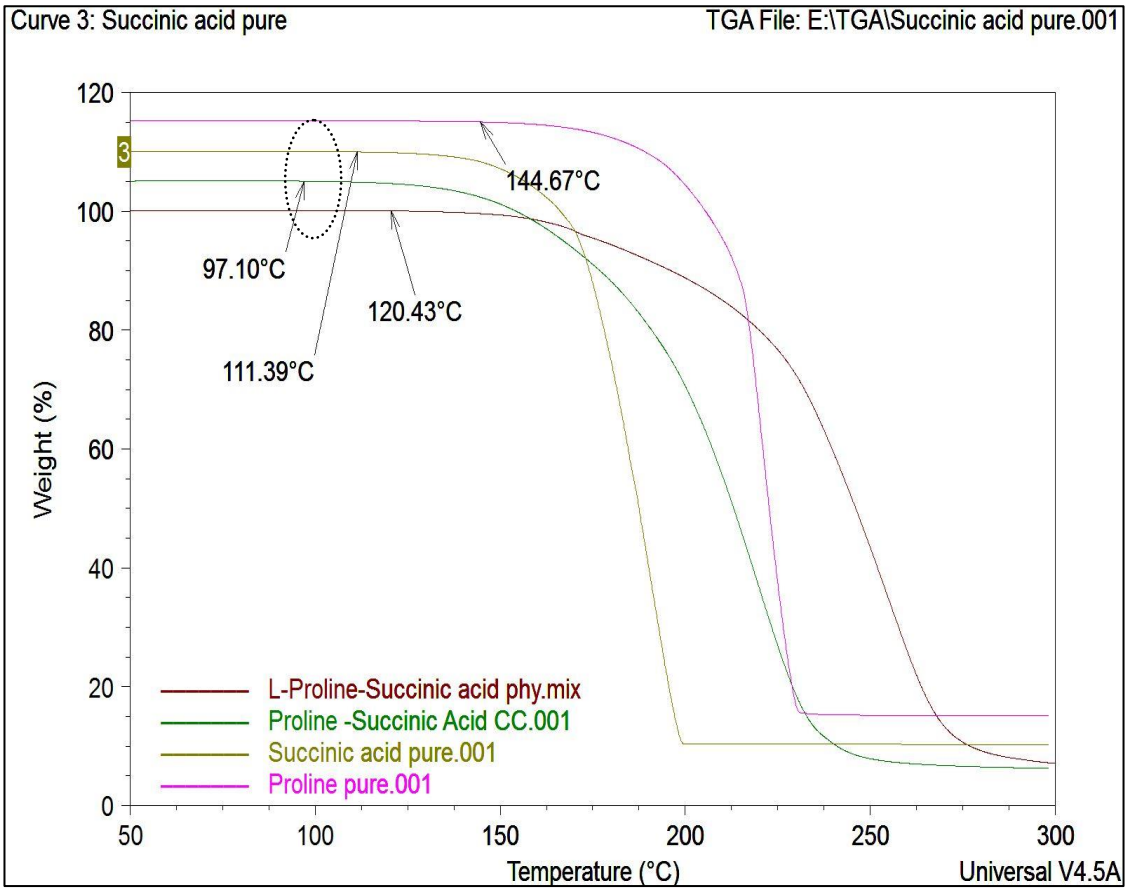

Figure 5.14 TGA of L-proline, succinic acid and their cocrystal.

3 DVS data

Absorption profile of L-proline, succinic acid raw materials, physical mixture and cocrystal was generated using DVS analyser (n=3; s.d.≤ 0.03). Below Table 5.6 reveals that L-proline-succinic acid cocrystal displayed very negligible moisture absorption until 80%RH followed by an increase in the moisture absorption profile. Negligible moisture absorption was observed in case of succinic acid as it is non-hygroscopic. L-proline, as it is hygroscopic, 15.70% absorption was observed at 80% RH followed by 148.70% absorption at 90%RH turning it into deliquescent.

This states that the hygroscopic property of L-proline is minimised by preparing cocrystal of L-proline and succinic acid. Below Figure 5.15 represents the

graphical representation of absorption profile of individual starting material, physical mixture and end cocrystal product.

Table 5.6 DVS of L-proline-succinic acid and their cocrystal and physical mixture (1:1).

RH (%)	Succinic acid (dm/dt)	L-proline-Succinic acid physical mix (dm/dt)	L-proline-Succinic acid CC (dm/dt)	L-proline pure (dm/dt)
0.0	0.0001	0.00	0.00	0.0
10.0	-0.0001	0.00	0.01	0.0
20.0	0.0011	0.00	0.00	0.1
30.0	0.0018	0.01	0.00	0.2
40.0	0.0014	0.01	0.00	15.5
50.0	0.0026	0.02	0.01	15.7
60.0	0.0045	4.76	0.03	15.7
70.0	0.0083	**16.52**	**1.83**	**16.0**
80.0	0.1002	24.87	44.12	89.6
90.0	0.5149	**42.96**	**80.78**	**148.7**

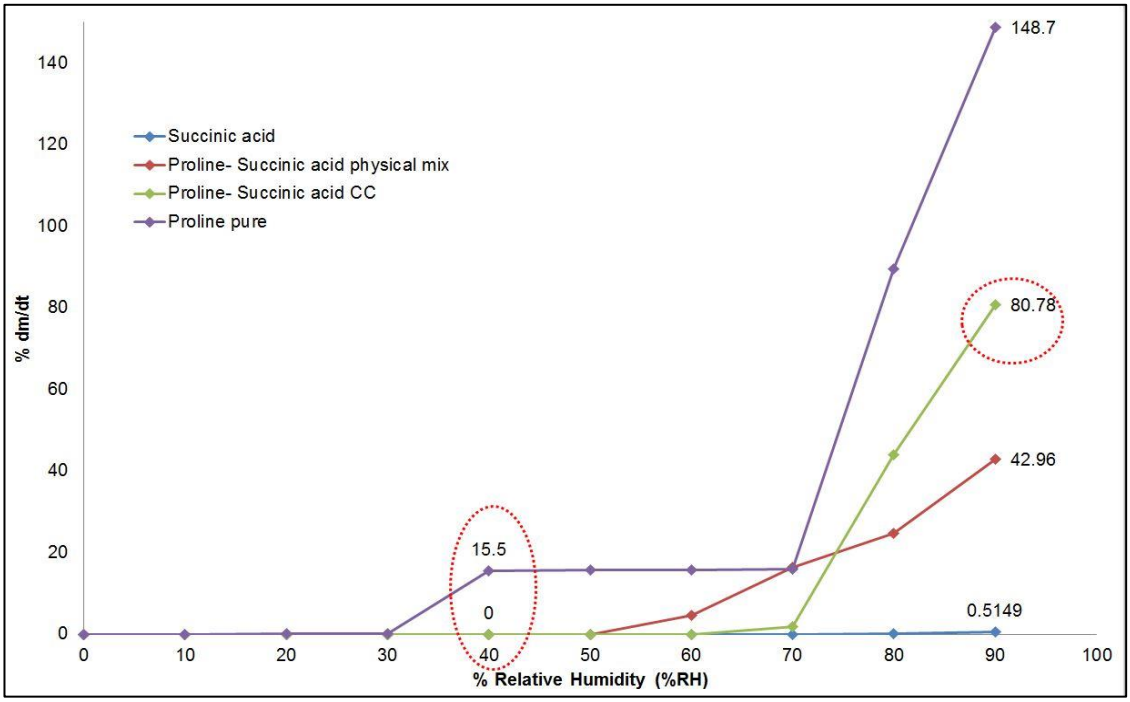

Figure 5.15 DVS of L-proline, succinic acid and their cocrystal and physical mixture (1:1).

4 Raman spectroscopy data

Raman spectroscopic analysis was performed to elucidate further the formation of bonding between L-proline and succinic acid cocrystal produce using liquid assisted grinding (n=3).

Raman spectroscopy analysis of L-proline-succinic acid co-crystal reveals that there was no salt formation occurred. It means that there may be the formation of a co-crystal. If there had been a salt formation, then the primary amine salts absorption of $-NH3^{+}$ would have been in the region of $3350cm^{-1}$ and $3100cm^{-1}$ of Raman shift. However, in this case, no such bands were observed. The Amines with $>NH2^{+}$ and $C=NH^{+}$ would have been absorbed in between $2700\text{-}2250cm^{-1}$ Raman shift (Larkin 2017). However, no such bands/peaks were observed. It means that the obtained material is co-crystal of L-proline and succinic acid (1:1). It has been supported by the PXRD and DSC data of the same. See the Figure 5.16.

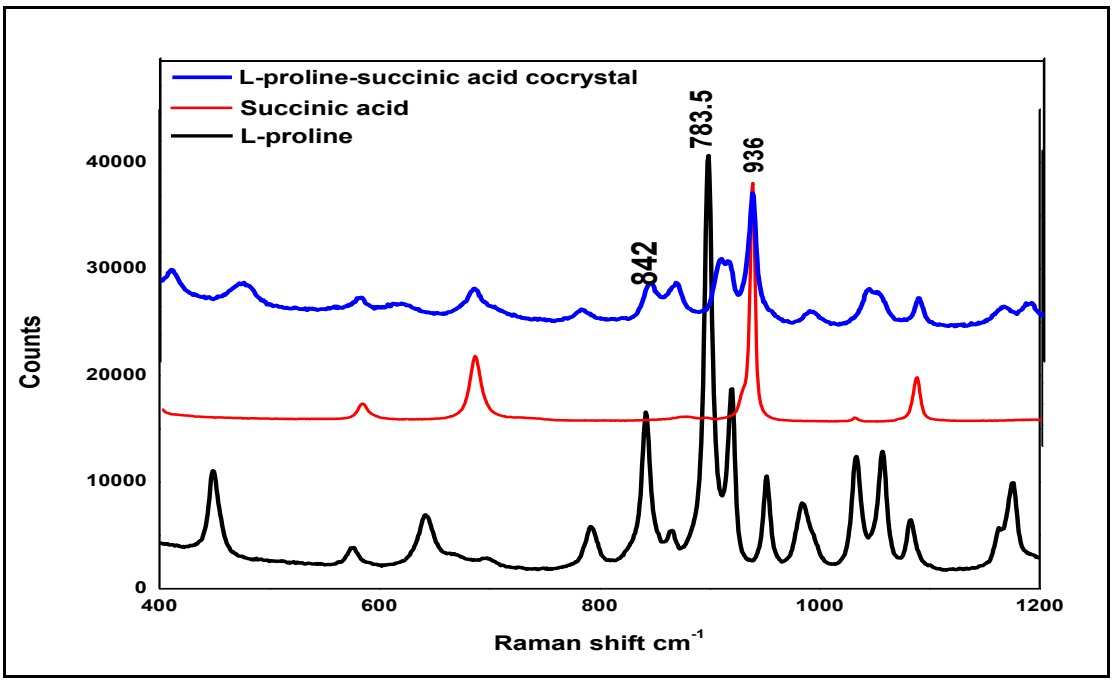

Figure 5.16 Raman spectrograph of L-proline-succinic acid cocrystal with starting material.

5 Summary

The cocrystal process of L-proline with carboxylic acids was carried out for all the powdered samples out of which L-proline failed to generate cocrystals with citric and tartaric acid and successfully generated cocrystal with fumaric, adipic and succinic acid. Cocrystallisation of L-proline and fumaric acid was already explored by Tilborg *et al*. in 2013. New crystalline phase was observed in all the L-proline-carboxylic acid cocrystal pairs which were further supported by thermal data. The hygroscopic property of L-proline had decreased considerably in all the cocrystal pairs compared to L-proline as starting material.

5.2 L-proline and non-steroidal anti-inflammatory drugs (NSAIDs) cocrystallisation

Based on the hydrogen bonding capability of L-proline, we have further explored the cocrystal formation between L-proline and different active pharmaceutical ingredients. Recently, Shimpi and group have reported the cocrystallisation of L-proline molecule with certain imidazole and ezetimibe categorised active components (Shimpi *et al*. 2014). Tilborg and group have recently published the cocrystallisation of L-proline with different profen groups of NSAID (Tilborg *et al.* 2014). Thus, based on the previous studies we have selected different API molecule which belong to NSAID group such as ibuprofen, flurbiprofen, ketoprofen and aspirin. Both L-proline and NSAID were selected in 1:1 molar stoichiometric ratio and further cocrystals screening were done using liquid assisted grinding technique.

5.2.1 Characterisation studies of L-proline- NSAIDs co-crystals

1 PXRD

Different characterisation studies using PXRD and thermal analysis were performed to reveal the formation of cocrystals with amino acids.

1.1 L-proline - aspirin

The LAG processed sample of L-proline-aspirin and L-proline, aspirin original samples were analysed using PXRD analyser to investigate the crystal phase (n=3). In the following Figure 5.17, it is observed that new characteristic crystalline phase peaks at 5.4 2θ° and 11.2 2θ° are observed in L-proline-aspirin 1:1 ratio LAG sample. The PXRD pattern of the L-proline-aspirin sample is completely different from individual starting material as the characteristic peaks of L-proline at 15 2θ° and aspirin at 15.5 2θ° are absent in the PXRD pattern of L-proline-aspirin processed sample. This change in the PXRD pattern and generation of new peaks reveals the formation of new crystal phase.

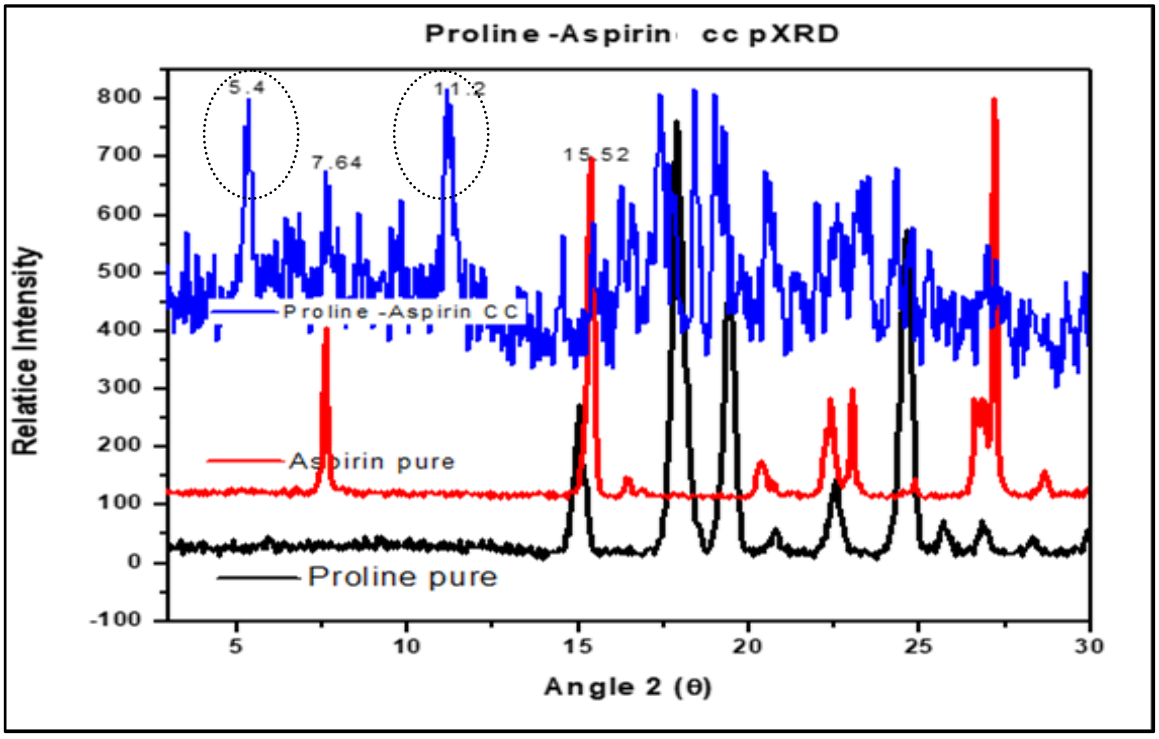

Figure 5.17 PXRD of L-proline- aspirin LAG (1:1) sample with starting material

1.2 L-proline-flurbiprofen

The Figure no. 5.18 represents the PXRD pattern of L-proline, flurbiprofen starting material and L-proline-flurbiprofen 1:1 LAG sample (n=3). The PXRD pattern reveals the formation of new characteristic peaks at 8.2,14.8 and 18.64 2θ°values. However, the strong characteristic peaks of L-proline from 15,18 and 19 2θ° and of aspirin from 7.5, 11.5, 21 and 23 2θ° values are absent in the newly formed crystalline phase. It indicates that there is new crystal phase formed.

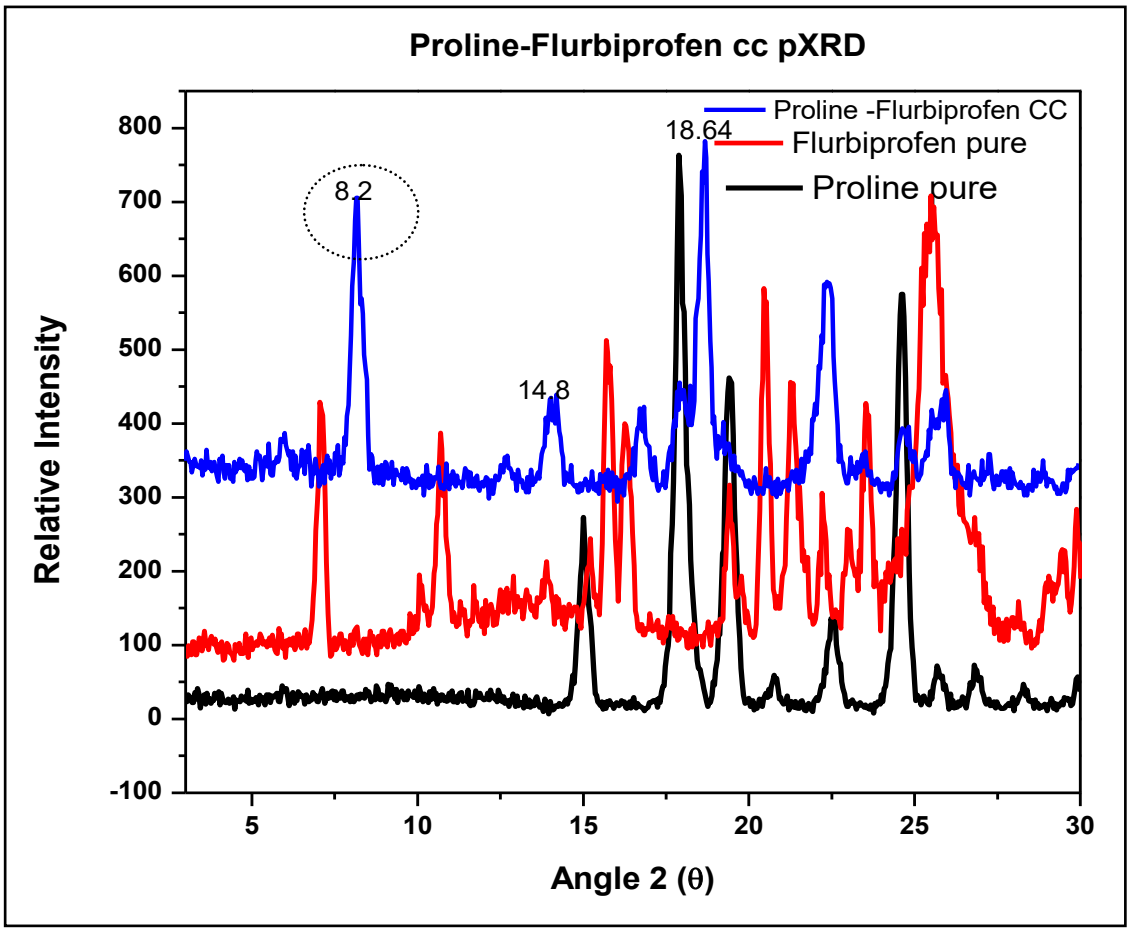

Figure 5.18 PXRD of L-proline-flurbiprofen LAG (1:1) sample with starting material

1.3 L-proline – ketoprofen PXRD results

The LAG processed sample of L-proline-ketoprofen and starting material samples were analysed using PXRD analyser to investigate the crystal phase

(n=3). In the following Figure 5.19, it is observed that new characteristic crystalline phase peaks at 8.12, 24.76 2θ° angle and 25.88 2θ° angle are observed in L-proline-ketoprofen 1:1 ratio LAG sample. The PXRD pattern of the L-proline-ketoprofen sample is completely different from individual starting material as the characteristic peaks of starting materials are absent in the newly developed crystalline phase sample. This change in the PXRD pattern and generation of new peaks reveals the formation of new crystal phase.

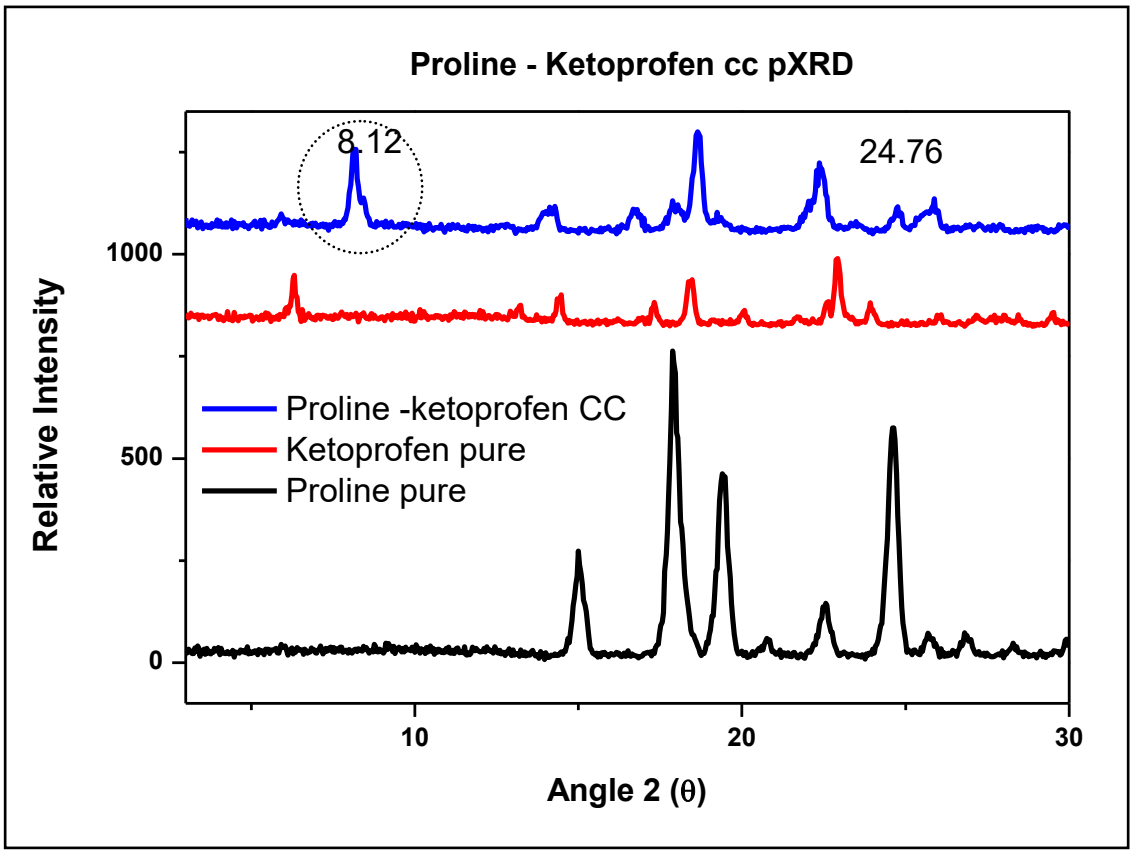

Figure 5.19 PXRD of L-proline-ketoprofen 1:1 LAG sample with starting material

1.4 L-proline – Ibuprofen PXRD results

The PXRD analysis of the L-proline-ibuprofen 1:1 LAG sample along with starting material was performed using Bruker D8 PXRD analyser to investigate the crystal phase (n=3). (Figure 5.20) Through this PXRD analysis, it was

observed that there are two characteristic peaks were generated at 4.12 and 5.12 2θ° values in the L-proline-ibuprofen LAG sample. These two peaks are absent in the original starting material. Original L-proline peak at 15 2θ° and that of ibuprofen at 6.092θ° values are absent in the newly formed crystal phase. This change in the PXRD pattern and newly generated peaks indicate the formation of new crystal phase. While working on these NSAIDs and amino acids co-crystal, similar kind of work was published by Othman (Othman *et al.* 2016). The PXRD pattern of L-proline-ibuprofen 1:1 LAG sample is correctly coinciding with the reported PXRD pattern by Othman.

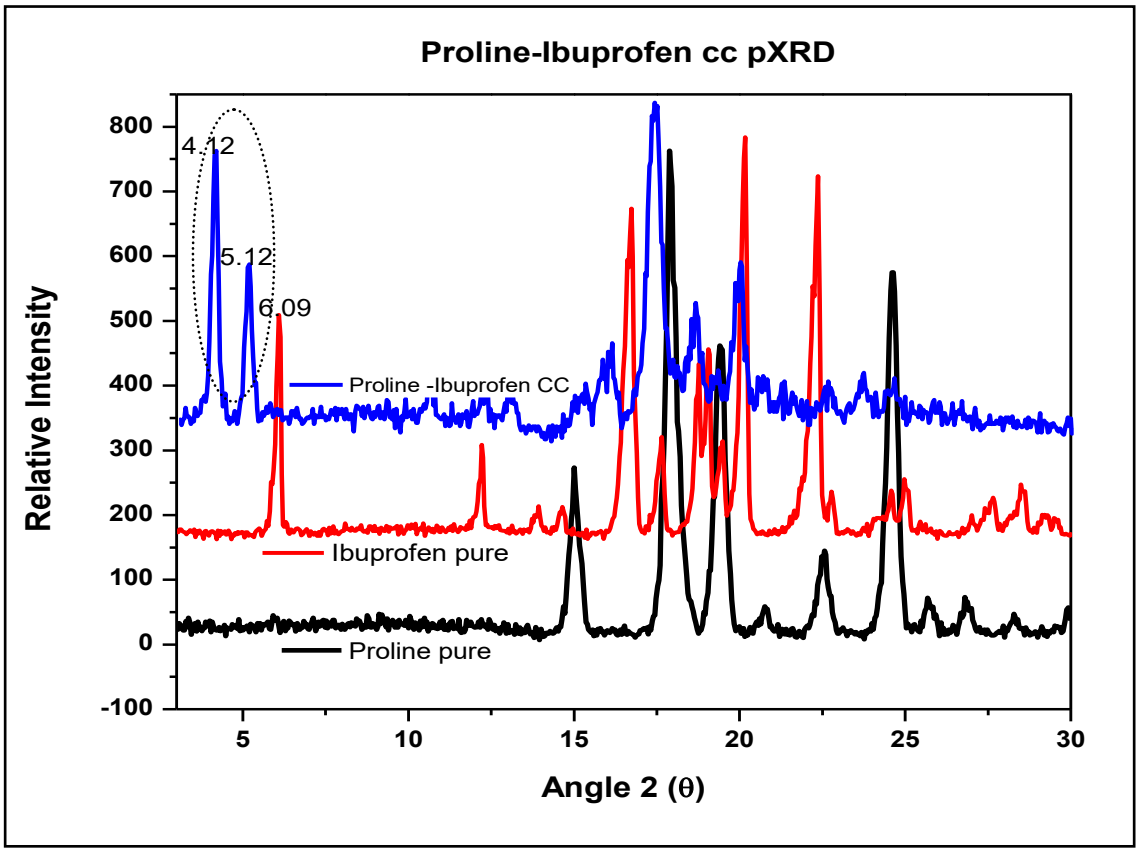

Figure 5.20 PXRD of L-proline- ibuprofen 1:1 LAG sample with starting material

2 DSC

Table 5.7 describes the DSC thermograms of starting materials and processed samples of L-proline and NSAIDs (n=3). Based on the presence of the melting

endotherms of L-proline and NSAIDs used in 1:1 LAG sample it is observed that single distinct melting endotherm followed by degradation was observed for the processed samples of L-proline-NSAIDs (Figure 5.21). This melting endotherm is different from the melting event of L-proline (221°C) (Ash and Ash 2006; Hautala et al. 2016). The melting point of ibuprofen is at 74.45°C and ketoprofen is at 92.85°C (Xudong and Capomacchia 2010).The flurbiprofen has shown the melting point at 116°C (Varma and Pandi 2005) and aspirin melting point is at 135°C (Huang et al. 2005). Based on the previous studies the melting endotherm of L-proline-ibuprofen (Othman et al. 2016) rightly matches with the cocrystal phase.

Table 5.7 Melting points of L-proline and NSAIDs with their 1:1 LAG samples.

Sr.No.	Name of Compound/Drug	Melting point (°C)
1	L-proline pure	221
2	Aspirin	135
3	Flurbiprofen	116
4	Ketoprofen	92.9
5	Ibuprofen	74.5
6	L-pro-asp (1:1) LAG sample	86.4
7	L-pro-flurb (1:1) LAG sample	150.7
8	L-pro-keto (1:1) LAG sample	63.1
9	L-pro-ibu (1:1) LAG sample	111.5

L-pro=L-proline, asp=aspirin, flurb=flurbiprofen, keto=ketoprofen and ibu=ibuprofen.

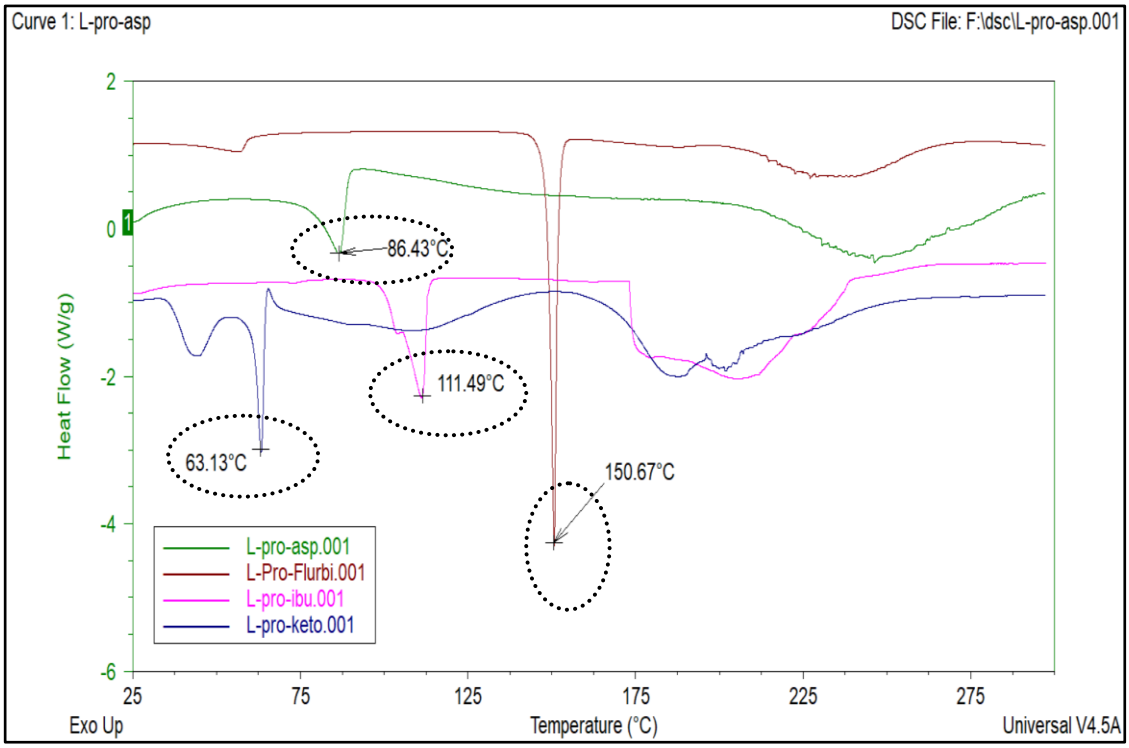

Figure 5.21 DSC thermogram of L-proline-NSAIDs and their 1:1 LAG samples.

3 Summary

Amino acid L-proline was screened for cocrystallisation development with the NSAIDs molecules. Total four drugs were screened under this experimental study.

The DSC and PXRD characterisation study results were promising for the consideration as a new cocrystal formation. After careful observation of the difference in the melting points of cocrystals with their original starting materials one can assume that the cocrystals are changing their physicochemical properties. Such as, aspirin melting point is 135°C and its cocrystal showed melting point around 86.43°C, mean it could be more soluble form of aspirin. Similarly, ketoprofen has melting point as 92.85°C and its cocrystal with L-proline has melting point around 63.13°C, means it may be more soluble than

the original ketoprofen. However, in the case of ibuprofen and flurbiprofen, it is reverse. These both cocrystals showed more melting points than their pure forms. During this study, the similar work was published by Othman *et al.* (Othman *et al.* 2016). This work was could not go further. However, it could be possible to explore in future.

5.3 Citric acid – amino acids cocrystallisation

Based on the application of amino acid in the formation of molecular bonding with organic molecules we have selected citric acid as model component and explored the possibility of cocrystallisation with different amino acid molecules. Citric acid is widely used an organic molecule in pharmaceutical and food industry. The use of citric acid is limited due to its hygroscopic nature which on exposure to higher moisture conditions, readily absorbs moisture and loses its structural integrity.

Initially, to understand the moisture absorption profile of citric acid we have performed DVS analysis for citric acid only (n=3). Below Figure 5.22 reveals the DVS isotherm of citric acid, it demonstrates that it is stable until 70% RH followed by drastic absorption of moisture and forming deliquescence.

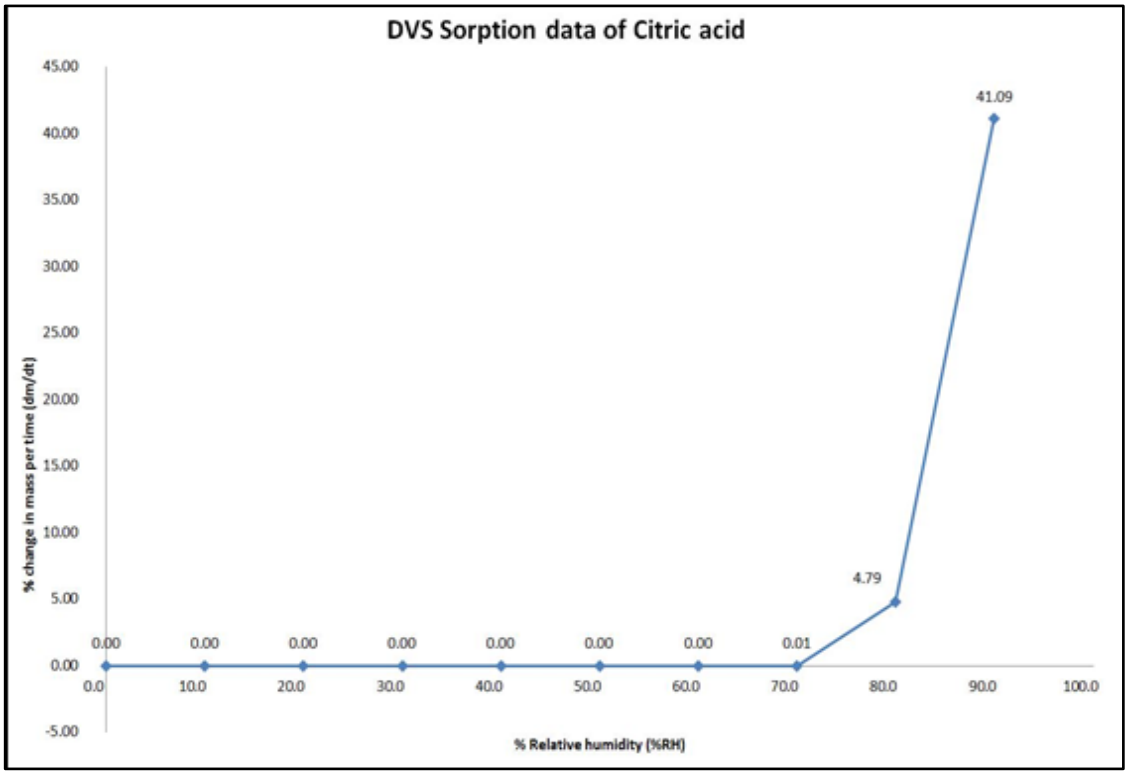

Figure 5.22 DVS of citric acid

In all the experiments of citric acid and amino acids, they were accurately weighed in 1:1 stoichiometric ratio and ethanol was used as the solvent system for liquid assisted grinding (n=3;s.d.≤ 0.03). Table 5.8 reveals the experimental data.

Table 5.8 Screening of amino acids co-crystals with citric acid.

Sr. No.	Molecules selected	Molar ratio	Solvent Liquid	Obtained material phase	PXRD	DSC	DVS	Raman	FT-IR
1	L-Alanine: citric acid	1:1	H_2O/EtOH	sticky	x	x	X	x	x
2	L-proline: citric acid	1:1	H_2O/EtOH	sticky	x	x	X	x	x
3	L-Valine: citric acid	1:1	H_2O/EtOH	sticky	x	x	X	x	x
4	L-Leucine: citric acid	1:1	H_2O/EtOH	Dry, free flow	✓	✓	✓	✓	✓
5	L-Isoleucine: citric acid	1:1	H_2O/EtOH	Dry, free flow	✓	✓	✓	✓	✓
6	L-Phenylalanine: citric acid	1:1	H_2O/EtOH	sticky	x	x	X	x	x
7	L-Serine: citric acid	1:1	H_2O/EtOH	Dry, free flow	✓	✓	✓	✓	✓
8	L-Threonine: citric acid	1:1	H_2O/EtOH	sticky	x	x	X	x	x
9	L-Asparagine: citric acid	1:1	H_2O/EtOH	sticky	x	x	X	x	x
10	L-Aspartate: citric acid	1:1	H_2O/EtOH	sticky	x	x	X	x	x
11	L-Arginine: citric acid	1:1	H_2O/EtOH	sticky	x	x	X	x	x
12	L-Histidine: citric acid	1:1	H_2O/EtOH	sticky	x	x	X	x	x
13	L-Methionine: citric acid	1:1	H_2O/EtOH	Dry, free flow	✓	✓	✓	✓	✓
14	L-lysine: citric acid	1:1	H_2O/EtOH	sticky	x	x	X	x	x
15	L-Tryptophan: citric acid	1:1	H_2O/EtOH	sticky	x	x	X	x	x
16	L-Glutamate: citric acid	1:1	H_2O/EtOH	sticky	x	x	X	x	x
17	L-Cysteine: citric acid	1:1	H_2O/EtOH	Dry, free flow	✓	✓	✓	✓	✓

✓ = selected for characterisation x = not selected

Based on the above experimental data, citric acid has failed to generate any cocrystal phase with 12 of the amino acids; this may be due to the molecular structure of the amino acids or binding affinity of citric acid with amino acids. Only five amino acids successfully generated cocrystals with citric acid.

They are namely citric acid - L-leucine, citric acid - L-isoleucine, citric acid - L-serine, citric acid - L-methionine, and citric acid - L-cysteine. These five samples were further examined for characterisation.

5.3.1 Citric acid - L- leucine study

1 PXRD data:

Based on the PXRD data it was observed that new peaks at 6.68, 18.68 and 19.64 2θ° were observed for citric acid-L-leucine processed samples (n=3). Citric acid and L-leucine amino acid pattern displayed characteristic peaks at 15 and 6.1 2θ° respectively. These characteristic peaks of individual components were absent in citric acid-L-leucine processed samples. Instead, generation of new peaks were detected. Thus, PXRD pattern indicates the formation of a new crystalline complex which is different from starting material. Below Figure 5.23 represents the PXRD pattern for citric acid, L-leucine starting materials and their processed samples.

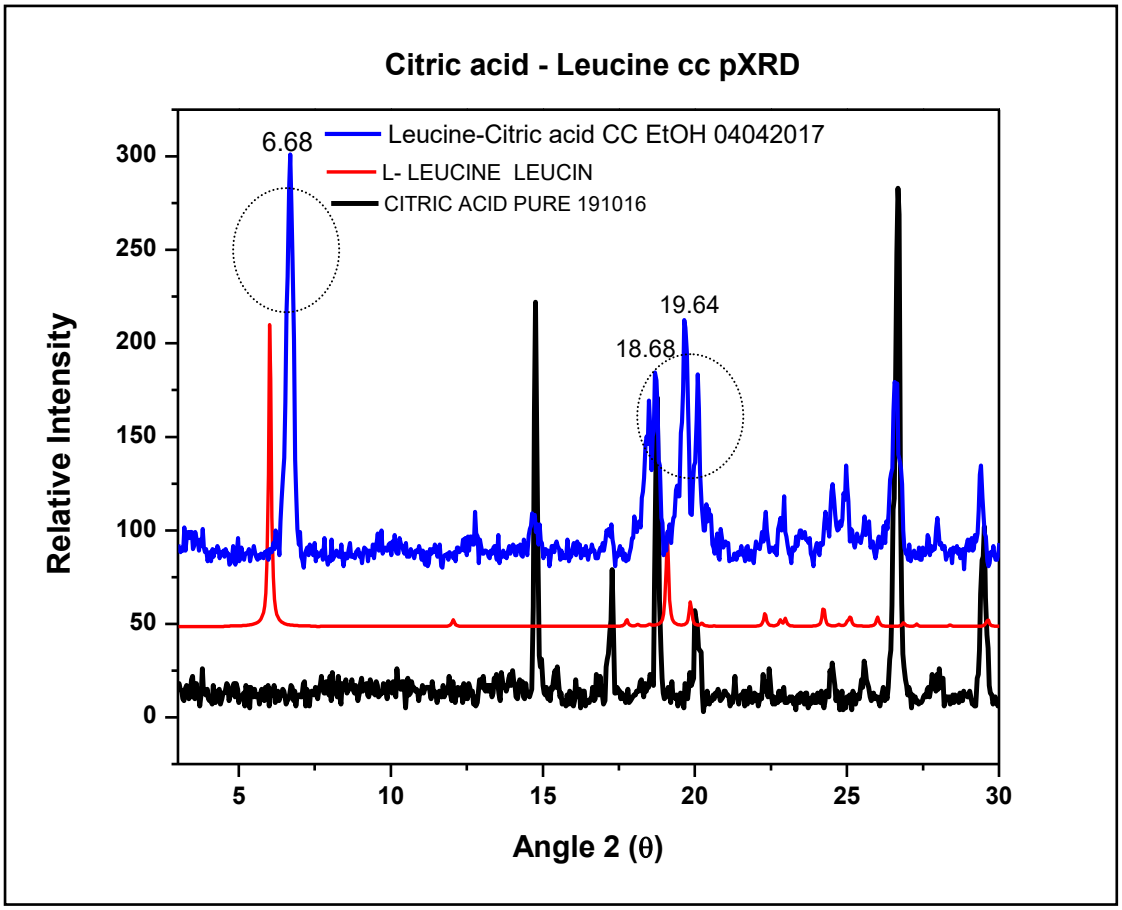

Figure 5.23 PXRD of citric acid, L-leucine starting material and their LAG processed material

2 DSC data

Based on the literature review and experimental data, the citric acid melting point is 153°C (Barbooti and Al-Sammerrai 1986; NCBI 2018a) and the leucine melting point is 293°C (NCBI 2017b). (See-Figure 5.24). In the DSC thermograms of citric acid-leucine LAG material (n=3), it was observed that there is single endothermal melting point showed at 126.20°C, which is different from the original starting material melting points. Which might be suggest that this product will be highly soluble than the starting material. It correlates with its DVS studies, where it absorbs more moisture and become deliquescent. It indicates that there may be a cocrystal formation occurred between leucine and citric acid. As there was no endothermic event observed in the region between

80 to 110°C no bound or unbound residual solvent is present in the final sample.

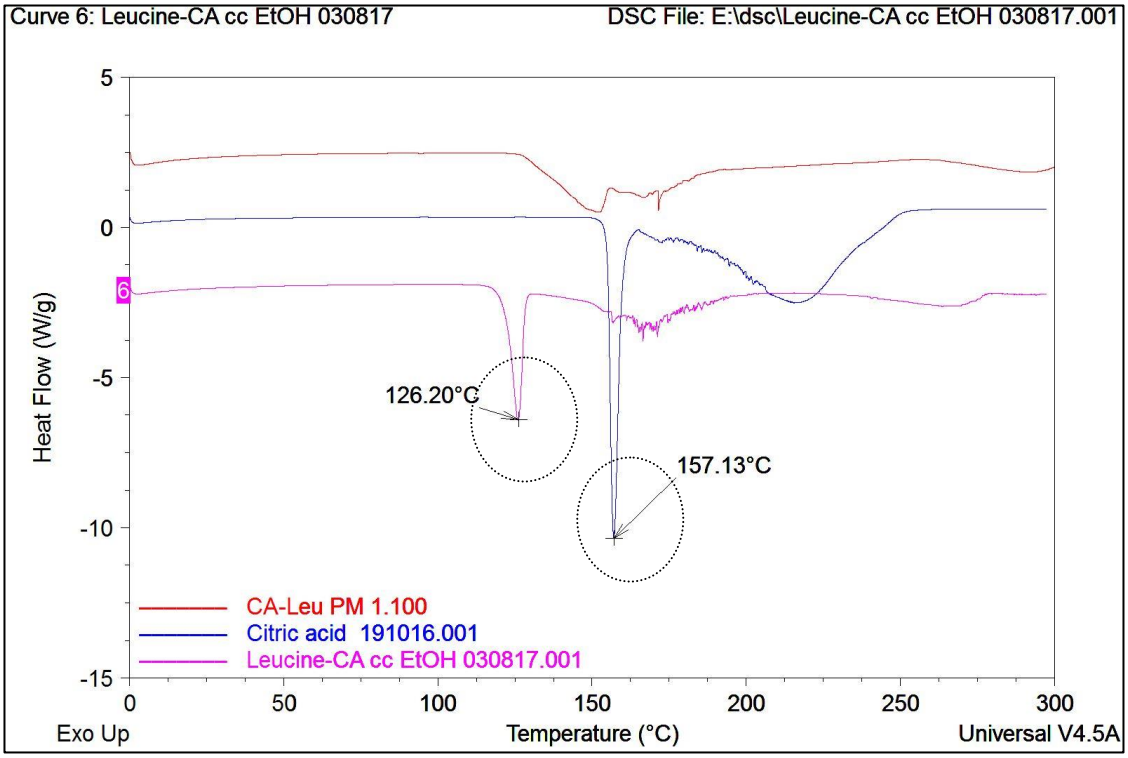

Figure 5.24 DSC thermogram of citric acid - L-leucine physical mixture (1:1), starting material and LAG complex of citric acid- L-leucine.

3 Spectroscopic data

Spectroscopic analysis was performed to further investigate the formation of hydrogen bonding between the two components.

3.1 Raman spectroscopy

In the below Raman spectra (Figure 5.25) analysis it was observed that there is no similarity in the peaks of the newly formed material by LAG of leucine and citric acid when compared with the individual starting material (n=3). It indicates that there may be the co-crystals formed between L- leucine and citric acid molecules.

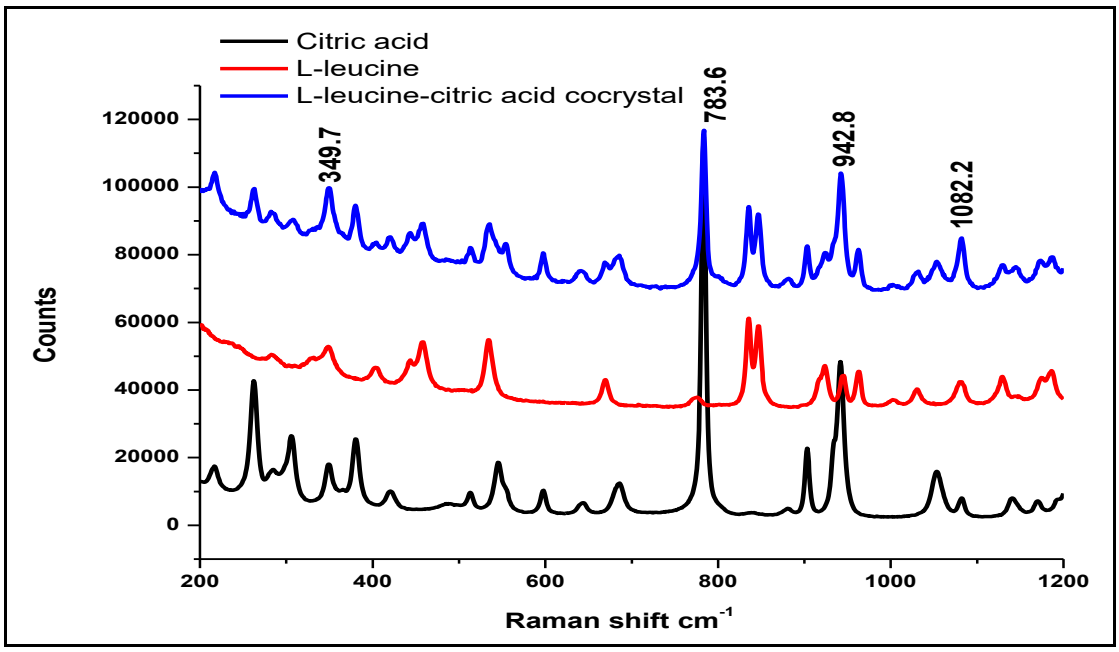

Figure 5.25 Raman spectra of L- leucine - citric acid co-crystals.

In Raman spectrum analysis, CH_2-CH torsion was not observed in the co-crystal at 209.2 cm^{-1}. A Raman shift occurred at 679 to 670 cm^{-1} for C=O stretching, for NH_3 rock from 1085 to 1081.5 cm^{-1}, CH_2 wag from 1217 to 1237.8 cm^{-1}. Then, O-CO bending of COOH occurred from 1345.2 to 1342.2 cm^{-1}, NH_3 symmetric bend from 1511 to 1506 and asymmetric bending from 1558 to 1554.1 cm^{-1} occurred.

Table 5.9 shows the Raman spectrum bands of L-leucine- citric acid and their co-crystal.

Table 5.9 Raman spectra band and associated functional groups in L-leucine, citric acid and their co-crystal

Transition energies (cm-1) with mode descriptions of L-leucine		citric acid		L-leucine -citric acid cc Raman spectra observed
Raman	A functional group associated.	Raman	A functional group associated.	Raman
209.2	CH_2-CH torsion	212		
258.8		258m broad		
296.2	CH_2-CH-CO_2 bend			
		301m		
331.2				
		345m		348.6
367.2	S-H out-of-plane bend			362.1
	N-CH-CO_2 bend	417m		
452	CH_2-CH-SH bend			457.8
513		499w		
531.3	CH_2-CH-N bend	539sh		533.8
	NH_3 torsion	550m		
		593m	sC-CH_3	599.2
	CH-CO_2 stretch	636w		
679.2		682m	C=O stretching	670.1
	C-S stretch			
				725.8
777.6	CH_2 rock	780s		783.5
	CH_2 Scissors			
841.5				846.3
	CO_2 wag			
		877w		
921.1		900m	C-C bends and OH out-of-plane bending	
	N-CH stretch	939s	C-C symmetric stretch	943.1
959.2				

996	CH_2-CH stretch			
				1029.4
1034.6	S-H in-plane bend	1050m	C-O stretch	1054.4
1,085	NH_3 rock	1082m	C-O stretch	1081.5
1126	NH_3 rock	1141m		1128.6
1178		1165w		1187.8
	CH_2 twist	1205m	C-C stretching	1213.8
1,231	CH_2 wag	1217m		1237.8
1260, 1274	C-H bend			
1294, 1326	C-H bend			
1309.1				
1345.2	CO_2 symmetric stretch	1346w	O-CO bending of COOH	1342.2
1410	CH_2 Scissors	1387s	CH_2 scissors	1407.1
		1430m broad	C-OH def.	
1465		1466 m broad	CH_2 scissors	1454.2
1511	NH_3 symmetric bend			1506.1
1558	NH_3 asymmetric bend			1554.1
	NH_3 asymmetric bend			
1627		1630 m broad		1625.1
1678	CO_2 asymmetric bend			1689, 1719

Symbols used are r: rocking, v: stretching, δ: deformation, t: twisting, ω: wagging, γ: deformation out of the plane, τ: torsion, as: antisymmetric, s: symmetric, skel.: skeleton, sh: shoulder, w: weak peak intensities

3.2 FT-IR spectroscopy

FT-IR spectroscopic analysis was performed on raw and processed samples (n=3) (refer Figure 5.26).

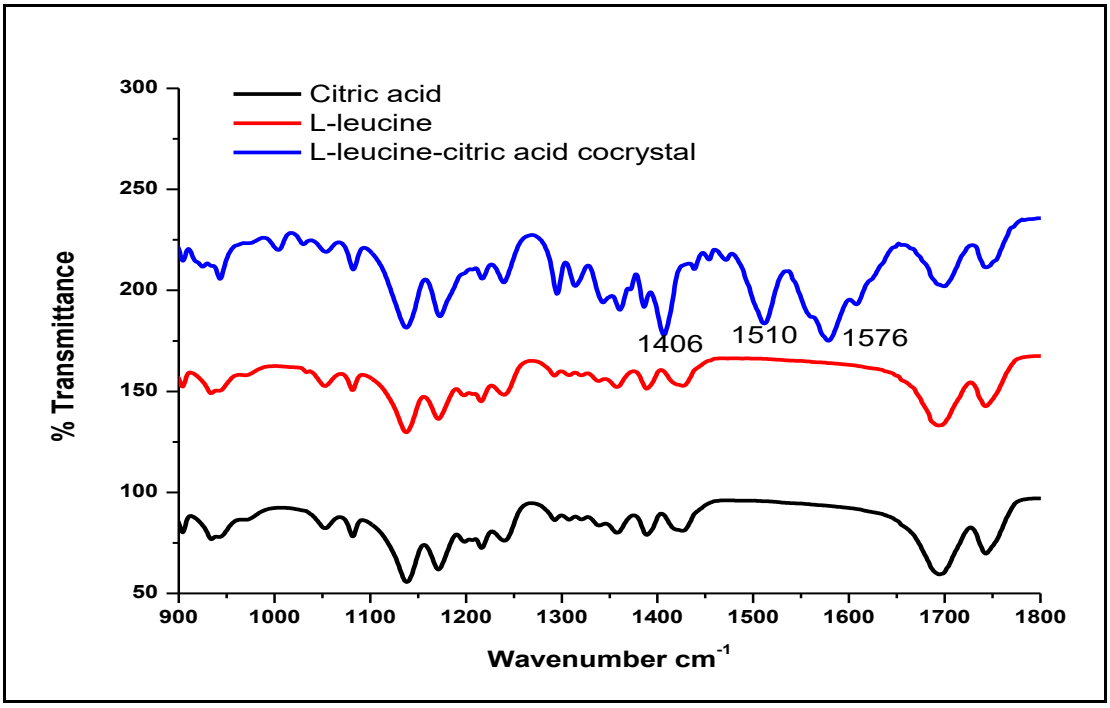

Figure 5.26 FT-IR spectra of citric acid, L-leucine and their co-crystal.

The obtained results with peak bands with their associated functional groups are represented in Table 5.10.

Table 5.10 FT-IR spectra peak band and associated group of L-leucine, citric acid and their co-crystal

L-leucine cm^{-1}	associated group	citric acid	associated group	L-leucine - citric acid cc IR
	CH-CO_2 stretch	639.6		648.8
668	C-S stretch	686.2m	C=O stretching	
768.2	CH_2 rock	770.5		744.6
	CH_2 Scissors	818.4s		818.5
847				
865.8	CO_2 wag			882
		881.2w		885.5
943	N-CH stretch	900m	C-C bends and OH	910

			out-of-plane bending	
1003	CH_2-CH stretch	934.3s	C-C symmetric stretch	981.8
	S-H in-plane bend	1.053.82		1049
1032	NH_3 rock	1050m	C-O stretch	
1085	NH_3 rock	1082m	C-O stretch	
1134		1138m		1138
1,185	CH_2 twist	1171w		
1239	CH_2 wag	1216.72m	C-C stretching	1215
	C-H bend	1217m		1272
1295	C-H bend	1293.86		1308
1362	CO_2 symmetric stretch	1358.80		1356
	CH_2 Scissors	1389.78w	O-CO bending of COOH	1416
		1387s	CH_2 scissors	
1405		1426m broad	C-OH def.	1461
	NH_3 symmetric bend	1466 m broad	CH_2 scissors	
1511				1517
1575	NH_3 asymmetric bend			1574
	NH_3 asymmetric bend			1616
	CO_2 asymmetric bend	1630 m broad		
		1695 vs	C=O stretching	1687
	S-H stretch	1743s	n(COOH)	
2124.9				
2617	N-H stretch			
2869	N-H stretch			2869

		2949w		
2957		2956w		2961
		2979w		2972
	C-H stretch	2993w		
	CH_2 symmetric stretch			3136
	CH_2 asymmetric stretch			
	N-H stretch	3283		
		3494		3447

The FT-IR analysis of L-leucine, citric acid and their co-crystals showed CH-CO_2 stretch at 648.8 cm^{-1}. The CH_2 rock was observed at 744.6 cm^{-1} and CH_2 scissors was observed at 818.5 cm^{-1} and CO_2 wag was observed at 882 cm^{-1}. The N-CH stretch and C-C bends and OH out-of-plane bending peak was observed at 910 cm^{-1}. S-H in-plane bend was observed at 1049, CH_2 wag and C-C stretching were observed at 1215 cm^{-1}. CH_2 scissors and O-CO bending of COOH was observed at 1416 cm^{-1}. NH_3 asymmetric bends were observed at 1574 cm^{-1} and 1616 cm^{-1}. These IR peaks suggest that there may be bonding between these two molecules and due to the co-crystal hydrate formation. Though there are chances of proton transfer in these reacting molecules as leucine has –NH group and –COOH functional groups and citric acid has –COOH groups, but no such proton transfers occurred. Therefore, the obtained pair is a cocrystal and not salt.

4 DVS data

DVS analyser was used to investigate the moisture absorption capability of the synthesised cocrystal (n=3;s.d.≤ 0.03). Below Table 5.11 reveals that citric acid-leucine cocrystal displayed higher absorption profile than individual component. It indicates that the cocrystal formation of leucine-citric acid could

not improve citric acids hygroscopic nature rather it absorbs more moisture than the pure citric acid molecule. The obtained cocrystal material was mixed with sodium bicarbonate in the molar ratio of 1.5 times of sodium bicarbonate to the citric acid content in the cocrystal to understand the stability property of cocrystals during formulation of effervescent tablets. When this mixture subjected to the DVS, it was observed that it showed less moisture absorption than the pure citric acid molecule. Figure 5.27 represents the DVS isotherm for raw and processed samples.

Table 5.11 DVS of L-leucine, citric acid and their co-crystal.

%RH	citric acid	L-leucine-CA cc	L-leucine pure	L-leucine - CA cc +1.5x SBC
0.0	0.00	0.00	0.0005	0.00
10.0	0.00	0.06	0.0318	0.02
20.0	0.00	0.12	0.0454	0.00
30.0	0.00	0.18	0.0842	-0.01
40.0	0.00	0.18	0.1110	0.03
50.0	0.00	0.23	0.1493	0.03
60.0	0.01	0.28	0.1967	0.01
70.0	0.02	5.13	0.2865	0.78
80.0	**4.65**	**35.91**	0.4439	**4.54**
90.0	**31.21**	**56.58**	**0.9806**	**12.85**

CA= Citric acid, cc= cocrystal, SBC= Sodium bicarbonate

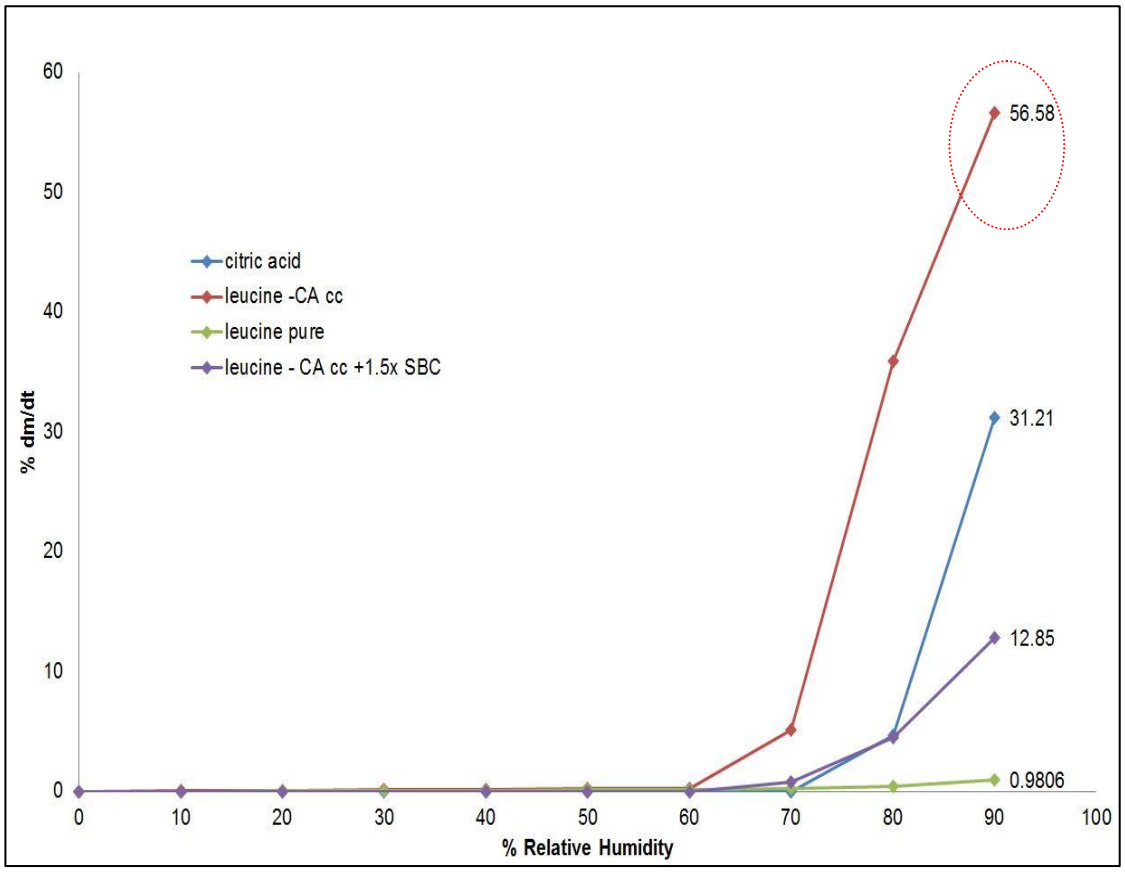

Figure 5.27 DVS of L-leucine, citric acid and their co-crystal.

5.3.2 Citric acid - L- isoleucine study

1 PXRD data

Based on the PXRD data (Figure 5.28) it is observed that citric acid and isoleucine starting materials retain their characteristic peaks at 15 and six 2θ°. When citric acid- isoleucine LAG sample was analysed through PXRD (n=3), new peaks were detected at 6.92, 8.88 and 13.24 2θ° which reveal that new crystal phase of citric acid-isoleucine is formed which can be attributed to cocrystal generation. The characteristics peaks of starting materials are absent in the processed samples.

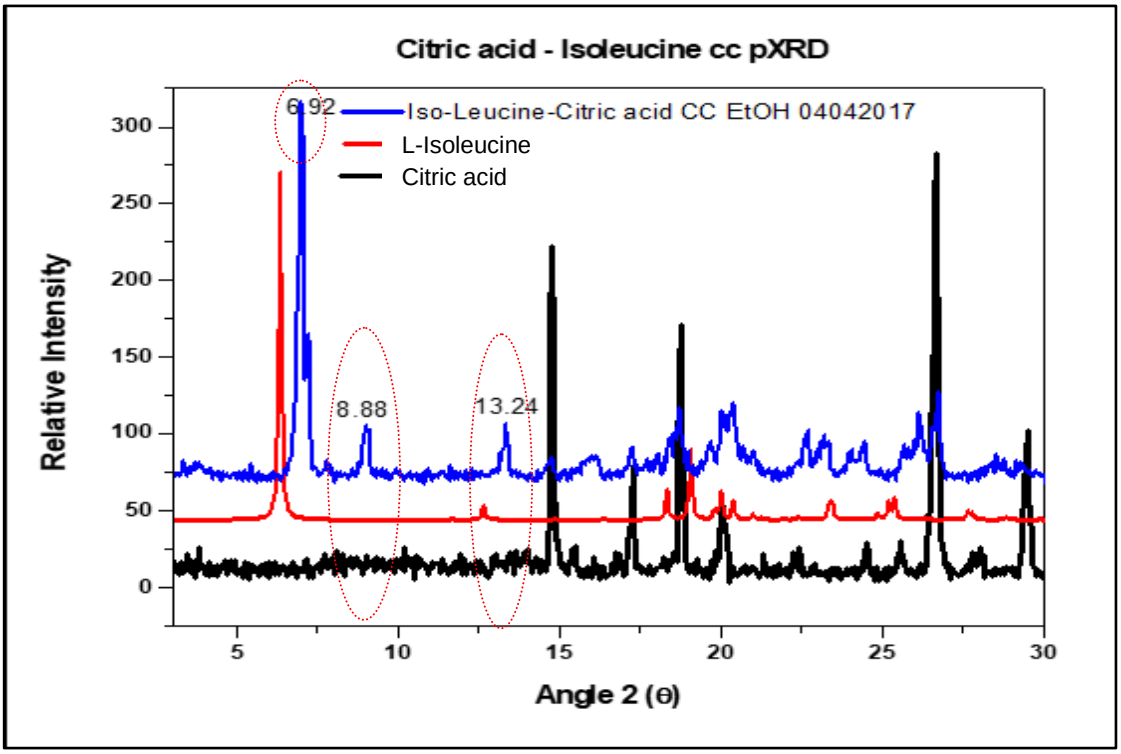

Figure 5.28 PXRD of citric acid, L- isoleucine and their LAG processed material.

2 DSC data

To further analyse the formation of the new crystal phase of citric acid and isoleucine thermal analysis was performed (n=3). Figure 5.29 represents the DSC thermogram of citric acid raw, isoleucine raw and citric acid-isoleucine LAG processed sample in 1:1 stoichiometric ratio. Based on the DSC data it is observed that single endotherm event at 126.84°C was obtained for citric acid-isoleucine cocrystal complex. This melting point is completely different compared to melting endotherm of individual starting materials. The absence of any major endothermic event between 80-110°C reveals that no solvent interactions have occurred.

Thus, based on PXRD and DSC data we can conclude that new crystal phase has been generated in citric acid-isoleucine processed samples which can be attributed to the weak hydrogen bonding between two components. To further

investigate the type of interactions and bonding involved between the two components spectroscopic analysis was performed.

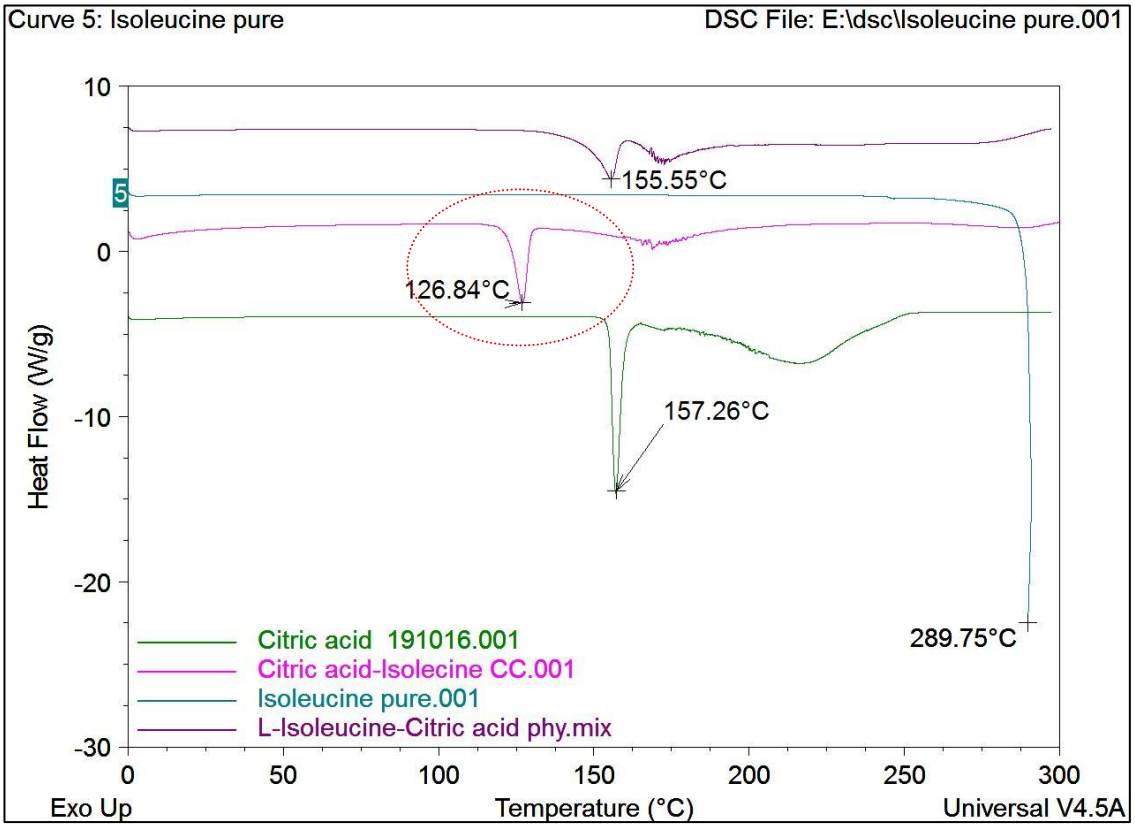

Figure 5.29 DSC of citric acid, L- isoleucine and their LAG processed material.

3. Spectroscopic analysis

3.1 Raman spectroscopy

On comparison of Raman spectra of raw and processed samples (n=3), it is observed that molecular interactions have occurred between the two components and new events at 310 cm^{-1}, 1361 cm^{-1} and 1087 cm^{-1} have been detected. Below Figure 5.30 represents the Raman spectra of citric acid, isoleucine and LAG processed citric acid-isoleucine complex.

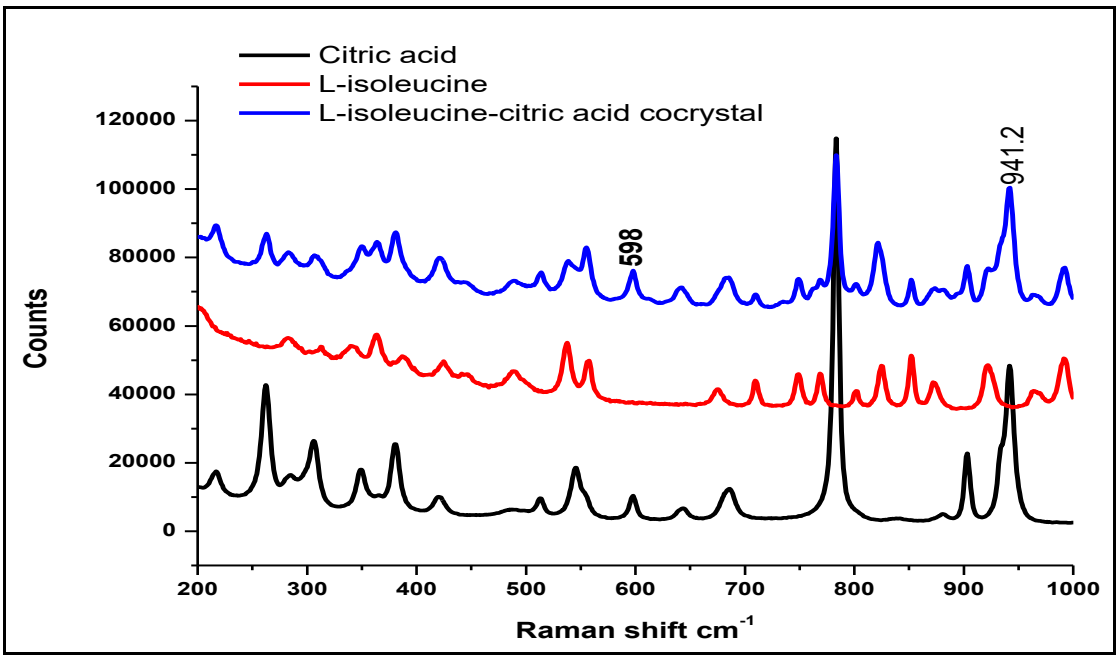

Figure 5.30 Raman spectrum of L-isoleucine- citric acid co-crystals.

Based on Raman spectra isoleucine-citric acid, the CH_2-CH-CO_2 bend at 310 cm^{-1} was observed with Raman shift from 296.2 cm^{-1}. The NH_3 torsion was observed at 564 cm^{-1}. The CH-CO_2 stretch 635-650 cm^{-1}, NH_3 rock and C-O stretch was observed at 1087 with Raman shift from 1082 cm^{-1} and the CO_2 symmetric stretch and O-CO bonding of COOH was observed at 1361 cm^{-1} Raman shift from 1346 cm^{-1}. This indicates that there is hydrogen bonding occurred in between the isoleucine and citric acid molecule. Thus, these interactions may attribute to cocrystal formation.

Table 5.12 for Raman spectra details of citric acid, isoleucine and their co-crystal.

Table 5.12 Raman spectra band and associated functional groups in L-isoleucine, citric acid and their co-crystal

Transition energies (cm^{-1}) with mode descriptions of L-isoleucine		citric acid		L-isoleucine - citric acid cc Raman spectra observed
Raman	A functional group associated.	Raman	A functional group associated.	Raman
				125.1
137.1				176.4
	CH_2-CH torsion	212		
		258m broad		268
	CH_2-CH-CO_2 bend			310
		301m		
		345m		
	S-H out-of-plane bend			356
381.6				
	N-CH-CO_2 bend	417m		414
452	CH_2-CH-SH bend			
485		499w		505
533.1	CH_2-CH-N bend	539sh		
	NH_3 torsion	550m		564
		593m	sC-CH_3	598
	CH-CO_2 stretch	636w		650
671.6		682m	C=O stretching	
705.7	C-S stretch			
				748
764.8	CH_2 rock	780s		783.5
820	CH_2 Scissors			822
848				
	CO_2 wag			
		877w		
917		900m	C-C bends and OH out-of-plane bending	890
	N-CH stretch	939s	C-C symmetric	942.7

			stretch	
987	CH_2-CH stretch			986.9
1028	S-H in-plane bend	1050m	C-O stretch	1048
1,087	NH_3 rock	1082m	C-O stretch	1087
1131	NH_3 rock	1141m		1145
1186		1165w		1191
	CH_2 twist	1205m	C-C stretching	
1,231	CH_2 wag	1217m		
1253	C-H bend			
1323	C-H bend			
1349	CO_2 symmetric stretch	1346w	O-CO bending of COOH	1361
1391	CH_2 Scissors	1387s	CH_2 scissors	
1444		1430m broad	C-OH def.	1446
		1466 m broad	CH_2 scissors	1470
1509	NH_3 symmetric bend			1502
1551, 1576	NH_3 asymmetric bend			
1617	NH_3 asymmetric bend			
		1630 m broad		
1678	CO_2 asymmetric bend			1,658

Symbols used are r: rocking, v: stretching, δ: deformation, t: twisting, ω: wagging, γ: deformation out of the plane, τ: torsion, as: antisymmetric, s: symmetric, skel.: skeleton, sh: shoulder, w: weak peak intensities.

3.2 FT-IR spectra:

Below Figure 5.31 represents the spectral overlay of citric acid starting material, isoleucine starting material and citric acid-isoleucine cocrystal (n=3).

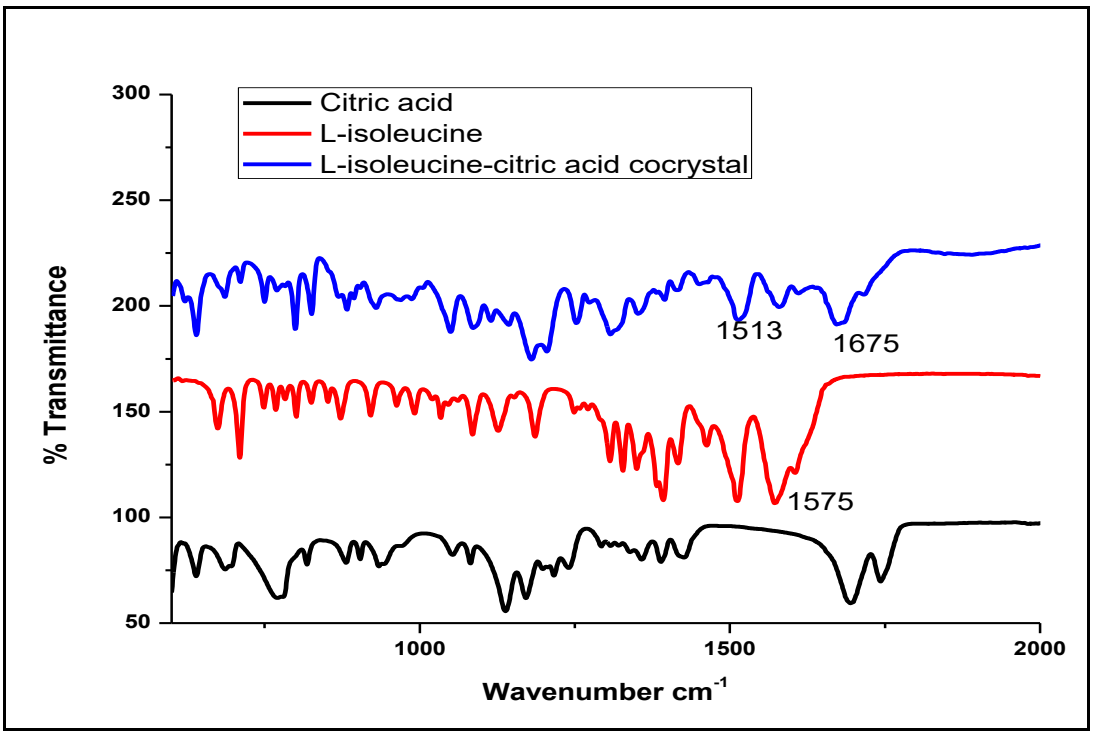

Figure 5.31 FT-IR spectra of L-isoleucine, citric acid and their co-crystal.

In FT-IR spectroscopy of L-isoleucine - citric acid cocrystal and starting materials, it was observed that there are some new peaks at different wavelength are detected. The bending of functional groups, wag and stretch pattern is observed, l. The C-S stretch and C=O stretching was observed at 685.6 cm^{-1}, CH_2 rock was observed at 749 cm^{-1}, CH_2 scissors was observed at 825 cm^{-1}, CO_2 wag was observed at 882 and N-CH stretch as well as C-C bends and OH out-of–plane bending was observed at 929.2cm^{-1}. CH_2-CH stretch, and C-C symmetric stretch was observed at 987.3 cm^{-1}. The S-H in-plane bend was observed at 1050 cm^{-1}, NH_3 rock and C-O stretch were observed at 1086 cm^{-1} and CO_2 symmetric stretch was observed at 1351 cm^{-1}. CH_2 scissors and O-CO bending of COOH was observed at 1394 and NH_3 symmetric bending was observed at 1453 cm^{-1}. In this pair also, a peak was detected at 3492 cm^{-1} confirming the presence of a water molecule. This may be because the citric acid has a strong affinity towards the water molecule. However, there was no any proton transfer observed. No peaks dedicated to –

COO^- and $–NH^+$ were observed. It indicates that there is no salt formation occurred. Table 13 represents the FT-IR spectra.

Table 5.13 L-isoleucine, citric acid and their co-crystal FT-IR peaks with associated groups.

L-isoleucine cm^{-1}	associated group	citric acid	associated group	L-isoleucine - citric acid cc IR
	CH-CO_2 stretch	639.6		639.9
674	C-S stretch	686.2m	C=O stretching	685.6
709.9				
768.8	CH_2 rock	770.5		749.8
800.9				799.4
825.1	CH_2 Scissors	818.4s		825.2
872.4	CO_2 wag	881.2w		882
920.9	N-CH stretch	900m	C-C bends and OH out-of-plane bending	929.2
962.9	CH_2-CH stretch	934.3s	C-C symmetric stretch	987.3
991.7				
1034	S-H in-plane bend	1.053.82		1050
	NH_3 rock	1050m	C-O stretch	
1085	NH_3 rock	1082m	C-O stretch	1086
1126		1138m		
1,186	CH_2 twist	1171w		1180
	CH_2 wag	1216.72m	C-C stretching	
1249	C-H bend	1217m		1252
1328	C-H bend	1293.86		1307
1350	CO_2 symmetric stretch	1358.80		1351
1393	CH_2 Scissors	1389.78w	O-CO bending of COOH	1394
		1387s	CH_2 scissors	
		1426m broad	C-OH def.	
1463	NH_3 symmetric bend	1466 m broad	CH_2 scissors	1453
1573	NH_3 asymmetric bend			1579

	NH_3 asymmetric bend			1673
	CO_2 asymmetric bend	1630 m broad		
		1695 vs	C=O stretching	
	S-H stretch	1743s	n(COOH)	
2124.9				
2607	N-H stretch			
2692	N-H stretch			2878
2876				
2930		2949w		
2961		2956w		2966
		2979w		2972
	C-H stretch	2993w		
	CH_2 symmetric stretch			3112
	CH_2 asymmetric stretch			
	N-H stretch	3283		
		3494		3492

4 DVS analysis

Based on the DVS isotherm data for citric acid-isoleucine cocrystal (n=3; s.d.≤ 0.03) it is observed that negative values or sample weight loss is observed which is attributed to the non-stable nature of the sample at 30%RH. Table 5.14 and Figure 5.32 represent the numerical and graphical data for raw and processed samples of citric acid and isoleucine respectively.

Table 5.14 DVS study of L-isoleucine - citric acid cocrystal

%RH	citric acid	isoleucine pure	isoleucine-CA cc
0.0	0.00	-0.01	0.00
10.0	0.00	-0.01	0.01
20.0	0.00	0.00	0.00
30.0	0.00	0.01	-1.29
40.0	0.00	0.02	-1.97
50.0	0.00	0.03	-3.01
60.0	0.01	0.05	-3.66
70.0	0.02	0.08	-3.75
80.0	4.65	0.12	2.40
90.0	**31.21**	**0.23**	**25.01**

CA= citric acid

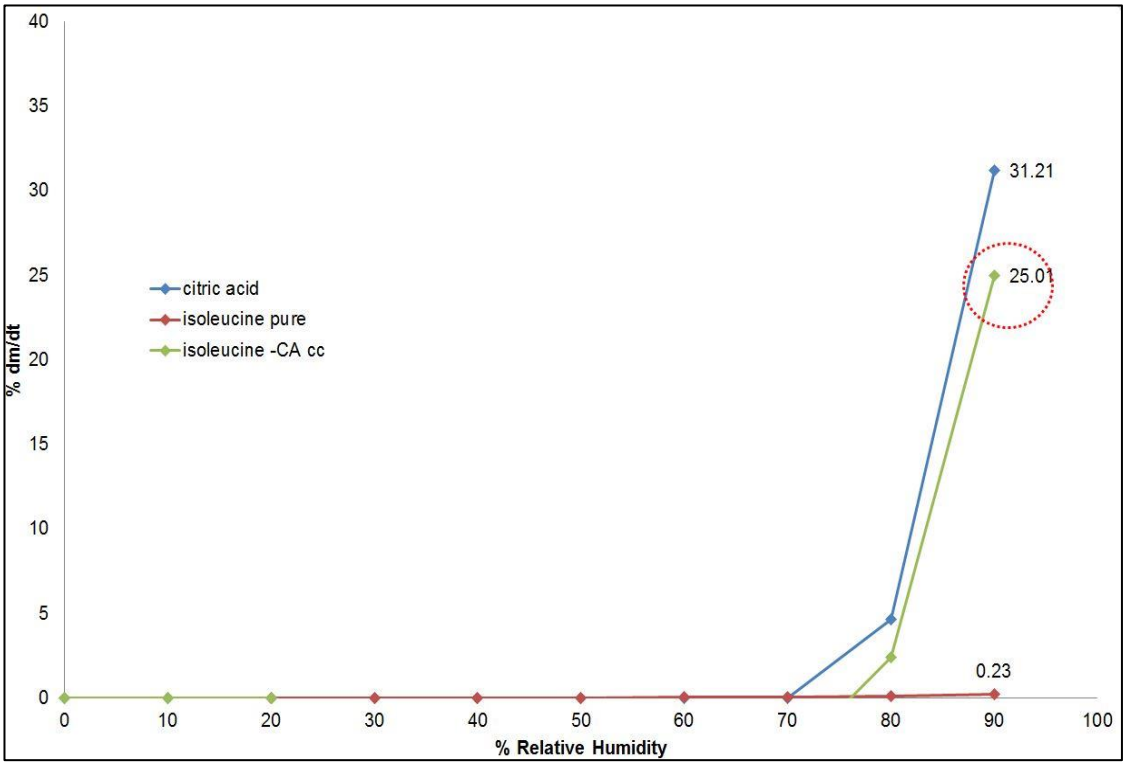

Figure 5.32 DVS isotherm of L-isoleucine, citric acid and their co-crystal.

5.3.3 Citric acid – L- serine cocrystals

1 PXRD data

Based on the PXRD pattern (Figure 5.33), in citric acid-serine LAG sample (n=3), new crystal peaks were detected at 6.32, 13, 17.68, 21, 23 and 25.5 2θ° which does not coincide with any of the characteristic peaks of citric acid and

serine starting material. Thus, based on this new crystal phase has been generated which can be attributed to cocrystal phase.

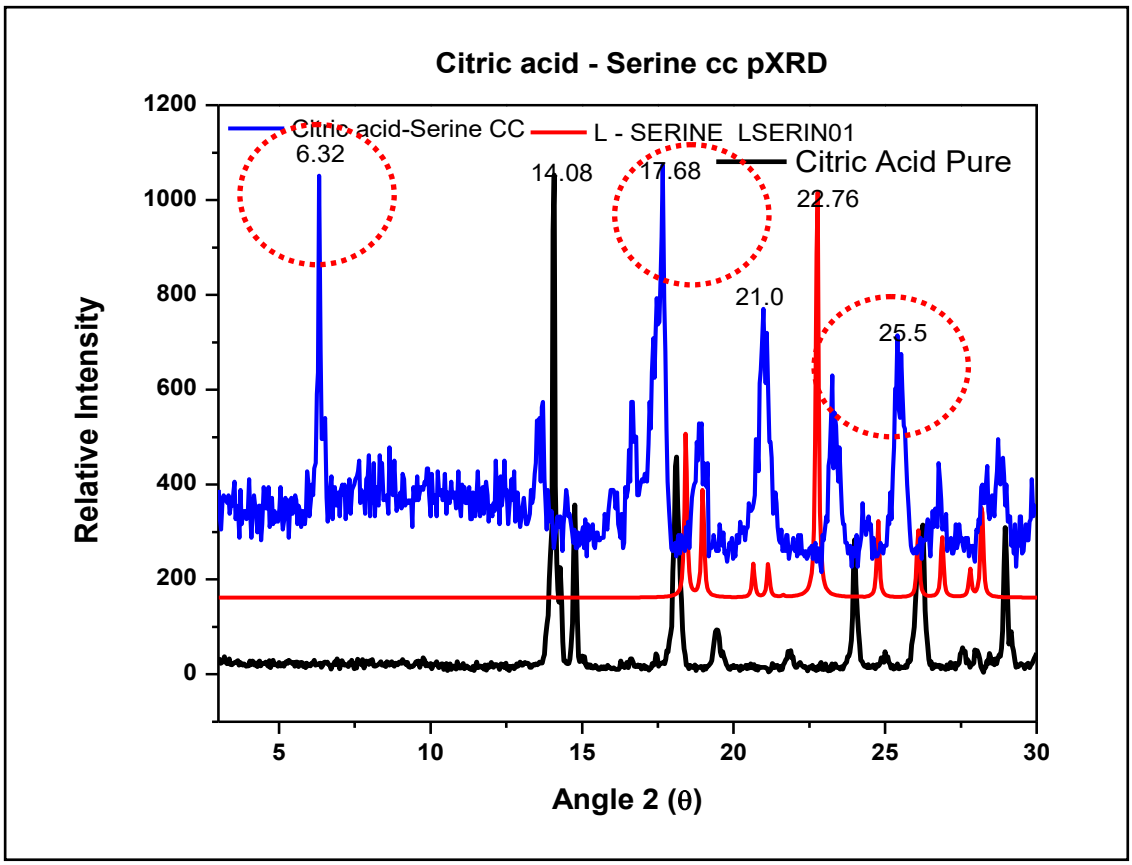

Figure 5.33 PXRD pattern of citric acid - L- serine LAG material.

2 DSC data

Below Figure 5.34 represents the overlay of DSC thermogram of citric acid and serine amino acid starting material and LAG processed sample (n=3). According to the PubChem records the melting point of the citric acid is 153°C and the melting point of the serine is 228°C (NCBI 2017c). The experimental endotherm melting events for citric acid and serine amino acid is similar to previously reported values (Rehder et al. 2011). In the DSC thermogram of citric acid-serine LAG material, it was observed that there is a single broad endothermic peak at 116.15°C followed by degradation this can be attributed to new crystal phase generation or even presence of bound solvent along with

cocrystal phase. This is different than the original starting materials melting points.

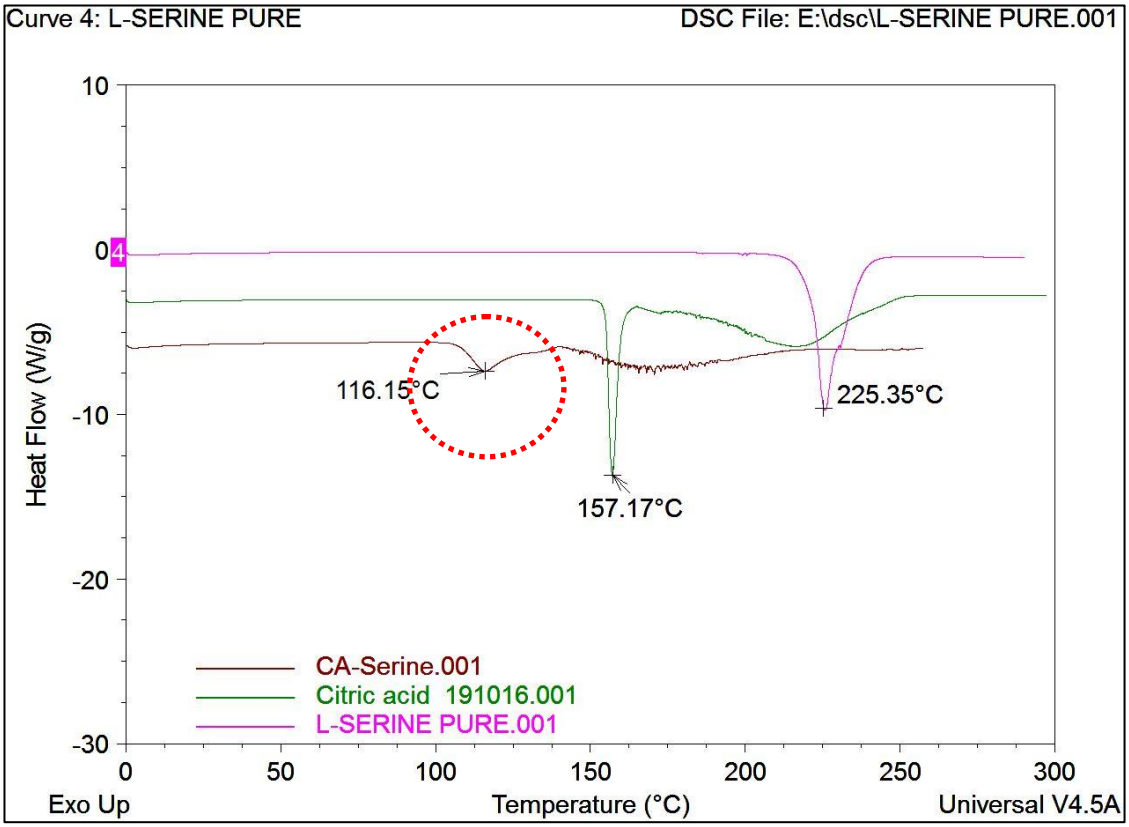

Figure 5.34 DSC of L- serine-citric acid and their LAG material.

3 Spectroscopic analysis

3.1 Raman spectroscopy

In the Raman analysis of the L-serine-citric acid LAG mixture (n=3), it was observed that Raman shifts occurred in some regions of the citric acid-L-serine complex which indicates that there is stretching, and new bond formation has happened. (See Figure 5.35)

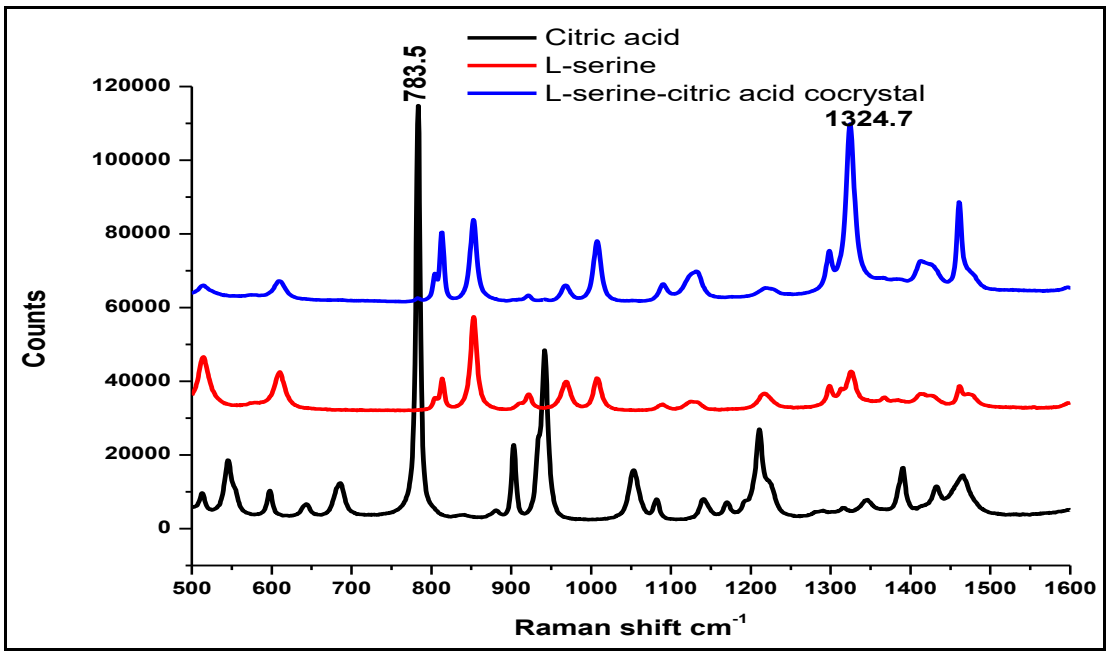

Figure 5.35 Raman spectrum of L-serine- citric acid co-crystals.

It was observed that, in the region 1090, -NH_3 rock shifted slightly from 1082 to 1090. The -O-CO bonding of COOH was found to be absent around 1345, 1354, 1346 regions. The NH_3- symmetric band from 1525 and -NH_3 asymmetric band from 1610.1 were absent. The details of Raman spectrum observed in the experiment are shown below in Table 5.15.

Table 5.15 Raman spectra band and associated functional groups in L-serine, citric acid and their co-crystal.

Transition energies (cm^{-1}) with mode descriptions of L-serine		citric acid		L-serine - citric acid cc Raman spectra observed
Raman	A functional group associated.	Raman	A functional group associated.	Raman
137.7				140.3
209	CH_2-CH torsion			
222.2		212		
258.8		258m broad		260.9
296.2	CH_2-CH-CO_2 bend			296.7

		301m		
		345m		
363.2	S-H out-of-plane bend			362.1
	N-CH-CO_2 bend	417m		
441,450	CH_2-CH-SH bend			
513		499w		514.5
536	CH_2-CH-N bend	539sh		
	NH_3 torsion	550m		
608.8		593m	sC-CH_3	609.8
639	CH-CO_2 stretch	636w		
		682m	C=O stretching	
693	C-S stretch			
773	CH_2 rock	780s		
813.6	CH_2 Scissors			813.3
852.1	CO_2 wag			852.6
		877w		
920.9		900m	C-C bends and OH out-of-plane bending	
968.1	N-CH stretch	939s	C-C symmetric stretch	968.1
1,007	CH_2-CH stretch			1007.3
1067	S-H in-plane bend	1050m	C-O stretch	
1005, 1011	NH_3 rock	1080m	C-O stretch	1090.1
1134.5	NH_3 rock	1141m		1132.1
		1165w		
1,199	CH_2 twist	1205m	C-C stretching	
1,218	CH_2 wag	1217m		1220.1
1260, 1274	C-H bend			
1294, 1326	C-H bend			1324.9
1345, 1354	CO_2 symmetric stretch	1346w	O-CO bending of COOH	
1398, 1425	CH_2 Scissors	1387s	CH_2 scissors	1413.2

		1430m broad	C-OH def.	
1461.1		1466 m broad	CH_2 scissors	1461.5
1525	NH_3 symmetric bend			
1574, 1581	NH_3 asymmetric bend			1597.1
1610.1	NH_3 asymmetric bend			
		1630 m broad		1627.1
1644	CO_2 asymmetric bend			

Symbols used are r: rocking, v: stretching, δ: deformation, t: twisting, ω: wagging, γ: deformation out of the plane, τ: torsion, as: antisymmetric, s: symmetric, skel.: skeleton, sh: shoulder, w: weak peak intensities.

3.2 FT-IR spectra:

The FT-IR spectroscopy was carried out on the citric acid, L-serine and the resulting co-crystal obtained through the LAG process (n=3). The overlay of FTIR spectra and tabular data of raw and processed data is demonstrated in Figure 5.36 and Table 5.16 respectively.

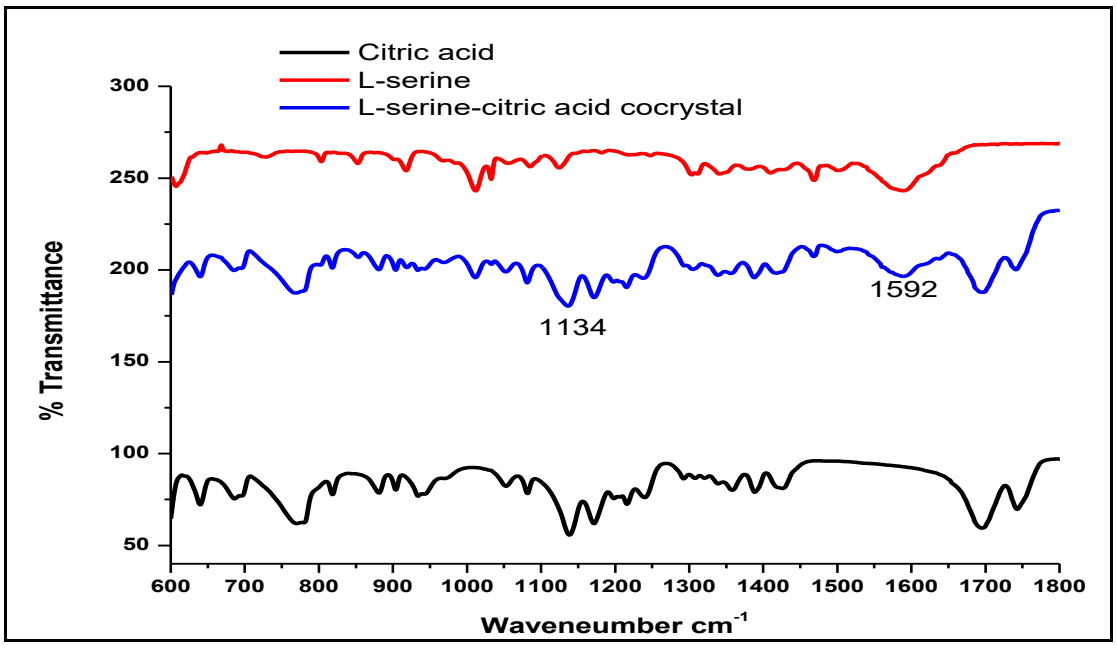

Figure 5.36 FT-IR spectra of L-serine-citric acid cc with starting material

Table 5.16 FT-IR spectra peak bands and associated functional groups of citric acid – L- serine cc and starting material.

L-serine cm^{-1}	associated group	citric acid	associated group	L-serine-citric acid cc IR
607.8				617.4
	CH-CO_2 stretch	639.6		640.1
	C-S stretch	686.2m	C=O stretching	696.7
727.9				
	CH_2 rock	770.5		780.4
803.1				
	CH_2 Scissors	818.4s		818.7
852.2	CO_2 wag	881.2w		881.8
917.7	N-CH stretch	900m	C-C bends and OH out-of-plane bending	902.5
	CH_2-CH stretch	934.3s	C-C symmetric stretch	934.2
1011.8	S-H in-plane bend	1.053.82		1028.5

	NH_3 rock	1050m	C-O stretch	1082
1085	NH_3 rock	1082m	C-O stretch	1094
1124		1138m		1139
1,182	CH_2 twist	1171w		1172
1219	CH_2 wag	1216.72m	C-C stretching	1217
1247	C-H bend	1217m		
1303	C-H bend	1293.86		1311.6
1341				
1360.9	CO_2 symmetric stretch	1358.80		1352
	CH_2 Scissors	1389.78w	O-CO bending of COOH	1390
		1387s	CH_2 scissors	
1410		1426m broad	C-OH def.	1429
1468	NH_3 symmetric bend	1466 m broad	CH_2 scissors	
1501				1503
1589	NH_3 asymmetric bend			1570
	NH_3 asymmetric bend			1592
	CO_2 asymmetric bend	1630 m broad		1632
		1695 vs	C=O stretching	1695
	S-H stretch	1743s	n(COOH)	1741
2040				2052
2116				2114
2163				2152
2325				
2384				2387
2597	N-H stretch			2560
2731	N-H stretch			2648
				2773
2942		2949w		2943

		2956w		
		2979w		
	C-H stretch	2993w		
	CH_2 symmetric stretch			
	CH_2 asymmetric stretch			
	N-H stretch	3283		3288
		3494		3496
3711				

The FT-IR spectra of L-serine-citric acid showed many similarities to the original citric acid material. However, after careful observation, it was revealed that there are differences between a few peaks intensities. C-S stretch and C=O stretch showed at 696.7 cm^{-1}, which is slightly different from the 686 of Citric acid. N-CH stretch and C-C and OH out of plane bending were observed to be at 902.5 cm^{-1}. There was a more significant difference between NH_3 rock and C-O stretch as compared to the original materials at 1094 cm^{-1}. O-CO bending of COOH was observed at 1390 cm^{-1}. Therefore, this data reveals that slight changes in the bend and stretch of the co-crystal molecule confirm it is a new form rather than the original material.

4 DVS data

The DVS isotherms (Figure 5.37) of L-Serine, Citric acid and their co-crystal (n=3; s.d.≤ 0.03), showed some different results from the previous two pairs of co-crystals. Although L-serine itself showed the non - hygroscopic nature, its co-crystal with citric acid becomes more hygroscopic. Again, this could be correlate with the DSC studies of these all. Where the cocrystal showed a lower melting point than that of their original materials. It absorbs 58.80% of moisture at 90 %

RH. At 30% RH it showed 0.48% moisture absorption, but after 50% RH, it starts to absorb more moisture. See Table 5.17.

Table 5.17 DVS of L-serine, citric acid and their co-crystal.

% RH	citric acid	serine-CA cc	serine pure
0.0	0.00	0.00	0.00
10.0	0.00	0.00	0.00
20.0	0.00	0.06	0.00
30.0	0.00	0.48	0.00
40.0	0.00	2.02	0.00
50.0	0.00	4.27	0.00
60.0	0.01	9.85	0.01
70.0	0.02	20.71	0.01
80.0	4.65	36.03	0.01
90.0	**31.21**	**58.80**	**0.01**

CA= citric acid.

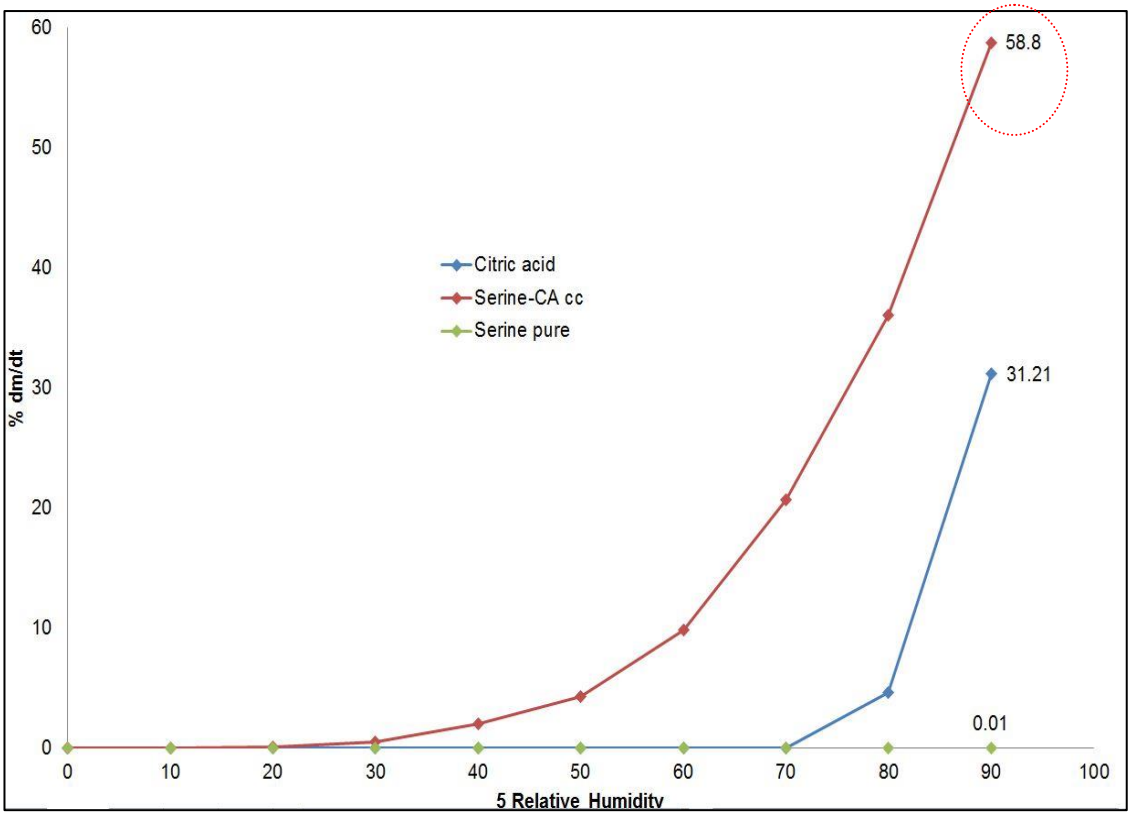

Figure 5.37 DVS of L-serine, citric acid and their co-crystal.

5.3.4 Citric acid–L-methionine study

1 PXRD

In the PXRD analysis of the citric acid-L-methionine LAG material (n=3), it was observed that new peaks were generated at 6.8, 19, 20.44 and 22.4 2θ° which significantly vary from characteristic peaks of individual starting materials. Thus, based on the PXRD pattern new crystal phase of citric acid-methionine is generated. See Figure 5.38.

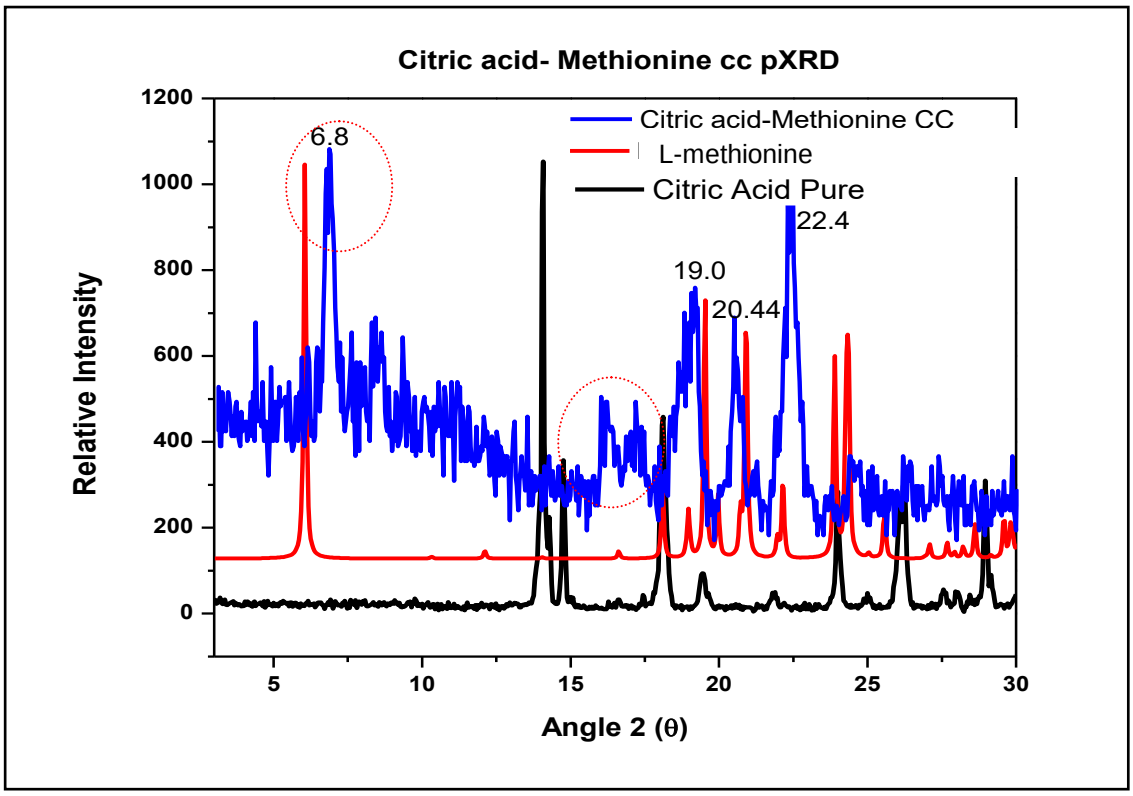

Figure 5.38 PXRD of citric acid–L-methionine LAG sample with starting material

2 DSC data

As per the PubChem database records, the melting point of citric acid is 153°C and the melting point of methionine is 283°C (Hautala et al. 2016).

The DSC analysis of citric acid-methionine LAG material (n=3), showed a single endothermal melting peak at 124.65°C which is different from the starting materials melting points. See Figure 5.39.

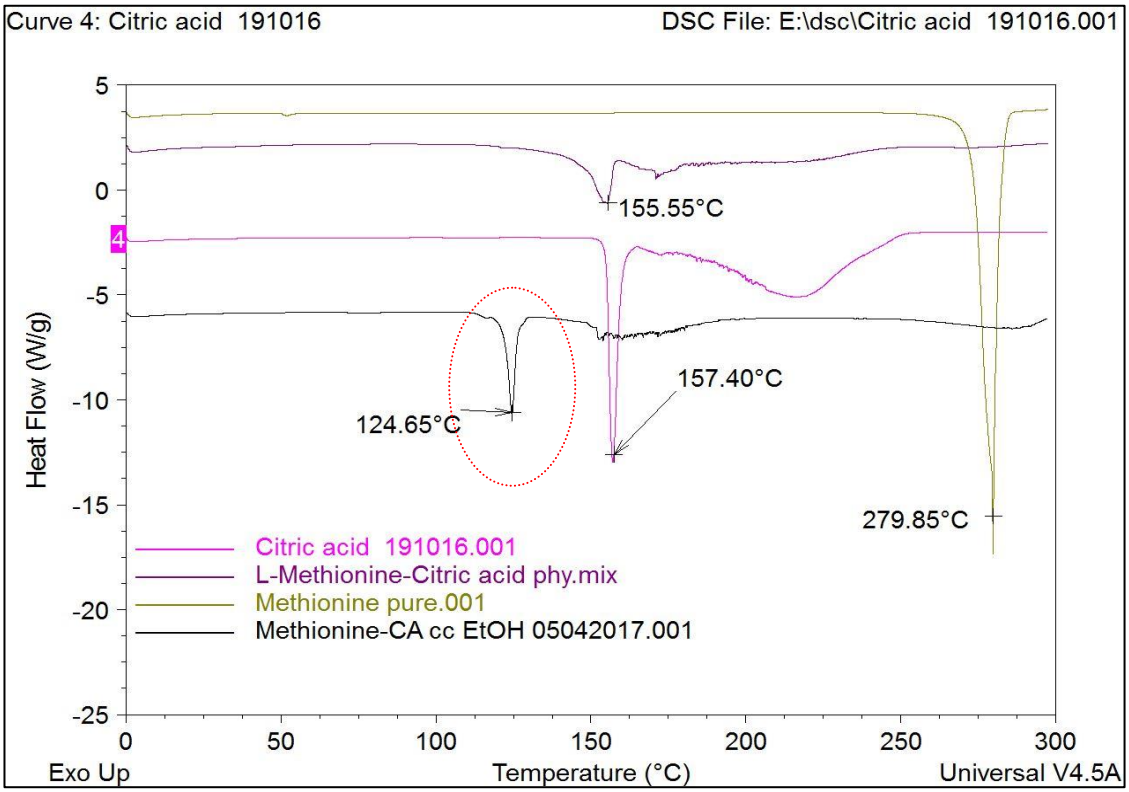

Figure 5.39 DSC of citric acid, L-methionine and their LAG material

3 Spectroscopic analysis

3.1 Raman spectroscopy

Based on the Raman spectral overlay of raw and LAG processed sample of methionine and citric acid (n=3), it was observed that new distinct peaks were generated which are different from starting materials (right the region of new peaks) are different from the starting materials. It indicates that there may be interactions occurring between L-methionine and citric acid molecules. See Figure 5.40.

In Raman analysis of the citric acid, L-methionine and their LAG mixture, it was observed that there are some stretch and wag and bends which are the indication of some kinds of bonding and attraction between atoms happened in the co-crystal molecule. Therefore, the Raman shift was observed at those points. This bonding or reaction by force was predicted around the -NH_2 group of amino acid and -COOH group of citric acid.

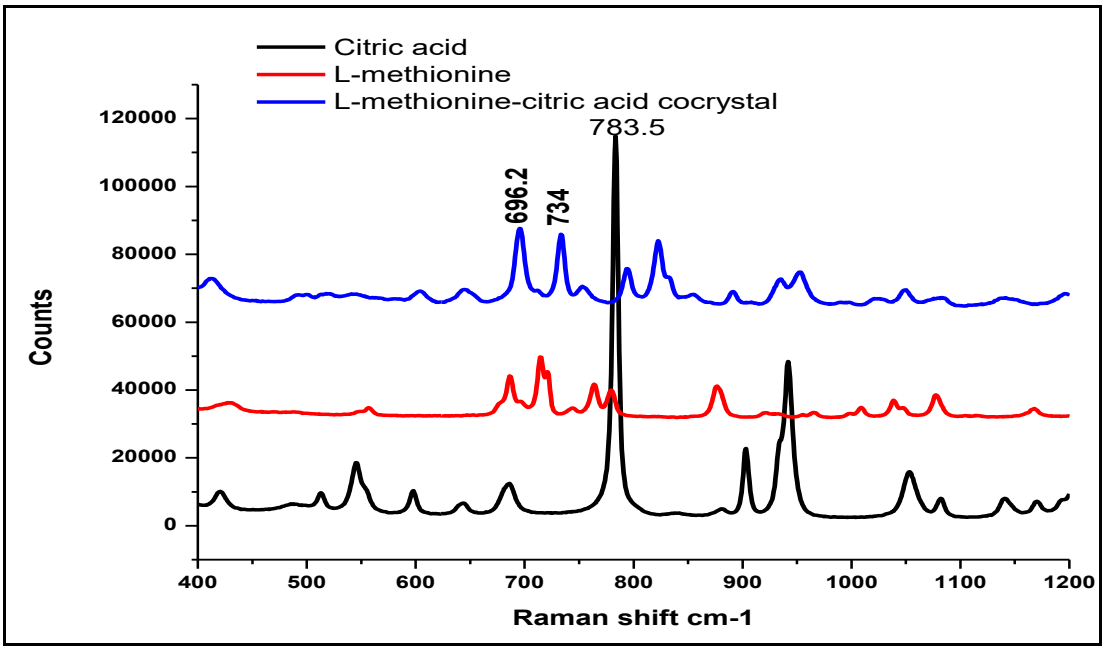

Figure 5.40 Raman spectra of citric acid–L-methionine LAG processed sample with starting material.

This citric acid–L-methionine co-crystal compound showed, NH_3 torsion at 518 cm^{-1}, which showed a Raman shift from their original molecule from 552.4 of L-methionine and 550 of Citric acid. C=O stretch was not observed. NH_3 rock and C-O stretch were observed at 1076 cm^{-1} which showed a Raman shift from 1082 of Citric acid and 1073 cm^{-1} of L-methionine. CO_2 symmetric stretch and O-CO bending of COOH was observed at 1337 cm^{-1} and a Raman shift from 1362 cm^{-1} of L- methionine and 1346 cm^{-1} of Citric acid were observed at the same point.

The Raman spectrometric analysis of citric acid and methionine co-crystals did not show the salt formation functional group (like CO_2^-, NH_4^+) peaks. Thus, it reveals that these are the co-crystals and not salts. Table 5.18 represents the Raman spectra observed in L-methionine and citric acid and their co-crystal.

Table 5.18 Raman spectra band and associated functional groups in citric acid - L- methionine and their co-crystal

Transition energies (cm^{-1}) with mode descriptions of L-methionine		citric acid		L-methionine-citric acid cc Raman spectra observed
Raman	A Functional group associated.	Raman	A Functional group associated.	Raman
126.7		127		129.9
137.1		182.8		
	CH_2-CH torsion	215.9		
257.1		258m broad		
	CH_2-CH-CO2 bend			
		301m		
345.7		345m		
	S-H out-of-plane bend			
426.1	N-CH-CO_2 bend	417m		417
	CH_2-CH-SH bend			
		499w		489
	CH_2-CH-N bend	539sh		
552.4	NH_3 torsion	550m		518
		593m	sC-CH_3	599
	CH-CO_2 stretch	636w		655
682.7		682m	C=O stretching	
710	C-S stretch			694
				731
759	CH_2 rock	780s		
	CH_2 Scissors			795

				818
	CO_2 wag			
872		877w		876
		900m	C-C bends and OH out-of-plane bending	
	N-CH stretch	939s	C-C symmetric stretch	935
1,005	CH_2-CH stretch			
1035	S-H in-plane bend	1050m	C-O stretch	1048
1,073	NH_3 rock	1082m	C-O stretch	1076
	NH_3 rock	1141m		1137
1165		1165w		
	CH_2 twist	1205m	C-C stretching	1183
	CH_2 wag	1217m		
1273	C-H bend			
1303	C-H bend			
1362	CO_2 symmetric stretch	1346w	O-CO bending of COOH	1337
1411	CH_2 Scissors	1387s	CH_2 scissors	
		1430m broad	C-OH def.	1430
		1466 m broad	CH_2 scissors	
	NH_3 symmetric bend			
	NH_3 asymmetric bend			
	NH_3 asymmetric bend			
		1630 m broad		
	CO_2 asymmetric bend			1,688

Symbols used are r: rocking, v: stretching, δ: deformation, t: twisting, ω: wagging, γ: deformation out of the plane, τ: torsion, as: antisymmetric, s: symmetric, skel.: skeleton, sh: shoulder, w: weak peak intensities

3.2 FTIR spectra

The vibrational spectroscopy FT-IR was carried out for L- methionine, citric acid and their co-crystal through the LAG mixture (n=3). The overlay of collected spectra is demonstrated in below Figure 5.41 and regions corresponding the spectral events are included in Table 5.19

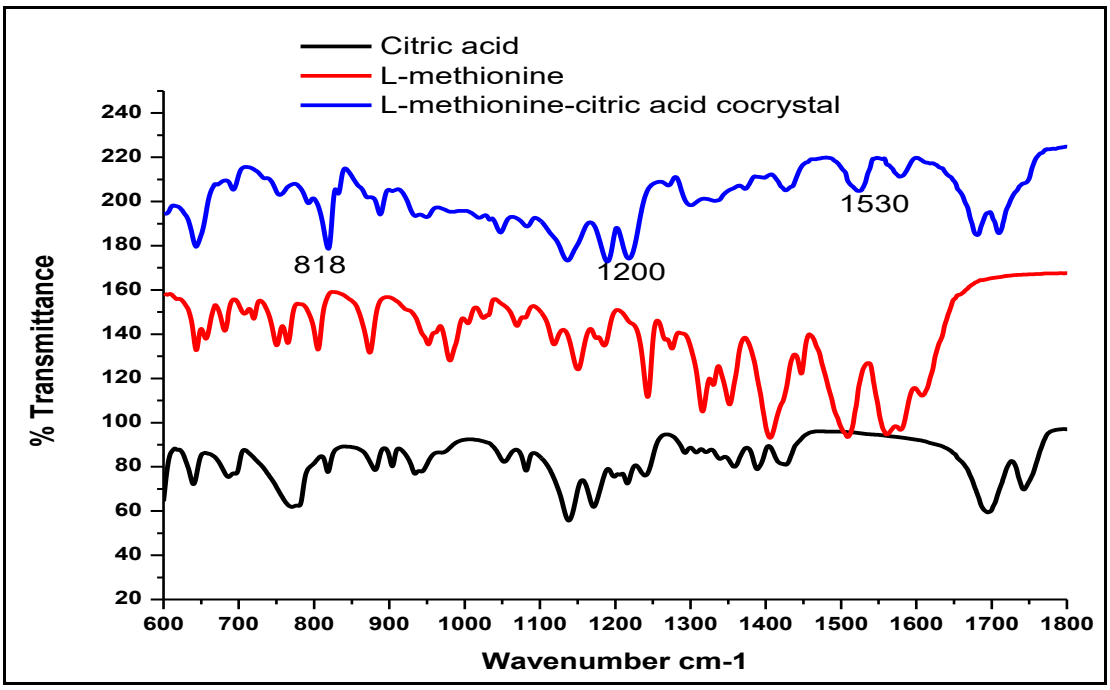

Figure 5.41 FT-IR spectra of citric acid–L-methionine cc with starting material.

Table 5.19 FT-IR spectra band and associated group of L-methionine, citric acid and their co-crystal.

L-methionine cm^{-1}	Associated group	Citric acid	Associated group	L-methionine-citric acid cc IR
643.4	CH-CO_2 stretch	639.6		645.4
681	C-S stretch	686.2m	C=O stretching	692
720				
750	CH_2 rock	770.5		755
805				
	CH_2 Scissors	818.4s		818.3
874	CO_2 wag	881.2w		887
917.7	N-CH stretch	900m	C-C bends and OH out-of-plane bending	887
951	CH_2-CH stretch	934.3s	C-C symmetric stretch	950
980	S-H in-plane bend	1.053.82		980
	NH_3 rock	1050m	C-O stretch	1048
1070	NH_3 rock	1082m	C-O stretch	1085
1119		1138m		1137
1,150	CH_2 twist	1171w		
1185				1191
	CH_2 wag	1216.72m	C-C stretching	1219
1243	C-H bend	1217m		
1275	C-H bend	1293.86		1304
1316				
1352	CO_2 symmetric stretch	1358.80		
	CH_2 Scissors	1389.78w	O-CO bending of COOH	
		1387s	CH_2 scissors	
1406		1426m broad	C-OH def.	1427

	NH_3 symmetric bend	1466 m broad	CH_2 scissors	
1509				
1561	NH_3 asymmetric bend			1524
	NH_3 asymmetric bend			1581
	CO_2 asymmetric bend	1630 m broad		
		1695 vs	C=O stretching	1682
	S-H stretch	1743s	n(COOH)	1711
				1980
				2030
2108				
				2164
				2215
	N-H stretch			
2736	N-H stretch			
2915		2949w		2927
		2956w		
		2979w		
	C-H stretch	2993w		
	CH_2 symmetric stretch			
3144	CH_2 asymmetric stretch			3100
	N-H stretch	3283		3288
		3494		3439

Symbols used are r: rocking, v: stretching, δ: deformation, t: twisting, ω: wagging, γ: deformation out of the plane, τ: torsion, as: antisymmetric, s: symmetric, skel.: skeleton, sh: shoulder, w: weak

The FT-IR spectra of L-methionine–citric acid co-crystal showed CH-CO_2 stretch at 645 cm^{-1}. The C-S stretch and C=O stretching was observed at 692 cm^{-1}. N-CH stretch and C-C bends and OH out–of–plane bending was observed at 887 cm^{-1}. S-H in-plane bend was observed at 980 cm^{-1}. NH_3 rock and C-O stretch were observed at 1048,1085 cm^{-1}. CH_2 wag and C-C stretching were observed at 1219 cm^{-1}. The stretch and bend observed in the co-crystals are slightly different as compared to the original materials indicating the formation of a new compound. The bend and stretch pattern supports the formation of H - O bonds but salt form functional groups were not observed. It indicates that there may be the co-crystals formed in between L-methionine and citric acid.

4 DVS data

Based on the DVS isotherm of L-methionine, citric acid and their co-crystal (n=3; s.d.≤ 0.03), that co-crystal process can improve the non-hygroscopicity of the Citric acid molecule. The co-crystal of citric acid and L-methionine only absorbed 0.46% moisture was absorbed in 90% RH.

Therefore, to understand its absorption profile in the presence of sodium bicarbonate, in the ratio of 1.5:1 to the citric acid amount in the cocrystal was added to this mixture and subjected to different humidity conditions. Figure 5.42 and Table 5.20 represents the DVS isotherm for SBC, based on the data generated it is observed that loss in weight is occurring which is due to the instability of citric acid-methionine cocrystal in the presence of SBC.

Table 5. 20 DVS of L - methionine, citric acid and their co-crystal

%RH	Citric acid	Methionine pure	Met-CA cc 280716	Met-CA cc + 1.5x $NaHCO_3$
0.0	0.00	0.00	0.001	0.001
10.0	0.00	0.01	0.013	-0.246
20.0	0.00	0.02	0.047	-0.337
30.0	0.00	0.02	0.094	-0.443
40.0	0.00	0.03	0.150	-0.575
50.0	0.00	0.04	0.221	-0.730
60.0	0.01	0.05	0.307	-0.866
70.0	0.02	0.07	0.460	-0.765
80.0	4.65	0.09	1.027	0.388
90.0	**31.21**	**0.16**	**1.817**	**8.340**

Met=L-methionine, CA=citric acid, cc=cocrystal, $NaHCO_3$=Sodium bicarbonate.

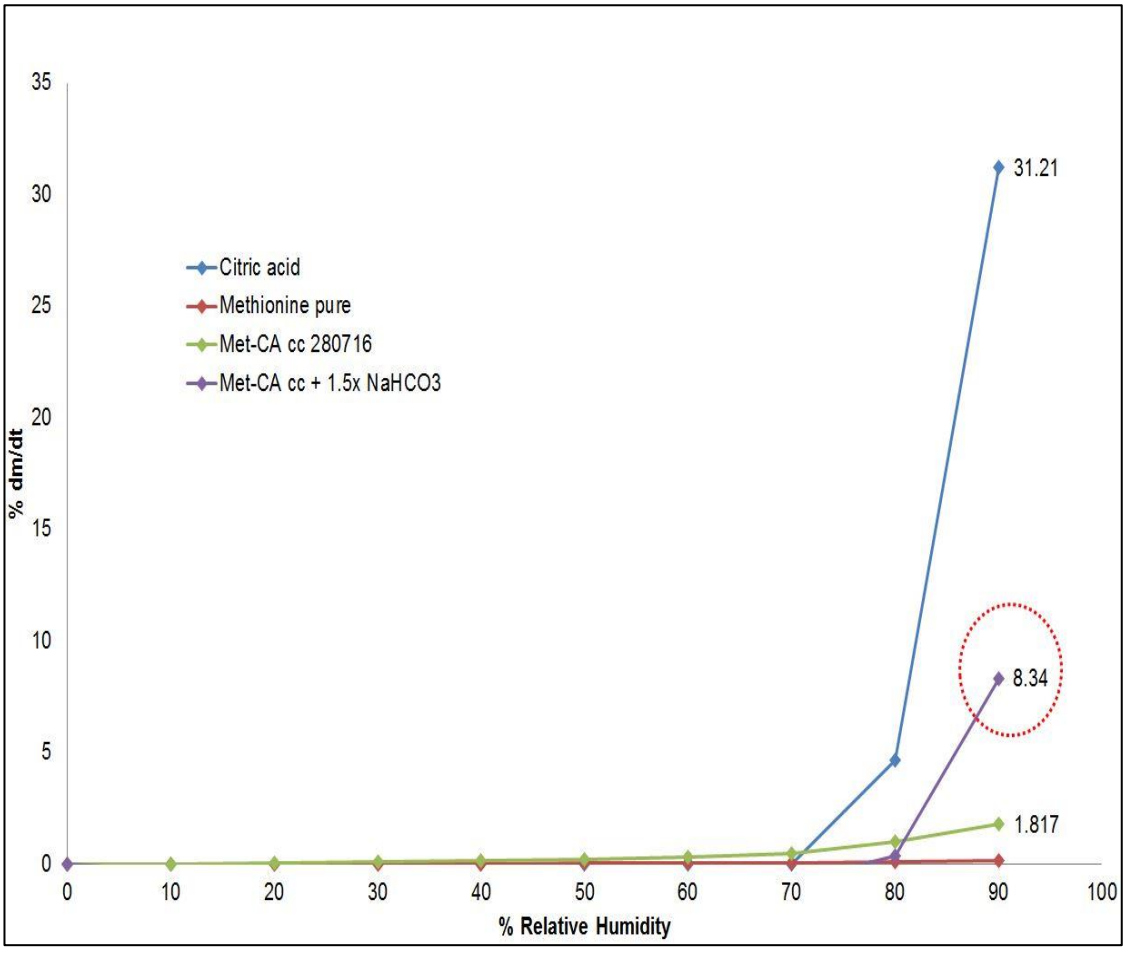

Figure 5.42 DVS of citric acid, L- methionine and their co-crystal.

5.3.5 Citric acid –L-cysteine study

1 PXRD data

Based on the overlay of PXRD patterns of citric acid, cysteine starting materials and LAG processed samples (n=3) (Figure 5.43) change in crystal phase is identified. In LAG processed sample new peaks at 7.96, 11.36 and 22.92 2θ° were detected which are absent in both the starting materials. Thus, based on the PXRD data new crystal phase of citric acid-cysteine in 1:1 ratio is obtained.

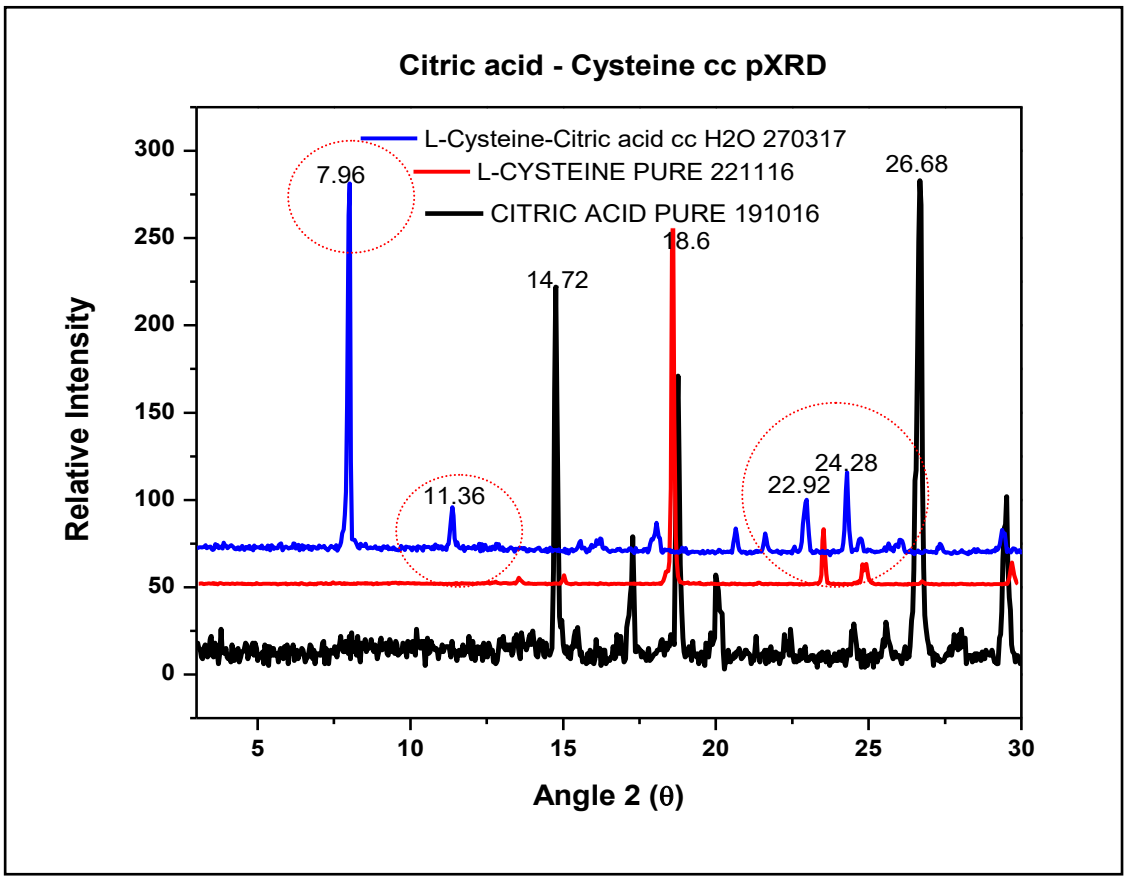

Figure 5.43 PXRD of citric acid, L- cysteine and their cocrystal

2 DSC data

To further investigate the presence of a residual solvent and phase impurity thermal analysis using DSC analyser was performed for all processed and raw samples (Figure 5.44).

In the DSC analysis of citric acid- cysteine 1:1 LAG mixture (n=3), a sharp single endothermal peak of melting point was observed around 72.77°C, which is different from the starting materials melting points. As per the previous record, the melting point of citric acid is 153°C (Rehder et al. 2011) and a melting point of L-cysteine is 240°C (NCBI 2017a). The observed results suggest that there is new crystalline phase formed, which could be a cocrystal of citric acid –L-cysteine in 1:1 stoichiometry. This result is supporting to the PXRD data.

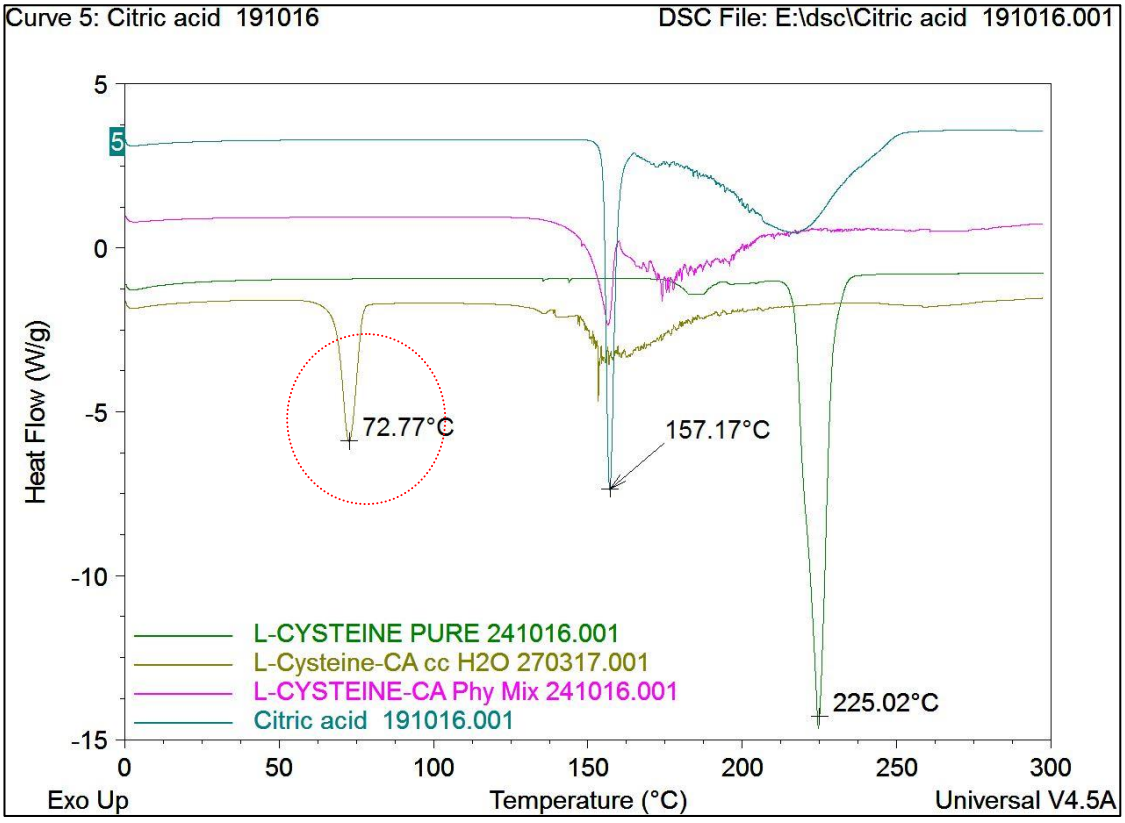

Figure 5.44 DSC results of citric acid - L - cysteine cocrystal

3 Spectroscopic analysis

3.1 Raman spectroscopy

Based on the spectral overlay of citric acid, L- cysteine and cocrystal sample (n=3), it was observed that the cocrystal has no significant peaks similarity to

characteristic peaks of starting materials. This indicates that there may be the formation of a new molecule. See Figure 5.45.

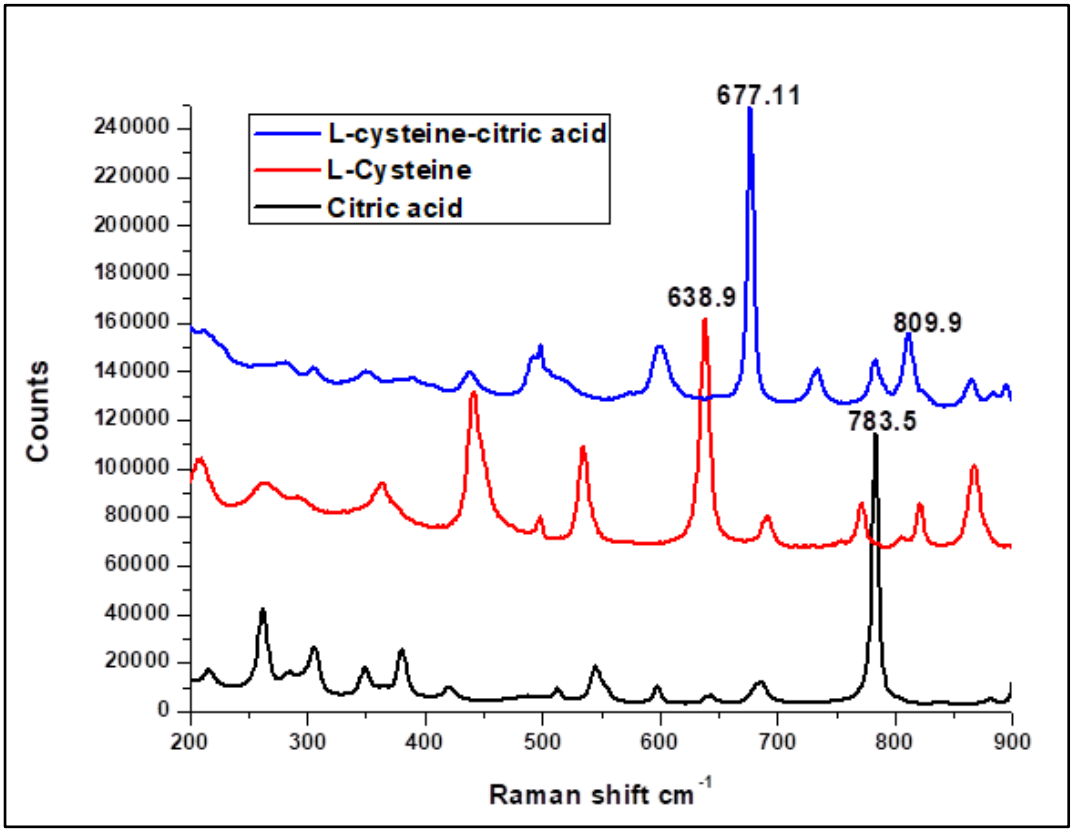

Figure 5.45 Raman spectrum of citric acid – L- cysteine co-crystals processed by Spectragryph version 1.2.7.

The study of the structures of these two molecules indicates that both molecules can donate as well as to accept the H-bonds/hydrogen bonds. See Figure 5.46.

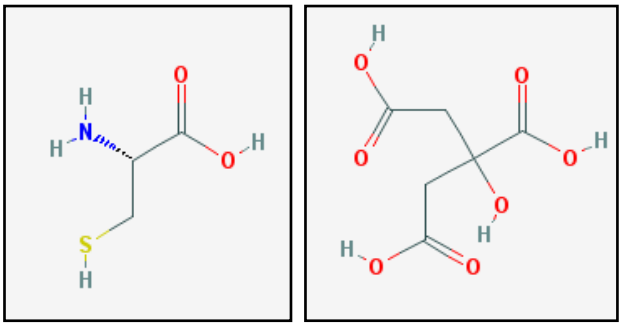

Figure 5.46 L-cysteine (left), citric acid (right) .

From Raman, it was observed that there is a slight Raman shift in the region of -NH_2^+ group. It was noticed that NH_3 rock changed slightly from 1005, 1011, 1080 to 1070. C-S stretch peak was absent from 692-693 region. CH_2-CO_2 stretch was absent from 636-639 region. NH_3 torsion was absent at 550 regions. CH_2-CH-N bend at 536 regions was also absent from the co-crystal molecule. It reveals that there may be stretching, and new bond formation occurs in between citric acid and L-cysteine molecules at -NH_3^+ region of L-cysteine and COOH group of citric acid. Table 5.21 shows the Raman spectra results of citric acid, L-cysteine and their co-crystal.

Table 5. 21 Raman spectra band and associated functional groups in citric acid, L-cysteine and their co-crystal.

Transition energies (cm^{-1}) with mode descriptions of L-cysteine		citric acid		L-cysteine-citric acid cc Raman spectra observed
Raman	A functional group associated.	Raman	A functional group associated.	Raman
167				128.8
209	CH_2-CH torsion			175.3
		212		
		258m broad		
298	CH_2-CH-CO_2 bend			281.3
		301m		
		345m		349.9
364	S-H out-of-plane bend			389.7
	N-CH-CO_2 bend	417m		
441,450	CH_2-CH-SH bend			438.1
		499w		498.4
536	CH_2-CH-N bend	539sh		
	NH_3 torsion	550m		
		593m	sC-CH_3	600.1

639	CH-CO_2 stretch	636w		
		682m	C=O stretching	677.4
693	C-S stretch			
				733.3
773	CH_2 rock	780s		783.3
806	CH_2 Scissors			811.5
868	CO2 wag			865.1
		877w		
		900m	C-C bends and OH out-of-plane bending	894.8
941	N-CH stretch	939s	C-C symmetric stretch	932.7
996, 1008	CH_2-CH stretch			1002.8
1067	S-H in-plane bend	1050m	C-O stretch	1042
1005, 1011	NH_3 rock	1080m	C-O stretch	1070
1140	NH_3 rock	1141m		1131
		1165w		1166.1
1,199	CH_2 twist	1205m	C-C stretching	
	CH_2 wag	1217m		1217.3
1260, 1274	C-H bend			1281.1
1294, 1302	C-H bend			1302.1
1345, 1354	CO_2 symmetric stretch	1346w	O-CO bending of COOH	1353.2
1398, 1425	CH_2 Scissors	1387s	CH_2 scissors	1403.1
		1430m broad	C-OH def.	1433.2
		1466 m broad	CH_2 scissors	
1525	NH_3 symmetric bend			
1574, 1581	NH_3 asymmetric bend			
1616	NH_3 asymmetric bend			1610
		1630 m		

		broad		
1644	CO_2 asymmetric bend			
		1691 vs	C=O stretching	1683
		1734s	n(COOH)	
2545, 2553	S-H stretch			2563
	N-H stretch			
2958, 2968	N-H stretch	2949w		2929
		2956w		
		2979w		2975
		2993w		
3000	C-H stretch			
	CH_2 symmetric stretch			
	CH_2 asymmetric stretch			
	N-H stretch			

Symbols used are r: rocking, v: stretching, δ: deformation, t: twisting, ω: wagging, γ: deformation out of the plane, τ: torsion, as: antisymmetric, s: symmetric, skel.: skeleton, sh: shoulder, w: weak

3.2 FTIR data

The Fourier transform infrared spectra (FT-IR) analysis of citric acid, L-cysteine and their 1:1 cocrystal by LAG was processed (n=3) and it showed the pattern as in Figure 5.47 and the bands were recorded in the Table 5.22 as follows.

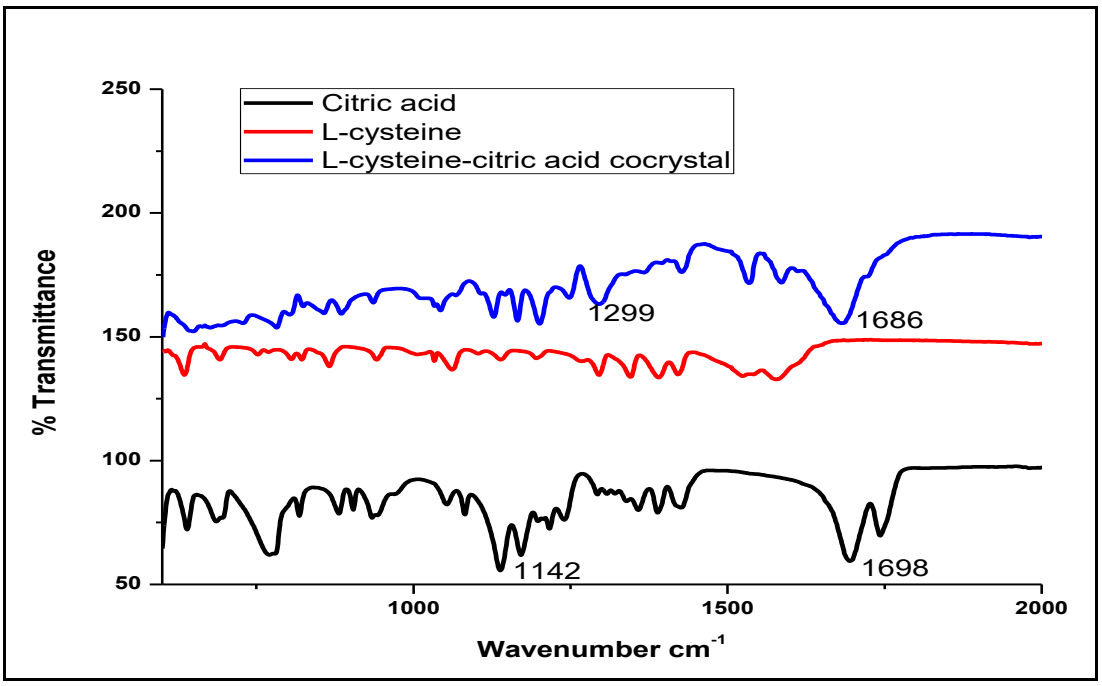

Figure 5.47 FT-IR spectra of citric acid, L- cysteine and their co-crystal.

The change in the patterns of the wavenumber gives an idea of the new bonding formation or stretch and bend pattern of the molecules. Obtained peaks were compared with the original material peak patterns and changes noted. S-H in-plane bend was observed around wavenumber 1043 cm^{-1}. The NH_3 rock and C-O stretch were observed at 1128 cm^{-1} in the new co-crystal molecule. CH wag and C-C stretching were observed at 1201 cm^{-1}. C-H bend was observed at 1248, 1296 cm^{-1}. C-OH deformation peak was observed at 1427 cm^{-1}. C=O stretching was observed at 1681 and n(COOH) S-H stretch peak was observed at 2564 cm^{-1}. A water peak of OH stretch was observed at 3478 cm^{-1}. It indicates that there may be a water molecule is present in this co-crystal, which suggests that there is co-crystal hydrate formation occurred.

Table 5. 22 FT-IR spectra band and an associated functional group of citric acid, L-cysteine and their co-crystal molecule.

L-cysteine cm^{-1}	associated group	citric acid	associated group	L-cysteine-citric acid cc IR
	NH_3 torsion	550m		
		593m	$sC-CH_3$	
635.1	$CH-CO_2$ stretch	639.6		649
691.7	C-S stretch	686.2m	C=O stretching	
				728.6
752.3	CH_2 rock	770.5		782.5
806	CH_2 Scissors	818.4s		
822.3				
865.8	CO_2 wag			857.4
		881.2w		885.5
941.2	N-CH stretch	900m	C-C bends and OH out-of-plane bending	
996, 1006	CH_2-CH stretch	934.3s	C-C symmetric stretch	936.1
1062	S-H in-plane bend	1.053.82		1043
1103	NH_3 rock	1050m	C-O stretch	
1139	NH_3 rock	1082m	C-O stretch	1128
		1138m		
1,196	CH_2 twist	1171w		1166
	CH_2 wag	1216.72m	C-C stretching	1201
1260, 1274	C-H bend	1217m		1248
1295	C-H bend	1293.86		1296
1345	CO_2 symmetric stretch	1358.80		1367
1390, 1421	CH_2 Scissors	1389.78w	O-CO bending of COOH	
		1387s	CH_2 scissors	

		1426m broad	C-OH def.	1427
1524	NH_3 symmetric bend	1466 m broad	CH_2 scissors	1534
1577	NH_3 asymmetric bend			1586
1616	NH_3 asymmetric bend			
1644	CO_2 asymmetric bend	1630 m broad		
		1695 vs	C=O stretching	1681
2080				
2506				
2550	S-H stretch	1743s	n(COOH)	2564
2633	N-H stretch			2665
2779	N-H stretch			
		2949w		2931
		2956w		
2965		2979w		2972
	C-H stretch	2993w		
	CH_2 symmetric stretch			3128
	CH_2 asymmetric stretch			
3162.9	N-H stretch	3283		
		3494		3476

Symbols used are r: rocking, v: stretching, δ: deformation, t: twisting, ω: wagging, γ: deformation out of the plane, τ: torsion, as: antisymmetric, s: symmetric, skel.: skeleton, sh: shoulder, w: weak peak intensities

4 DVS data

After DVS study of L-cysteine, citric acid and their LAG processed samples (n=3; s.d.≤ 0.03), it was observed that it remains in powder form at 90 % RH

with only 12.07% of moisture absorption. After obtaining single crystal of the same pair through slow solvent evaporation method, it was observed that it has further improved its non-hygroscopic nature and absorb only 3.18 % of moisture at 90% RH. However, when tested with 1.5 times addition of sodium bicarbonate equivalent to citric acid content, it reacted at 80% RH by -2.76 %, but still, only 5.74 % of moisture was absorbed in 90 % RH. It means that up to 70% RH condition, there was no reaction in the mixture of co-crystallised citric acid and sodium bicarbonate. It will help in reducing the cost of maintenance regarding environmental conditions in the manufacturing of effervescent tablets. Please see table 5.23 and Figure 5.48.

Table 5.23 DVS study of citric acid-L-cysteine and their co-crystal.

%RH	citric acid	L-cysteine pure sigma	CA-L-cysteine	CA-L-cysteine single crystal	CA-L-CYS SC +1.5x SBC
0.0	0.00	0.00	0.00	0.001	0.000
10.0	0.00	0.04	0.07	0.015	0.000
20.0	0.00	0.07	0.26	0.062	0.003
30.0	0.00	0.10	0.61	0.394	0.008
40.0	0.00	0.13	0.87	0.586	0.013
50.0	0.00	0.15	1.06	0.677	0.016
60.0	0.01	0.18	1.31	0.740	0.015
70.0	0.02	0.21	1.72	0.813	0.046
80.0	4.65	0.27	2.43	0.886	-2.760
90.0	**31.21**	**0.43**	**12.07**	**3.184**	**5.740**

RH: relative humidity, CA: citric acid, L-CYS: L-cysteine, SC: single crystal, SBC: sodium bicarbonate.

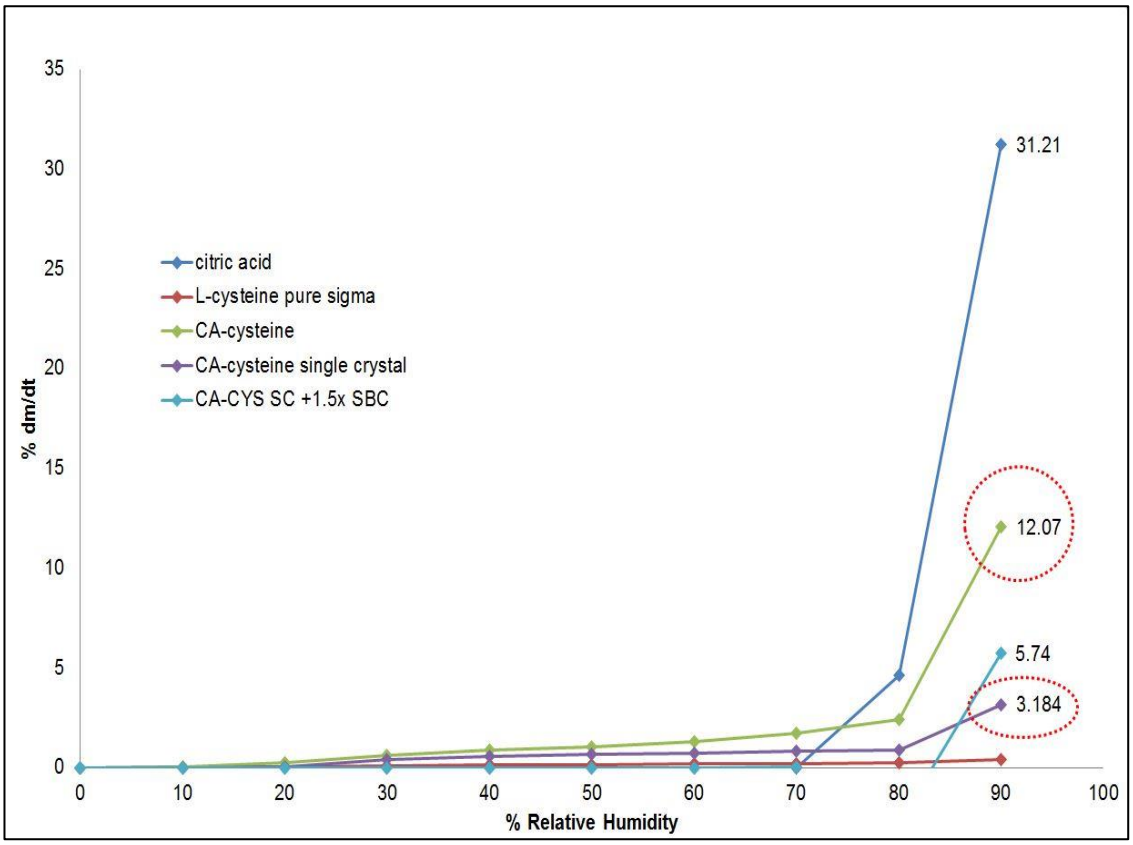

Figure 5.48 DVS study of citric acid –L- cysteine and their co-crystal.

5 Summary

The DVS study of citric acid showed that citric acid compound has high affinity towards water. It was observed that citric acid could tolerate moisture up to 70% relative humidity condition but after 70% RH reacts and starts absorbing moisture and becomes deliquescent at 90%RH. Therefore, it was attempted through the co-crystallisation process in this current study, to reduce the hygroscopicity of citric acid in order to improve its storage capability by making it non-hygroscopic. The amino acids were found to be prominent to form cocrystal with citric acid. Total five amino acids amongst 17 were screened for successful cocrystal formation in 1:1 ratio with citric acid. Obtained LAG samples were characterised by PXRD, DSC, and spectroscopic analysis and finally checked for their moisture absorption by DVS. Through DVS study only

one cocrystal (L-cysteine-citric acid in 1:1 ratio) was observed to be less hygroscopic at various moisture conditions as compared to the citric acid.

All obtained cocrystals were further examined for single crystal development study.

5.3.6 Citric acid-amino acid solution crystallisations

All five pairs of amino acid-citric acid co-crystals were selected in 1:1 stoichiometric ratio and subjected to solution/solvent slow evaporation crystallisation process (n=2) to generate single crystals. The range of solvent systems like methanol, ethanol, water, a mixture of ethanol and water (1:1 v/v) as well as methanol and water (1:1 v/v) were used for this study. Molar equivalents of citric acid-amino acid was selected in 1:1 stoichiometry ratio and completely dissolved in the solvent system under external heating conditions of 70°C temperature with continuous stirring. This solution was further filtered through Whatmann filter paper no.1 and left for solvent evaporation at room temperature until crystallisation occurs. In some cases, crystallisation occurs after 4-5 days such as citric acid – L-methionine, citric acid-L-leucine, citric acid -L-isoleucine; but in other cases (citric acid-L-serine and citric acid -L-cysteine) no crystallisation was observed even after 22 days. Instead they form a jelly like glassy transparent material. Then the sticky mass was agitated using a clean spatula, which led to nucleation at the bottom of the conical flask and eventually a complete crystalline phase was observed in the conical flask after 40 days with citric acid-L-cysteine (see Figure 5.49).

Based on the solution evaporation experiments, citric acid failed to generate any crystals with L-leucine, L-isoleucine and L-methionine. In these experiments due to the solubility of amino acids in the solvent system, they crystallised out first as an impurity. For amino acid L-serine and L-cysteine water was used as

the solvent system for generation of crystals with citric acid. The generated crystalline material (Figure 5.49) was used as a seed to generate good quality single crystals from a saturated solution (made up of only 1ml of deionised water and mixture of citric acid and L-cysteine in 1:1 stoichiometry) of citric acid-L-cysteine amino acid.

Figure 5.49 A crystalline material obtained from citric acid-L-cysteine 1:1 mixture solution in water after complete evaporation of water.

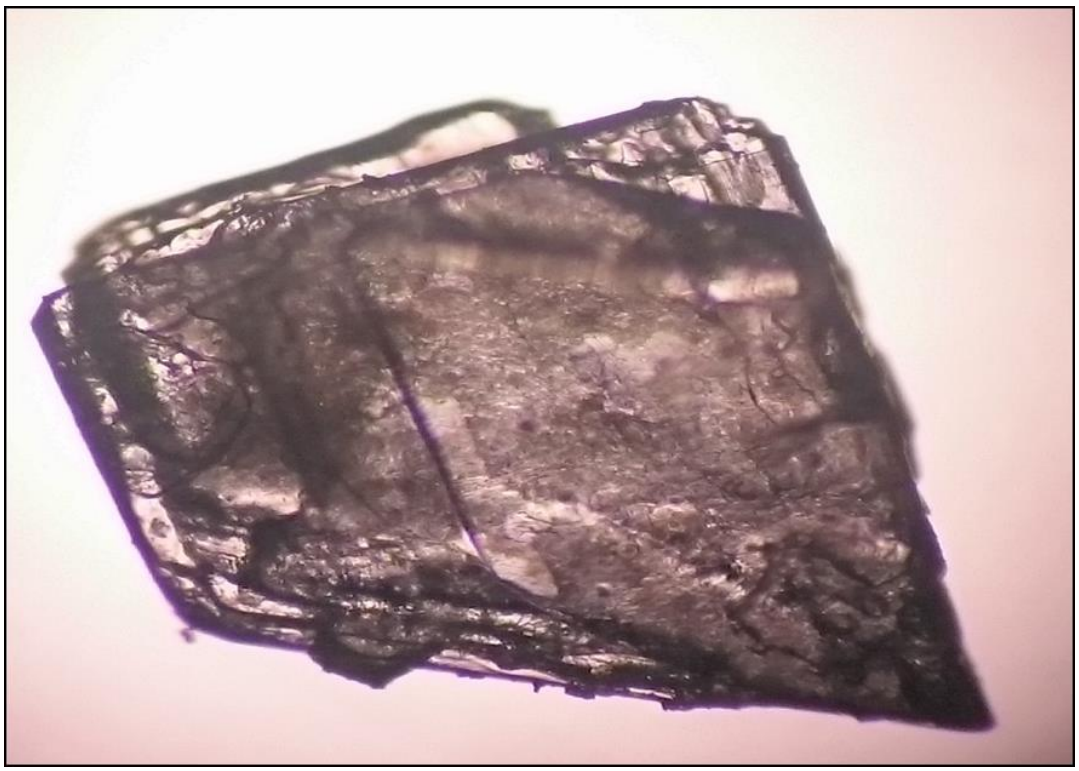

Figure 5.50 A single crystal of citric acid-L-cysteine monohydrate 1:1 co-crystal.

The generated single crystals were dried properly and subjected to further different characterisation techniques to investigate the cocrystal phase. One of the best single crystal has been observed and imaged under compound microscope at 40x (See Figure 5.50).

1.0 PXRD

Below Figure 5.51 represents the PXRD pattern of citric acid, L-cysteine starting material and single crystal of citric acid-L-cysteine solution crystallised (n=3). It is observed that solution crystallised citric acid-L-cysteine crystal material displayed distinct characteristic peaks at 8.32, 14.76 and 24.56 2θ°angle. These peaks are absent in the PXRD pattern of starting materials. This generated PXRD pattern of the single crystal is similar to the pattern obtained in a LAG experiment in our previous experiments.

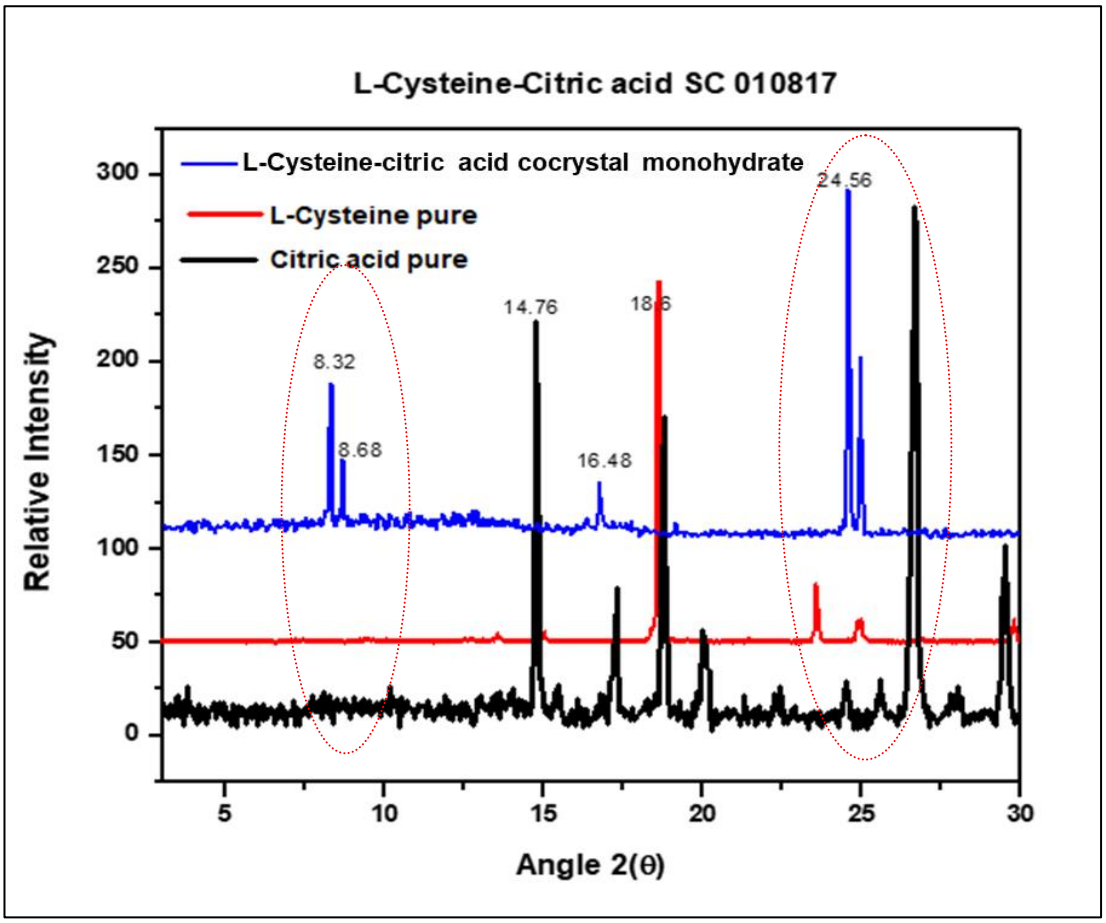

Figure 5.51 PXRD of a single crystal of citric acid-L-cysteine monohydrate (SC= single crystal).

2.0 Thermal analysis

2.1 DSC

Below Figure 5.52 demonstrates the overlay of DSC thermogram of citric acid-L-cysteine single crystal and starting material (n=3). The single crystal of citric acid-L-cysteine displayed a single distinct endothermic peak at 78.25°C which is quite different from the melting point of citric acid (157.17°C) and L-cysteine (225.84°C) respectively.

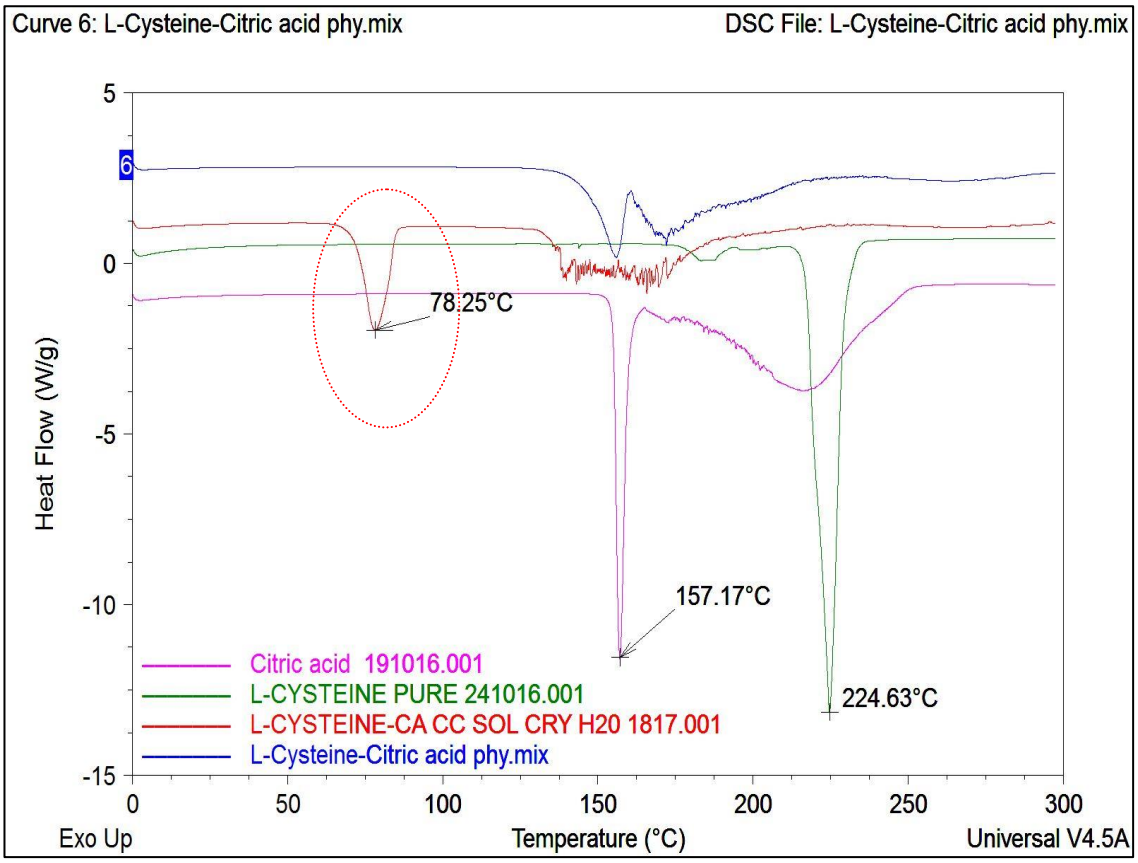

Figure 5.52 DSC of a single crystal of citric acid -L-cysteine monohydrate and their original material, physical mixture (1:1) ratio.

2.2 TGA

The thermogravimetric analysis of single crystal (n=2) (Figure 5.53) showed the difference in degradation and melting point pattern from the original starting material. The onset melting point of the obtained cocrystal is at 53.13˚C. This was earlier compared to the starting material onset melting points. The onset melting point of citric acid and cysteine was at 128.50°C and 164.98°C respectively.

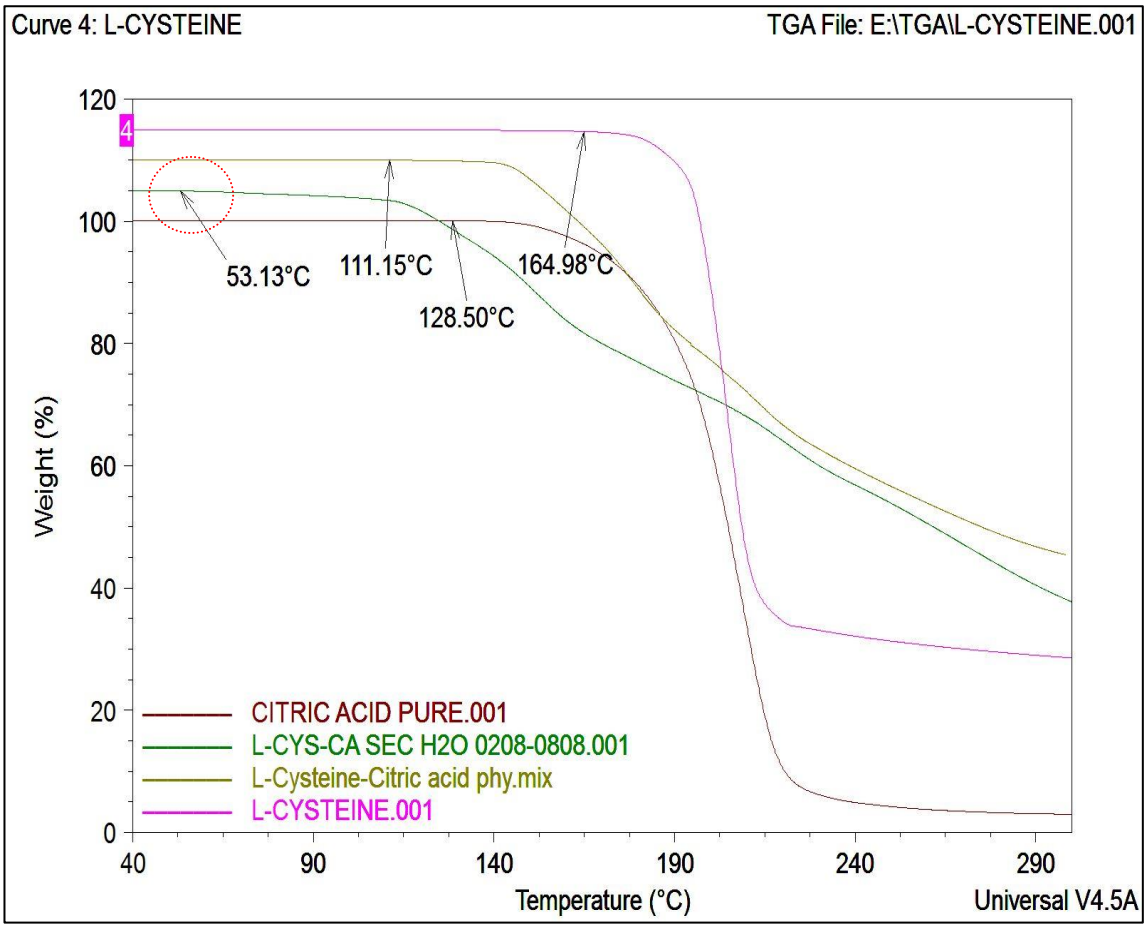

Figure 5.53 TGA of the single crystal of citric acid-L-cysteine monohydrate and starting material

3.0 DVS data

The DVS analysis (n=3; s.d.≤ 0.03), showed that the obtained single crystal absorbs only

3.18 % of moisture at 90% RH. In the presence of 1.5 x sodium bicarbonate to that of citric acid content in the cocrystal, showed stable low moisture absorption up to 70% RH. Please see Table 5.24 and Figure 5.54.

Table 5.24 DVS of a single crystal of citric acid-L-cysteine monohydrate cocrystal.

% RH	Dm/Dt
0.0	0.001
10.0	0.015
20.0	0.062
30.0	0.394
40.0	0.586
50.0	0.677
60.0	0.740
70.0	0.813
80.0	0.886
90.0	3.184

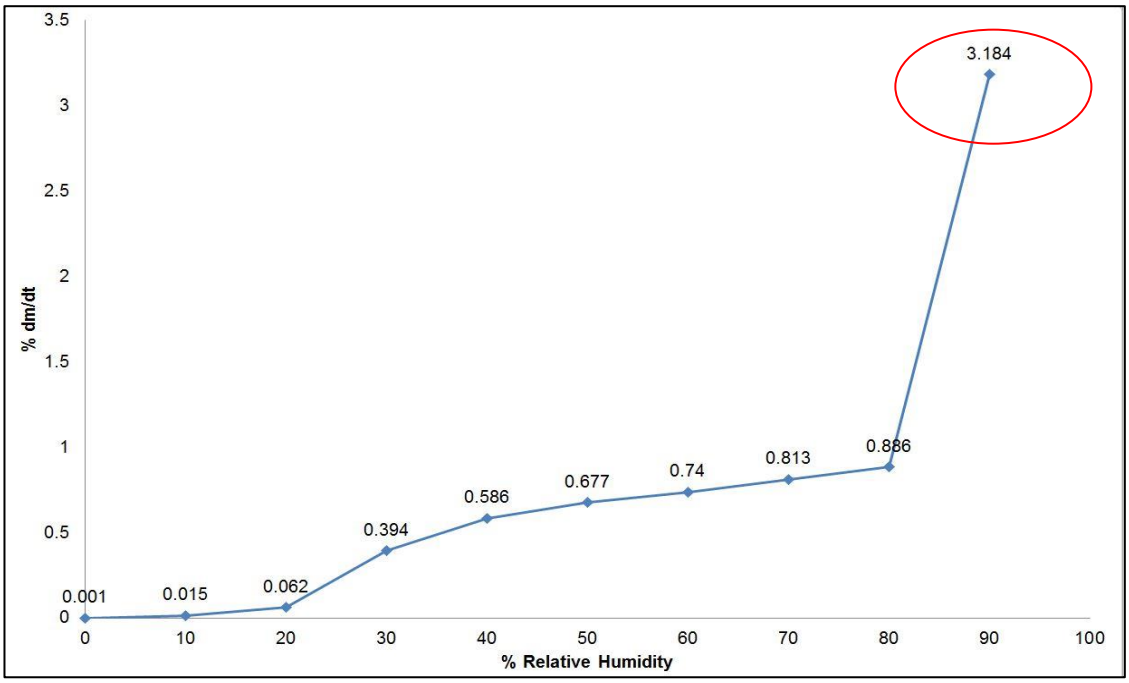

Figure 5.54 DVS of a single crystal of L-cysteine–citric acid-H_2O cocrystal

4.0 Scanning electron microscopy of L-cysteine-citric acid-monohydrate cocrystal

Scanning electron microscopy (SEM) of L-cysteine-citric acid monohydrate cocrystal (single crystals) and its starting materials were carried out. The observed results are showed in the Figure 5.55 to 5.58.

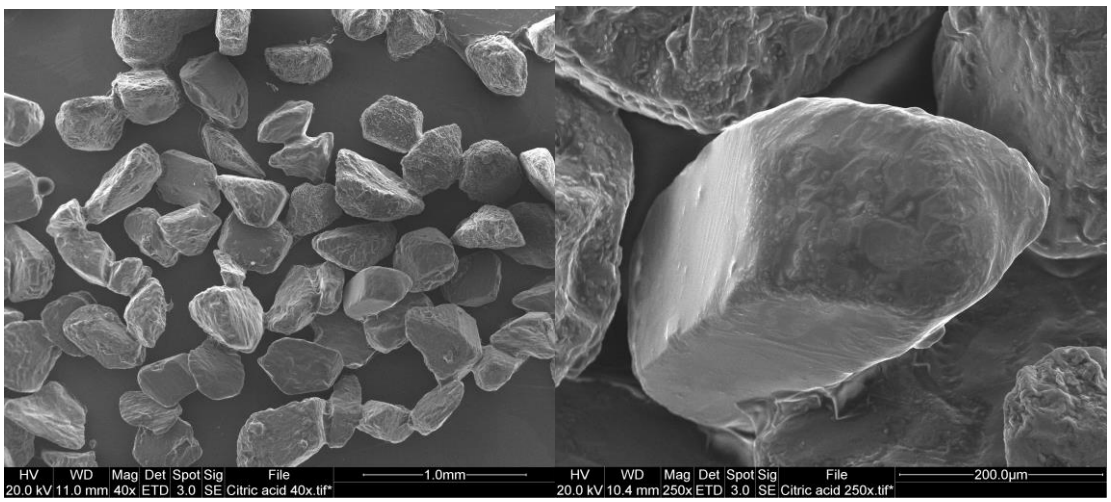

Figure 5.55 SEM images of citric acid 40x and 250x magnification.

SEM of citric acid showed a rough surface of crystalline material containing cavities which could contribute for moisture absorption.

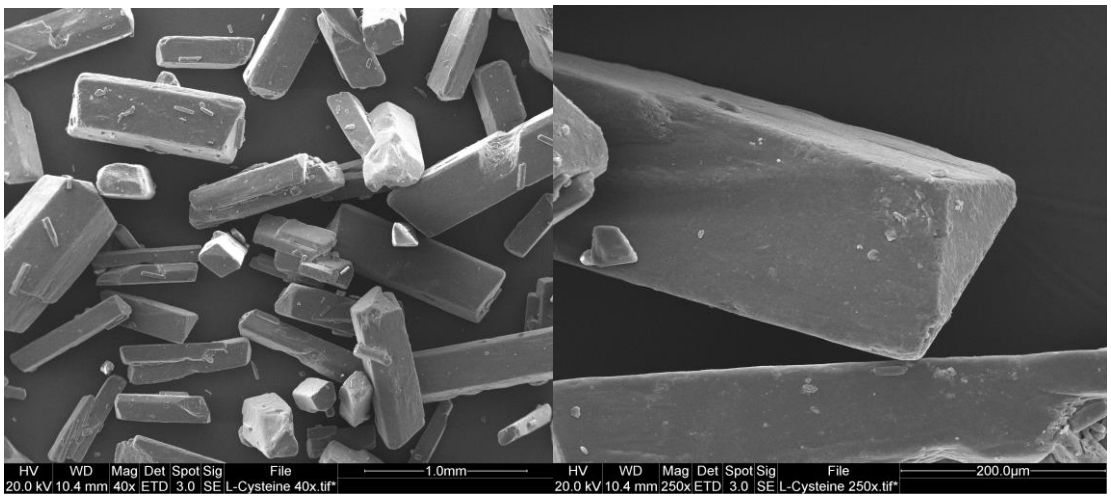

Figure 5.56 SEM images of L-cysteine 40x and 250x magnification.

SEM of L-cysteine reveals that some triangular shaped long bars with smooth surface which could attribute to low moisture attraction.

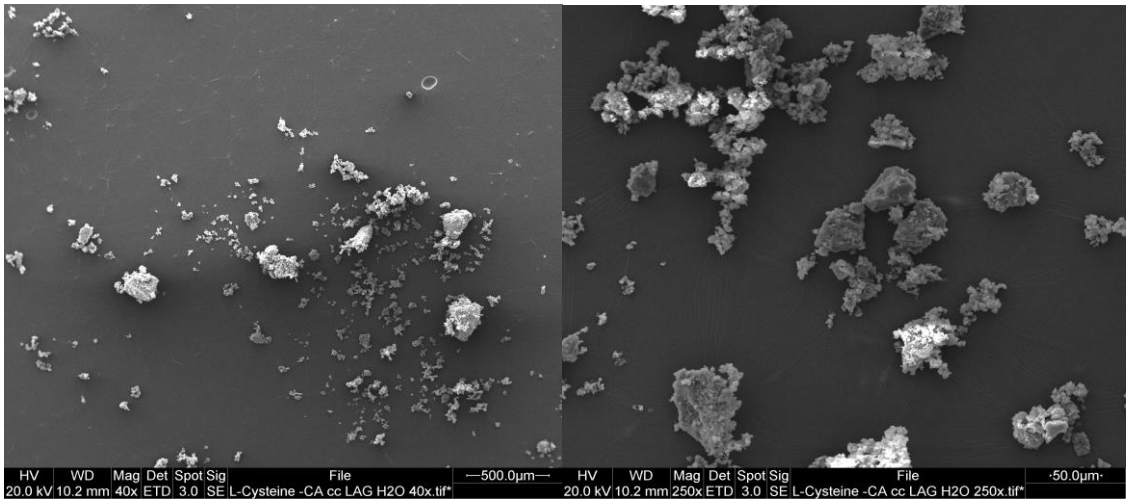

Figure 5. 57Figure 5.57 SEM images of L-cysteine-citric acid LAG sample 1:1 ratio 40x and 100x.

SEM of LAG mixture of L-cysteine-citric acid shown an agglomerated material.

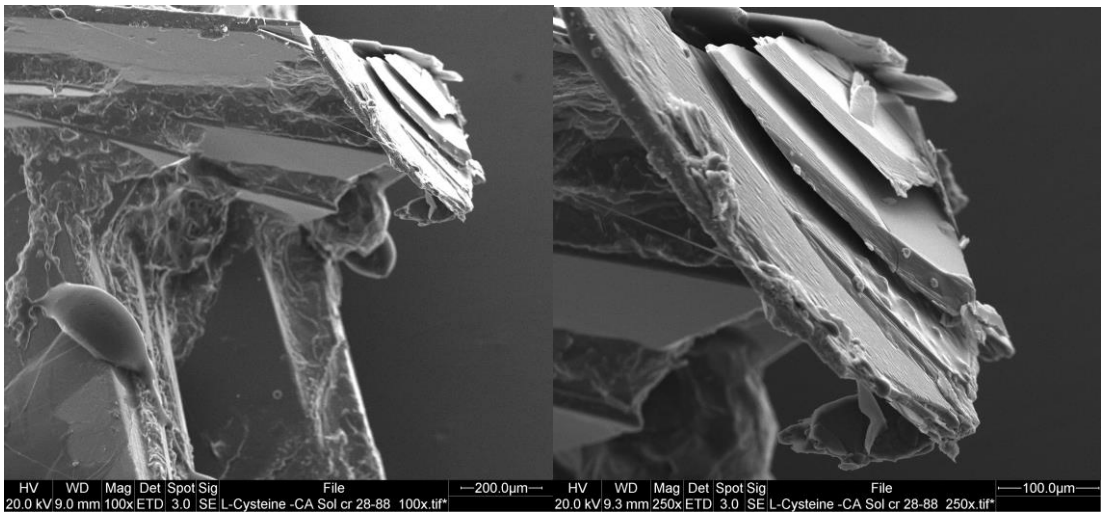

Figure 5.58 SEM images of single crystal of L-cysteine-citric acid-monohydrate cocrystal 100x and 250x.

SEM images of L-cysteine-citric acid monohydrate (single crystals) reveals that many plates stacking arrangement of crystal with smooth surface could be attribute to low moisture attraction.

5.0 Single crystal X-ray diffraction analysis

The obtained good quality single crystals were subjected to single crystal X-ray crystallography (n=2). This involved the mounting of a single crystal on the

goniometer of Xcalibur Gemini EOS CCD diffractometer (Oxford Diffraction, Yarnton, UK). Reflections from the crystals were collected using Mo-Kα, radiation at 298K. CrysAlisPro (Version 1.171.33.55) software was used for data reduction. The reflection data and crystal structure were refined and solved using OLEX2-1.0 and SHELX-TL 97 software with the anisotropic refinement of non-hydrogen atoms. In a crystal, hydrogen atoms present in oxygen and nitrogen were located experimentally through difference electron density maps. The HFIX command in SHELX-TL was used for geometrical fixing of all C–H atoms. The final CIF file was checked using PLATON for any missed symmetry. The packing diagram was prepared using X-Seed program.

The single crystal data showed the formation of L-cysteine - Citric acid co-crystal hydrate in 1:1 stoichiometric ratio. Figure 5.59 shows ORTEP plot. Figure 5.60 shows the 1:1 stoichiometric ratio. Figure 5.61 reveals how these two molecules are bound to each other and the trapping of one water molecule in between them. Table 5.25 summarises the crystallographic parameters.

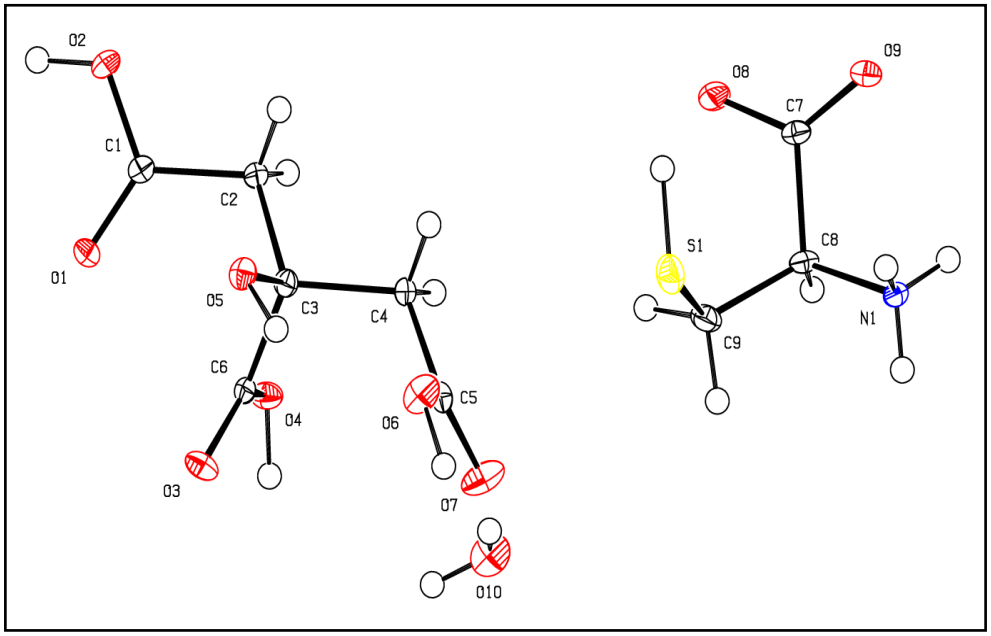

Figure 5.59 ORTEP plot drawn at 50% probability level.

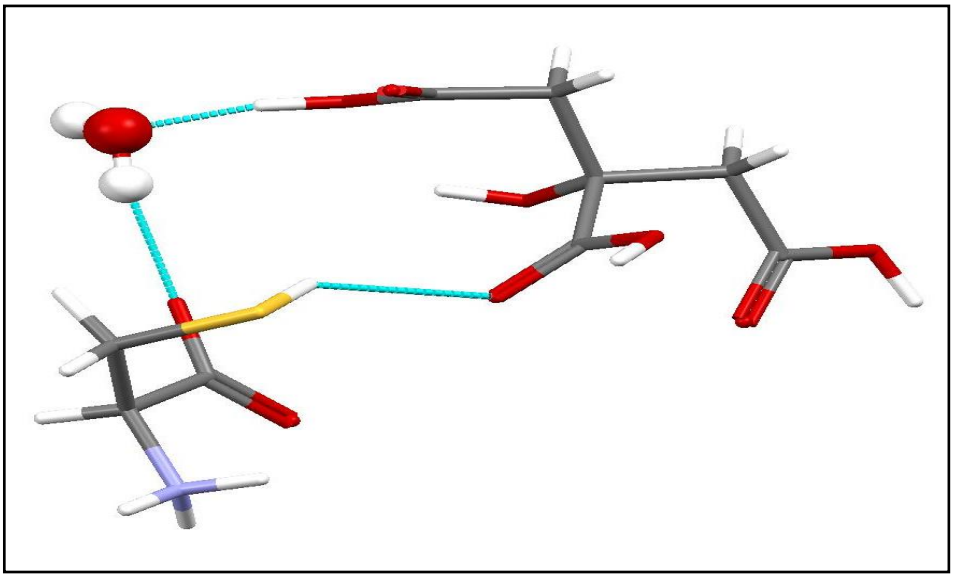

Figure 5.60 L-cysteine with citric acid co-crystal monohydrate in 1:1 stoichiometric ratio.

In Figure 5.60, the L-cysteine molecule bonded to the citric acid molecule through water molecule as C-H…H-O…H bonding. The bond between S-H…O observed is weak bonding.

However, the main key interactions are revealed on the other side of bonding which is shown in Figure 5.61.

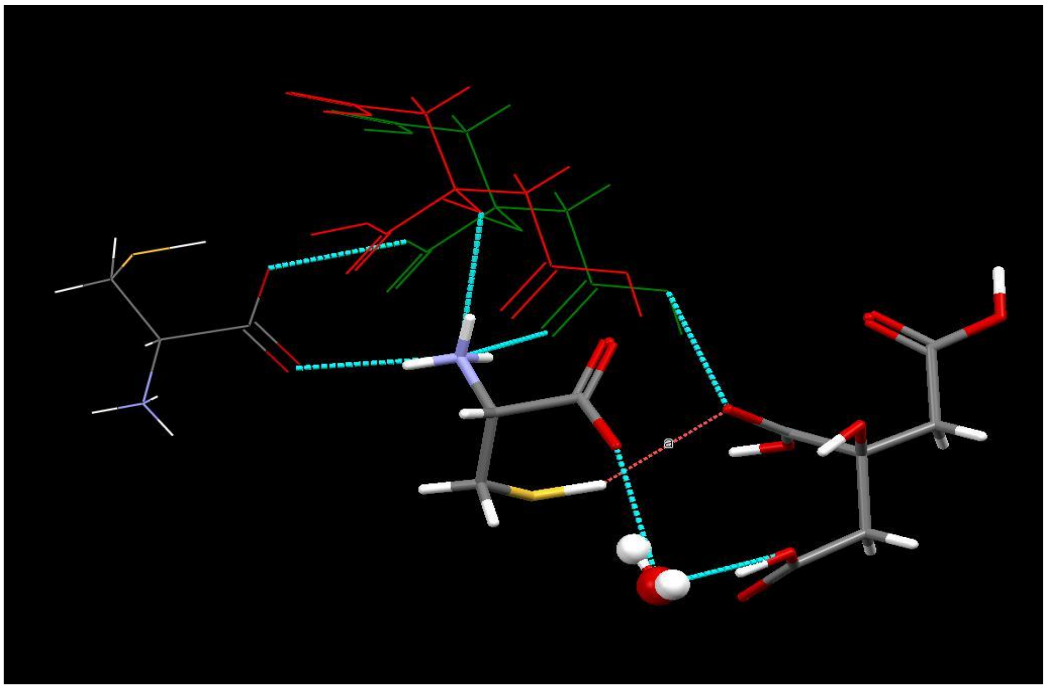

Figure 5.61 Key interactions in the co-crystal of L-cysteine-citric acid-H_2O

Figure 5.61 reveals the key interactions of this co-crystal, through which the other side of bonding was exposed. There is bonding between the hydrogen of the amino group of L-cysteine and two molecules of citric acid and one molecule of L-cysteine. There is bonding between first L-cysteine molecules -NH^{3+} group, as N-H…O-C with another L-cysteine molecule. The other two hydrogen bonding was also observed with the same -NH^{3+} molecule of first L-cysteine molecule to the two citric acid molecules. This bonding occurred -N-H…O-C of 1st citric acid and -N-H…O – H group of a 2nd citric acid molecule. However, the -COOH group of the 1st L-cysteine molecule connected to the water molecule as C-O….H bonding, which is another side bonded to the 3rd citric acid molecule. This 3rd citric acid molecule was bonded weakly to the 1st L-cysteine molecule. Based on these various bonds, it can be predicted that, if tried carefully, L-cysteine-citric acid co-crystal can be formed without involving water molecule. However, here in this current study water was used in solvent evaporation method. It is well known that citric acid molecule has a strong affinity towards a water molecule. Thus, it was easier to adopt a water molecule in between the L-cysteine and citric acid crystal lattice. Other solvents were used, but they failed to work.

Table 5.25 Crystallographic data of citric acid-L-cysteine-H_2O

	citric acid-L-cysteine-H_2O
Crystal Shape	Plate-like clear crystals
Colour	Colourless, clear
Empirical formula	$(C_3H_7NO_2S)\cdot$ $(C_6H_8O_7).(H_2O)$
Formula weight	331.29
Crystal system	Monoclinic
Space group	$P\ 2_1$
T [K]	170(2)
a [Å]	5.7524(NCBI)
b [Å]	10.8433
c [Å]	11.1221
α [°]	90
β [°]	102.285(2)
γ [°]	90
Z	4
V [Å^3]	677.86
D_{calc} [g cm^{-3}]	1.623
μ [mm^{-1}]	0.152
Reflections used	9783
Unique reflections	2259
Observed reflections	2271
Parameters	258
R1[I > 2σ(I)]	0.0326
wR_2 [all]	0.0769
GOF	1.153

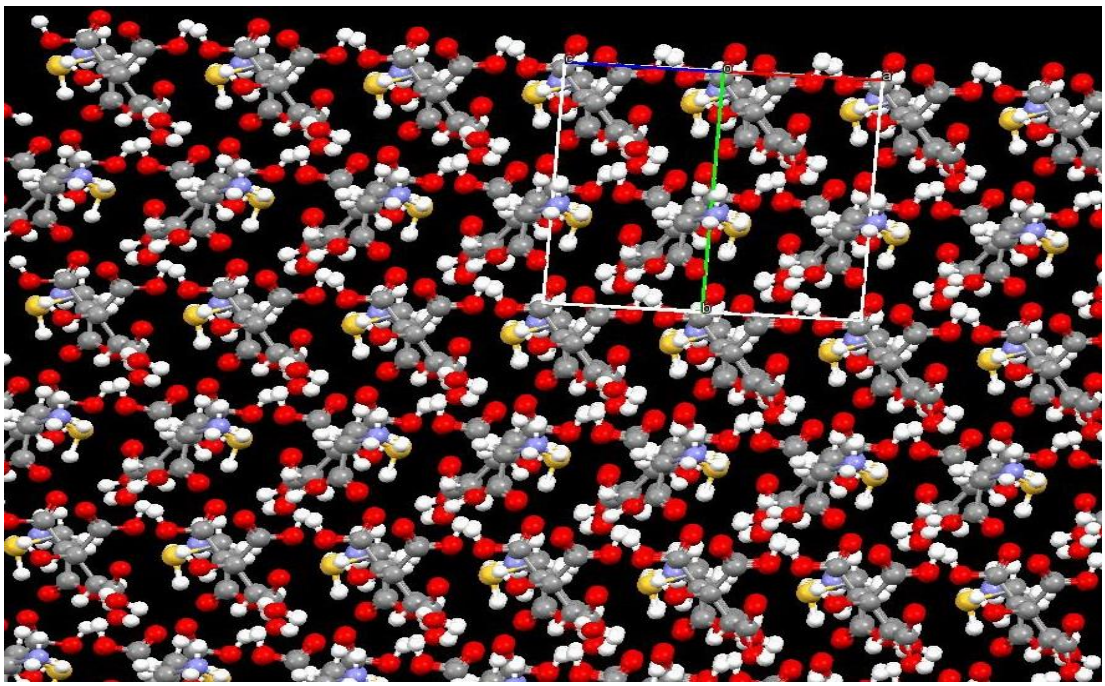

Figure 5.62 shows the packing of citric acid-L-cysteine-H_2O co-crystal monohydrate.

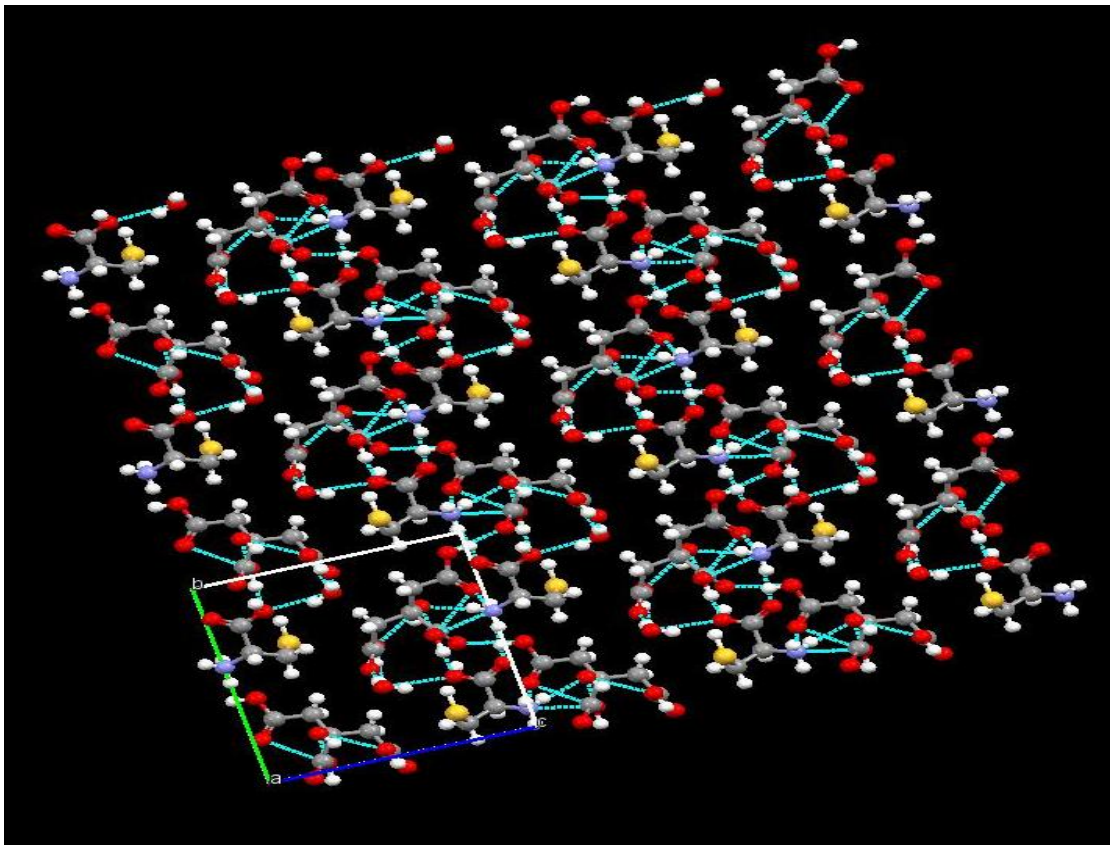

Figure 5.63 Packing of citric acid-L-cysteine-H_2O co-crystal monohydrate.

Thus, amino acids were screened for co-crystals formation, and five co-crystals with citric acid, four of L-proline-NSAIDs, and three of L-proline- carboxylic acid were successfully developed and characterised through PXRD, DSC, TGA, Raman and FT-IR. However, it is still a difficult task to obtain a single crystal from these. Only one single crystal was obtained in this study.

The obtained single crystal and their ability to be less hygroscopic directed to further formulation studies. This improvement in effervescent tablet formulation process and their stability studies were carried out. Detailed information is presented in the next chapter.

6 Summary

Amino acids were successfully screened for the cocrystal formation with citric acid molecule through this study. Total five amino acids–citric acid cocrystals were obtained and confirmed through characterisation studies. However, as per the hypothesis design of this experiment to reduce the hygroscopicity of the citric acid molecule was not achieved with four cocrystals except one. After DVS studies of all obtained cocrystals, it was observed that only one citric acid-L-cysteine cocrystal showed promising results where hygroscopic property of citric acid is reduced. Single crystal XRD examined the obtained single crystal and observed that there is the presence of one water molecule in the crystal lattice of 1:1, citric acid: L-cysteine. After careful observation, it was assumed that if carefully tried it could be possible to develop as an anhydrous cocrystal. The obtained cocrystal hydrate proved to be less hygroscopic. Thus, it could be used in the formulations as a physically stable component.

5.4 Application of co-crystals in effervescent tablet formulations

5.4.1 Background

This current study focuses on physical stability improvement of effervescent formulations by incorporating physically stable non-hygroscopic citric acid molecule. This citric acid non-hygroscopicity was achieved through successful cocrystallisation with the biologically safe amino acid molecule. The obtained co-crystal monohydrate of citric acid : L-cysteine (1:1) has shown good physicochemical characteristic improvement in stability. Therefore, it is selected to explore the stability in effervescent tablet formulation studies. This co-crystal has shown improvement in reducing the hygroscopicity of the involving molecules like citric acid. Citric acid has excellent pharmaceutical relevance and it plays a vital role in effervescent formulations. Hence, obtained co-crystals of citric acid and L-cysteine amino acid can stand as a great influencing application in this field.

As per the recent study, it was revealed that effervescent formulation had gained more popularity in Europe for decades as well as growth in the US also because they offer a new way for expansion to the pharmaceutical and nutraceutical companies (Lee 2000).

At the production site of effervescent tablets, it was observed that effervescent tablets and powders are produced in much the same manner as conventional tablets and powders. However, there is a prerequisite that, production must occur in very low humidity conditions. This required controlled humidity condition maintenance could add a cost to the company. However, it could be reduced by the newly developed co-crystal based formula. Effervescent granulations can be mixed in conventional blending equipment, such as ribbon, twin-cone, and V-type blenders. All equipment should be well grounded and

should be allowed to make it entirely dry after wash-down. Any traces of moisture in the equipment will give erratic granulation results and most likely result in lost batches of product (Lee 2000).

However, the in-house production of effervescent formulation using the newly formed co-crystal of L-cysteine-citric acid monohydrate bypasses all the problems mentioned above. It can be successfully scalable at an industrial level.

5.4.1.1 Effervescent tablet formulations

Below Table 5.26 and 5.27 represents the description of tablet formulation used in the present study.

Effervescent tablet formulation carried out as per the formula 1 to 4, as (see Table 5.26 and Table 5.27) shown below.

In this study, formula 1 and 3 are the general formula with pure chemicals as available as with Sigma-Aldrich standard. However, in the formula 2 and 4, instead of a pure form of citric acid, the citric acid co-crystal compound was used. All the ingredients were kept under vacuum at 60^0C temperature for 1 hour before the tablet being pressed. As per the requirement, each ingredient was weighed carefully and transferred into a clean glass vial as per tablet formula and the airlock cap was placed on it. These vials were shaken thoroughly to mix the ingredients before the tablet was pressed. Six tablets of each formula (n=6) were pressed using Karnavati make Rimek mini press tablet machine (See Figure 5.64).

Table 5.26 Citric acid effervescent tablets

Citric acid-based tablets *(Formula 1)*		**Citric acid co-crystal-based tablets *(Formula 2)***	
Citric acid	400 mg (we took 800 mg)	Cocrystal equivalent to 400mg of citric acid	652.25 mg (We took 1304.5mg)
Sodium bicarbonate	600 mg (1200mg)	Sodium bicarbonate	600 mg (1200mg)

Table 5.27 Ibuprofen (sodium salt) effervescent tablets

Citric acid-based tablets *(Formula 3)*		**Citric acid co-crystal-based tablets *(Formula 4)***	
Ibuprofen sodium salt	0.2213 gm	Ibuprofen sodium salt	0.2213 gm
Sodium bicarbonate	0.6818 gm	Sodium bicarbonate	0.6818 gm
Polyvinylpyrrolidone (PVP K30) (In this study K-17)	0.1 gm	Polyvinylpyrrolidone (PVP K30) (In this study K-17)	0.1 gm
Mannitol	0.150 gm	Mannitol	0.150 gm
Citric acid	0.198 gm	Cocrystal equivalent to 0.198 gm of citric acid	0.322 gm

Figure 5.64 Mini tablet press machine Rimek by Karnavati at CPES, University of Bradford.

Compact tablets were prepared for all the listed formulations and their stability was investigated using different standard stability conditions. The standard stability conditions used were 40°C/75% RH, 25°C/60% RH and 25°C/50% RH. The morphological stability of all the tablets was tracked at different time points ranging from day 0 to the 1month period.

5.4.2 Results and Discussion

Below Table 5.28 represents the tabular image format for all the stability tablets at different stability conditions.

Table 5.28 Stability of tablets at day 0 (time T_0)

<table>
<tr><td colspan="2">Time in Days ⟹</td><td>0 Day
Citric acid tablet</td><td>0 Day
Ibuprofen tablet</td></tr>
<tr><td>Experimental conditions</td><td>compositions</td><td></td><td></td></tr>
<tr><td rowspan="2">50 % RH at 25°C,
60% RH at 25°C and
75% RH at 40° C</td><td>Conventional method</td><td> 
1</td><td> 
3</td></tr>
<tr><td>CA-L-Cyst cc hydrate new formula</td><td> 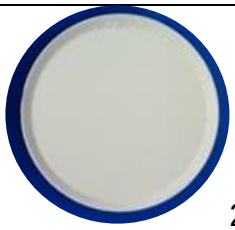
2</td><td> 
4</td></tr>
<tr><td colspan="2">Results and comments</td><td>At time T_0 both conventional and newly developed formula citric acid tablets were stable under all experimental conditions.</td><td>At time T_0 both conventional and newly developed formula’s ibuprofen salt citric acid tablets were stable at all experimental conditions</td></tr>
</table>

Table 5.29 Stability of tablet at day 8.

Time in Days →		8 Days Citric acid tablet	8 Days Ibuprofen tablet
Experimental conditions	compositions		
50 % RH at 25°C,	Conventional method	 1 US	 3 US
	CA-L-Cystcc hydrate new formula	 2 S	 4 S
60% RH at 25°C	Conventional method	 1 US	 3US
	CA-L-Cystcc hydrate new formula	 2 S	 4 S
75% RH at 40° C	Conventional method	 1 US	 3US
	CA-L-Cystcc hydrate new formula	 2 S	 4 S
Results and comments		1,2,3 and 4: formula US: unstable S: stable	1,2,3 and 4: formula US: unstable S: stable

Table 5.30 Stability of tablet at day 28.

Time in Days →		28 Days Citric acid tablet	28 Days Ibuprofen tablet
Experimental conditions	compositions		
50 % RH at 25°C,	Conventional method	 1 US	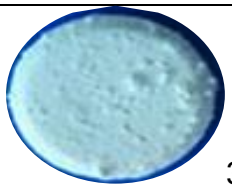 3 US
	CA-L-Cystcc hydrate new formula	 2 S	 4 S
60% RH at 25°C	Conventional method	 1 US	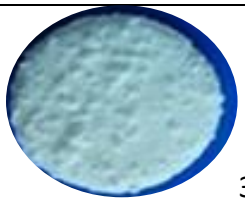 3US
	CA-L-Cystcc hydrate new formula	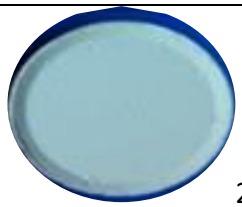 2 S	 4 S
75% RH at 40° C	Conventional method	 1 US	 3US
	CA-L-Cystcc hydrate new formula	 2 S	 4 S
Results and comments		1,2,3 and 4: formula US: unstable S: stable	1,2,3 and 4: formula US: unstable S: stable

Based on the observations demonstrated in Table 5.28, 5.29 and 5.30, it is revealed that initially at T_0 or day 0 time point all the tablets were stable and intact with a smooth surface. After 1-day it was identified that tablet of formulation 1 and 3 were became unstable at all stability conditions as the surface of the tablets started interacting with the moisture content and generating bubbled like rough surface. Under similar conditions tablet of formulation 2 and 4 were remained stable till day 8 at all stability condition. Whereas tablets at 40°C/75 % RH stability conditions were started interacting with moisture which states that they became unstable. The tablets of formulation 2 and 4 at 25°C/60% RH and 25°C/50% RH were remained stable after 8 days' time point till 28 days stability studies. Slight decolouration of the formulation 4 tablets was observed at 25°C/60% RH after 18 days; this can be attributed to solid state degradation of actives in the formulation. Based on the images of the tablets of formulation 2 and 4 displayed minimum changes compared to formulation 1 and 3 at all the stability conditions.

Thus, based on the stability studies, it is proved that formulation 4 displayed greater stability at 25°C/50% RH for one-month stability studies. Thus, we have explored the application of cocrystallisation approach to enhance the hygroscopic stability of citric acid and further attenuate the cost of processing effervescent formulations.

The other characteristic features of the newly developed formulation and original in-house formulation are shown in Table 5.31.

Table 5.31 Effervescent tablet studies

Tablet formula number	Thickness in mm Average	Hardness in KP	pH after	Disintegration time in min.	Complete solubilisation in a min.	Weight loss after solubilisation
1	3.658	1.15	5.83	0.32	0.38	0.14
2	4.67	14.0	5.93	0.39	0.46	0.13
3	2.796	1.17	6.58	2.07	5.35	0.04
4	3.015	5.79	6.71	3.39	4.10	0.02

The average size of the tablet was 20.59 mm in diameter. The pH of the distilled water was 6.89. All four formula tablets were checked for thickness (n=6) and the average thickness of tablets shown in Table 5.31. The hardness of each formula tablet was measured using 4M Hardness Tester (Schleuniger) (n=2) and the results are shown in Table 5.31.

It was observed that the in-house developed formulation of effervescent tablet and the newly developed citric acid -L-cysteine monohydrate cocrystal based formulation tablets showed differences in their pH after disintegration. The time of disintegration, hardness, thickness, complete solubility time and weight loss were measured as 2 tablets (n=2) per formula and obtained results are noted in Table 5.31. As per the formulation, the amount of component varied, but still the obtained results are significant as compared with normal formulation. It proves the physicochemical properties have been changed due to the co-crystallisation process.

5.4.3 Summary

The obtained co-crystal of citric acid –L-cysteine-H_2O monohydrate was successfully applied in the effervescent tablet formulations. Through this study, it was observed that the obtained cocrystal could be scalable to industrial level and has tremendous scope in the effervescent tablet productions. It improves

the stability of the product during processing as well as storage. It may be useful for the reduction in production and packaging costs of effervescent tablets.

Chapter 6 – Global Discussion and Conclusion

6.1 Discussion

The molecular interactions involved in the pharmaceutical preformulation limited to drug-PPB were studied through this current work.

In this current study, high-performance liquid chromatography technique was utilised to carry out the structural properties governing drug-PPB. This is the first study to investigate and quantify the factors involved in the drug-PPB interaction by using the HPLC method. This method employs the stationary phases immobilised with plasma proteins (HSA and AGP). The drug-plasma protein binding was investigated for a set of compounds with a broad range of structural diversity. Based on the findings the LFER model was developed for it.

The LFER model shows that for neutral compounds the structural parameters S, B and V are the prominent factors governing drug binding with HPLC stationary phases immobilised with HSA and AGP. Whereas E is less important, and A is not of statistical significance in both systems. For ionic compounds, electrostatic interactions play a major role in binding. The ionised acids, as anions, show very strong interaction with immobilised HSA stationary phase compared to immobilise AGP phase, whereas ionised basic compounds, as cations, interact with immobilised AGP phase stronger than the HSA phase.

The structural diversity-based compounds showed different behaviours based on their molecular interactions like dipole-dipole moments, ionic behaviour at physiological pH conditions. Total hydrogen bond basicity and total hydrogen bond acidity are found to be essential to consider for the drug-PPB interaction. Drug displacement and strong or less affinity towards the plasma proteins play an important role in drug distribution, metabolism and concentration at the site

of action and excretion. Thus, the molecular behaviour in between drugs and plasma protein interaction was revealed by this study.

Another area where such intermolecular interactions are widely observed is in the area of supramolecular complexes. The best example of it is the cocrystals. This study explores the molecular interactions involved in between two reacting molecules during the co-crystallisation process.

Interestingly, in both cases, the interactions involve the hydrogen bonding, Van der Walls forces involvement and π-π interactions. In both cases, the interacting molecule has competent molecules. Like in drug-PPB interaction a strong affinity candidate and less affinity candidate compete to fulfil the binding site on the plasma proteins. It may be drug-protein, drug-drug or plasma protein with other serum components. However, in the co-crystallisation process, the coformer and solvent or hydrate molecule compete for binding with the APIs or the reacting molecule.

This study reveals that amino acids are potent coformer molecules. These are biologically safe to a human being and thus necessary to be considered for coformer compared with other chemical coformers. As per FDA guidelines, amino acids are coming under the GRAS category and have excellent RDA (recommended dosage daily allowance) values.

When amino acids entered the physiological condition, they become zwitterion and hence have more chances to develop better solubility and good permeability.

The co-crystals synthesis of amino acids with various carboxylic acids, NSAIDs, and citric acid gives very good co-crystals. Single crystal obtaining process is, though, time-consuming and very much specific to solvent selection. However, this study has shown it is possible by using just water as a solvent that can

produce good single crystal of citric acid - L-cysteine monohydrate co-crystal. This hydrate formation is straight forward for the molecular interactions involving citric acid and amino acids and notably when there is water used as a solvent. The citric acid molecule has a greater affinity towards a water molecule. Hence once it encounters a water molecule, it changes physically and becomes a liquid deliquescent form. The used amino acid has good hydrogen bond donor capacity as well as accepting capacity.

The single crystal X-ray diffraction analysis reveals that there is might be a possibility to develop anhydrous co-crystal from the same pair with using solvent system other than water. However, it requires time to selection of such system through range of polar and non-polar solvents in which both reacting molecules can be dissolved completely. The L-proline adipic acid and fumaric acid pairs have been already studied. However, succinic acid and L-proline showed very promising data of co-crystal formation. The Raman and FT-IR data revealed that there was no salt forming functional group peaks. It suggests that there is a formation of hydrogen bonds means co-crystals between L-proline and succinic acid.

The L-proline and NSAIDs co-crystal screening also showed promising data. The data suggest that there may be the formation of co-crystals in between L-proline and aspirin, ibuprofen, ketoprofen, flurbiprofen. However, L-proline - ibuprofen co-crystal work was published by other researchers (Othman *et al.* from Malaysia) during this study.

The obtained single crystal of L-cysteine and citric acid co-crystal monohydrate proves to be non-hygroscopic. It can tolerate the moisture absorption up to 28 days (672 hrs at 25°C/60% RH). It has shown good improvement in the

effervescent tablet manufacturing process. It can be helpful in reducing the production cost.

6.2 Conclusion

Structural properties governing drug-plasma protein binding study was successfully carried out by using high-performance liquid chromatography. An HPLC method was utilised to quantify the factors involved in the drug-PPB binding interaction. The ionic behaviour which is responsible for the drug-PPB was quantified for the first time through this current study. LFER method has been used to develop a statistical equation for quantifying the drug-PPB interaction studies. The molecular interaction involved in the pharmaceutical preformulation limited to drug-PPB was studied successfully.

Amino acid and citric acid co-crystals were developed, and one single crystal was successfully obtained through green synthesis process by using water as a solvent. Amino acids can be used as an alternative source for the chemical coformer which is more promising than the chemical coformer. The molecular interactions involved in preformulation and supramolecular complexes limited to the co-crystal study were explored and understood

6.3 Recommended Future Work

Based on the findings of this current study the following areas could be developed as future work: -

1) LFER implementation in drug-drug interaction studies and quantification of commonly used drugs displacement studies.
2) HPLC based techniques development for various interactions in biopharmaceutical applications for *in-vivo* and *in-vitro* analysis studies.
3) To develop the amino acids co-crystals with BCS class II and IV drugs to draw them into mainstream drug development field.

4) To study the amino acid and NSAIDs cocrystals to improve their characteristic physicochemical properties.

Chapter 7

References

Aakeroy, C. B., Panikkattu, S., Chopade, P. D. and Desper, J. (2013) Competing hydrogen-bond and halogen-bond donors in crystal engineering. *CrystEngComm* 15 (16), 3125-3136.

Abraham, M. H. (1993) Hydrogen-bonding .31. Construction of a scale of solute effective or summation hydrogen-bond basicity. *Journal of Physical Organic Chemistry* 6 (12), 660-684.

Abraham, M. H. (2003) The determination of air/water partition coefficients for alkyl carboxylic acids by a new indirect method. *Journal of Environmental Monitoring* 5 (5), 747-752.

Abraham, M. H. (2011) The permeation of neutral molecules, ions, and ionic species through membranes: Brain permeation as an example. *Journal of Pharmaceutical Sciences* 100 (5), 1690-1701.

Abraham, M. H. and Acree, W. E. (2005) Characterisation of the water-isopropyl myristate system. *International Journal of Pharmaceutics* 294 (1-2), 121-128.

Abraham, M. H. and Acree, W. E., Jr. (2010a) Equations for the transfer of neutral molecules and ionic species from water to organic phases. *Journal of Organic Chemistry* 75 (4), 1006-1015.

Abraham, M. H. and Acree, W. E., Jr. (2010b) Solute descriptors for phenoxide anions and their use to establish correlations of rates of reaction of anions with iodomethane. *Journal of Organic Chemistry* 75 (9), 3021-3026.

Abraham, M. H. and Acree, W. E., Jr. (2010c) The transfer of neutral molecules, ions and ionic species from water to ethylene glycol and to propylene

carbonate; descriptors for pyridinium cations. *New Journal of Chemistry* 34 (10), 2298-2305.

Abraham, M. H. and Acree, W. E., Jr. (2010d) The transfer of neutral molecules, ions and ionic species from water to wet octanol. *Physical Chemistry Chemical Physics* 12 (40), 13182-13188.

Abraham, M. H., Acree, W. E., Jr., Fahr, A. and Liu, X. (2013) Analysis of immobilized artificial membrane retention factors for both neutral and ionic species. *J Chromatogr A* 1298, 44-9.

Abraham, M. H., Ibrahim, A. and Zissimos, A. M. (2004) Determination of sets of solute descriptors from chromatographic measurements. *Journal of Chromatography A* 1037 (1-2), 29-47.

Abraham, M. H. and Martins, F. (2004) Human skin permeation and partition: General linear free-energy relationship analyses. *Journal of Pharmaceutical Sciences* 93 (6), 1508-1523.

Abraham, M. H. and Zhao, Y. H. (2005) Characterisation of the water/o-nitrophenyl octyl ether system in terms of the partition of nonelectrolytes and of ions. *Physical Chemistry Chemical Physics* 7 (12), 2418-2422.

Aher, S., Dhumal, R., Mahadik, K., Paradkar, A. and York, P. (2010) Ultrasound assisted cocrystallization from solution (USSC) containing a non-congruently soluble cocrystal component pair: Caffeine/maleic acid. *European Journal of Pharmaceutical Sciences* 41 (5), 597-602.

Aitipamula, S., Banerjee, R., Bansal, A. K., Biradha, K., Cheney, M. L., Choudhury, A. R., Desiraju, G. R., Dikundwar, A. G., Dubey, R. and Duggirala, N. (2012a) Polymorphs, salts, and cocrystals: What's in a name? *Crystal growth & design* 12 (5), 2147-2152.

Aitipamula, S., Chow, P. S. and Tan, R. B. (2010) Conformational and enantiotropic polymorphism of a 1: 1 cocrystal involving ethenzamide and ethylmalonic acid. *CrystEngComm* 12 (11), 3691-3697.

Aitipamula, S., Chow, P. S. and Tan, R. B. (2012b) Co-crystals of caffeine and piracetam with 4-hydroxybenzoic acid: Unravelling the hidden hydrates of 1: 1 co-crystals. *CrystEngComm* 14 (7), 2381-2385.

Alsirawan, M. B., Vangala, V. R., Kendrick, J., Leusen, F. J. and Paradkar, A. (2016) Coformer replacement as an indicator for thermodynamic instability of cocrystals: competitive transformation of caffeine: dicarboxylic acid. *Crystal growth & design* 16 (6), 3072-3075.

Amidon, G. L., Lennernäs, H., Shah, V. P. and Crison, J. R. (1995) A theoretical basis for a biopharmaceutic drug classification: the correlation of in vitro drug product dissolution and in vivo bioavailability. *Pharmaceutical Research* 12 (3), 413-420.

Apshingekar, P. P., Aher, S., Kelly, A. L., Brown, E. C. and Paradkar, A. (2016a) Synthesis of caffeine/maleic acid co-crystal by ultrasound-assisted slurry co-crystallization. *Journal of Pharmaceutical Sciences* 106 (1), 66-70.

Apshingekar, P. P., Aher, S., Kelly, A. L., Brown, E. C. and Paradkar, A. (2016b) Synthesis of caffeine/maleic acid co-crystal by ultrasound-assisted slurry co-crystallization. *Journal of Pharmaceutical Sciences*.

Artursson, P. and Karlsson, J. (1991) Correlation between oral drug absorption in humans and apparent drug permeability coefficients in human intestinal epithelial (Caco-2) cells. *Biochemical and Biophysical Research Communications* 175 (3), 880-885.

Ash, M. and Ash, I. (2006) *Handbook of flavors and fragrances.* Synapse Information Resources, Incorporated.

Barbooti, M. M. and Al-Sammerrai, D. A. (1986) Thermal decomposition of citric acid. *Thermochimica Acta* 98, 119-126.

Batisai, E., Ayamine, A., Kilinkissa, O. E. and Báthori, N. B. (2014) Melting point–solubility–structure correlations in multicomponent crystals containing fumaric or adipic acid. *CrystEngComm* 16 (43), 9992-9998.

Bergström, C. A. (2005) In silico predictions of drug solubility and permeability: two rate-limiting barriers to oral drug absorption. *Basic & Clinical Pharmacology & Toxicology* 96 (3), 156-161.

Bhogala, B. R., Basavoju, S. and Nangia, A. (2005) Tape and layer structures in cocrystals of some di- and tricarboxylic acids with 4,4′-bipyridines and isonicotinamide. From binary to ternary cocrystals. *CrystEngComm* 7 (90), 551.

Bolla, G. and Nangia, A. (2016) Pharmaceutical cocrystals: walking the talk. *Chemical Communications (Cambridge, England)* 52 (54), 8342-60.

Borchardt, R., Kerns, E., Lipinski, C., Thakker, D. and Wang, B. (2005) *Pharmaceutical profiling in drug discovery for lead selection.* American Association of Pharmaceutical Scientists.

Buxton, E. (2017) *Principles of solid dosage forms.* University of Wisconsin - Madison: Divison of Pharmacy Professional Development of University of Wisconsin -Madison. *https://ce.pharmacy.wisc.edu/pd/soliddosage/* Accessed 3 October 2017.

Chattoraj, S. and Sun, C. C. Crystal and particle engineering strategies for improving powder compression and flow properties to enable continuous

tablet manufacturing by direct compression. *Journal of Pharmaceutical Sciences* 107 (4), 968-974.

Chow, S. F., Chen, M., Shi, L., Chow, A. H. L. and Sun, C. C. (2012) Simultaneously improving the mechanical properties, dissolution performance, and hygroscopicity of ibuprofen and flurbiprofen by cocrystallization with nicotinamide. *Pharmaceutical Research* 29 (7), 1854-1865.

Datta, S. and Grant, D. J. W. (2004) Crystal structures of drugs: advances in determination, prediction and engineering. *Nature Reviews Drug Discovery* 3 (1), 42-57.

Dhumal, R., Kelly, A. and Paradkar, A. (2010) Development of solvent free continuous cocrystallisation (sfcc) technique. *Journal of Pharmacy and Pharmacology* 62 (10), 1418-1419.

FDA (2000) *Q6A specifications: test procedures and acceptance criteria for new drug substances and new drug products: chemical substances.* March 29, 2001. Rockville, MD: Food and Drug Administration. *https://www.fda.gov/Drugs/GuidanceComplianceRegulatoryInformation/Guidances/ucm134966.htm* Accessed November 14, 2017.

FDA (2016) *FDA to reclassify pharmaceutical co-crystals.* RAPS. *http://www.raps.org/Regulatory-Focus/News/2016/08/16/25611/FDA-to-Reclassify-Pharmaceutical-Co-Crystals/* Accessed 16 August 2016.

Friščić, T., Trask, A. V., Jones, W. and Motherwell, W. (2006) Screening for inclusion compounds and systematic construction of three-component solids by liquid-assisted grinding. *Angewandte Chemie International Edition* 118 (45), 7708-7712.

Ghafourian, T. and Amin, Z. (2013) QSAR models for the prediction of plasma protein binding. *BioImpacts : BI* 3 (1), 21-27.

Ghosh, M., Basak, A. K. and Mazumdar, S. K. (1991) Structure and conformation of the 1:1 molecular complex of sulfaproxyline-caffeine. *Acta Crystallographica* C47, 577.

Gil-Agusti, M., Esteve-Romero, J. and Abraham, M. H. (2006) Solute-solvent interactions in micellar liquid chromatography - Characterization of hybrid micellar systems of sodium dodecyl sulfate-pentanol. *Journal of Chromatography A* 1117 (1), 47-55.

Guo, K., Sadiq, G., Seaton, C., Davey, R. and Yin, Q. (2009) Co-crystallization in the caffeine/maleic acid system: lessons from phase equilibria. *Crystal Growth & Design* 10 (1), 268-273.

Hage, D. S., Jackson, A., Sobansky, M. R., Schiel, J. E., Yoo, M. J. and Joseph, K. S. (2009) Characterization of drug-protein interactions in blood using high-performance affinity chromatography. *J Sep Sci* 32 (5-6), 835-53.

Hautala, J., Airaksinen, S., Naukkarinen, N., Vainio, O. and Juppo, A. M. (2016) Evaluation of new flavors for feline mini-tablet formulations. *Journal of Excipients and Food Chemicals* 5 (2).

Hein, K. L., Kragh-Hansen, U., Morth, J. P., Jeppesen, M. D., Otzen, D., Moller, J. V. and Nissen, P. (2010) Crystallographic analysis reveals a unique lidocaine binding site on human serum albumin. *Journal of Structural Biology* 171 (3), 353-360.

Howard, M. L., Hill, J. J., Galluppi, G. R. and McLean, M. A. (2010) Plasma protein binding in drug discovery and development. *Combinatorial Chemistry & High Throughput Screening* 13 (2), 170-187.

Huang, Z., Sun, G.-B., Chiew, Y. C. and Kawi, S. (2005) Formation of ultrafine aspirin particles through rapid expansion of supercritical solutions (RESS). *Powder Technology* 160 (2), 127-134.

Iwama, S., Kuyama, K., Mori, Y., Manoj, K., Gonnade, R. G., Suzuki, K., Hughes, C. E., Williams, P. A., Harris, K. D. and Veesler, S. (2014) Highly Efficient Chiral Resolution of dl-Arginine by Cocrystal Formation Followed by Recrystallization under Preferential-Enrichment Conditions. *Chemistry-a European Journal* 20 (33), 10343-10350.

Jayasankar, A., Good, D. J. and Rodríguez-Hornedo, N. (2007) Mechanisms by which moisture generates cocrystals. *Molecular Pharmaceutics* 4 (3), 360-372.

Jones, W., Motherwell, W. S. and Trask, A. V. (2006) Pharmaceutical cocrystals: an emerging approach to physical property enhancement. *MRS Bulletin* 31 (11), 875-879.

Kaliszan, R., Nasal, A. and Turowski, M. (1995) Binding-site for basic drugs on alpha (1)-acid glycoprotein as revealed by chemometric analysis of biochromatographic data. *Biomedical Chromatography* 9 (5), 211-215.

Kamble, S., Loadman, P., Abraham, M. H. and Liu, X. (2018) Structural properties governing drug-plasma protein binding determined by high-performance liquid chromatography method. *Journal of Pharmaceutical and Biomedical Analysis* 149, 16-21.

Kelly, A. L., Gough, T., Dhumal, R., Halsey, S. and Paradkar, A. (2012) Monitoring ibuprofen–nicotinamide cocrystal formation during solvent free continuous cocrystallization (SFCC) using near infrared spectroscopy as a PAT tool. *International Journal of Pharmaceutics* 426 (1), 15-20.

Kennedy, T. (1997) Managing the drug discovery/development interface. *Drug Discovery Today* 2 (10), 436-444.

Kim, H. S. and Wainer, I. W. (2008) Rapid analysis of the interactions between drugs and human serum albumin (HSA) using high-performance affinity chromatography (HPAC). *J Chromatogr B Analyt Technol Biomed Life Sci* 870 (1), 22-6.

Kremer, J. M. H., Wilting, J. and Janssen, L. H. M. (1988) Drug-binding to human alpha-1-acid glycoprotein in health and disease. *Pharmacological Reviews* 40 (1), 1-47.

Larkin, P. (2017) *Infrared and Raman spectroscopy: principles and spectral interpretation.* Elsevier.

Lee, R. E. (2000) *Effervescent tablets*. CSC publishing, Tablets & capsules.

Lindup, W. and Orme, M. (1981) Clinical pharmacology: plasma protein binding of drugs. *British Medical Journal (Clinical Research Ed.)* 282 (6259), 212.

Liu, M., Hong, C., Yao, Y., Shen, H., Ji, G., Li, G. and Xie, Y. (2016) Development of a pharmaceutical cocrystal with solution crystallization technology: Preparation, characterization, and evaluation of myricetin-proline cocrystals. *European Journal of Pharmaceutics and Biopharmaceutics* 107, 151-159.

Lloyd, D. J. and Phillips, H. (1933) Protein structure and protein hydration. *Transactions of the Faraday Society* 29 (140), 132-146.

Losev, E. A., Zakharov, B. A., Drebushchak, T. N. and Boldyreva, E. V. (2011) Glycinium semi-malonate and a glutaric acid-glycine cocrystal: new structures with short O-H...O hydrogen bonds. *Acta Crystallographica Section C: Crystal Structure Communications* 67 (Pt 8), o297-300.

McNamara, D. P., Childs, S. L., Giordano, J., Iarriccio, A., Cassidy, J., Shet, M. S., Mannion, R., O'donnell, E. and Park, A. (2006) Use of a glutaric acid cocrystal to improve oral bioavailability of a low solubility API. *Pharmaceutical Research* 23 (8), 1888-1897.

NCBI (2017a) *L-Cysteine.* Bethesda: NCBI. *https://pubchem.ncbi.nlm.nih.gov/compound/5862* Accessed Mar. 15, 2017.

NCBI (2017b) *L-Leucine.* Bethesda: NCBI. *https://pubchem.ncbi.nlm.nih.gov/compound/6106* Accessed March 15, 2017.

NCBI (2017c) *L-Serine* Bethesda: NCBI. *https://pubchem.ncbi.nlm.nih.gov/compound/5951* Accessed March 15, 2017.

NCBI (2018a) *Citric acid.* Bethesda: NCBI. *https://pubchem.ncbi.nlm.nih.gov/compound/311* Accessed Mar. 22, 2018.

NCBI (2018b) *Flurbiprofen.* Bethesda: NCBI. *https://pubchem.ncbi.nlm.nih.gov/compound/3394* Accessed Mar. 10, 2018.

NCBI (2018c) *L-proline* Bethesda: NCBI. *https://pubchem.ncbi.nlm.nih.gov/compound/145742* Accessed Mar. 10, 2018.

Oravcova, J., Bo, B. and Lindner, W. (1996) Drug-protein binding studies new trends in analytical and experimental methodology. *Journal of Chromatography B: Biomedical Sciences and Applications* 677 (1), 1-28.

Othman, M. F., Jamburi, N., Anuar, N., Rahim, S. A. and Rohalim, N. H. (2016) Ibuprofen-amino acids co-crystal screening via co-grinding methods. *MATEC Web of Conferences.* Vol. 69. EDP Sciences.

Pagire, S., Korde, S., Ambardekar, R., Deshmukh, S., Dash, R. C., Dhumal, R. and Paradkar, A. (2013a) Microwave assisted synthesis of caffeine/maleic acid co-crystals: the role of the dielectric and physicochemical properties of the solvent. *CrystEngComm* 15 (18), 3705-3710.

Pagire, S. K., Korde, S. A., Whiteside, B. R., Kendrick, J. and Paradkar, A. (2013b) Spherical crystallization of carbamazepine/saccharin co-crystals: selective agglomeration and purification through surface interactions. *Crystal Growth & Design* 13 (10), 4162-4167.

Paradkar, A. and Pagire, S. (2017) *Effervescent compositions containing co-crystals of the acid part*. Google Patents.

Paradkar, A. R., Maheshwari, M., Ketkar, A. R. and Chauhan, B. (2003) Preparation and evaluation of ibuprofen beads by melt solidification technique. *International Journal of Pharmaceutics* 255 (1), 33-42.

Parsons, M. T., Mak, J., Lipetz, S. R. and Bertram, A. K. (2004) Deliquescence of malonic, succinic, glutaric, and adipic acid particles. *Journal of Geophysical Research: Atmospheres* 109 (D6).

Patil, S. P., Modi, S. R. and Bansal, A. K. (2014) Generation of 1: 1 carbamazepine: nicotinamide cocrystals by spray drying. *European Journal of Pharmaceutical Sciences* 62, 251-257.

Poole, C. F. (2003) *The essence of chromatography.* Amsterdam;London;: Elsevier.

Rehder, S., Klukkert, M., Löbmann, K. A., Strachan, C. J., Sakmann, A., Gordon, K., Rades, T. and Leopold, C. S. (2011) Investigation of the formation process of two piracetam cocrystals during grinding. *Pharmaceutics* 3 (4), 706-722.

Reilly, J., Etheridge, D., Everatt, B., Jiang, Z., Aldcroft, C., Wright, P., Clemens, I., Cox, B., Press, N. J. and Watson, S. (2011) Studies in drug albumin binding using HSA and RSA affinity methods. *Journal of Liquid Chromatography & Related Technologies* 34 (4), 317-327.

Saha, B. K., Nangia, A. and Jaskolski, M. (2005) Crystal engineering with hydrogen bonds and halogen bonds. *CrystEngComm* 7 (58), 355-358.

Salameh, A. K., Mauer, L. J. and Taylor, L. S. (2006) Deliquescence lowering in food ingredient mixtures. *Journal of Food Science* 71 (1).

Salameh, A. K. and Taylor, L. S. (2006a) Deliquescence-induced caking in binary powder blends. *Pharmaceutical Development and Technology* 11 (4), 453-464.

Salameh, A. K. and Taylor, L. S. (2006b) Role of deliquescence lowering in enhancing chemical reactivity in physical mixtures. *The Journal of Physical Chemistry B* 110 (20), 10190-10196.

Savjani, K. T., Gajjar, A. K. and Savjani, J. K. (2012) Drug solubility: Importance and enhancement techniques. *ISRN Pharmaceutics* 2012, 195727.

Schonfeld, D. L., Ravelli, R. B., Mueller, U. and Skerra, A. (2008) The 1.8-A crystal structure of alpha1-acid glycoprotein (Orosomucoid) solved by UV RIP reveals the broad drug-binding activity of this human plasma lipocalin. *Journal of Molecular Biology* 384 (2), 393-405.

Schultheiss, N. and Newman, A. (2009) Pharmaceutical Cocrystals and Their Physicochemical Properties. *Crystal Growth & Design* 9 (6), 2950-2967.

Scott, R. P. (1995) *Techniques and practice of chromatography.* Vol. 70. CRC Press.

Sebille, B., Zini, R., Madjar, C. V., Thuaud, N. and Tillement, J. P. (1990) Separation procedures used to reveal and follow drug protein-binding. *Journal of Chromatography-Biomedical Applications* 531, 51-77.

Şengül, Ü. (2016) Comparing determination methods of detection and quantification limits for aflatoxin analysis in hazelnut. *Journal of Food and Drug Analysis* 24 (1), 56-62.

Shah, V. P. and Amidon, G. L. (2014) A theoretical basis for a biopharmaceutic drug classification: the correlation of in vitro drug product dissolution and in vivo bioavailability. *The American Association of Pharmaceutical Scientists Journal, The AAPS Journal* 16 (5), 894-898.

Shan, N. and Zaworotko, M. J. (2008) The role of cocrystals in pharmaceutical science. *Drug Discovery Today* 13 (9-10), 440-6.

Sheikh, A. Y., Rahim, S. A., Hammond, R. B. and Roberts, K. J. (2009) Scalable solution cocrystallization: case of carbamazepine-nicotinamide I. *CrystEngComm* 11 (3), 501-509.

Shete, A., Murthy, S., Korpale, S., Yadav, A., Sajane, S., Sakhare, S. and Doijad, R. (2015) Cocrystals of itraconazole with amino acids: Screening, synthesis, solid state characterization, in vitro drug release and antifungal activity. *Journal of Drug Delivery Science and Technology* 28, 46-55.

Shevchenko, A., Bimbo, L. M., Miroshnyk, I., Haarala, J., Jelínková, K., Syrjänen, K., van Veen, B., Kiesvaara, J., Santos, H. A. and Yliruusi, J. (2012) A new cocrystal and salts of itraconazole: Comparison of solid-

state properties, stability and dissolution behavior. *International Journal of Pharmaceutics* 436 (1–2), 403-409.

Shimpi, M. R., Childs, S. L., Bostrom, D. and Velaga, S. P. (2014) New cocrystals of ezetimibe with l-proline and imidazole. *CrystEngComm* 16 (38), 8984-8993.

Singh, S. S. and Mehta, J. (2006) Measurement of drug-protein binding by immobilized human serum albumin-HPLC and comparison with ultrafiltration (vol 834, pg 108, 2006). *Journal of Chromatography B-Analytical Technologies in the Biomedical and Life Sciences* 837 (1-2), 153-153.

Soares, F. L. F. and Carneiro, R. L. (2013) Green Synthesis of Ibuprofen–Nicotinamide Cocrystals and In-Line Evaluation by Raman Spectroscopy. *Crystal Growth & Design* 13 (4), 1510-1517.

Soares, F. L. F. and Carneiro, R. L. (2014) Evaluation of analytical tools and multivariate methods for quantification of co-former crystals in ibuprofen-nicotinamide co-crystals. *Journal of Pharmaceutical and Biomedical Analysis* 89, 166-175.

Soewandhi, S. N. Preparation and Solid State Characterization of Binary Mixtures of Acyclovir–Succinic Acid.

Sprunger, L., Blake-Taylor, B. H., Wairegi, A., Acree, W. E., Jr. and Abraham, M. H. (2007) Characterization of the retention behavior of organic and pharmaceutical drug molecules on an immobilized artificial membrane column with the Abraham model. *Journal of Chromatography A* 1160 (1-2), 235-245.

Stenberg, P., Norinder, U., Luthman, K. and Artursson, P. (2001) Experimental and computational screening models for the prediction of intestinal drug absorption. *Journal of Medicinal Chemistry* 44 (12), 1927-1937.

Sudlow, G., Birkett, D. J. and Wade, D. N. (1975) Characterization of 2 specific drug binding-sites on human-serum albumin. *Molecular Pharmacology* 11 (6), 824-832.

Sudlow, G., Birkett, D. J. and Wade, D. N. (1976) Further characterization of specific drug binding-sites on human-serum albumin. *Molecular Pharmacology* 12 (6), 1052-1061.

Tan, T.-F., Han, J., Pang, M.-L., Song, H.-B., Ma, Y.-X. and Meng, J.-B. (2006) Achiral benzoic acid derivatives as chiral cocrystal building blocks in supramolecular chemistry: adducts with organic amines. *Crystal Growth & Design* 6 (5), 1186-1193.

Taverniers, I., De Loose, M. and Van Bockstaele, E. (2004) Trends in quality in the analytical laboratory. II. Analytical method validation and quality assurance. *TRAC Trends in Analytical Chemistry* 23 (8), 535-552.

Thakuria, R., Delori, A., Jones, W., Lipert, M. P., Roy, L. and Rodriguez-Hornedo, N. (2013) Pharmaceutical cocrystals and poorly soluble drugs. *International Journal of Pharmaceutics* 453 (1), 101-25.

Tilborg, A., Leyssens, T., Norberg, B. and Wouters, J. (2013) Structural study of prolinium/fumaric acid zwitterionic cocrystals: focus on hydrogen-bonding pattern involving zwitterionic (ionic) heterosynthons. *Crystal Growth & Design* 13 (6), 2373-2389.

Tilborg, A., Norberg, B. and Wouters, J. (2014) Pharmaceutical salts and cocrystals involving amino acids: A brief structural overview of the state-of-art. *European Journal of Medicinal Chemistry* 74, 411-426.

Trainor, G. L. (2007) The importance of plasma protein binding in drug discovery. *Expert Opinion on Drug Discovery* 2 (1), 51-64.

Trask, A. V. and Day, J. (2007) An overview of pharmaceutical cocrystals as intellectual property. *Molecular Pharmaceutics* 4 (3), 301-309.

Trask, A. V., Motherwell, W. D. S., Jones, W. and Pharmaceutical Cocrystallization, n. (2005a) Engineering a remedy for caffeine hydration. *Crystal Growth and Design* 5, 1013.

Trask, A. V., Motherwell, W. S. and Jones, W. (2004) Solvent-drop grinding: green polymorph control of cocrystallisation. *Chemical Communications* (7), 890-891.

Trask, A. V., Motherwell, W. S. and Jones, W. (2005b) Pharmaceutical cocrystallization: engineering a remedy for caffeine hydration. *Crystal Growth & Design* 5 (3), 1013-1021.

Urien, S., Tillement, J.-P. and Barré, J. (2001) *The significance of plasma-protein binding in drug research.* Wiley VCH: Zürich, Switzerland.

Valko, K., Nunhuck, S., Bevan, C., Abraham, M. H. and Reyncilds, D. P. (2003) Fast gradient HPLC method to determine compounds binding to human serum albumin. Relationships with octanol/water and immobilized artificial membrane lipophilicity. *Journal of Pharmaceutical Sciences* 92 (11), 2236-2248.

Van De Waterbeemd, H. and Gifford, E. (2003) ADMET in silico modelling: towards prediction paradise? *Nature reviews. Drug discovery* 2 (3), 192.

Vangala, V. R., Chow, P. S. and Tan, R. B. (2011) Characterization, physicochemical and photo-stability of a co-crystal involving an antibiotic drug, nitrofurantoin, and 4-hydroxybenzoic acid. *CrystEngComm* 13 (3), 759-762.

Varma, M. M. and Pandi, J. K. (2005) Dissolution, Solubility, XRD, and DSC Studies on flurbiprofen-nicotinamide solid dispersions. *Drug Development and Industrial Pharmacy* 31 (4/5), 417-423.

Vishweshwar, P., McMahon, J. A., Bis, J. A. and Zaworotko, M. J. (2006) Pharmaceutical co-crystals. *Journal of Pharmaceutical Sciences* 95 (3), 499--516.

Vuignier, K., Guillarme, D., Veuthey, J.-L., Carrupt, P.-A. and Schappler, J. (2013) High performance affinity chromatography (HPAC) as a high-throughput screening tool in drug discovery to study drug-plasma protein interactions. *Journal of Pharmaceutical and Biomedical Analysis* 74, 205-212.

Vuignier, K., Schappler, J., Veuthey, J. L., Carrupt, P. A. and Martel, S. (2010a) Drug-protein binding: a critical review of analytical tools. *Analytical and Bioanalytical Chemistry* 398 (1), 53-66.

Vuignier, K., Schappler, J., Veuthey, J. L., Carrupt, P. A. and Martel, S. (2010b) Improvement of a capillary electrophoresis/frontal analysis (CE/FA) method for determining binding constants: Discussion on relevant parameters. *Journal of Pharmaceutical and Biomedical Analysis* 53 (5), 1288-1297.

Wa, C. L., Cerny, R. L. and Hage, D. S. (2006) Identification and quantitative studies of protein immobilization sites by stable isotope labeling and mass spectrometry. *Analytical Chemistry* 78 (23), 7967-7977.

Wan, H. and Holmen, A. G. (2009) High throughput screening of physicochemical properties and in vitro ADME profiling in drug discovery. *Combinatorial Chemistry & High Throughput Screening* 12 (3), 315-329.

Wang, Y., Sun, J., Liu, H., Liu, J., Zhang, L., Liu, K. and He, Z. (2009) Predicting skin permeability using liposome electrokinetic chromatography. *Analyst* 134 (2), 267-272.

Wermuth, C. G., Stahl, P. H. and International union of pure and applied, c. (2002) *Handbook of pharmaceutical salts : properties, selection, and use.* Zürich; Weinheim [etc.]: VHCA ; Wiley-VCH.

Xudong, Y. and Capomacchia, A. C. (2010) Physicochemical studies of binary eutectic of ibuprofen and ketoprofen for enhanced transdermal drug delivery. *Drug Development and Industrial Pharmacy* 36 (10), 1168-1176.

Yadav, S., Gupta, P. C., Sharma, N. and Kumar, J. (2015) Cocrystals: An alternative approach to modify physicochemical properties of drugs. *International Journal of Pharmaceutical, Chemical and Biological Sciences* 5 (2), 427-436.

Yang, F., Zhang, Y. and Liang, H. (2014) Interactive association of drugs binding to human serum albumin. *International Journal of Molecular Sciences* 15 (3), 3580-3595.

Zakharov, B. A., Losev, E. A. and Boldyreva, E. V. (2013) Polymorphism of “glycine–glutaric acid” co-crystals: the same phase at low temperatures and high pressures. *CrystEngComm* 15 (9), 1693.

Zakharov, B. A., Losev, E. A., Kolesov, B. A., Drebushchak, V. A. and Boldyreva, E. V. (2012) Low-temperature phase transition in glycine-glutaric acid co-crystals studied by single-crystal X-ray diffraction, Raman spectroscopy and differential scanning calorimetry. *Acta Crystallographica. Section B: Structural Crystallography and Crystal Chemistry* 68 (Pt 3), 287-96.

Zhang, K., Chen, M., Scriba, G. K. E., Abraham, M. H., Fahr, A. and Liu, X. (2012) Human skin permeation of neutral species and ionic species: Extended linear free-energy relationship analyses. *Journal of Pharmaceutical Sciences* 101 (6), 2034-2044.

Zhang, K. D., Chen, M., Scriba, G. K. E., Abraham, M. H., Fahr, A. and Liu, X. L. (2011) Linear Free Energy Relationship Analysis of Retention Factors in Cerasome Electrokinetic Chromatography Intended for Predicting Drug Skin Permeation. *Journal of Pharmaceutical Sciences* 100 (8), 3105-3113.

Zhao, Y. H., Abraham, M. H., Hersey, A. and Luscombe, C. N. (2003) Quantitative relationship between rat intestinal absorption and Abraham descriptors. *European Journal of Medicinal Chemistry* 38 (11-12), 939-947.

Zhao, Y. H., Le, J., Abraham, M. H., Hersey, A., Eddershaw, P. J., Luscombe, C. N., Boutina, D., Beck, G., Sherborne, B., Cooper, I. and Platts, J. A. (2001) Evaluation of human intestinal absorption data and subsequent derivation of a quantitative structure-activity relationship (QSAR) with the Abraham descriptors. *Journal of Pharmaceutical Sciences* 90 (6), 749-784.

Appendix-1

Drug-plasma protein binding study:

Preparation of stock solutions for HPLC analysis

Each compound/drug molecule weighed adequately to get 10^{-2}M (0.01M) stock solution in MeOH/ACN (Total stock 20ml)

For better UV detection and retention time prepare a solution from further stock dilution to get 0.001-0.00001M in Methanol.

Column

HSA 100.4 CHIRAL-HSA 4mm ID 100 x 4 mm

Installation

The column is filled with 10% propanol in distilled water. (Storage condition)

Wash the column with distilled water

Start the low flow rate and increase to 0.5 ml /min, maintain for 2min.

Increase the flow rate to 0.8- 0.9 ml/min and continue the washing for 10min.

Equilibrate the column with the mobile phase to be used and stable baseline to appear.

Recommended flow rate with a 4.0 mm ID column is 0.8-0.9 ml/min.

Mobile Phases

Buffer

Sodium or potassium phosphate buffers

Ammonium or sodium acetate buffers

Formate or citrate buffers

Concentrations

0.01– 0.1M

Normally 10-20 mM (0.01-0.02M)

pH:

Can be used in the range of 5-7.

However, if used at pH>7 or <5 for a longer period, may decrease the column lifetime

Organic modifier

Recommended 1-Propanol,2-Propanol, methanol, ethanol, acetonitrile <10%

Temp

R.T.

Samples injection volume 10-20microlitre

Potassium phosphate buffer

Compound	Mol.wt	1M/1000ml	0.1M/1000ml	0.01M/1000ml
K_2HPO_4	174.18	174.18gms	17.418gms	1.7418 gms
KH_2PO_4	136.09	136.09gms	13.609 gms	1.3609 gms

.

Add slowly second compound required molar solution into first until pH becomes7.0.

First K_2HPO_4 buffer pH around 9.13.

Second KH_2PO_4 buffer pH around 4.60.

Calculations

SP= c+eE+sS+aA+bB+vV

SP= c+ eE+ sS + aA + bB + vV + j+J+ + j- J-

Average of E = Em = [E1+E2+E3+E4+…….E60]/ 60

Similarly, S,A,B,V calculated. For 20% 15% and 25% IPA

Relative contribution = %E = eE/ (eE+sS+aA+bB+vV) x 100

Similarly, for % S, A,B and V calculated

Using Minitab16 calculate the e.s.a.b.v values through MLR.

Regression Analysis: log kAGP versus E, S, A, B, V, J+, J-

Method

Rows unused 7

Analysis of Variance

Source	DF	Seq SS	Contribution	Adj SS	Adj MS	F-Value	P-Value
Regression	7	10.1263	79.65%	10.1263	1.44661	27.96	0.000
E	1	1.9050	14.98%	1.0071	1.00714	19.47	0.000
S	1	1.1069	8.71%	1.3589	1.35888	26.27	0.000
A	1	0.2328	1.83%	0.2399	0.23990	4.64	0.036
B	1	0.4326	3.40%	4.1650	4.16500	80.51	0.000
V	1	0.5819	4.58%	5.2455	5.24546	101.39	0.000
J+	1	0.2586	2.03%	0.0206	0.02056	0.40	0.531
J-	1	5.6086	44.12%	5.6086	5.60863	108.41	0.000
Error	50	2.5867	20.35%	2.5867	0.05173		
Total	57	12.7130	100.00%				

Model Summary

S	R-sq	PRESS	R-sq(pred)
0.227451	79.65%	76.80%	4.13625	67.46%

Coefficients

Term	Coef	SE Coef	95% CI	T-Value	P-Value	VIF
Constant	-0.756	0.111	(-0.979, -0.533)	-6.81	0.000	
E	0.4274	0.0969	(0.2328, 0.6219)	4.41	0.000	2.33
S	-0.3539	0.0691	(-0.4927, -0.2152)	-5.13	0.000	19.31
A	-0.1566	0.0727	(-0.3026, -0.0105)	-2.15	0.036	6.58
B	-1.254	0.140	(-1.534, -0.973)	-8.97	0.000	22.80
V	1.279	0.127	(1.024, 1.534)	10.07	0.000	9.77
J+	-0.0511	0.0811	(-0.2139, 0.1117)	-0.63	0.531	10.40
J-	1.562	0.150	(1.261, 1.864)	10.41	0.000	13.05

Regression Equation

log kAGP = -0.756 + 0.4274 E - 0.3539 S - 0.1566 A - 1.254 B + 1.279 V - 0.0511 J+ + 1.562 J-

Amino acids cocrystals:

Total experiment and characterisation studies carried out.

Serial number	Name of compound	PXRD	DSC	TGA	Raman	FT-IR	DVS
1	**L-proline**	Yes	Yes	Yes	Yes	Yes	Yes
2	**Adipic acid**	Yes	Yes	Yes	Yes	Yes	Yes
3	**Fumaric acid**	Yes	Yes	Yes	Yes	Yes	Yes
4	**Succinic acid**	Yes	Yes	Yes	Yes	Yes	Yes
5	**L-proline-Adipic acid cc**	Yes	Yes	Yes	Yes	Yes	Yes
6	**L-proline-Fumaric acid cc**	Yes	Yes	Yes	Yes	Yes	Yes
7	**L-proline-Succinic acid cc**	Yes	Yes	Yes	Yes	Yes	Yes
8	**L-leucine**	Yes	Yes	Yes	Yes	Yes	Yes
9	**L-isoleucine**	Yes	Yes	Yes	Yes	Yes	Yes
10	**L-serine**	Yes	Yes	Yes	Yes	Yes	Yes
11	**L-methionine**	Yes	Yes	Yes	Yes	Yes	Yes
12	**L-cysteine**	Yes	Yes	Yes	Yes	Yes	Yes
13	**Citric acid**	Yes	Yes	Yes	Yes	Yes	Yes
14	**L-leucine-Citric acid cc**	Yes	Yes	Yes	Yes	Yes	Yes
15	**L-isoleucine – Citric acid cc**	Yes	Yes	Yes	Yes	Yes	Yes
16	**L-serine-Citric acid cc**	Yes	Yes	Yes	Yes	Yes	Yes
17	**L-methionine-Citric acid cc**	Yes	Yes	Yes	Yes	Yes	Yes
18	**L-cysteine-Citric acid cc**	Yes	Yes	Yes	Yes	Yes	Yes
19	**Physical mixtures (1:1)**	Yes	Yes	Yes	Yes	Yes	Yes

Amino Acids and reported cocrystals

Name	Short	code	structure	Reported co-crystals
non-polar, aliphatic residues				
L-Glycine	Gly	G	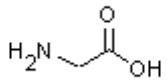	Yes. L-gly-glutaric acid, L-gly-tartaric acid,L-gly-phthalic acid, L-gly-urea.
L-Alanine	Ala	A	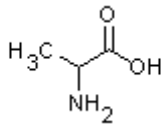	L-ala-val-ala.H_2O, L-ala-mandelic acid,
L-Valine	Val	V	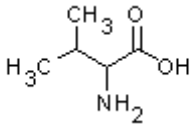	L-val-D-2 amino butanoic acid, L-val-fumaric acid, D-val-L-leu
L-Leucine	Leu	L	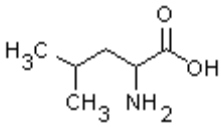	L-leu-D-val
L-Isoleucine	Ile	I	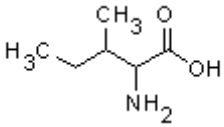	D-val-L-isoleucine
L-proline	Pro	P	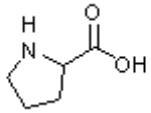	L-pro-fumaric acid
aromatic residues				
L-Phenylalanine	Phe	F	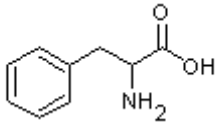	No
L-Tyrosine	Tyr	Y	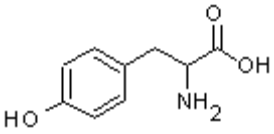	No
L-Tryptophan	Trp	W	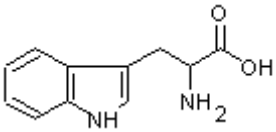	No
polar, non-charged residues				
L-Serine	Ser	S	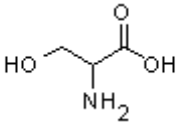	L-ser/pyridine-2,4dicarboxilic acid
L-Threonine	Thr	T	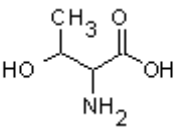	L-thr/L-all-thr

L-Cysteine	Cys	C	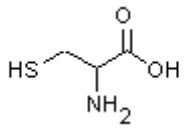	1) L-cys/S mandelic acid/R mandelic acid
L-Methionine	Met	M	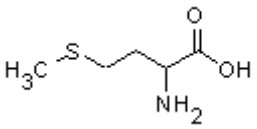	No
L-Asparagine	Asn	N	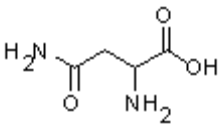	2) L-asn / L tartaric acid
L-Glutamine	Gln	Q	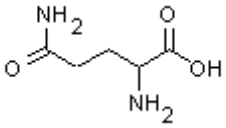	No
positively charged residues				
L-Lysine	Lys	K	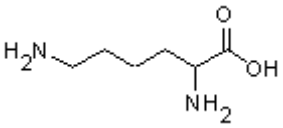	No
L-Arginine	Arg	R	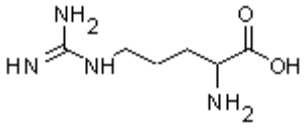	No
L-Histidine	His	H	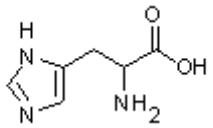	No
negatively charged residues				
L-Aspartate	Asp	D	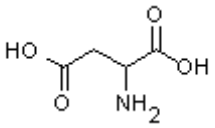	No
L-Glutamate	Glu	E	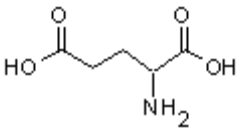	No

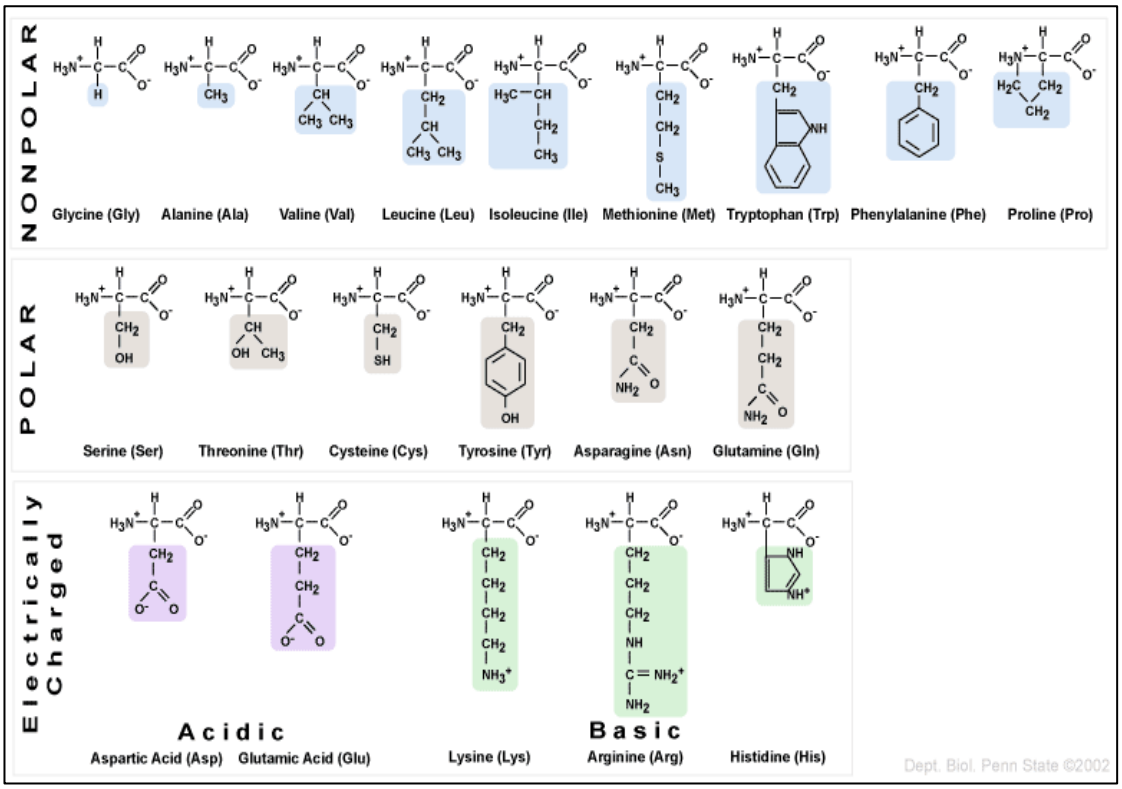

A single crystal of citric acid - L-cysteine monohydrate co-crystal pattern

Figure A 1 Crystal habit of single crystal citric acid-L-cysteine-H_2O

Figure A2 Crystal pattern – the plate-like habit of a single crystal of citric acid-L-cysteine-H_2O cocrystal hydrate.

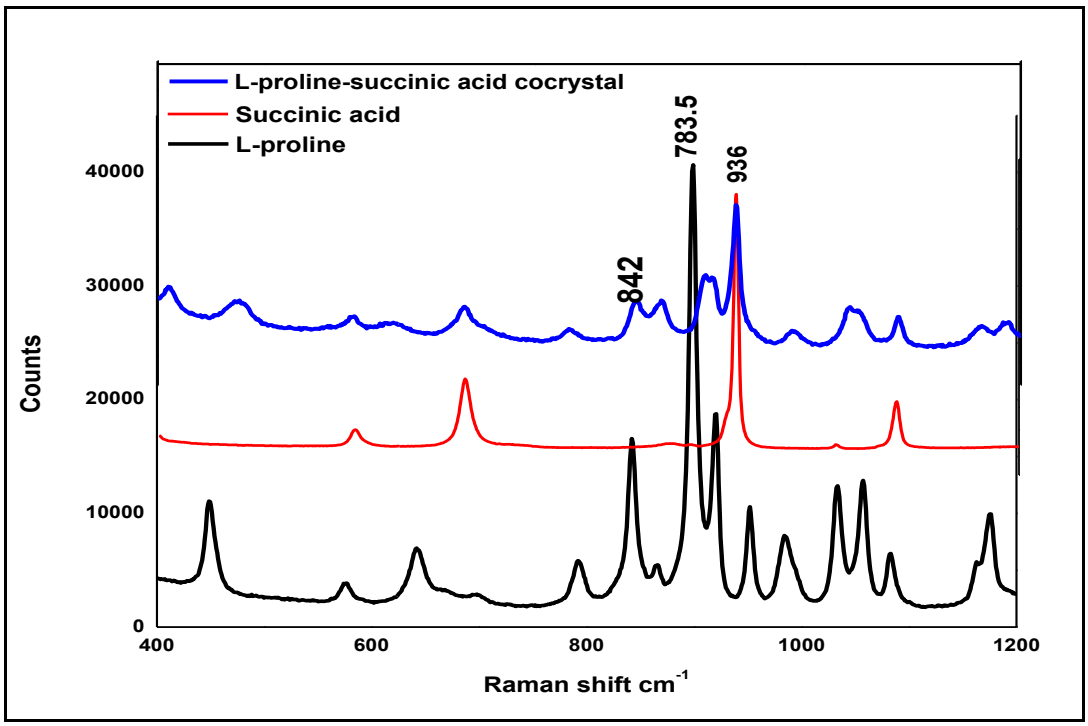

Figure A3 L-proline-succinic acid cocrystal Raman spectroscopy analysis

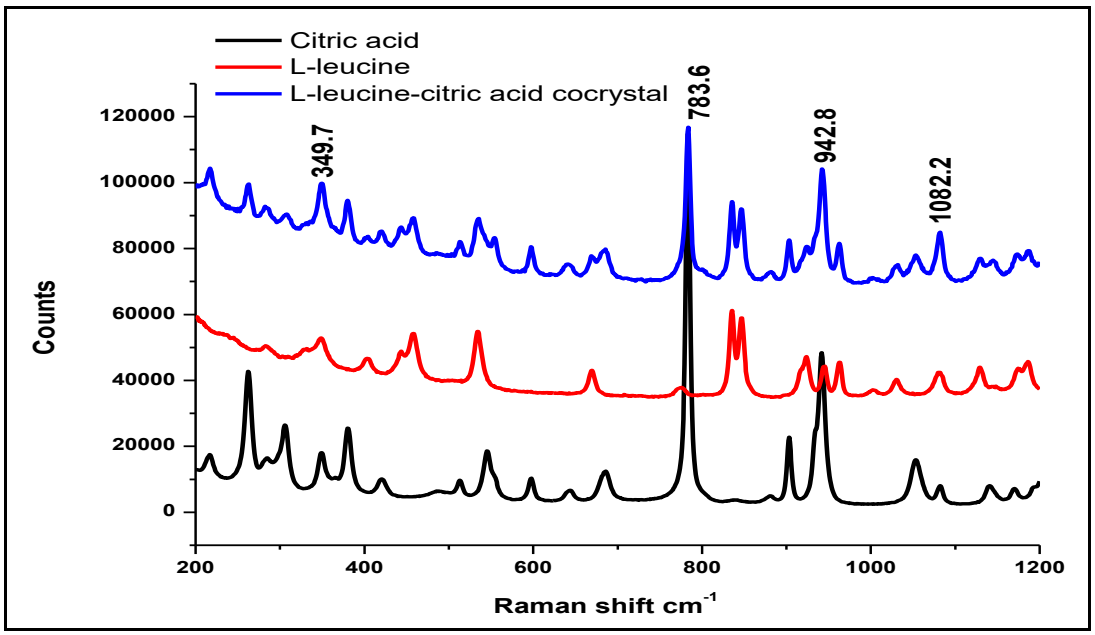

Figure A4 Raman spectroscopic analysis of L-leucine-citric acid cocrystal and starting material.

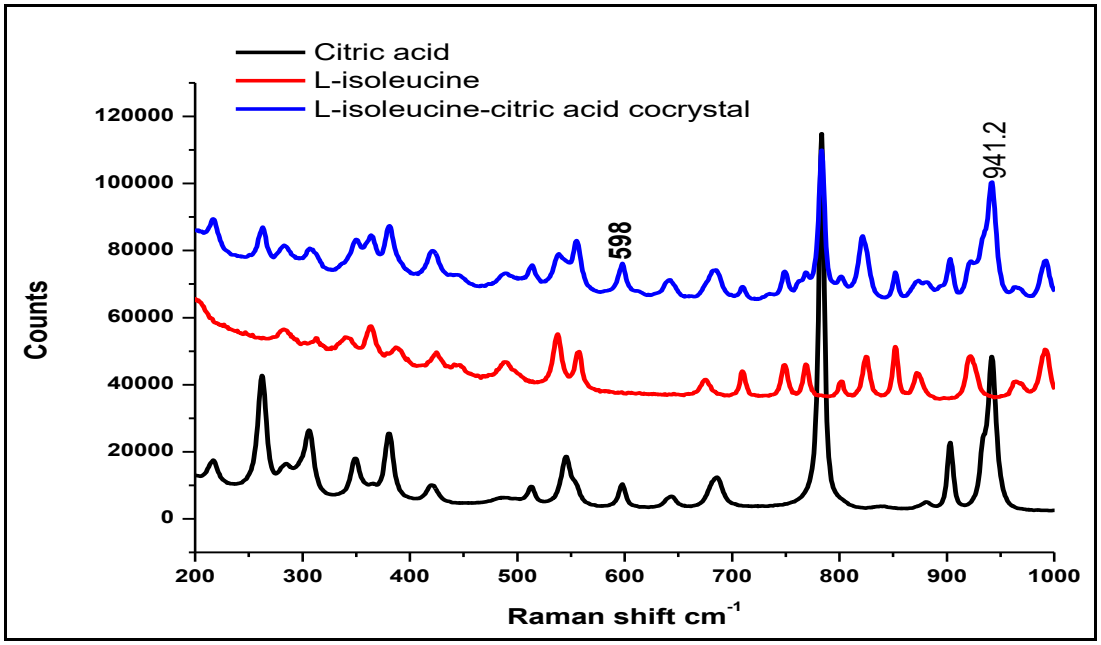

Figure A 5 L-isoleucine-citric acid cocrystal and their original material Raman spectroscopy.

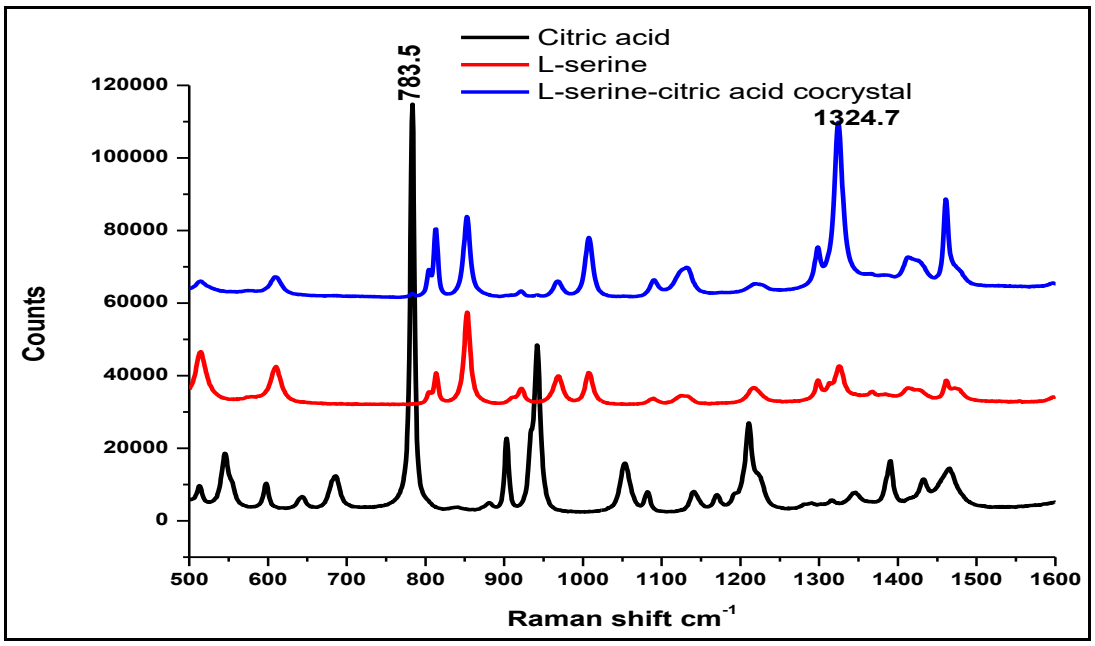

Figure A 6 L-serine-citric acid and their starting material Raman spectroscopy.

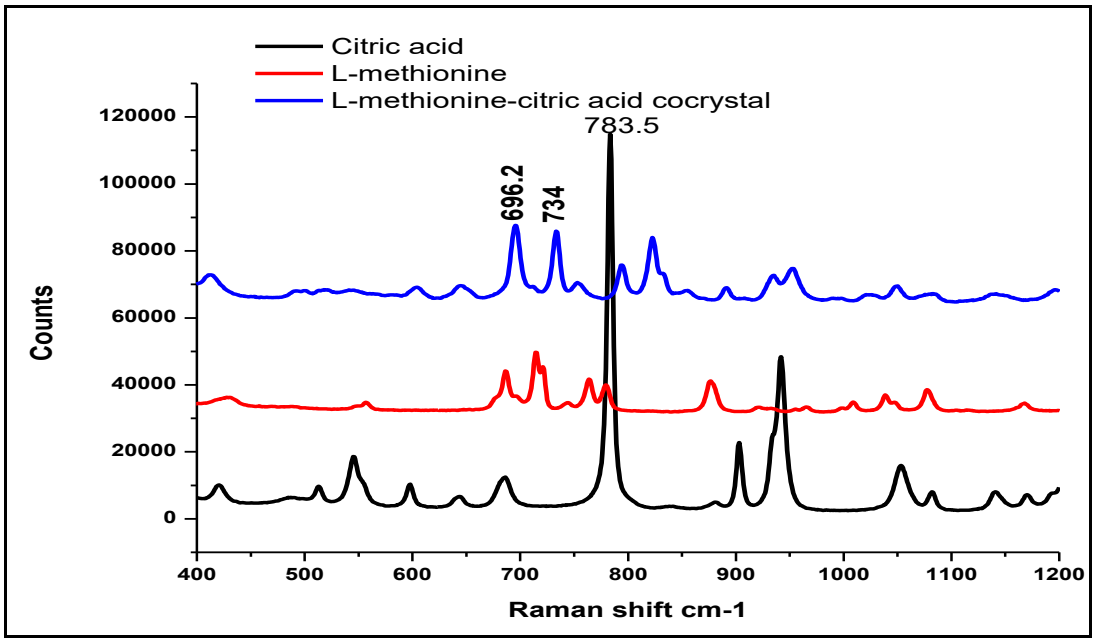

Figure A 7 L-methionine-citric acid cocrystal and their starting material Raman spectroscopy.

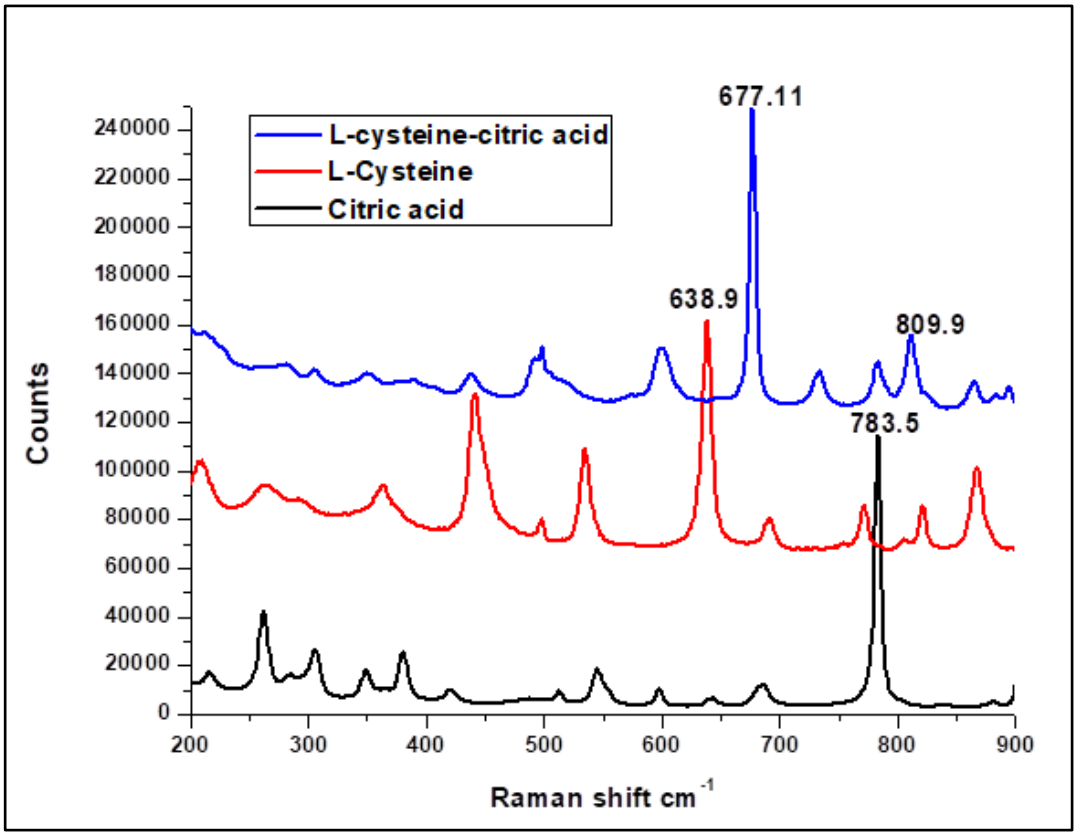

Figure A 8 L-cysteine-citric acid cocrystal and their starting material Raman spectroscopy.

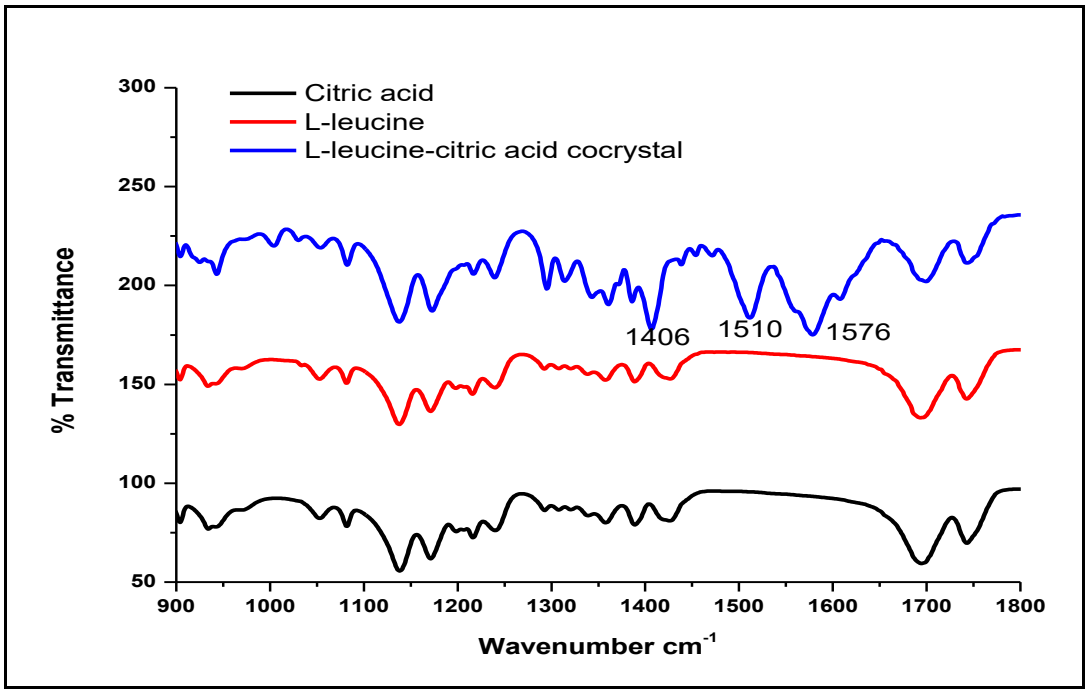

Figure A 9 L-leucine-citric acid cocrystal and their starting material FT-IR spectrum.

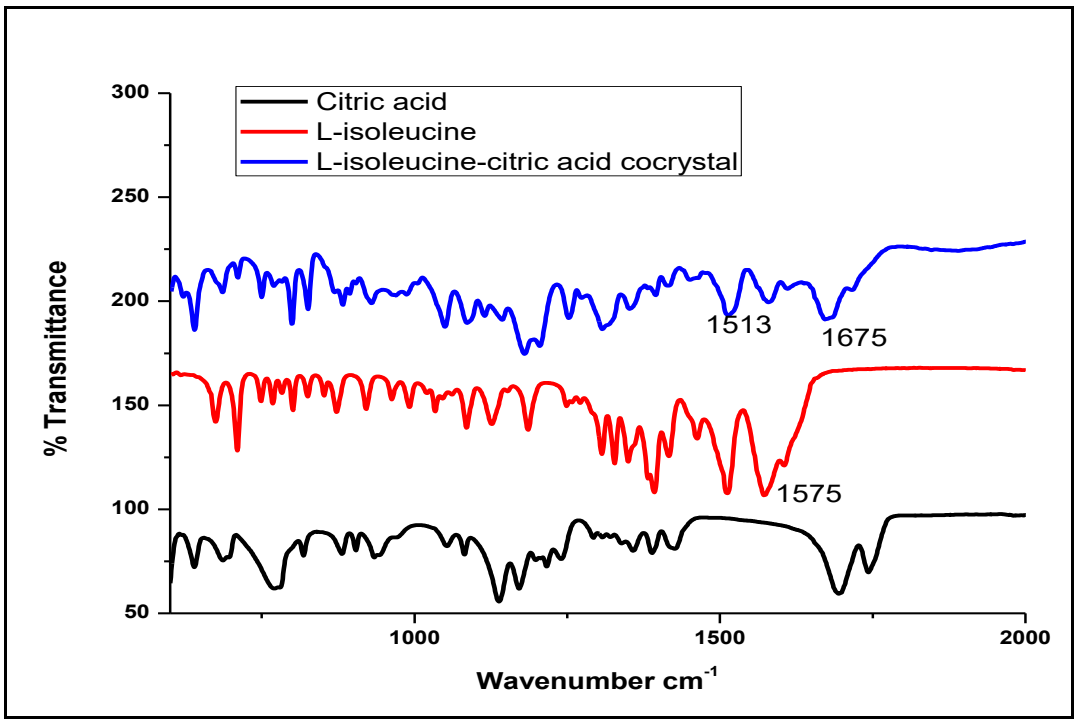

Figure A 10 L-isoleucine-citric acid cocrystal and their starting material FT-IR spectrum.

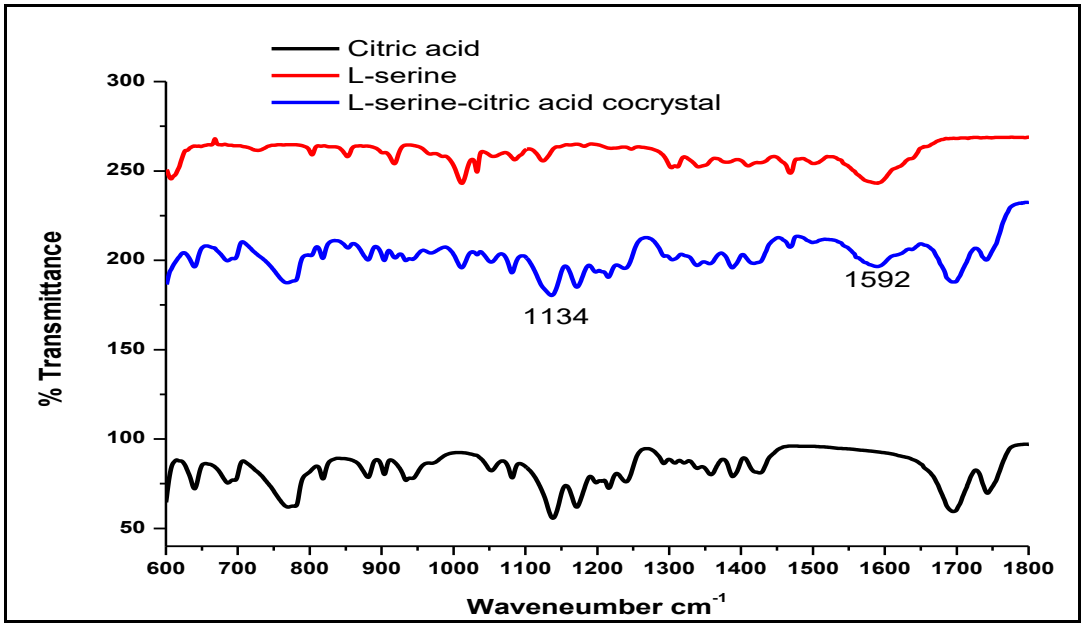

Figure A 11 L-serine-citric acid cocrystal and their starting material FT-IR spectra.

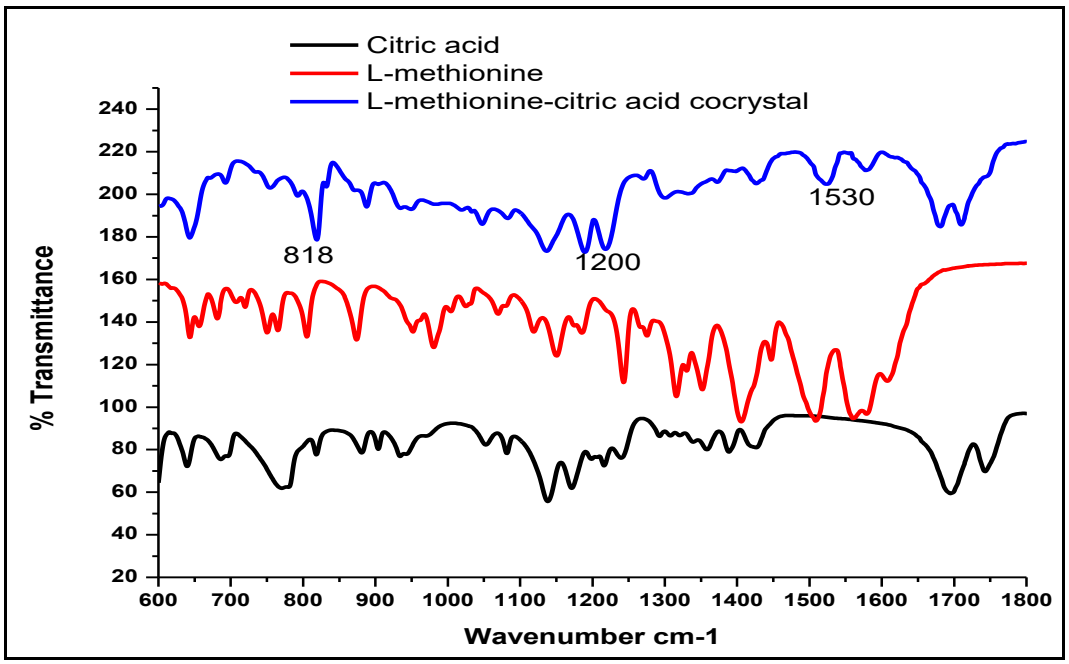

Figure A 12 L-methionine-citric acid cocrystal and their starting material FT-IR spectra.

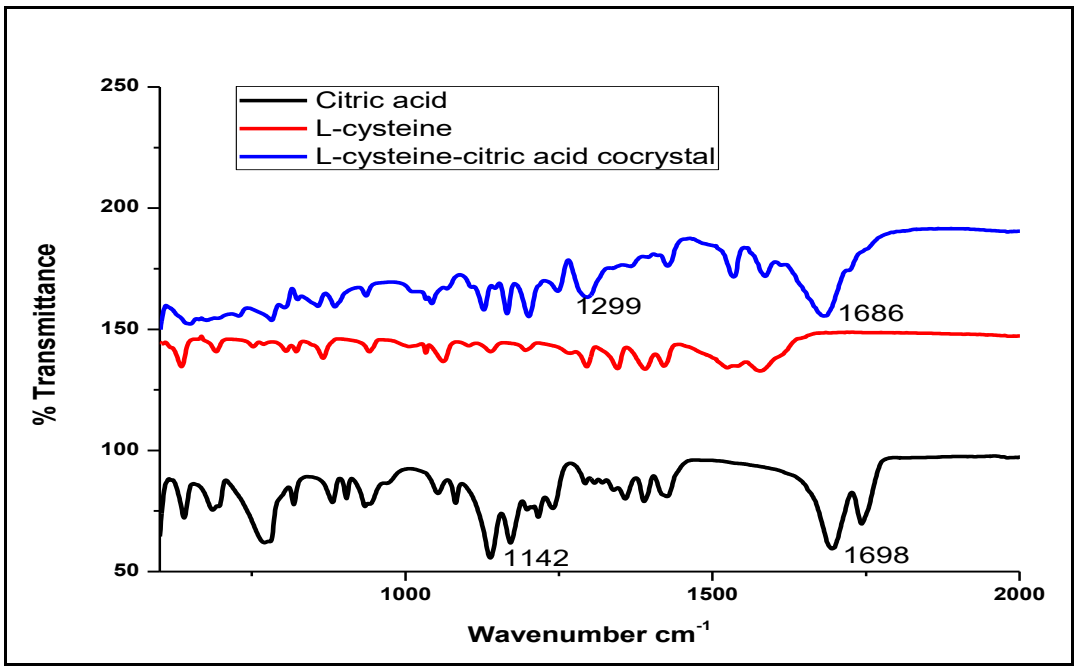

Figure A 13 L-cysteine-citric acid cocrystal and their starting material FT-IRspectra.

Journal of Pharmaceutical and Biomedical Analysis 149 (2018) 16–21

Contents lists available at ScienceDirect

Journal of Pharmaceutical and Biomedical Analysis

j ournal homepage: www.elsevier.com/locate/jpba

Structural properties governing drug-plasma protein binding determined by high-performance liquid chromatography method

Sharad Kamble[a], Paul Loadman[a], Michael H. Abraham[b], Xiangli Liu[a,*]

[a] School of Pharmacy and Medical Sciences, Faculty of Life Sciences, University of Bradford, Bradford, BD7 1DP, UK
[b] Department of Chemistry, University College London, 20 Gordon Street, London, WC1H 0AJ, UK

a r t i c l e i n f o

Article history:
Received 23 September 2017
Received in revised form 16 October 2017
Accepted 22 October 2017
Available online 28 October 2017

Keywords:
Plasma proteins
Binding
HPLC
Retention factors (k)
Linear free energy relationship
Abraham (Absolv) descriptors

a b s t r a c t

The high-performance liquid chromatography (HPLC) method employing stationary phases immobilized with plasma proteins was used for this study to investigate the structural properties governing drug-plasma protein binding. A set of 65 compounds with a broad range of structural diversity (in terms of volume, hydrogen-bonding, polarity and electrostatic force) were selected for this purpose. The Abraham linear free energy relationship (LFER) analyses of the retention factors on the immobilized HSA (human serum albumin) and AGP (α_1-acid glycoprotein) stationary phases showed that McGowan's characteristic molecular volume (V), dipolarity/polarizability (S) and hydrogen bond basicity (B) are the three significant molecular descriptors of solutes determining the interaction with immobilized plasma proteins, whereas excess molar refraction (E) is less important and hydrogen bond acidity (A) is not of statistical significance in both systems, for electrically neutral compounds. It was shown that ionised acids, as carboxylate anions, bind very strongly to the immobilized HSA stationary phase and that ionised bases, as cations bind strongly to the AGP stationary phase. This is the first time that the effect of ionised species on plasma protein binding has been determined quantitatively; the increased binding of acids to HSA is due almost entirely to acids in their ionised form.

1. Introduction

The binding of drugs to plasma proteins is an important process that determines the activity and pharmacokinetics of many drugs in the body. After being distributed around the circulating system, drugs bind to plasma proteins in varying degrees. In general, such binding is reversible, and an equilibrium exists between bound and free molecular forms. In most cases, only the free drug molecules are able to cross membrane barriers, be distributed to tissues and then exert therapeutic effects [1,2]. Drug-plasma protein binding acts as a reservoir for free drug concentration and prolongs the duration of drug action. Therefore drug-plasma protein binding is considered as an important property and needs to be characterized in the early stage of drug discovery [3].

In plasma, two major proteins, human serum albumin (HSA) and α_1-acid glycoprotein (AGP) are present in relatively high quantities. They are able to bind a variety of drugs with considerable affinity [4]. It is found that HSA with the highest concentration (5–7.5 $\times$ 10^{-4} mol/L) in plasma has two major binding sites and can bind acidic drugs with high association constants. AGP is an acidic protein with a lower concentration (0.9–2.2$\times$$10^{-5}$ mol/L). It exhibits a preference for binding basic and neutral drugs. Lipoproteins which are macromolecular complexes of lipid and proteins also play a role to a lesser degree [5].

There are different techniques to determine drug-plasma protein binding *in vitro*. Among these techniques, equilibrium dialysis, ultra-filtration and ultra-centrifugation have been most widely used. However, these methods show a number of limitations such as a very low throughput and poor reproducibility [6]. In comparison to these conventional methods, the HPLC method that employs stationary phases immobilized with plasma proteins appears an interesting approach because of the speed of analysis and automation capability [7,8]. In this method, drugs with high affinities interact strongly with the immobilized protein and are eluted later than drugs with no or less affinities. The affinity is expressed by the retention factor k, which is calculated through Eq. (1)

$$k = (t_r - t_0)/t_0 \quad (1)$$

where t_r and t_0 are the retention times of the solute and of an unretained compound, respectively.

A number of studies have been carried out to investigate drug-plasma protein interaction by using special classes of drugs [9–13].

* Corresponding author.
E-mail address: x.liu18@bradford.ac.uk (X. Liu).

https://doi.org/10.1016/j.jpba.2017.10.022
0731-7085/